

Ph.D. Thesis – C.N. Tsai; McMaster University – Biochemistry and Biomedical Sciences

ANTI-INFECTIVE DISCOVERY IN SALMONELLA TYPHIMURIUM

Ph.D. Thesis – C.N. Tsai; McMaster University – Biochemistry and Biomedical Sciences

**EXPLOITING HOST IMMUNITY FOR ANTI-INFECTIVE DISCOVERY IN
SALMONELLA TYPHIMURIUM**

By Caressa Natalie Tsai, B.Sc.

A Thesis Submitted to the School of Graduate Studies in Partial Fulfillment of the
Requirements for the Degree of Doctor of Philosophy

McMaster University © Copyright Caressa Natalie Tsai, June 2021

Ph.D. Thesis – C.N. Tsai; McMaster University – Biochemistry and Biomedical Sciences

McMaster University DOCTOR OF PHILOSOPHY (2021) Hamilton, Ontario
(Biochemistry and Biomedical Sciences)

TITLE: Exploiting host immunity for anti-infective discovery in *Salmonella*
Typhimurium

AUTHOR: Caressa N. Tsai, B.Sc. (University of Toronto)

SUPERVISOR: Dr. Brian K. Coombes

NUMBER OF PAGES: xiii, 220

FOREWORD

Abstract

Salmonella enterica serovar Typhimurium (*Salmonella*) is a Gram-negative bacterial pathogen capable of causing both gastroenteritis and bacteraemia in human hosts. During infection, *Salmonella* invokes a complex network of virulence factors, regulatory systems, and metabolic pathways to promote immune evasion, sometimes demanding antibiotic treatment for resolution. Unfortunately, antibiotic resistance has reached critical levels in this and other pathogens, necessitating the discovery of new anti-infective targets and treatment options. Herein, we have sought to exploit the dynamic interactions between *Salmonella* and the host immune system to identify new, conditionally active anti-*Salmonella* therapies. In chapter 2, we aim to identify chemical compounds that are selectively antimicrobial against intracellular *Salmonella*, and discover that the anxiolytic drug metergoline inhibits *Salmonella* survival in cultured macrophages and systemically infected mice. In chapter 3, we screen for anti-virulence compounds that target regulatory signaling in *Salmonella*, and characterize the inhibitory activity of methyl-3,4-dephostatin, which perturbs SsrA/B and PmrB/A signaling and enhances sensitivity to colistin *in vitro* and *in vivo*. In chapter 4, we identify several host-directed compounds that modulate macrophage immunity and investigate their ability to attenuate a multidrug resistant *Salmonella* infection. Together, the work presented in this thesis demonstrates the potential for drug screening in infection-relevant conditions to identify new anti-infectives with non-traditional targets.

Acknowledgements

Dr. Brian Coombes – thank you for five years of exceptional mentorship. I truly appreciate the time you have devoted in teaching me scientific rigor, compelling prose, and unwavering professionalism – all of which you epitomize. Your faith gave me the freedom and confidence to pursue intriguing science, and I will always be proud to have been a member of the Coombes lab.

Dr. Eric Brown – the stories in these chapters could not have been formed without tremendous input from not only you, but so many of your lab members. Thank you for your generosity with your time, and for fostering so much creativity and enthusiasm for research in this institute.

Dr. Dawn Bowdish – I am deeply grateful for all of your advice and support throughout my time here. Thank you for gifting my committee meetings with an immunological perspective, thought-provoking questions, and excitement for my research.

Past and present Coombes lab – thank you to all for many years of companionship and encouragement, especially: Bushra and Alex, for always sharing in my excitement and frustration and for every fun adventure; Wael and Dustin, for the advice and guidance that I credit so much of this work to and for never failing to make me laugh; Liz, for your friendship and thoughtfulness through every day of grad school and for always lending a kind ear; Jordyn, John and Angelica, for all of your efforts in bringing my ideas to fruition and for shaping me into a better teacher.

Mom, Dad, Pascale, Raewyn – your belief in me has allowed me to chase after my dreams and made every day a little easier. Thank you for supporting me

through nine years of post-secondary education, and for never letting the time between our visits be felt.

Craig – none of this work would have been possible without your unending support and insight. Thank you for always believing in me, for finding the excitement in every day, for helping me piece together my data, and for the endless sacrifices you have made to support my decisions and goals. Your love, in every facet of its meaning, has made this journey a happy one. I love you.

Table of Contents

| | |
|---|------------|
| FOREWORD | iv |
| Abstract | iv |
| Acknowledgements | v |
| Table of Contents | vii |
| List of Figures | ix |
| List of Tables | xi |
| List of Abbreviations | xii |
| CHAPTER 1 – Introduction | 1 |
| Preface | 2 |
| Epidemiology of <i>Salmonella enterica</i> | 3 |
| Modelling <i>Salmonella</i> infection <i>in vivo</i> | 4 |
| Genetic determinants of <i>Salmonella</i> virulence | 6 |
| Two-component regulatory systems and environmental signals | 7 |
| Interplay between extracellular <i>Salmonella</i> and the host immune system | 9 |
| Adaptation of <i>Salmonella</i> to the intracellular environment | 11 |
| Antibiotic resistance and highly invasive <i>Salmonella</i> | 13 |
| Modern approaches in antibiotic and anti-infective discovery | 14 |
| Purpose and contents of this thesis | 17 |
| Figures | 19 |
| CHAPTER 2 – A macrophage-based screen identifies antibacterial compounds selective for intracellular <i>Salmonella</i> Typhimurium | 22 |
| Preface | 23 |
| Summary | 24 |
| Introduction | 25 |
| Results | 27 |
| Discussion | 39 |
| Methods | 43 |
| Acknowledgements | 54 |
| Author Contributions | 54 |
| Figures | 55 |
| Tables | 65 |
| Supplementary Figures | 66 |
| Supplementary Tables | 89 |
| Supplementary Methods | 92 |
| CHAPTER 3 – Targeting two-component systems uncovers a small molecule inhibitor of <i>Salmonella</i> virulence | 105 |
| Preface | 106 |
| Summary | 107 |

| | |
|---|------------|
| Keywords | 107 |
| Introduction | 108 |
| Results | 110 |
| Discussion | 122 |
| Significance | 125 |
| Acknowledgements | 127 |
| Author Contributions | 127 |
| Declaration of Interests | 127 |
| STAR Methods | 128 |
| Figures | 141 |
| Supplementary Figures | 151 |
| Supplementary Tables | 161 |
| CHAPTER 4 – Host-directed small molecules sensitize multidrug resistant <i>Salmonella</i> to macrophage immunity | 162 |
| Preface | 163 |
| Abstract | 164 |
| Introduction | 165 |
| Results | 167 |
| Discussion | 170 |
| Methods | 173 |
| Figures | 179 |
| CHAPTER 5 – Conclusions | 184 |
| Summary | 185 |
| Conditional antimicrobial activity and outer membrane disruption | 185 |
| Advantages and disadvantages of inhibiting bacterial virulence | 188 |
| Direct targeting of the host immune system during infection | 190 |
| Final remarks | 192 |
| REFERENCES | 193 |

List of Figures

| | |
|---|-----|
| Figure 1.1. Stages of <i>Salmonella</i> spread during infection. | 19 |
| Figure 1.2. Regulatory systems governing virulence gene expression in <i>Salmonella</i> | 20 |
| Figure 1.3. Overview of the intracellular immune response to <i>Salmonella</i> infection. | 21 |
| Figure 2.1. Genetic requirements for <i>S. Tm</i> growth in host-mimicking media and macrophages. | 55 |
| Figure 2.2. Chemical screen identifies novel compound activities against intracellular <i>S. Tm</i> | 57 |
| Figure 2.3. Impact of OM integrity and efflux on metergoline activity in MHB and LPM. | 59 |
| Figure 2.4. Atomic force microscopy (AFM) on <i>S. Tm</i> grown in MHB, LPM, or bone-marrow derived macrophages. | 61 |
| Figure 2.5. Metergoline is bacteriolytic and perturbs the <i>S. Tm</i> cytoplasmic membrane. | 62 |
| Figure 2.6. <i>In vivo</i> efficacy of metergoline in a murine model of systemic <i>S. Tm</i> infection. | 64 |
| Figure 3.1. Identifying chemical repressors of virulence gene transcription. | 141 |
| Figure 3.2. Dephostatin represses intracellular virulence through SsrB. | 142 |
| Figure 3.3. Dephostatin inhibits non-SPI-2 virulence genes. | 144 |
| Figure 3.4. Dephostatin selectively potentiates polymyxin antibiotics against <i>Salmonella</i> | 146 |
| Figure 3.5. Synergy between dephostatin and colistin requires PmrA-regulated genes. | 148 |
| Figure 3.6. <i>In vivo</i> efficacy of dephostatin and colistin in a murine infection model. | 150 |
| Figure 4.1. Immunomodulatory compounds restrict <i>Salmonella</i> replication in macrophages. | 179 |
| Figure 4.2. Potency analysis of putative HDT compounds. | 181 |
| Figure 4.3. Immunomodulatory activity of hit compounds. | 182 |
| Supplementary Figure 2.1. Optimization of intracellular screening workflow. | 66 |
| Supplementary Figure 2.2. Impact of LPM or mutants on metergoline activity. .. | 68 |
| Supplementary Figure 2.3. Activity of metergoline against methicillin-resistant <i>Staphylococcus aureus</i> (MRSA). | 69 |
| Supplementary Figure 2.4. Serial-passage experiment with metergoline and control experiments for DiSC ₃ (5) and ATP assays. | 71 |
| Supplementary Figure 2.5. <i>In vivo</i> efficacy of metergoline following delayed treatment administration. | 73 |
| Supplementary Figure 2.6. Structure of metergoline analogues. | 74 |

| | |
|---|-----|
| Supplementary Figure 2.7. NMR spectra for aminomethyl ergoline (S1). | 75 |
| Supplementary Figure 2.8. NMR spectra for ethyl carbamate derivative (S2). ... | 76 |
| Supplementary Figure 2.9. NMR spectra for N-Boc ergoline derivative (S3). | 77 |
| Supplementary Figure 2.10. NMR spectra for N-Acetyl ergoline derivative (S4). .. | 78 |
| Supplementary Figure 2.11. NMR spectra for N-(N'-Benzyl) urea derivative (S5). | 79 |
| Supplementary Figure 2.12. NMR spectra for N-(2-Phenylethylsulfonyl) ergoline derivative (S6)..... | 80 |
| Supplementary Figure 2.13. NMR spectra for N-(3-Phenylpropyl) ergoline derivative (S7)..... | 81 |
| Supplementary Figure 2.14. NMR spectra for N-Benzoyl ergoline derivative (S8). | 82 |
| Supplementary Figure 2.15. NMR spectra for N-Phenylacetyl ergoline derivative (S9)..... | 83 |
| Supplementary Figure 2.16. NMR spectra for N-(3-Phenylpropanoyl) ergoline derivative (S10)..... | 84 |
| Supplementary Figure 2.17. NMR spectra for N-L-Phenylalanyl ergoline derivative (S11)..... | 85 |
| Supplementary Figure 2.18. NMR spectra for N-(N-Boc-L-Phenylalanyl) ergoline derivative (S12)..... | 86 |
| Supplementary Figure 2.19. NMR spectra for N-trans-Cinnamoyl derivative (MLBC-01). | 87 |
| Supplementary Figure 2.20. NMR spectra for N-trans-Cinnamoyl derivative (MLBC-02). | 88 |
| Supplementary Figure 3.1. Screening workflow to identify chemical repressors of virulence gene transcription, related to Figure 3.1..... | 151 |
| Supplementary Figure 3.2. Dephostatin represses transcription of SPI-2 and other virulence genes, related to Figure 3.3. | 153 |
| Supplementary Figure 3.3. Selectivity of dephostatin-polymyxin synergy, related to Figure 3.4..... | 155 |
| Supplementary Figure 3.4. Screening of the <i>Salmonella</i> single-gene deletion (SGD) collection, related to Figure 3.5. | 157 |
| Supplementary Figure 3.5. Analysis of genetic suppressors to dephostatin-colistin synergy, related to Figure 3.5. | 159 |
| Supplementary Figure 3.6. Dephostatin synthesis route, related to STAR Method: Synthesis of Dephostatin. | 160 |

List of Tables

| | |
|---|-----|
| Table 2.1. Structure activity relationship analysis of metergoline and two synthetic analogues. | 65 |
| Supplementary Table 2.1. Small molecule screening data..... | 89 |
| Supplementary Table 2.2. Activity of metergoline and 17 structurally related compounds. | 90 |
| Supplementary Table 2.3. NMR data for N-acetyl ergoline derivative S4. | 91 |
| Supplementary Table 3.1. Primers used in this study, related to STAR Method: Cloning and mutant generation..... | 161 |

List of Abbreviations

| | |
|-------------------------------|--|
| AFM | atomic force microscopy |
| ATP | adenosine triphosphate |
| BMM | bone marrow-derived macrophage |
| cAMP | cationic antimicrobial peptide |
| CAT | chloramphenicol acetyltransferase |
| CCCP | carbonyl cyanide m-chlorophenyl hydrazone |
| CFU | colony-forming units |
| CRAMP | cathelicidin-related antimicrobial peptide |
| DiSC ₃ (5) | 3,3'-dipropylthiadicarbocyanine iodide |
| DMEM | Dulbecco's modified eagle medium |
| DMSO | dimethyl sulfoxide |
| DNA | deoxyribonucleic acid |
| EDTA | ethylenediaminetetraacetic acid |
| FBS | fetal bovine serum |
| HDT | host-directed therapy |
| HK | histidine kinase |
| IL | interleukin |
| iNTS | invasive non-typhoidal <i>Salmonella</i> |
| L-SUP | L929 fibroblast conditioned medium |
| LB | lysogeny broth |
| LDH | lactate dehydrogenase |
| LPM | low phosphate low magnesium media |
| LPS | lipopolysaccharide |
| M | microfold |
| MHB | mueller hinton broth |
| MIC | minimum inhibitory concentration |
| MOI | multiplicity of infection |
| MRSA | methicillin-resistant <i>Staphylococcus aureus</i> |
| N ₂ O ₃ | dinitrogen trioxide |
| NLR | nod-like receptor |
| NO ₂ ⁻ | nitrite |
| NPN | N-phenyl-1-naphthylamine |
| NRAMP | natural resistance associated macrophage protein |
| OD | optical density |
| OM | outer membrane |
| PBS | phosphate buffered saline |
| PMB | polymyxin B |
| PMBN | polymyxin B nonapeptide |
| PMF | proton motive force |
| PTP | protein tyrosine phosphatase |
| RLU | relative light unit |

RNA ribonucleic acid
RR..... response regulator
RT-qPCR reverse transcriptase-quantitative polymerase chain reaction
S. Tm *Salmonella enterica* serovar Typhimurium
Salmonella *Salmonella enterica* serovar Typhimurium
SCV *Salmonella*-containing vacuole
SDS sodium dodecyl sulfate
SGD single-gene deletion
SPI *Salmonella* pathogenicity island
ST sequence type
T3SS..... type 3 secretion system
TCS..... two-component regulatory system
TLR..... toll-like receptor
WT wild-type

CHAPTER 1 – Introduction

Preface

Some parts of this chapter were adapted from the previously published review:

Tsai CN, Coombes BK. The role of the host in driving phenotypic heterogeneity in *Salmonella*. *Trends in Microbiology* (2019) 27, 6.

I wrote the manuscript with input from Coombes BK.

Permission has been granted by the publishers to reproduce the material herein.

*References within this and all other chapters have been compiled into one list at the end of the thesis, to avoid redundancy between sections.

Epidemiology of *Salmonella enterica*

Salmonella enterica is a species of pathogenic Gram-negative bacteria in the Enterobacteriaceae family. Strains within this species are capable of causing disease in a wide range of animal hosts, producing a spectrum of illness from mild to severe (Wheeler et al., 2018). *S. enterica* is divided into over 2500 individual serotypes based on antigenic classification, which may be further classified into those that are typhoidal and human-restricted (few in number), or non-typhoidal with a broad vertebrate host range (thousands) (Feasey et al., 2012). In addition to differences in host range, salmonellae may also be grouped by clinical presentation in human infection, typically manifesting as one of the following: enteric fever, bacteraemia, or gastroenteritis (Eng et al., 2015).

Cases of enteric fever are caused exclusively by the typhoidal serotypes *S. Typhi* or *S. Paratyphi*, and produce symptoms of headache, abdominal pain, diarrhea, and fever (Bhan et al., 2005). In these instances, antibiotic treatment is required for infection resolution, with ciprofloxacin, azithromycin, and ceftriaxone as first-line options. Comparatively, *Salmonella*-associated bacteraemia can be caused by both typhoidal and non-typhoidal serotypes, the latter including *S. Dublin*, *S. Choleraesuis*, *S. Enteritidis*, and *S. Typhimurium*, amongst others. Symptoms of bacteraemia are quite similar to those of enteric fever, with antibiotic treatment also necessitated. Finally, the majority of non-typhoidal serotypes cause mild cases of gastroenteritis, which includes symptoms of diarrhea, vomiting, nausea, headache, and abdominal pain (Gordon et al., 2008). These infections are typically self-limiting and often resolve quickly without antibiotic treatment; individuals who are young, elderly, or immunocompromised are at the highest risk of more severe illness.

Globally, *S. enterica* infections constitute a significant health burden. An estimated 11-21 million typhoidal infections and 93 million non-typhoidal infections occur each year worldwide (Majowicz et al., 2010). Given a significant animal reservoir, transmission of *S. enterica* is primarily zoonotic, aggravated by industrial production of meat, egg, and processed food products (Feasey et al., 2012). Infections are typically acquired by the oral consumption of contaminated food or water, occurring much more frequently in regions within the African and Asian continents (Stanaway et al., 2019).

Modelling *Salmonella* infection *in vivo*

Most of what we know of *S. enterica* infection biology has been gleaned from laboratory strains of the non-typhoidal *S. Typhimurium* serotype (hereinafter *Salmonella*), a generalist pathovar that is capable of infecting a wide range of animals (Branchu et al., 2018). Leveraging these natural hosts, *Salmonella* strains are routinely used to infect genetically susceptible *Nramp*-deficient mice (lacking a transporter of essential metals) through oral, intraperitoneal, and intravenous routes. In the oral infection model, streptomycin pretreatment is often used to transiently suppress the natural gut microbiota that confers colonization resistance (Sorbara and Pamer, 2018). With this, all three infection routes can produce significant pathology in the intestinal tract, spleen, and liver, resulting in lethality within a week of infection – not unlike what is seen in serious instances of enteric fever and/or bacteraemia in untreated, *Salmonella*-infected humans (Monack et al., 2004b). Genetically resistant mice that harbor the wild-type *Nramp* allele can also be used in chronic infection models, which can sustain *Salmonella* infections for months without significant pathology (Monack et al., 2004a). This phenotype more closely resembles the chronic carrier state occasionally seen during human infection, where *Salmonella* may be shed in the stool for over a year after inoculation (Eng et al., 2015). Additional exploration of

Salmonella pathogenicity has been performed in culture with immortalized fibroblast, epithelial, and macrophage cell lines, as well as in ileal loop and calf infection models of gastroenteritis.

The murine infection model has yielded tremendous insights into *Salmonella* pathogenicity, as well as the interplay between this bacterium and the host immune system. The course of systemic infection in orally infected mice may be viewed in three stages: invasion and inflammation in the intestinal tract, intracellular residence in and immune evasion within phagocytic cells, and growth and spread of *Salmonella* in systemic circulation (Figure 1.1). The initial invasion of the intestinal epithelium is central to *Salmonella* pathogenesis, where after oral infection of streptomycin-pretreated mice, bacterial colonization occurs in the terminal ileum, cecum and colon (Barthel et al., 2003). Here, *Salmonella* begins interacting with host cell subtypes in several ways: invasion of epithelial cells, endocytosis by microfold (M) cells, sampling by dendritic cells, and/or phagocytosis by macrophages and neutrophils. Systemic infections then proceed through infiltration of the gut mucosa and exit from the intestinal tract (Mastroeni and Grant, 2017). In this phase, adaptation to intracellular environments becomes more important, as *Salmonella* populations begin to mostly occupy dendritic cells, macrophages, neutrophils, and fibroblasts (Geddes et al., 2007). Once infected, these cells attempt to restrict the growth of internalized *Salmonella* with several unique antimicrobial pathways, differentiating several subpopulations of bacteria throughout the host (Bumann and Cunrath, 2017).

In the first 24 hours after infection, the total *Salmonella* burden within infected hosts is thought to initially decrease, due to a net balance of host-mediated killing over bacterial replication (Mastroeni and Grant, 2017). As infection proceeds, bacterial survival then becomes favoured by the transcriptional reprogramming that occurs in *Salmonella*. These changes allow *Salmonella* to express virulence

genes that confer resistance to the natural antimicrobial mechanisms of the host immune system (Behnsen et al., 2015). A partitioned bacterial population is created and sustained, with one fraction of cells remaining in the intestinal tract to intensify enterocyte inflammation, and another shuttled to the mesenteric lymph node and then systemic sites through the reticuloendothelial system (Mastroeni et al., 2009). Ultimately, the extraintestinal phase of *Salmonella* pathogenesis drives the formation of several distinct bacterial subpopulations in the lymph nodes, spleen, liver, and bloodstream, where unique colonization dynamics are adopted in each multicellular lesion to facilitate the infection and reinfection of host cells.

Genetic determinants of *Salmonella* virulence

Salmonella pathogenicity is understood to have evolved by “quantum leaps” through horizontal gene acquisition (Bäumler et al., 1998). This process – the transfer of genetic elements by bacterial conjugation, phage transduction, or DNA uptake – has contributed significantly to the pathoadaptive evolution of *Salmonella*, such that acquiring new virulence determinants has maximized fitness across infective environments (Ochman et al., 2000). Virulence-associated horizontally acquired elements in *Salmonella* are referred to as *Salmonella* pathogenicity islands (SPIs); at present, 21 such islands have been identified within the species (Ilyas et al., 2017).

Within the SPI pan-genome, the islands SPI-1 and SPI-2 are critically important and demarcate the two pathogenic lifestyles of *Salmonella*: invasive (SPI-1) and intracellular (SPI-2). Both SPI-1 and SPI-2 individually encode type 3 secretion systems (T3SSs), molecular nanomachines that translocate host-modulating effector proteins outside of bacteria into host cells. Effectors secreted by both T3SSs mediate different aspects of the *Salmonella* virulence program, subject to

highly precise regulatory control at distinct stages of infection (Haraga et al., 2008). The SPI-1 T3SS is required for invasion of intestinal epithelial cells via bacterial-mediated endocytosis, secreting effector proteins that induce actin rearrangements and membrane ruffling to permit bacterial uptake (Galán, 1996). After traversal of the epithelial layer and initiation of immune cell infection in the lamina propria and submucosa, the SPI-2 T3SS is required for intracellular survival (Jennings et al., 2017). Following its phagocytosis into host immune cells, *Salmonella* translocates over 30 unique SPI-2 effector proteins that interfere with host signaling pathways and convert the normally antimicrobial phagosome into a *Salmonella*-containing vacuole (SCV) (Figueira and Holden, 2012). *Salmonella* continues to reside and replicate in SCVs throughout infection, acquiring host nutrients through tubular extensions out of the SCV (Knuff and Finlay, 2017).

Two-component regulatory systems and environmental signals

The SPI-2 T3SS is one of the most important determinants of *Salmonella* virulence, as the systemic phase of infection relies upon bacterial replication in intracellular environments. As such, there has been considerable research into understanding the regulation of SPI-2 gene expression, highlighting the activity of several two-component regulatory systems (TCSs). TCSs are one of the most common forms of bacterial signal transduction mechanisms, are widely conserved across taxa, and function to translate environmental perturbations into biochemical triggers for gene expression (Fass and Groisman, 2009). Over 20 TCSs have been identified in *Salmonella*, forming a complex regulatory network that controls virulence genes within and outside of the SPIs (Ilyas et al., 2017).

Canonical TCSs consist of sensor histidine kinase (HK) and response regulator (RR) proteins (Capra and Laub, 2012). These systems regulate gene expression

through the initiation of a phosphorelay cascade that is initiated with the sensing of an environmental stimulus. Within each TCS, the HK fulfills the role of signal detection, where ligands, osmolarity, pH, or other environmental factors are recognized from the cytoplasm, membrane, or periplasm of bacterial cells (Mascher et al., 2006). In response, the HK will autophosphorylate on a conserved histidine residue within its cytoplasmic dimerization domain (Casino et al., 2009), then transfer this phosphoryl group to a conserved aspartate within the receiver domain of the cognate RR (Cheung and Hendrickson, 2010). Once phosphorylated, RRs are able to interact with downstream DNA or protein targets, with which they may activate or repress certain functions to elicit an appropriate cellular response (Jacob-Dubuisson et al., 2018).

The TCSs SsrA/B, PhoQ/P, EnvZ/OmpR and PmrB/A contribute significantly to *Salmonella* virulence (Figure 1.2). The SsrA/B TCS was co-inherited with SPI-2 and is crucial for its regulation (Walthers et al., 2007; Walthers et al., 2011). Upon activation in conditions similar to the host environment (acidic pH, low Mg^{2+}) (Mulder et al., 2015), the SsrA sensor kinase phosphorylates the SsrB response regulator at a conserved aspartate residue to create an active transcription factor that binds to and activates *cis*-regulatory elements in promoters within and outside of SPI-2. However, SsrB on its own is insufficient for complete SPI-2 activation, as SPI-2 promoters are also under the control of the PhoQ/P TCS, which responds to pH, Mg^{2+} , and cationic antimicrobial peptides (Bijlsma and Groisman, 2005); the EnvZ/OmpR TCS, which responds to pH and osmolarity (Lee et al., 2000); and the accessory regulatory protein SlyA, which is under the transcriptional control of PhoP (Navarre et al., 2005). Signaling through the PhoQ and EnvZ HKs also results in activation of the Hil regulatory proteins and eventually, SPI-1 genes (Ellermeier and Schlauch, 2007). The PmrB/A TCS, while not previously reported to transcriptionally activate SPI-2 (Choi and Groisman, 2013), also contributes significantly to virulence by controlling the addition of

outer membrane-fortifying chemical modifications to bacterial lipopolysaccharide (LPS) (Chen and Groisman, 2013). PmrA is activated by PmrB in environments with acidic pH (Perez and Groisman, 2007) or high $\text{Fe}^{3+}/\text{Al}^{3+}$ (Wösten et al., 2000), but also through the PhoQ/P system in environments with low Mg^{2+} due to posttranslational regulation of phosphorylated PmrA by the PhoP-activated gene *pmrD* (Kato and Groisman, 2004; Kato et al., 2003).

Interplay between extracellular *Salmonella* and the host immune system

One of the first immune defenses encountered by extracellular *Salmonella* during infection in its target niche is the harsh environment of the intestinal lumen, containing bile at concentrations of 0.2-2%. Bile salts are potent antimicrobial agents capable of degrading lipids and inducing DNA damage through point mutations and rearrangements (Gunn, 2001). Upon exposure to bile, *Salmonella* increases expression of the AcrAB-TolC efflux pump to export bile salts from the periplasm, and decrease OmpF porin expression via *marRAB* operon regulation to reduce influx (Prouty et al., 2004). These resistance mechanisms confer protection to bile salt concentrations at and above those encountered during infection (Velkinburgh and Gunn, 1999).

In the small intestine, *Salmonella* is also exposed to high concentrations of cationic antimicrobial peptides (cAMPs) at the base of villus crypts, secreted by Paneth cells (Bevins and Salzman, 2011). These host defense molecules target and perturb bacterial membranes through pore formation, leading to permeabilization and cell death (Brown and Hancock, 2006). Membrane lysis is facilitated by the amphipathic and positively charged nature of 15-20 amino acid-long cAMPs, which can adopt a wide range of secondary structures but are conserved in their electrostatic attraction towards negatively charged bacterial membranes (Hancock and Sahl, 2006). In addition to their membrane-targeting

activity, cAMPs have also been shown to possess cytosolic targets, and may act as immunomodulatory agents by binding bacterial LPS and nucleic acids to promote proinflammatory signaling (Bowdish and Davidson, 2005). The TCSs PhoQ/P and PmrB/A are particularly important for cAMP resistance, as they regulate many genes that encode for LPS-modifying enzymes (Bader et al., 2005; Groisman and Parra-Lopez, 1992; Gunn et al., 1998; Navarre et al., 2005; Shi et al., 2004). LPS modifications involving protein content or acyl chain count alter the surface charge of the bacterial outer membrane, and in turn, decrease the electrostatic attraction of cAMPs to microbial surfaces (Peschel, 2017). cAMP resistance has also been linked to transcriptional changes that modulate outer membrane protease and efflux pump expression (Ernst et al., 2001). It is worth noting that *Salmonella* also encounters cAMPs in intracellular environments, often through fusion of neutrophil granules to the SCV (Hood and Skaar, 2012).

Another immune defense that *Salmonella* encounters in the extracellular milieu is the lytic activity of the complement system. Over 30 complement proteins are naturally present in the bloodstream and at mucosal surfaces, comprising a major axis of the innate immune response to pathogens. Activation of complement occurs after contact with invading microbes; this triggers a proteolytic cascade that ultimately decorates bacterial membranes with complement proteins (Ricklin et al., 2010). Bacteria are then either coated and opsonized for eventual phagocytosis, or killed through lysis via membrane attack complex pore insertion (Heesterbeek et al., 2019). *Salmonella* has a high level of intrinsic complement resistance, mostly through proteolytic inactivation of complement proteins (Lambris et al., 2008), variation of LPS O-antigen length to prevent membrane attack complex localization (Bravo et al., 2008), or modulation of nucleotide metabolism through the stringent response (Chau et al., 2021).

Adaptation of *Salmonella* to the intracellular environment

In subsequent stages of infection, the stressors encountered by *Salmonella* become largely intracellular, as bacteria are internalized into SCVs within phagocytic host immune cells (Behnsen et al., 2015) (Figure 1.3). After formation of the SCV, vacuolar ATPase is assembled on its membrane (Lukacs et al., 1991), which gradually exposes *Salmonella* to low pH stress through the pumping of protons from the cytosol into the phagosome (Bang et al., 2002). Rather than inducing bacterial death, however, adaptation within *Salmonella* has allowed for rapid sensing of acid stress – this signal primarily acts as a cue to initiate virulence gene expression (Arpaia et al., 2011; Coombes et al., 2004; Wong et al., 2009) through the SsrB/A (Mulder et al., 2015), PhoQ/P (Bearson et al., 1998), and PmrB/A (Perez and Groisman, 2007) TCSs.

Intracellular *Salmonella* is also exposed to sources of oxidative stress produced by specialized phagocytic cells (Fang, 2004). After phagocytosis, components of NADPH oxidases are rapidly assembled on the SCV membrane, which then generates superoxide via electron transfer to molecular oxygen. Superoxide is rapidly disproportionated into hydrogen peroxide by superoxide dismutases, which then can be converted into either hydroxyl radicals via the Fenton reaction, back into molecular oxygen by catalases, or into hypochlorous acid by myeloperoxidases in neutrophils (Winterbourn and Kettle, 2013). Neutrophils also produce hydrogen peroxide as a by-product during D-amino acid oxidation, adding another source of oxidative stress to the infective environment (Tuinema et al., 2014). Superoxide, hydrogen peroxide, and hypochlorous acid all have high antimicrobial potential, inducing bacterial death by targeting DNA, proteins, and iron-sulfur clusters (Slauch, 2011). *Salmonella* evades these stressors by preventing NADPH oxidase trafficking to the SCV membrane and expressing enzymes such as superoxide dismutases, catalases, and peroxidases to detoxify

reactive oxygen species (Aussel et al., 2011; Fang et al., 1999; Vazquez-Torres et al., 2000).

The canonical NAIP/NLRC4 inflammasome is another important arm of the intracellular immune response to *Salmonella*. Inflammasomes are multiprotein complexes that detect and respond to cytosolic bacterial ligands with Caspase-mediated cytokine processing and the pore-forming Gasdermin-D protein, culminating in pyroptotic lysis of the infected host cell (Latz et al., 2013). Although the majority of intramacrophage *Salmonella* remains confined within the SCV (and thus, protected from the inflammasome) during infection (Birmingham et al., 2006), cytosolic escape can occasionally occur due to spurious pore-forming activity of the SPI-1 T3SS (Deng et al., 2017). The presence of bacterial flagellin (Franchi, 2006; Miao et al., 2006) and/or SPI-1 T3SS needle components (Miao et al., 2010) in the macrophage cytosol induces a rapid response from the NLRC4 inflammasome, involving activation of caspase-1, maturation of pro-inflammatory IL-1 β and IL-18, and pyroptosis. *In vivo*, this process is thought to expel cytosolic *Salmonella* into the extracellular milieu, where bacteria become trapped within the products of cellular lysis (Jorgensen et al., 2016). In these cases, the release of IL-1 β and IL-18 from lysed cells promotes the recruitment of secondary phagocytes such as neutrophils and natural killer cells, which may later engulf trapped bacteria (Müller et al., 2016). The NLRP3 inflammasome is also active within macrophages and responds to *Salmonella* infection in a similar way, although its activation has been partially attributed to oxidative stress and may not require cytosolic bacterial ligands (Broz et al., 2012; Man and Kanneganti, 2015).

Within and outside of immune cells, infected hosts restrict access to amino acids, essential transition metals, and other nutrients in an attempt to prevent pathogen growth. NRAMP metal transporters, for example, pump Fe²⁺ and Mn²⁺ out of the

SCV; transferrin and lactoferrin proteins bind and sequester extracellular Fe^{2+} ; neutrophil-derived calprotectin binds and sequesters Mn^{2+} and Zn^{2+} . Collectively, these processes make up the 'nutritional immunity' defense strategy (Hood and Skaar, 2012). Because nutritional limitation negatively impacts bacterial replication, adaptation of *Salmonella* to the intracellular environment includes significant transcriptional reprogramming that successfully circumvents host-mediated sequestration of free nutrients. Within the SCV, *Salmonella* has access to all nutrients required for growth, mostly facilitated by *Salmonella*-induced filaments (Knuff and Finlay, 2017) that extend from the SCV and establish an endosomal network for metabolite exchange between the host cytosol and the SCV (Liss et al., 2017). Proteomic and metabolic characterization has further confirmed that *Salmonella* has access to at least 31 different nutrients during infection (Steeb et al., 2013). Nutritional deprivation can also be countered by *Salmonella* with the production of siderophores for iron acquisition or upregulation of divalent metal transporter expression (Behnsen et al., 2015; Campoy et al., 2002).

Antibiotic resistance and highly invasive *Salmonella*

As discussed previously, most strains of *Salmonella* cause mild gastroenteritis in immunocompetent individuals; only some are capable of causing bacteraemia. However, recent years have seen the emergence of new clades within the Typhimurium serovar, which are capable of causing illness more similar to that induced by typhoidal *S. enterica* (Wheeler et al., 2018). Clinically referred to as invasive nontyphoidal *Salmonella* (iNTS) disease, these variants cause lethal bloodstream infection in humans, and disproportionately impact HIV-positive, malaria-infected, or malnourished individuals (Gordon et al., 2008). Globally, the highest incidence of iNTS disease cases occur in sub-Saharan Africa, where the majority of infections are caused by the single sequence type (ST) 313 (Feasey

et al., 2012). Case fatality rates of iNTS disease range from an estimated 25% in children to 50% in adults, causing almost 50,000 deaths each year (Kingsley et al., 2009). It is hypothesized that ST313 infections undergo human-human transmission, as no zoonotic source has been identified (Kariuki et al., 2006).

ST313 isolates are largely multi-drug resistant, rendering the former first-line treatments ampicillin, chloramphenicol, and trimethoprim-sulfamethoxazole ineffective against iNTS infection (Su et al., 2004). Extended-spectrum beta-lactamases have also been identified in certain ST313 isolates; their presence confers resistance to the important cephalosporin ceftriaxone, which is often used to treat complicated cases of iNTS (Feasey et al., 2014). More recently, an extensively drug resistant lineage of ST313 has emerged in the Democratic Republic of the Congo, which produces extended spectrum beta-lactamases and is also resistant to azithromycin (Van Puyvelde et al., 2019).

The emergence of antibiotic-resistant *S. enterica* strains is a significant global health concern, particularly within iNTS lineages. For both typhoidal and non-typhoidal *S. enterica* variants, the frequency of resistance to one or more antimicrobial agents continues to rise each year, with ciprofloxacin resistance rates in *S. Typhi* and nontyphoidal *S. enterica* infections reaching 74% and 10%, respectively, in 2017 (CDC, 2019). Antibiotic treatment – particularly with fluoroquinolones such as ciprofloxacin – is often essential to eradicate typhoidal and iNTS infections. Any further restriction in therapeutic options for these cases has the potential to greatly increase mortality rates around the world.

Modern approaches in antibiotic and anti-infective discovery

Within and outside of the *Salmonella* genus, antibiotic resistance has reached critical levels. Decades of antibiotic misuse in healthcare and agricultural settings

has selected for pathogens with intrinsic or acquired mechanisms of antibiotic resistance, gradually eroding our once numerous treatment options for infection (Davies and Davies, 2010). This ongoing issue has motivated several research efforts in antibiotic development, with considerable academic investment directed towards non-traditional approaches in drug discovery (Theuretzbacher and Piddock, 2019).

The initial discovery of antibiotics was one of the greatest achievements of modern medicine. Now decades past its prime, antibiotic research saw a golden era between 1940 and 1960, launched by Alexander Fleming's discovery of penicillin (Fleming, 1929). By screening Actinomycetes and other soil-dwellers for the production of antibacterial secondary metabolites, researchers were able to characterize over 20 different classes of antibiotics (Hutchings et al., 2019). These miracle drugs largely extinguished the previous lethality of bacterial infections, allowing clinicians to transform healthcare with invasive surgeries, chemotherapy treatments, organ transplants and more (Brown and Wright, 2016).

By the 1960s, the Waksman platform – used for metabolite screening – became plagued with rediscovery, and new antibiotics became increasingly difficult to find (Lewis, 2013). To overcome this hurdle, researchers looked to medicinal chemistry approaches to improve antibiotic potency around existing scaffolds (Theuretzbacher et al., 2020), and later, high-throughput robotics to examine large-scale libraries of synthetic molecules (Brown and Wright, 2016). While these efforts did and will continue to contribute significantly to our antibiotic armamentarium, they have been unable to keep pace with increasing resistance evolution (Tommasi et al., 2015). With pharmaceutical companies rapidly exiting the discovery space in favour of more profitable endeavors, we now find ourselves in a post-antibiotic age that begs for a resurrection in innovation (Årdal et al., 2020).

In academic labs working on antibiotic and anti-infective research, there is a focus on unconventional drug discovery and treatment options. Briefly, some such strategies include adjuvant compounds to enhance antibiotic activity (Wright, 2016), combinatorial treatments to leverage synergistic drug pair interactions (Fischbach, 2011), host-directed immunomodulatory therapies (Zumla et al., 2016), anti-virulence compounds (Rasko and Sperandio, 2010), and screening in infection-relevant conditions to illuminate targets that are conditionally essential *in vivo* (Brown and Wright, 2016).

For the purposes of this thesis, the concept of conditionally essential genes is especially important to consider. Gene essentiality has been traditionally defined as the smallest subset of genes required for growth under optimal growth conditions; as such, for most pathogens this has been determined from growth in rich laboratory media (Farha and Brown, 2015). In line with this, antibiotic activity has also been primarily assayed under similar growth conditions (Leekha et al., 2011), and most antibiotics target a limited range of essential bacterial processes. Now, it is understood that gene essentiality varies across environmental conditions, and thus should be viewed as conditional (D'Elia et al., 2009). This holds particularly true for pathogens in the setting of infection, where the host immune system restricts access to important nutrients and imposes other antimicrobial defenses upon invading microbes (Brown and Wright, 2016). This, in turn, necessitates that bacterial genes in virulence, metabolism, and other pathways be expressed to evade immune-based killing. Integrating this view with current techniques in high-throughput screening is beginning to reveal hundreds of genes to be conditionally essential for bacterial survival only in infection-relevant growth conditions (Karinsey et al., 2019; McCarthy et al., 2018; Nichols et al., 2011; Turner et al., 2015), and similarly, several unique anti-infectives to be conditionally active in those same settings (Colquhoun et al.,

2015; Ersoy et al., 2017; Fahnoe et al., 2012; Farha et al., 2017; Weber et al., 2020; Zlitni et al., 2013).

Purpose and contents of this thesis

Salmonella is a host-adapted pathogen that has evolved a complex network of virulence genes and regulatory systems that promote immune evasion. As these gene products and pathways are likely to be conditionally essential during infection, they may be valuable entry points and targets for new anti-infective discovery. My thesis work has focused on identifying unconventional anti-*Salmonella* therapies that exploit its interactions with the host immune system, leveraging the unique conditions of the intracellular environment (chapter 2), the TCSs required for virulence gene expression (chapter 3), and the host-specific antimicrobial pathways that restrict *Salmonella* survival (chapter 4). In these studies, I have focused primarily on the contextual environment of host macrophages, as these phagocytes have been identified as the primary *Salmonella*-containing cells at infection foci (Geddes et al., 2007).

Chapter 2 describes our work to identify chemical compounds with intracellular-specific antibacterial activity against *Salmonella*. Using an intramacrophage screening platform, we discover the anxiolytic drug, metergoline, to be an inhibitor of *Salmonella* replication in both cultured macrophages and an animal model of systemic salmonellosis. Within this work, we also report that several virulence genes, TCSs, and other regulatory factors are conditionally essential for intracellular *Salmonella* survival. Chapter 3 expands on this observation, where we aim to identify anti-virulence compounds that perturb TCS signaling, given the importance of these systems for *Salmonella* pathogenesis. From a cell-based, promoter reporter screen, we discover the anti-virulence activity of the natural product, methyl-3,4-dephostatin, which inhibits the expression of several genes

regulated by the SsrA/B and PmrB/A two-component systems, enhances sensitivity to the last-resort antibiotic, colistin, and attenuates *Salmonella* virulence *in vitro* and *in vivo*. Chapter 4 then implements a screening approach targeted towards the host rather than pathogenic viability or virulence, wherein we discover several small molecules that modulate macrophage immunity to indirectly restrict *Salmonella* survival. With an intramacrophage screening platform modified from that initially described in chapter 2, we focus on a strain of ST313 *Salmonella* that causes iNTS disease, as a prototypical multidrug resistant pathogen that may be sensitized to unconventional anti-infective therapies. Chapter 5 concludes this thesis by integrating the new anti-*Salmonella* compounds identified herein with current perspectives in modern drug discovery and evaluating the potential of these screening approaches for clinical implementation.

Figures

Figure 1.1

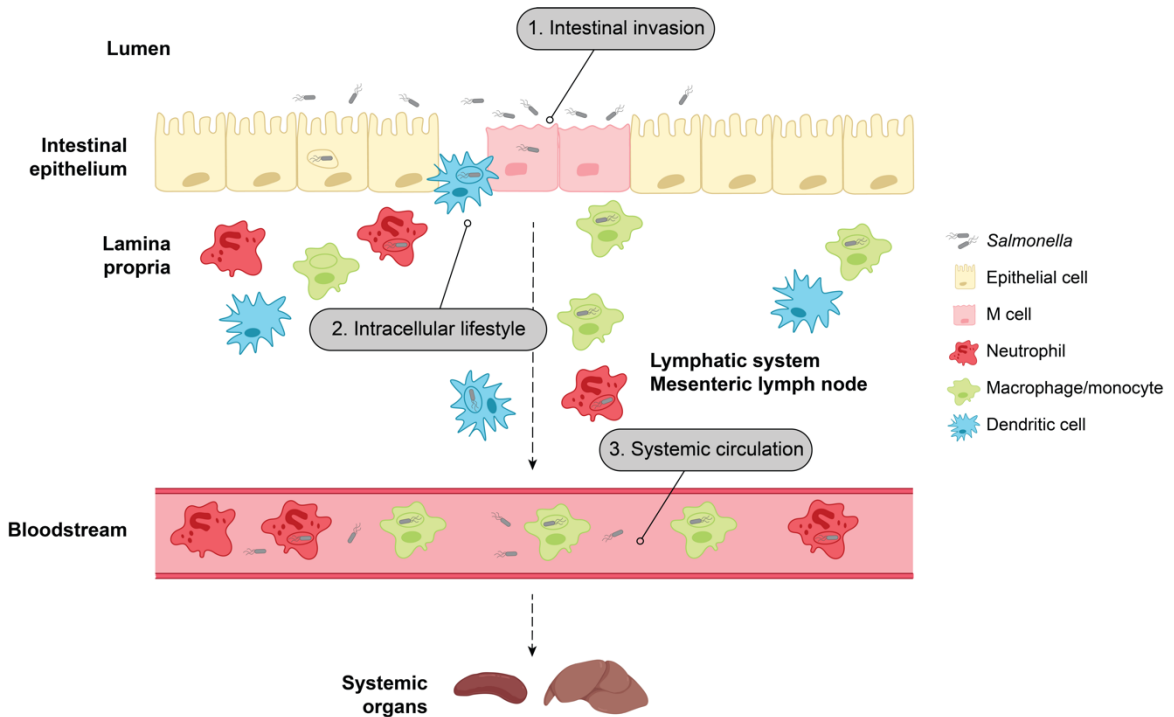


Figure 1.1. Stages of *Salmonella* spread during infection.

Salmonella infections are typically acquired via oral ingestion of contaminated food or water, and after surviving the acidic environment of the stomach, will reach the intestinal lumen. To begin inducing inflammation in enterocytes, *Salmonella* first begins to invade cells in the intestinal epithelium. As this area becomes increasingly disrupted, *Salmonella* cells begin to enter into the underlying lamina propria, and rapid recruitment of dendritic cells, neutrophils, and macrophages begins. These phagocytes engulf *Salmonella*, triggering a shift into its intracellular lifestyle. Host immune cells facilitate systemic spread of *Salmonella* through the lymphatic system, mesenteric lymph node, and ultimately, the bloodstream. Phagocytosis continues to occur in these areas with the eventual creation of multicellular pathogenic lesions in the spleen and liver.

Figure 1.2

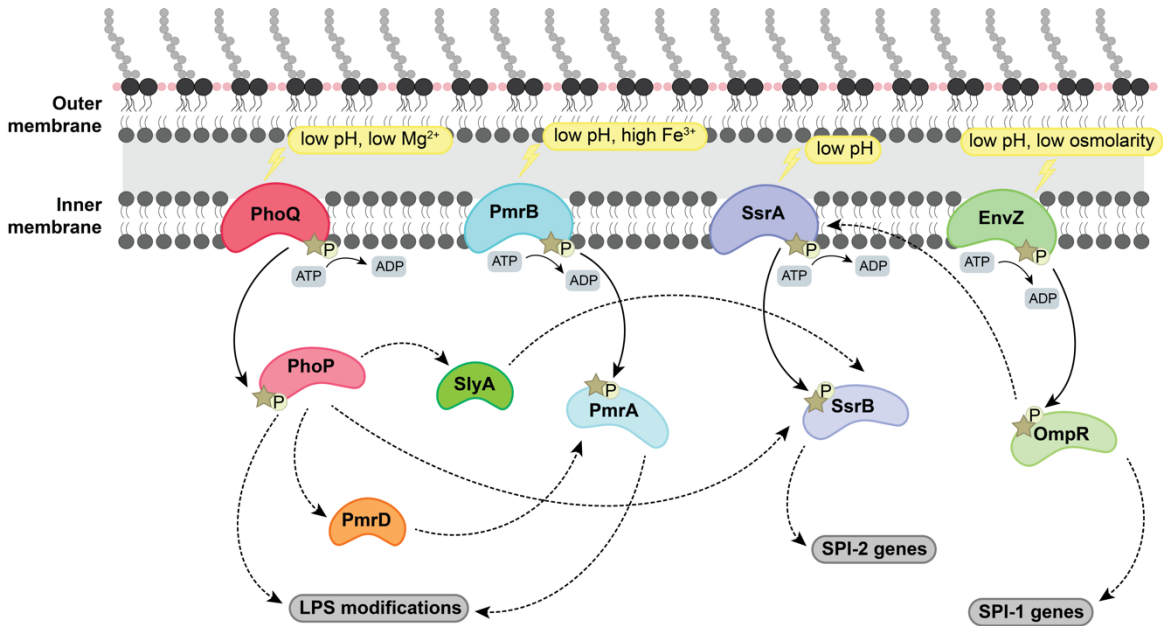


Figure 1.2. Regulatory systems governing virulence gene expression in *Salmonella*.

The two-component systems (TCSs) PhoQ/P, PmrB/A, SsrA/B, and EnvZ-OmpR control the expression of several important virulence loci in *Salmonella*, including genes within the SPI-1 and SPI-2 pathogenicity islands, as well as several lipopolysaccharide (LPS)-modifying enzymes that confer resistance to membrane disruption. Regulatory connections exist between and within the sensor histidine kinase (HK) proteins PhoQ, PmrB, SsrA, EnvZ and the response regulator (RR) proteins PhoP, PmrA, SsrB, and OmpR. Upon detection of environmental signals (indicated for each TCS in yellow), each HK is autophosphorylated, then transfers this phosphoryl group to its cognate RR, which becomes active and capable of modulating gene expression. The PhoP and PmrA RRs directly regulate genes that control LPS modifications, while the SsrA and OmpR RRs control SPI-2 and SPI-1 gene expression, respectively; upstream of these RRs there are several other connections between the four TCSs and the accessory proteins PmrD and SlyA.

Figure 1.3

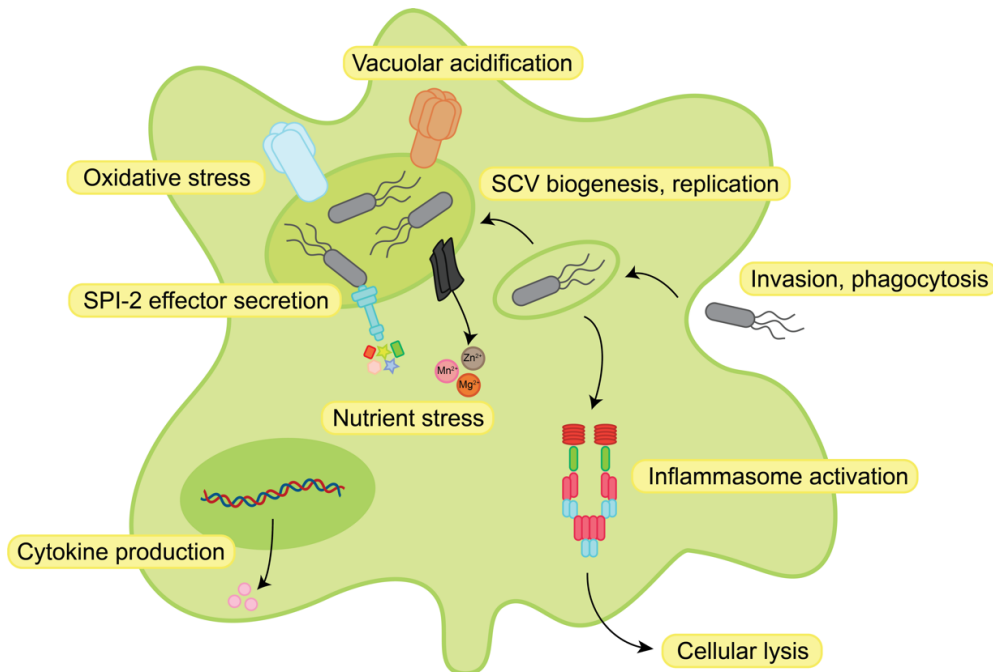


Figure 1.3. Overview of the intracellular immune response to *Salmonella* infection.

After internalization into host macrophages through invasion or phagocytic uptake, *Salmonella* is internalized into a phagosome that becomes modified to form a spacious *Salmonella*-containing vacuole (SCV). In the SCV, bacteria begin to express genes encoded on the SPI-2 pathogenicity island to secrete effector proteins that aid in SCV maintenance and immune evasion; replication begins to occur. Vacuolar ATPase and NADPH oxidase localize to the SCV membrane, which together acidify the environment and expose *Salmonella* to oxidative stress; metal transporters within the macrophage induce nutrient stress by pumping essential metals out of the SCV. In some cases, *Salmonella* may escape from the phagosomal compartment into the host cell cytosol, triggering inflammasome activation that results in pro-inflammatory cytokine production and potentially lysis of the infected macrophage.

CHAPTER 2 – A macrophage-based screen identifies antibacterial compounds selective for intracellular *Salmonella* Typhimurium

Preface

The work presented in this chapter was previously published in:

Ellis MJ, Tsai CN, Johnson JW, French S, Elhenawy W, Porwollik S, Andrews-Polymeris H, McClelland M, Magolan J, Coombes BK, Brown ED. A macrophage-based screen identifies antibacterial compounds selective for *Salmonella* Typhimurium. *Nature Communications* (2019) 10, 197.

Permission has been granted by the publisher to reproduce the material herein.

Ellis MJ and I contributed equally to this work. We wrote the manuscript with input from Coombes BK and Brown ED, and performed all experiments, with the following exceptions: Johnson JW and Magolan J designed and synthesized metergoline analogues (Supplementary Figures 2.6-2.20, Supplementary Table 2.3, Supplementary Methods). French S performed atomic force microscopy (Figure 2.4). Elhenawy W assisted with tissue culture experiments (Figure 2.1b). Porwollik S, Andrews-Polymeris H, and McClelland M constructed and supplied the *Salmonella* deletion library.

*References within this and all other chapters have been compiled into one list at the end of the thesis, to avoid redundancy between sections.

Summary

Salmonella Typhimurium (S. Tm) establishes systemic infection in susceptible hosts by evading the innate immune response and replicating within host phagocytes. Here, we sought to identify inhibitors of intracellular S. Tm replication by conducting parallel chemical screens against S. Tm growing in macrophage-mimicking media and within macrophages. We identify several compounds that inhibit *Salmonella* growth in the intracellular environment and in acidic, ion-limited media. We report on the antimicrobial activity of the psychoactive drug metergoline, which is specific against intracellular S. Tm. Screening an S. Tm deletion library in the presence of metergoline reveals hypersensitization of outer membrane mutants to metergoline activity. Metergoline disrupts the proton motive force at the bacterial cytoplasmic membrane and extends animal survival during a systemic S. Tm infection. This work highlights the predictive nature of intracellular screens for *in vivo* efficacy, and identifies metergoline as a novel antimicrobial active against *Salmonella*.

Introduction

The stagnant antibiotic discovery pipeline is particularly concerning for intracellular infections. Bacterial pathogens that survive within host cells evade the antimicrobial activity of the immune system and can form persister cells that tolerate antibiotic treatment (Helaine et al., 2014; Rycroft et al., 2018). As such, intracellular infections are often recurrent, warranting an increase in antimicrobial research specific for such pathogens and an improved understanding of the genetic requirements for intracellular survival. Intracellular bacteria occupy modified phagosomes (*Salmonella*, *Mycobacterium*, *Francisella*), inclusions (*Chlamydia*), lysosomes (*Legionella*, *Coxiella*) or the cytosol (*Listeria*, *Shigella*, *Rickettsia*) of host cells, which offer considerably different environments relative to standard nutrient-rich growth media (Mitchell and Isberg, 2017). Interestingly, emerging evidence suggests that pathogens such as *Staphylococcus aureus* and *Streptococcus pneumoniae* are also able to survive within host cells (Ercoli et al., 2018; Lehar et al., 2015). In these intracellular environments, genes that are otherwise dispensable for growth in nutrient-rich media often become essential, constituting a novel antimicrobial target space that is currently underexplored (Brown and Wright, 2016). Genes conditionally essential within host cells may be overlooked in experimental systems that do not resemble the intracellular environment; indeed, recent systematic studies of the genetic requirements for growth in infection-relevant conditions revealed additional essential genes relative to those required for growth *in vitro* (Ibberson et al., 2017; Nichols et al., 2011; Turner et al., 2015). High-throughput screening platforms in conditions that closely resemble the intracellular environment have the potential to uncover novel antimicrobials that target conditionally essential genes.

Salmonella enterica serovar Typhimurium (*S. Tm*) is an intracellular pathogen and one of the leading causes of gastroenteritis worldwide (Majowicz et al.,

2010). Enteric salmonellosis is typically self-limiting in healthy individuals, although in the elderly and immunocompromised, *S. Tm* can invade into phagocytes for systemic spread through the reticuloendothelial system (Watson and Holden, 2010). *Salmonella* infections are commonly treated with fluoroquinolones, cephalosporins, or macrolides (Phoon et al., 2015), although cephalosporins do not penetrate phagocytic cells (Hand et al., 1983). Unfortunately, resistance to these antibiotic classes is increasing worldwide (Cuypers et al., 2018; Nair et al., 2016). Of further concern are extensively drug-resistant *S. Typhi* (Klemm et al., 2018) and an invasive, multidrug-resistant variant of *S. Tm* that first emerged in sub-Saharan Africa (ST313) (Ashton et al., 2017). The emergence of antibiotic resistance across clades of *Salmonella* species threatens to intensify an already significant global health burden, underscoring the importance of novel antibiotic drug discovery.

During infection of macrophages and neutrophils, *S. Tm* occupies a modified phagosome called the *Salmonella*-containing vacuole (SCV). A predominantly intracellular lifestyle affords protection from extracellular host immune defenses, including bile salts, antimicrobial peptides, and serum complement (Watson and Holden, 2010). Host cells also act as reservoirs for dissemination to systemic sites, and often provide unique metabolic environments to shelter intracellular pathogens from nutrient competition with resident bacteria (Bumann and Schothorst, 2017). Several antimicrobial mechanisms intrinsic to the intracellular environment (i.e. metal depletion, vacuolar acidification, oxidative stress) (Castanheira and García-Del Portillo, 2017) serve as environmental signals for multiple two-component regulatory systems in *S. Tm* that detect and respond to immune stresses with alterations in virulence gene expression (Calva and Oropeza, 2006).

In line with previous work suggesting discordance between *in vitro* and *in vivo* drug susceptibility (Ersoy et al., 2017), we hypothesized that *S. Tm* displays altered sensitivity to antimicrobials within macrophages. In particular, genes or processes that become essential within the intracellular environment may represent new drug targets or even sensitize *S. Tm* to existing or novel antibiotics. We therefore screened an *S. Tm* ordered gene deletion collection (Santiviago et al., 2009) for growth impairment in media with ion availability and pH resembling the intracellular vacuolar environment. These data and subsequent experiments with bacteria internalized in macrophages reveal that *S. Tm* is sensitized to the intracellular environment following genetic perturbation of metabolic and cell envelope biogenesis pathways. A high-throughput compound screen against intracellular *S. Tm* in macrophages identifies several small molecules with conditional efficacy only in acidic, ion-limited media, or macrophages, and not in nutrient-rich media. Interestingly, we also observe potentiation of canonically Gram-positive targeting antibiotics in the intracellular environment, which we ascribe to a loss of normal outer membrane structure in macrophage-internalized *S. Tm*. Here, we report the identification of an intracellular-selective antimicrobial, metergoline, which disrupts the bacterial cytoplasmic membrane and prolongs animal survival in a murine model of systemic *S. Tm* infection.

Results

Screen for *S. Tm* genes required for intracellular growth

In the systemic phase of infection, different populations of *S. Tm* encounter varying degrees of nutrient limitation and immune stressors, whether internalized within macrophages and neutrophils, persisting extracellularly in the bloodstream, or invading intestinal epithelial cells. We sought to identify growth-inhibitory small

molecules that are specific for intra-macrophage *S. Tm*, as macrophages are one of the primary host cell types manipulated by *Salmonella* for replication and systemic dissemination. We reasoned that to be selective for intracellular bacteria, a compound should interfere with one or more biological processes that are required only for growth in this environment, so we aimed to survey the genetic requirements for intracellular *S. Tm* growth. While others have identified *Salmonella* genes that become required (i.e. conditionally essential) for growth in conditions mimicking those *in vivo* (Coombes et al., 2004; Fowler and Galán, 2018; Khatiwara et al., 2012; Lawley et al., 2006; Sabbagh et al., 2012; Wrande et al., 2016); to our knowledge, there has been no systematic, genome-scale survey of the impact of gene deletion on *S. Tm* survival in cultured macrophages.

The *S. Tm* str. 14028S genome contains ~4200 non-essential genes, ~3700 of which have been deleted in the ordered *Salmonella* single-gene deletion (SGD) collections (Porwollik et al., 2014; Santiviago et al., 2009). Traditional macrophage infection assays are not practical for high-throughput screening with this large a number of individual strains, so we first aimed to identify SGD mutants with impaired growth in acidic, low-phosphate, low-magnesium media (LPM) that was established to resemble conditions in the SCV (Coombes et al., 2004). Importantly, gene expression in *S. Tm* grown in LPM and other types of acidic, ion-limited media has been shown to resemble that within macrophages (Coombes et al., 2004; Kröger et al., 2013; Srikumar et al., 2015). We first measured the growth of 3725 SGD mutants in LPM, as a preliminary assessment of intracellular gene essentiality (Figure 2.1a). This screen identified 125 genes important for growth in LPM, most of which are involved in nutrient biosynthesis and metabolism, as well as biological processes related to cell envelope homeostasis. Among others, this included amino acid (e.g. *aroE*, *hisA*, *argH*, *argG*, *serB*) and nucleotide (e.g. *pyrF*, *pyrE*, *purG*, *purE*, *purF*) biosynthesis, as well as LPS modifications and maintenance (e.g. *rfc*, *pgm*, *rfaK*, *rfaH*, *rbK*, *rfaI*).

We sought to verify the intracellular sensitivity of this LPM-sensitive subset of SGD mutants directly within cultured phagocytes by monitoring replication of these 125 strains over 7 h of growth in RAW264.7 macrophages. For reference, we included several mutants with known intracellular replication defects. Surprisingly, we observed intracellular growth defects for only 62 LPM-sensitive mutants, while the remaining 63 genes were dispensable for intramacrophage growth (Figure 2.1b). From this, we inferred that macrophages may be more permissive for bacterial growth relative to LPM. However, we note that our preliminary LPM screen expanded the target space for intracellular-selective antimicrobials beyond growth in conventional media (Figure 2.1c).

Identification of chemical inhibitors of intracellular *S. Tm*

To identify putative antimicrobials effective against intracellular *S. Tm*, we conducted two parallel chemical screens with an annotated compound collection composed largely of previously-approved drugs (Supplementary Table 2.1). We screened *S. Tm* grown in (i) LPM and (ii) RAW264.7 macrophages. The collection of 1600 chemicals used in these screens includes ~250 known antibacterial compounds with defined targets in Gram-positive and -negative bacteria. Considering the discordance observed with the growth phenotypes in LPM and macrophages, for some of the SGD strains, we elected to conduct chemical screens in both of these conditions, to maximize our potential to access novel target space (Figure 2.2a). To perform the intracellular screen, we measured luminescence from a constitutively expressed luciferase reporter in *S. Tm* to enable *in situ* estimations of intramacrophage bacterial viability. Luminescence correlated linearly with the number of viable bacteria, and the presence of this reporter construct did not affect bacterial replication within macrophages or sensitivity to our control compound, rifampicin (Supplementary

Figure 2.1). Together, these high-throughput screens identified 130 compounds with growth-inhibitory activity. Notably, 63% of compounds active in LPM were also effective at limiting growth of macrophage-internalized bacteria. However, 54% of compounds active against intracellular *S. Tm* displayed no activity against *S. Tm* grown in LPM (Figure 2.2a). The latter class of compounds might exert antibacterial activity through targeting of macrophage-encoded proteins or a bacterial target that is not required for growth in LPM.

We next analyzed the potency of all 130 actives from our primary screens. Conditions included *S. Tm* grown in LPM, RAW264.7 macrophages, as well as standard nutrient-rich (cation-adjusted Mueller-Hinton Broth, MHB) and nutrient-poor (MOPS glucose minimal media) microbiological media. We also measured lactate dehydrogenase (LDH) release from uninfected macrophages as a measure of toxicity and did not pursue compounds with toxicity >25% (percentage relative to maximum LDH release, see Materials and Methods) (Figure 2.2b). Using an arbitrary cutoff for minimum inhibitory concentration (MIC) of 6.25 μ M, we eliminated compounds with activity in MHB, as these were least likely to be intramacrophage-selective *in vivo*. We found that nucleoside analogs (e.g. doxifluridine, fluorouracil, azacitidine, carmofur) were effective against intracellular *S. Tm* and bacteria grown in LPM or MOPS minimal media, but not MHB. As genes involved in nucleotide biosynthesis were required for intracellular growth (Figure 2.1, e.g. *pyrC*, *pyrE*, *pyrF*, *purE*, *purF*, *purG*), these data suggest that our genetic and chemical screens accurately probed the intramacrophage environment encountered by *S. Tm*. Further, when considering all compounds with an MIC \leq 3 μ M against intracellular *S. Tm*, 64% of these compounds were similarly potent in LPM compared to only 50% in MHB or MOPS. We prioritized 15 of the 31 compounds that were exclusively active in LPM/macrophages and not MHB/MOPS, based on low host cell cytotoxicity, potency, chemical diversity and commercial availability.

We tested the 15 priority actives for the ability to reduce intracellular replication (measured by CFU enumeration) of *S. Tm* in primary bone marrow-derived macrophages isolated from C57BL/6 mice (Figure 2.2c). Ciprofloxacin is an antibiotic routinely used in salmonellosis infection treatment and was therefore included as a positive control. Of the 15 compounds tested, 11 significantly reduced bacterial replication within 4 hours at a concentration of $128 \mu\text{g mL}^{-1}$ ($P < 0.05$, two-way ANOVA, Bonferroni multiple test correction). Excluding those with previously characterized antibacterial activity, 4 compounds reduced bacterial viability >2-fold at a concentration of $64 \mu\text{g mL}^{-1}$ or less: bromperidol, metergoline, ciclopirox, and ethopropazine. The four remaining compounds had moderately increased activity in LPM relative to MHB (Figure 2.2d), suggesting selectivity of these antimicrobials for an *in vivo*-mimicking environment. Metergoline was the most potent of these compounds and was the focus of subsequent studies of mechanism and *in vivo* efficacy.

The outer membrane antagonizes metergoline activity

The MIC of metergoline in primary macrophages is significantly lower ($\sim 8 \mu\text{g mL}^{-1}$) than in LPM ($128 \mu\text{g mL}^{-1}$) or MHB ($>256 \mu\text{g mL}^{-1}$). These discrepancies led us to hypothesize that one or more aspects of the SCV induce metergoline hypersensitivity in *S. Tm*. To identify potential contributors to this conditional susceptibility, we sought to identify conditions that would increase metergoline activity in standard growth media (MHB). We therefore conducted a chemical-genetic screen of the SGD collection in the presence of a sub-lethal concentration of metergoline in MHB ($100 \mu\text{g mL}^{-1}$) and compared the growth of each mutant to an untreated control (Figure 2.3a). In this experiment, gene deletions that resulted in metergoline hypersensitivity could provide insight to

bacterial processes that confer metergoline resistance in nutrient-rich growth media (MHB).

Our chemical-genetic data revealed that genes involved in assembly of LPS (*rfaG*, *rfaQ*), outer membrane (OM) integrity (*asmA*, *tolQ*, *tolR*, *yfgL*), synthesis and turnover of cell wall (*ldcA*, *prc*, *nlpI*), or RND efflux pumps (*tolC*, *acrB*) are required for normal growth in the presence of metergoline. Indeed, we confirmed that deletions of *tolC*, *tolR*, and *rfaQ* in *S. Tm* all resulted in hypersensitivity to metergoline in the intracellular environment (Figure 2.3b). From these data we inferred that (i) disruption of cell envelope integrity increases metergoline potency, (ii) metergoline is a likely substrate of the AcrAB-TolC efflux pump, and (iii) increased OM permeability and/or decreased efflux-pump activity might occur in LPM/macrophages to permit metergoline activity.

We noted in our chemical screens that several antibiotics with poor activity against Gram-negative bacteria (e.g. telithromycin, erythromycin, piperacillin, meropenem, rifampin, rifaximin, mupirocin, novobiocin) inhibited growth of *S. Tm* in LPM and/or macrophages. The activity of these antibiotics against Gram-negative bacteria is enhanced by OM permeabilization (Brennan-Krohn et al., 2018; Krishnamoorthy et al., 2017). Considering the hypersensitivity of OM mutants to metergoline, we reasoned that OM-perturbing agents would synergize with metergoline. In line with this, we observed synergy between metergoline and several OM-perturbing agents, including EDTA, polymyxin B, and polymyxin B nonapeptide (Figure 2.3c). We also speculated that metergoline potency in macrophages could be driven by the presence of bicarbonate as a buffer in tissue culture media, as we and others have previously reported bicarbonate-mediated potentiation of multiple antibiotic classes (Ersoy et al., 2017; Farha et al., 2017). Although physiological concentrations of bicarbonate (25 mM) alone had no

effect on metergoline's activity against *S. Tm* grown in MHB, it did enhance its antibacterial activity when combined with polymyxin B (Figure 2.3c).

Our chemical-genetic screen data also suggested a potential role for efflux in conferring metergoline resistance in MHB. Indeed, we observed a ≥ 8 -fold increase in potency of metergoline against a $\Delta toI/C$ strain of *S. Tm* grown in MHB, and polymyxin B potentiated metergoline against an efflux-deficient strain of *S. Tm* (Figure 2.3d). However, others have shown that TolC is required, and therefore active, for intracellular growth of *S. Tm* (Reens et al., 2018; Webber et al., 2009). We therefore reasoned that OM permeability, and not reduced efflux, contributes to metergoline activity in macrophages.

Growth of *S. Tm* in LPM results in a ≥ 4 -fold increase in sensitivity to metergoline compared to growth in MHB. In this media, *S. Tm* is resistant to polymyxin B; accordingly, it did not synergize with metergoline (Supplementary Figure 2.2a). However, a $\Delta phoP$ strain of *S. Tm* was sensitized to polymyxin B, and in this strain we observed strong synergy between polymyxin B and metergoline in both LPM and MHB (Supplementary Figure 2.2a, Supplementary Figure 2.2b).

We next sought to determine the component(s) of LPM that contribute to increased OM permeability. In addition to lower pH, LPM has decreased Mg^{2+} and PO_4^{3-} concentrations relative to MHB, reflective of the environment in the SCV. Since WT *S. Tm* was sensitized to metergoline, rifampicin, and mupirocin when grown in LPM, we measured the MIC of these compounds against bacteria grown in ion-supplemented (10 mM $MgCl_2$ or PO_4^{3-}) or pH-adjusted (pH 7.0) media. Additionally, we measured the activity of vancomycin in these media because similar to rifampicin and mupirocin, vancomycin has low activity against Gram-negative bacteria due to the OM permeability barrier (Krishnamoorthy et al., 2017). For all four compounds tested, addition of 10 mM $MgCl_2$ to LPM

suppressed activity by at least four-fold. The effect of increased pH or PO_4^{3-} supplementation was compound-dependent; for metergoline, only Mg^{2+} supplementation suppressed activity (Supplementary Figure 2.2c).

We observed antagonism between metergoline and Mg^{2+} in LPM, which we attribute to stabilization of the OM by Mg^{2+} and a corresponding decrease in metergoline penetration (Figure 2.3e). Accordingly, we observed >2-fold enhancement of N-phenyl-1-naphthylamine (NPN) uptake for bacterial cells grown in LPM relative to MHB, which was abrogated by supplementation with 10 mM MgCl_2 (Figure 2.3f). Measurement of NPN uptake offers a direct measurement of OM integrity, as an intact OM prevents entry of this hydrophobic fluorophore into the phospholipid bilayer where NPN exhibits the highest fluorescence (Helander and Sandholm, 2000). As expected, EDTA significantly increased NPN uptake of bacterial cells in MHB, consistent with the difference in metergoline MIC we observe between LPM and MHB supplemented with EDTA (Figure 2.3c, Figure 2.3f).

These data suggested that the antibacterial activity of metergoline was dependent on OM permeabilization and driven by Mg^{2+} limitation in LPM/macrophages, leading us to hypothesize that the OM of *S. Tm* is perturbed in the intracellular environment. We and others have shown that OM weakening by metal depletion or cationic molecules results in increased surface roughness and the appearance of pits in the OM (Amro et al., 2000; Oh et al., 2017; Stokes et al., 2017). To study these features of OM disruption in intracellular *S. Tm*, we used atomic force microscopy (AFM) to measure surface roughness of intracellular bacteria and compared this to bacteria grown in MHB or LPM. Cells grown in MHB had a largely uniform cell surface with a maximum peak to pit roughness of 9.37 nm. Remarkably, we observed deep pits on the surface of cells grown in LPM with a maximum roughness score of 22.6 nm (Figure 2.4a,

Figure 2.4b). We observed an almost 50% increase in surface roughness (13.7 nm vs 9.52 nm) for *S. Tm* directly isolated from primary bone marrow-derived macrophages (see Materials and Methods) relative to cells grown in MHB (Figure 2.4c). Given that OM integrity was protective against metergoline, we reasoned that metergoline might be readily active against Gram-positive bacteria, which do not possess an OM barrier. Indeed, metergoline was ≥ 16 -fold more potent against methicillin-resistant *Staphylococcus aureus* (MRSA) than *S. Tm* in MHB (MIC = 32 $\mu\text{g mL}^{-1}$, Supplementary Figure 2.3a), but roughly equipotent against both bacteria in primary macrophages (Figure 2.2c and Supplementary Figure 2.3b). Again, these observations are consistent with increased permeability of the Gram-negative OM in the intracellular environment.

Metergoline perturbs the bacterial cytoplasmic membrane

Sensitivity to metergoline could be induced *in vitro* through genetic disruption of efflux. We elected to use a ΔtolC strain of *S. Tm* to gain insight into metergoline's mechanism of action. To identify a possible protein target for metergoline, we sought to isolate spontaneously resistant mutants by plating at 4x MIC on MHB or LPM agar, but these attempts were unsuccessful. Moreover, we did not detect a significant increase in MIC during a 10-day serial passage experiment with MRSA or ΔtolC *S. Tm* (Supplementary Figure 2.4a). We were, however, able to observe rapid bacteriolytic activity of metergoline against ΔtolC *S. Tm* (Figure 2.5a). This led us to speculate that metergoline conditionally targets the bacterial cytoplasmic membrane in outer membrane-disrupted cells, in line with previous observations of antibiotic-induced bacterial lysis attributed to imbalanced proton homeostasis across this membrane (Bartek et al., 2016; Lobritz et al., 2015). This hypothesis would be consistent with the cryptic antifungal activity of metergoline that is related, in part, due to depolarization of mitochondrial membrane potential (Kang et al., 2011).

In Gram-negative bacteria, the inner cytoplasmic membrane regulates the proton motive force (PMF) to generate energy that is necessary for ATP synthesis by the F_1 - F_0 ATPase (Mitchell, 2011). The PMF is composed of electrical potential ($\Delta\psi$) and a transmembrane proton gradient (ΔpH), and perturbations to either component result in precise compensatory increases to the other (Bakker and Mangerich, 1981). This process may be targeted by membrane potential-uncoupling antibiotics, wherein the dissipation of either $\Delta\psi$ or ΔpH results in a collapse of the PMF (Farha et al., 2017; Farha et al., 2013; Feng et al., 2015). Remarkably, we found that metergoline caused a rapid release of 3,3'-dipropylthiadicarbocyanine iodide ($\text{DiSC}_3(5)$) (Figure 2.5b), a fluorescent probe that accumulates in the cytoplasmic membrane in a $\Delta\psi$ -dependent manner (Wu et al., 1999). Metergoline caused a similar $\text{DiSC}_3(5)$ response to the ionophore valinomycin, a known dissipator of $\Delta\psi$ (Supplementary Figure 2.4b). In contrast, the ΔpH dissipator carbonyl cyanide m-chlorophenyl hydrazone (CCCP) decreases fluorescence of $\text{DiSC}_3(5)$, due to a compensatory increase in $\Delta\psi$ (Supplementary Figure 2.4c). These data suggest that metergoline treatment rapidly decreases electrical potential at the cytoplasmic membrane. In line with this, metergoline synergized with CCCP against WT *S. Tm* grown in MHB supplemented with EDTA, or LPM (Figure 2.5c), consistent with previous observations of antibacterial synergy between dissipators of ΔpH and $\Delta\psi$ (Farha et al., 2013).

Disruption of the cytoplasmic membrane potential by metergoline would be expected to perturb cellular ATP levels. Indeed, we found that cellular ATP levels were reduced ~10-fold after a 30 min exposure to $128 \mu\text{g mL}^{-1}$ metergoline (Figure 2.5d). By comparison, CCCP at a concentration of $32 \mu\text{g mL}^{-1}$ led to a <2-fold change in ATP levels in this short experiment (Supplementary Figure 2.4d). Lastly, we observed a similar effect of metergoline on $\text{DiSC}_3(5)$ release in MRSA

(Supplementary Figure 2.3c), as well as synergy between CCCP and metergoline (Supplementary Figure 2.3d).

***In vivo* efficacy of metergoline in a murine infection model**

Given its selective potency *in vitro*, we tested the efficacy of metergoline in a systemic murine infection model with *S. Tm*. Genetically susceptible mice (*Nramp*-deficient C57BL/6) intraperitoneally infected with *S. Tm* typically succumb within ~72 hours. This route of infection recapitulates severe salmonellosis and bacteraemia is detectable as early as 1 hour post-injection (Xu and Hsu, 1992). Metergoline is a naturally occurring alkaloid compound derived from ergot fungus, and, to our knowledge, its *in vivo* efficacy has been explored solely in experiments to characterize its anxiolytic effects in mice as a serotonin antagonist (Commissaris and Rech, 1982; Hooker et al., 2010; Sastry and Phillis, 1977). We first administered metergoline at multiple doses to uninfected animals to test for potential adverse effects. We observed weight loss and increased agitation of otherwise healthy mice following administration of metergoline twice daily at 10 mg kg⁻¹, but more mild effects at 5 mg kg⁻¹ (average 6.5% weight loss over ~3 days). We therefore selected 5 mg kg⁻¹ as our therapeutic dose for metergoline.

We determined the efficacy of metergoline as a potential therapeutic by testing its ability to reduce bacterial load and prolong survival when administered either at the time of infection (Figure 2.6a, Figure 2.6b) or 12 hours after infection (Supplementary Figure 2.5e, Supplementary Figure 2.5f). Metergoline treatments were administered at 5 mg kg⁻¹, twice daily, until experimental endpoint was reached for both vehicle-treated and metergoline-treated groups. When administered at the time of infection, metergoline significantly reduced bacterial load in all organs harvested (Figure 2.6a) and significantly extended animal

survival time (Figure 2.6b). We also observed a statistically significant reduction in bacterial counts in the colon of *S. Tm*-infected mice when administered metergoline starting at 12 hours after infection, and a reduction in counts in the spleen, liver and cecum, although not statistically significant (Supplementary Figure 2.5a). Under this treatment regimen, metergoline also significantly prolonged animal survival (Supplementary Figure 2.5b).

Antibacterial activity of metergoline analogues

Given the potential to extend animal survival time following frequent administration of metergoline despite mildly adverse effects, we aimed to identify a chemical analog with increased potency against *S. Tm* and/or decreased toxicity against eukaryotic cells. We therefore pursued an in-depth structure-activity-relationship analysis to explore the chemical properties of the metergoline scaffold required for activity. We tested seventeen structurally related analogs for the ability to reduce growth of wildtype and $\Delta to/C$ *S. Tm* in MHB, LPM, and macrophages, as well as MRSA grown in MHB (Supplementary Figures 2.6-2.20, Supplementary Table 2.2). Four of the analogs we evaluated are FDA-approved therapeutics that contain the core ergot alkaloid scaffold but diverge structurally from metergoline in multiple regions. These compounds: nicergoline, pergolide, cabergoline, and methysergide, are neuroactive drugs that interact with dopamine and/or serotonin receptors, similar to metergoline. Of these, nicergoline showed modest antimicrobial efficacy while the remaining three drugs were inactive in our assays. Thirteen additional analogs were synthesized from metergoline by systematic replacement of the benzyl carbamate moiety with other groups (Supplementary Figure 2.6, compounds S1-S11, MLBC-01 and MLBC-02).

Given the mildly acidic pH of LPM and SCV, we considered the possibility that metergoline may be acting as a pro-drug by means of hydrolysis of the acid-labile carbamate moiety to release its corresponding amine (Supplementary Figure 2.6). Evaluation of compound S1, however, showed no *in vitro* efficacy at 128 $\mu\text{g mL}^{-1}$ in all but one assay (MHB supplemented with EDTA) and inferior intra-macrophage growth inhibition relative to metergoline. The remaining synthetic analogs consisted of two alkyl carbamates, seven amide derivatives, a benzyl urea derivative, a sulfonamide, and an amine (Supplementary Figure 2.6). Most of these analogs were inactive in our assays but the α,β -unsaturated amides MLBC-01 and MLBC-02 demonstrated antimicrobial activity superior to metergoline (Table 2.1). *In vitro*, MLBC-01 was 2-4 times as potent as metergoline while the -chlorophenyl derivative MLBC-02 was up to 64-fold more potent (against MRSA). Both compounds also inhibited intra-macrophage growth of *S. Tm* with similar potency to metergoline. However, compounds MLBC-01 and MLBC-02 were more toxic to macrophages (18.1% and 8.9% toxicity respectively) relative to metergoline (2.9% toxicity) as determined by lactate dehydrogenase release (Table 2.1). We are encouraged by the improved activity of these analogues against bacteria and further structural optimization of this novel scaffold is presently underway.

Discussion

Intracellular pathogens often occupy niches that are difficult to recapitulate *in vitro*; thus, we and others have developed fluorescence, luminescence, and colorimetric-based screening assays with readouts that approximate bacterial viability when compared to traditional cfu counting methods (Chiu et al., 2009; Czyz et al., 2014; Lo et al., 2014; Reens et al., 2018; Stanley et al., 2014). Here we describe a macrophage-based chemical screen specific for intracellular *S. Tm*, leading to the discovery of metergoline as an antibacterial with *in vivo*

efficacy, and the unexpected identification of outer membrane disruption in the intracellular environment. Further, we show that metergoline disrupts the proton motive force across the *S. Tm* cytoplasmic membrane, diminishes cellular ATP levels, reduces bacterial load in a murine model of systemic *S. Tm* infection, and significantly prolongs survival of infected animals. Interestingly, we found that metergoline activity *in vivo* was particularly potent in the cecum and colon, which is perhaps surprising given that the spleen and liver serve as the primary reservoirs for intraperitoneal *S. Tm* infection. Because the presence of bacteria in the intestinal tract after intraperitoneal infection is primarily due to transit from the hepatic biliary system (Monack et al., 2004b), we speculate that this phenotype merely reflects the lower bacterial burden in the liver, comprising a smaller reseeding population. Additionally, though we identify a disruption of the proton motive force and reduction in cellular ATP levels concomitant with metergoline treatment, we note that these effects may be indirect consequences of bacterial cell lysis. Indeed, future work remains to completely elucidate the mechanisms underlying metergoline activity.

Antimicrobials effective against intracellular pathogens are ideally multifaceted and with the following properties: (i) penetration of host cell membranes, (ii) penetration of bacterial membrane(s), (iii) the ability to perturb a conditionally essential bacterial target required for intracellular survival, and (iv) bacterial target specificity to limit host cell toxicity. Primary chemical screens directly against bacteria internalized within host cells are essential to identify molecules with all of these properties; however, these screens are technically challenging and poorly suited to high-throughput applications. Here, we adopted an alternative approach of screening in host-mimicking media (LPM) to perturb conditional bacterial targets (i.e. nutrient biosynthesis and cell envelope homeostasis) in the intracellular environment. Although we acknowledge that our genetic and chemical screen data suggest that LPM is an imperfect mimic of macrophages,

we were indeed able to identify intracellular-selective antimicrobials that are otherwise elusive using conventional screens in nutrient-rich growth media. Given that the intramacrophage screening platform described here is limited to approximately 1000 compounds/day, the alternative approach using unconventional growth media, such as LPM, is a preferable option for larger-scale chemical screening efforts.

We showed that Mg^{2+} depletion increased OM permeability and sensitized *S. Tm* to metergoline. OM disruption on depletion of Mg^{2+} is thought to arise because negatively charged neighbouring LPS molecules are stabilized through the binding of divalent cations (Nikaido, 2003). The low Mg^{2+} concentrations in LPM/macrophages offers a compelling explanation for the intracellular activity of metergoline. Considered with our observation of atypical cell surface characteristics of intracellular *S. Tm*, we speculate that the Gram-negative OM is disrupted in the intracellular environment. This is somewhat paradoxical given that the environmental cues in LPM/macrophages activate PhoPQ and PmrAB-regulated lipid A modifications (caused by, e.g., low pH, low Mg^{2+}/Ca^{2+} and antimicrobial peptides) (Needham and Trent, 2013), most of which are thought to confer resistance to cation depletion and antimicrobial peptide stress by altering OM charge. Nevertheless, the impact of these modifications on OM permeability has not been clearly tested *in vivo*, and further work is required to disentangle the relationship between lipid A modifications and resistance to antibiotics in the intracellular environment.

These findings have important implications for antibiotic drug discovery. By convention, Gram-negative bacteria are susceptible only to antibiotics capable of penetrating the OM (e.g. polymyxins and aminoglycosides) or to small hydrophilic antibiotics that can traverse the OM through porin channels (Delcour, 2009; Nikaido, 2003). Our work indicates that natural components of the innate immune

system may sensitize intracellular Gram-negative bacteria to otherwise poorly penetrating antibacterial compounds *in vivo*. Moreover, screening for compounds that are selective for bacteria within macrophages can reveal those that target conditionally essential genes, due to the unique conditions of the intracellular environment. Indeed, genes that are essential for growth under conditions that more closely resemble those during infection is a promising avenue in modern antibiotic research that has garnered increased attention in recent years (Brown and Wright, 2016). For complex *S. Tm* infections that include several bacterial subpopulations with highly varied gene expression and virulence phenotypes, the identification of novel antimicrobials with unique targets is critical. We conclude that intracellular-targeting chemical screening platforms have the potential to identify small molecules with relatively underexplored targets, a goal of paramount importance in the current antibiotic resistance era.

Methods

Ethics statement

All animal experiments were performed according to the Canadian Council on Animal Care guidelines using protocols approved by the Animal Review Ethics Board at McMaster University under Animal Use Protocol #17-03-10.

Reagents

Screening stocks (5 mM) of the Pharmakon-1600 (MicroSource) compound library were stored at -20 °C in DMSO. With the following exceptions, all chemicals were purchased from Sigma-Aldrich: Ciclopirox (Santa Cruz Biotechnology), Pergolide (Toronto Research Chemicals), Cabergoline (Toronto Research Chemicals), Methysergide (Toronto Research Chemicals). Compounds were routinely dissolved in DMSO at a concentration of 12.8 or 25.6 mg mL⁻¹ and stored at -20 °C. Synthetic analogs of metergoline are described in Supplementary Methods.

Bacterial strains and culture conditions

All experiments with *Salmonella enterica* subsp. *enterica* ser. Typhimurium (S. Tm) were performed with strain SL1344 or derivatives with the exception of the S. Tm single-gene deletion collection (Santiviago et al., 2009), which was constructed in the related S. Tm str. 14028s background. For consistency, in the experiments presented in Figures 2.1 and 2.3b, the wildtype S. Tm 14028s strain was used for comparison. For compound screening and secondary assays, S. Tm SL1344 was transformed with pGEN-*lux* (Lane et al., 2007), and SL1344 Δ *tolC* was generated by standard methods (Datsenko and Wanner, 2000).

Briefly, the chloramphenicol resistance cassette from pKD3 was amplified by PCR with primers Del ToIC F (5'-CAATTATTTTTACAAATTGATCAGCGCTAAATACTGCTTCACAACAAGGAGTAGGCTGGAGCTGC-3') and Del ToIC R (5'-AGACCTACAAGGGCACAGGTCTGATAAGCGCAGCGCCAGCGAATAACTTACATATGAATATCCTCCTTAGTTCC-3') and the resulting amplicon was transformed into electro-competent *S. Tm* SL1344 cells harboring the pSim6 plasmid as previously described (Côté et al., 2016; Datta et al., 2006). Successful recombinants were confirmed by colony PCR using primers Chk ToIC F (5'CGACCATCTCCAGCAGCCAC-3') and Chk ToIC R (5'GAAAAGGCGAGAATGCGGCG-3'). Experiments with *Staphylococcus aureus* used a Canadian isolate (CMRSA10) of community-acquired methicillin-resistant *S. aureus* USA300 (Christianson et al., 2007).

Overnight cultures of bacteria were inoculated with a single colony and routinely grown in LB media (10 g L⁻¹ NaCl, 10 g L⁻¹ Tryptone, 5 g L⁻¹ yeast extract) supplemented with antibiotics as appropriate (streptomycin, 150 µg mL⁻¹; chloramphenicol, 25 µg mL⁻¹; kanamycin, 50 µg mL⁻¹, ampicillin, 100 µg mL⁻¹). Where indicated, bacteria were subcultured 1:100 and grown to mid-log phase in cation-adjusted MHB (BBL™ Mueller Hinton II Broth – Cation Adjusted), LPM (5 mM KCl, 7.5 mM (NH₄)₂SO₄, 0.5 mM K₂SO₄, 10 mM Glucose, 49 µM MgCl₂, 337 µM PO₄³⁻, 0.05% casamino acids, 80 mM MES, pH 5.8), or MOPS glucose minimal medium (Teknova) supplemented with 40 µg mL⁻¹ histidine when growing *S. Tm* SL1344. For LPM supplementation experiments, MgCl₂ or KH₂PO₄ were added to a final concentration of 10 mM and media was pH adjusted prior to filter sterilizing. Bacteria were grown at 37°C.

Genetic Screening

The *Salmonella* single-gene deletion (SGD) library (Santiviago et al., 2009) was pinned from frozen DMSO stocks at 384-colony density onto LB agar medium containing 50 $\mu\text{g mL}^{-1}$ kanamycin using a Singer RoToR HDA (Singer Instruments) and grown for 18 h at 37°C. The SGD was then grown overnight in 384-well clear flat-bottom plates (Corning) in either MOPS glucose (Figure 2.1a) or LB (Figure 2.3a) supplemented with 50 $\mu\text{g mL}^{-1}$ kanamycin. The Singer RoToR HDA was then used to inoculate assay plates (containing 50 μL per well LPM without casamino acids, MHB, or MHB with 100 $\mu\text{g mL}^{-1}$ metergoline) with a starting inoculum of approximately 1.7×10^5 CFU per well. Optical density at 600 nm (OD_{600}) was measured with a Tecan M1000 Infinite Pro plate reader at the time of inoculation (T_0) and after 16 hrs (T_{16}) incubation at 37°C with shaking at 220 rpm. Growth was calculated by subtracting the pre-reads ($T_{16} - T_0$) and interquartile-mean normalization for plate and well effects (Mangat et al., 2014). The interaction score was calculated by dividing normalized growth in the presence of metergoline by the MHB control. Experiments were performed in duplicate or triplicate as noted.

Replication of SGD mutants in macrophages

Strains from the *Salmonella* single-gene deletion library were selected based on prioritization from genetic screening in LPM (growth $< 3.5\sigma$ from mean of screening data), along with SPI-1, SPI-2, virulence, motility, and regulatory genes, and WT to use as controls. Strains of interest were grown overnight in 96-well clear flat-bottom plates (Corning) in LB in duplicate.

RAW264.7 macrophages were seeded into 96-well plates in DMEM + 10% FBS at $\sim 10^5$ cells per well and left to adhere for 20-24 hours, incubated at 37°C with 5% CO_2 . Overnight cultures of bacteria were diluted to obtain an MOI of $\sim 50:1$, then opsonized for 30 min in 20% human serum in PBS at 37°C. Bacteria were

added to each well, and plates were spun down at 500 x g for 2 min, then incubated for 30 min at 37°C with 5% CO₂. Media was aspirated and replaced with fresh DMEM containing 100 µg mL⁻¹ gentamicin to kill extracellular bacteria for 30 min at 37°C with 5% CO₂. For half the plates, RAW264.7 cells were washed once with PBS, then scraped from the wells and lysed in PBS containing 1% (v/v) Triton-X100, 0.1% (w/v) SDS. Bacterial colony-forming units (CFU) from each well were enumerated by serially diluting in PBS and plating on LB plates (T₀ counts). For the other half of the plates, RAW264.7 cells were washed once with PBS, then fresh DMEM was added and cells were incubated at 37°C with 5% CO₂. After 7 h, RAW264.7 cells were washed once with PBS, then scraped from the wells and lysed in PBS containing 1% (v/v) Triton-X100, 0.1% (w/v) SDS. Bacterial CFU from each well were enumerated by serially diluting in PBS and plating on LB plates (T₇ counts). CFU were averaged (two technical replicates per assay plate) and a CFU ratio (CFU at T₇ divided by T₀) was calculated to represent fold replication over the course of the experiment.

High-throughput compound screening

For chemical screening in LPM, an overnight culture of *S. Tm* SL1344 was subcultured 1:100 in LB, grown to an OD₆₀₀ of 0.5, then diluted 40-fold into LPM and grown to an OD₆₀₀ of 0.3 before a final 1:150 dilution into LPM. Bacterial culture (50 µL) was dispensed into 96-well black, clear flat-bottom (Corning) plates and then 50 µL of each compound (diluted to 20 µM in LPM) was added for a final concentration of 10 µM compound and ~2x10⁴ CFU per well. The OD₆₀₀ was read immediately after compound addition (T₀) and then 16 hrs later (T₁₆). Plate and well effects were normalized by interquartile-mean based methods (Mangat et al., 2014) and compounds reducing growth more than 3σ below the mean were considered primary screen actives. Screening was performed in triplicate.

For the screen against intramacrophage *S. Tm*, RAW264.7 macrophages were seeded 16 hrs prior to infection at $\sim 2 \times 10^5$ cells per well in 96-well black, clear flat-bottom plates (Corning) in DMEM + 10% FBS and were incubated at 37°C with 5% CO₂. *S. Tm* str. SL1344 transformed with pGEN-*lux* was grown overnight in LB with 100 µg mL⁻¹ ampicillin, diluted to obtain a multiplicity of infection (MOI) of 100:1, then opsonized for 30 min in 20% human serum (Innovative Research) in PBS at 37°C. An equal volume of bacteria (100 µL) was added to macrophages and plates were centrifuged at 500 x *g* for 2 min followed by a 30 min incubation at 37°C with 5% CO₂. Media was then aspirated and replaced with fresh DMEM containing 100 µg mL⁻¹ gentamicin to eliminate extracellular bacteria, and plates were incubated for 30 mins at 37°C with 5% CO₂. Infected cells were washed with PBS prior to addition of 100 µL of DMEM containing compound at 10 µM. Luminescence was read immediately after compound addition (T₀) and plates were then incubated for 3 hr at 37°C with 5% CO₂. Luminescence was measured a second time after media was replaced with fresh DMEM + 10% FBS (T₃) and plates were incubated for a further 3hr before luminescence was measured a final time (T_{Final}).

Secondary screening of compounds in macrophages

130 priority compounds were selected based on prioritization from chemical screening in LPM and macrophages. Infection assays in RAW264.7 macrophages were performed as described above, with the following modifications: macrophages were seeded at 10⁵ cells per well, macrophages were pretreated with 100 ng mL⁻¹ LPS from *Salmonella enterica* serovar Minnesota R595 (Millipore), and an MOI of 50:1 was used. Compounds were serially diluted two-fold starting at 5 mM to achieve a final concentration of 50 µM with 1% DMSO in DMEM. Luminescence was read immediately after compound

addition (T_0), and plates were incubated for 20 h at 37°C with 5% CO₂ before luminescence was read again (T_{20}). Luminescence readings were averaged (two technical replicates per assay plate) and a luminescence ratio (luminescence at T_{20} divided by T_0) was calculated to represent fold replication over the course of the experiment. Minimal inhibitory concentrations (MICs) were estimated based on ability to reduce luminescence by at least 10-fold.

Cytotoxicity assays

RAW264.7 macrophages were seeded into 96-well plates in DMEM + 10% FBS and 100 ng mL⁻¹ LPS from *Salmonella enterica* serovar Minnesota R595 (Millipore) and left to adhere for 20-24 h, incubated at 37°C with 5% CO₂. Compounds were premixed into DMEM at a final concentration of 50 µM with 1% DMSO, then added to wells. After 2 hours of compound treatment, the culture supernatant was collected for analysis of lactate dehydrogenase release. Cytotoxicity was quantified colorimetrically with the Pierce LDH cytotoxicity kit where LDH activity is measured by subtracting Absorbance at 490 nm from Absorbance at 680 nm. Lysis control wells were treated with 10X lysis buffer for 1 hour. Percent cytotoxicity was calculated with the formula:

$$\frac{LDH_{Compound\ Treated} - LDH_{Spontaneous}}{LDH_{Maximum} - LDH_{Spontaneous}} \times 100\%$$

where LDH_{Spontaneous} is the amount of LDH activity in the supernatant of untreated cells and LDH_{Maximum} is the amount of LDH activity in the supernatant of lysis control wells. The LDH activity in cell-free culture medium was subtracted from each value prior to normalization.

Bone marrow-derived macrophage assays

Bone marrow-derived macrophages (BMMs) were collected from the femur and tibia of 6-10 week old female C57BL/6 mice (Charles River Laboratories) and differentiated in RPMI (Gibco) + 10% FBS + 10% L-sup (L929 fibroblast conditioned medium) + 100 U penicillin-streptomycin for 7 days at 37°C and 5% CO₂. Differentiated BMMs were seeded 20-24 h prior to infection in 96-well plates at 10⁵ cells per well in RPMI + 10% FBS + 100 ng mL⁻¹ *Salmonella enterica* serovar Minnesota R595 (Millipore) and incubated at 37°C with 5% CO₂. Infection assays were performed as described for RAW264.7 macrophages, with the following modifications: bacteria were not opsonized prior to infection, and an MOI of 50:1 was used. Compounds were added to wells as described previously (see Secondary screening of compounds in macrophages).

Chequerboard analyses and compound potency analysis

A single colony of freshly streaked bacteria was used to inoculate LB with appropriate antibiotics (150 µg mL⁻¹ streptomycin for *S. Tm* str. SL1344 and derivatives, 25 µg mL⁻¹ chloramphenicol for SL1344 Δ *tolC* or Δ *phoP*). Overnight cultures were diluted 100-fold into antibiotic-free MHB or LPM, as appropriate, and grown to mid-log phase (OD₆₀₀ = 0.4-0.8). Subcultures were then diluted to an OD₆₀₀ = 0.0001 (~1x10⁵ cfu mL⁻¹) in assay media and 150 µL of this dilution was added to each well of the 96-well assay plate. For chequerboard experiments, an 8x12 matrix of two compounds was created with two-fold serial dilutions of each compound. Metergoline, CCCP, nigericin, and valinomycin were dissolved in DMSO, and polymyxin B, polymyxin B nonapeptide, and EDTA were dissolved in water. After addition of bacteria, plates were incubated at 37°C with shaking for 16 hours, at which time the OD₆₀₀ was measured. The minimum inhibitory concentrations (MIC) for various compounds were determined using 11 two-fold dilutions and growth was measured after 16 hours. The MIC was the concentration that inhibited growth >95% when compared to the solvent control.

In all experiments, DMSO was present at a final concentration <2% (routinely 1%).

NPN Uptake Assay

Uptake of the lipophilic dye N-phenyl-1-naphthylamine (NPN) was measured essentially as previously described³⁷. Briefly, overnight cultures of *S. Tm* were diluted 50-fold into LB and grown to mid-log ($OD_{600} = 0.5$), then diluted again 100-fold into variants of LPM, MHB, or MHB with 10 mM EDTA, and grown to late-exponential phase ($OD_{600} \sim 1.2$). Cells were harvested by centrifugation, washed in 5 mM HEPES, pH 7.2, then resuspended to a final $OD_{600} = 1.0$. The cell suspension (50 μ L), 40 μ M NPN (50 μ L), and 5 mM HEPES, pH 7.2 (100 μ L) were mixed in black clear flat-bottom 96-well plates immediately before measuring fluorescence (excitation, 340 nm; emission 415 nm) in a Tecan M1000 Infinite Pro plate reader. Background fluorescence of each preparation of cells was subtracted along with background fluorescence of NPN in buffer.

Atomic force microscopy (AFM)

BMMs were differentiated as described above, and then seeded 16 hours prior to infection in 6-well plates at 5×10^6 cells per well in RPMI + 10% FBS + 100 ng mL^{-1} *Salmonella enterica* serovar Minnesota R595 (Millipore) and incubated at 37°C with 5% CO₂. Bacteria were added at an MOI of 100:1 and were allowed to infect for 30 minutes, after which media was aspirated and replaced with fresh RPMI containing 100 μ g mL^{-1} gentamicin (to kill extracellular bacteria) for 30 minutes at 37°C with 5% CO₂. Media was then aspirated and replaced with fresh RPMI, and macrophages were scraped into the media.

20 μL of suspended macrophages was then transferred to a hydrophilic polycarbonate 0.2 μm Millipore Isopore GTTP filter (Merck Millipore), with a Kimwipe (Kimberly-Clark Professional) underneath to remove liquid without vacuum. Filters were attached to a glass slide with an adhesive and examined using AFM. Macrophages lysed immediately upon removal of medium, with bacterial cells remaining intact for surface scanning. For bacteria grown in LPM or MHB, cells were grown to mid-log phase ($\text{OD}_{600} \sim 0.5$), then 20 μL of the suspension was placed on the same filter as above. The liquid was removed with a Kimwipe as previously described, then 20 μL of 10 mM MES pH 5.5 was overlaid, and liquid removed. Filters were mounted on a glass slide and examined with AFM.

A Bruker BioScope Catalyst AFM, with a Nanoscope V controller, was used to scan bacterial surfaces. For each sample, a 0.65 μm thick Si_3N_4 triangular cantilever was used (Scan Asyst AIR, Bruker), with a symmetric tip and spring constant of $\sim 0.4 \text{ N m}^{-1}$. All AFM was done at 25°C (ambient room temperature), with a scan rate of 0.5 Hz and 256 samples per line resolution. Scanning was done in PeakForce quantitative nanomechanical mapping mode. All downstream image processing was done using NanoScope software (Bruker). For scans of whole cells, scans were fit to a plane to normalize the Z-Height. For scans of bacterial surface topology, images were flattened using a second order transformation to account for subtle cell curvature, and surface topography was calculated from cross sections of these image scans.

DiSC₃(5) assay

Subcultures of WT *S. Tm* or MRSA were grown to late-exponential phase ($\text{OD}_{600} \sim 1$) in MHB (MRSA) or MHB with 10 mM EDTA (*S. Tm*). Gram-negative outer membrane disruption is required for the highly lipophilic 3'-

dipropylthiadicarbocyanine iodide (DiSC₃(5)) to access the cytoplasmic membrane (Zhang et al., 2000). Cells were harvested by centrifugation, washed twice in buffer (5 mM HEPES, pH 7.2, 20 mM glucose), and then resuspended in buffer to a final OD₆₀₀=0.085 with 1 μM DiSC₃(5). For the experiment presented in Supplementary Figure 2.4b, 100 mM KCl was added to the cell suspension containing DiSC₃(5). After a 20 min incubation at 37°C, 150 μL of DiSC₃(5) loaded cells was added to two-fold dilutions of metergoline, valinomycin, or CCCP in 96-well black clear-bottom plates (Corning) and fluorescence (excitation = 620 nm, emission = 685 nm) was read 1 min later using a Tecan M1000 Infinite Pro plate reader. The fluorescence of metergoline diluted in buffer was negligible (<200 a.u.). The fluorescence intensity was stable (<5% fluctuation) for at least 15 min when the plate was shielded from light.

Measurement of intracellular ATP levels

WT *S. Tm* was grown in MHB with 1 mM EDTA to early-log phase (OD₆₀₀ = 0.2) and then grown in the presence of metergoline or CCCP for 30 minutes in clear flat-bottom 96-well plates. The OD₆₀₀ was determined immediately before ATP levels were measured using a BacTiter-Glo™ Microbial Cell Viability Assay (Promega), according to manufacturer instructions, in a white 96-well plate using an EnVision plate reader (PerkinElmer). Relative ATP levels were calculated by dividing relative light units (RLU) by the OD₆₀₀ (RLU/OD).

Animal infections

Before infection, mice were relocated at random from a housing cage to treatment or control cages. Six- to ten-week-old female C57BL/6 mice (Charles River Laboratories) were infected intraperitoneally with ~10⁵ cfu *S. Typhimurium* SL1344 in 0.1 M Hepes (pH 8.0) with 0.9% NaCl. Metergoline was administered

at 5 mg kg⁻¹ via intraperitoneal injection, solubilized in 5% DMSO in DMEM. 5% DMSO in DMEM was given to vehicle control groups of mice. Metergoline treatments were administered every 12 hours for the duration of infection, beginning at either the time of infection or 12 hours post-infection, as indicated per experiment. Clinical endpoint was determined using body condition scoring analyzing weight loss, reduced motility, and hunched posture. Experimental endpoint was defined as 60 hours post-infection for CFU comparison experiments; at this time point *S. Tm*-infected mice have undergone ~10-12% weight loss and display signs of clinical illness. At experimental endpoint, mice were euthanized, and the spleen, liver, cecum, and colon were aseptically collected into ice-cold PBS and homogenized. Bacterial load in each tissue type was enumerated from organ homogenates serially diluted in PBS and plated onto solid LB supplemented with 100 µg mL⁻¹ streptomycin.

Serial passage in the presence of metergoline

Freshly streaked colonies of MRSA or $\Delta toIC$ *S. Tm* (3 colonies for each strain) were grown overnight in MHB. Each culture was diluted 500-fold into MHB and 150 µL of each sample was added to 2-fold dilutions of metergoline in a 96-well plate. After 24 h incubation at 37°C with shaking, the well with the highest concentration of metergoline and visible growth (defined as 1/2x MIC) was diluted 500-fold into fresh MHB and the assay repeated.

Statistical analysis

Data were analyzed using RStudio version 1.0.143 with R version 3.2.2, GraphPad Prism 6.0 software (GraphPad Inc., San Diego, CA). Specific statistical tests and multiple test corrections are indicated in figure legends. P values of <0.05 were considered significant.

Acknowledgements

We are grateful to Susan McCusker for excellent technical assistance in high-throughput compound screens, and Maya Farha for useful discussions throughout this work. M.J.E was supported by a post-doctoral Fellowship from the Canadian Institutes of Health Research (CIHR); C.N.T. was supported by a Canada Graduate Scholarship from the Natural Sciences and Engineering Research Council and an Ontario Graduate Scholarship. This work was supported by operating grants from CIHR to B.K.C (388221 and 376674) and E.D.B (FRN-143215), the Canada Research Chairs program (to B.K.C. and E.D.B), the Ontario Research Fund (RE07-048 to B.K.C., and E.D.B.), and a donation from the Boris Family Fund for Health Research Excellence (to B.K.C. and E.D.B.). J.W.J. and J.M. were supported by a startup grant from the McMaster Faculty of Health Sciences Dean's Fund. M.M., S.P. and H.A.P. were supported in part by NIH grant R01AI075093, and NIAID Contract No. HHSN272200900040C.

Author Contributions

M.J.E., C.N.T., B.K.C., and E.D.B conceived and designed the research. J.W.J and J.M designed metergoline analogues. M.J.E. and C.N.T. performed all experiments and analyzed data with the following exceptions: J.W.J. synthesized and analyzed metergoline analogues, S.F. performed atomic force microscopy, W.E. assisted with tissue culture. S.P., H.A-P., and M.M. constructed and supplied the *Salmonella* deletion library. M.J.E., C.N.T., B.K.C., and E.D.B wrote the paper. All authors commented on the manuscript.

Figures

Figure 2.1

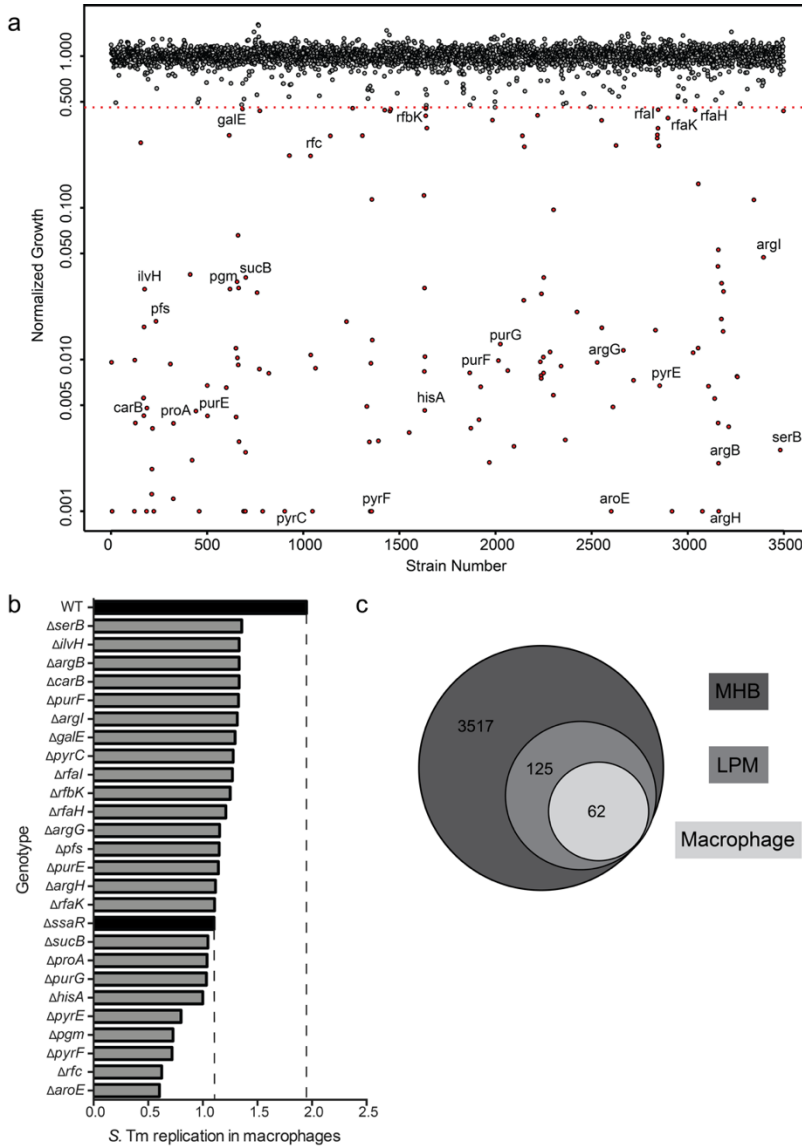


Figure 2.1. Genetic requirements for *S. Tm* growth in host-mimicking media and macrophages.

a Index plot showing normalized growth of mutant strains from the *Salmonella* single-gene deletion (SGD) collection in LPM media, sorted in order of

chromosomal position of deleted genes. Values shown per strain represent the calculated mean growth of three replicate screens, normalized to account for plate and positional effects. Points below the red dotted line represent genes with growth values less than 3.5 s.d. from the mean of the dataset. Strains that exhibited low growth and were used in follow-up experiments are labeled. **b** Replication of selected mutant strains from the SGD collection in RAW264.7 macrophages over 7 hours. Wildtype (WT) and Δ *ssaR* strains (black bars) were used as controls for high and low replication, respectively. Bar plots depict the mean fold-change in bacterial burden between 0 and 7 h of intracellular infection, measured from two technical replicates. **c** Cartoon representing the overlap between genes essential for growth in LPM or within RAW264.7 macrophages, and dispensable genes in *S. Tm* represented in the SGD.

Figure 2.2

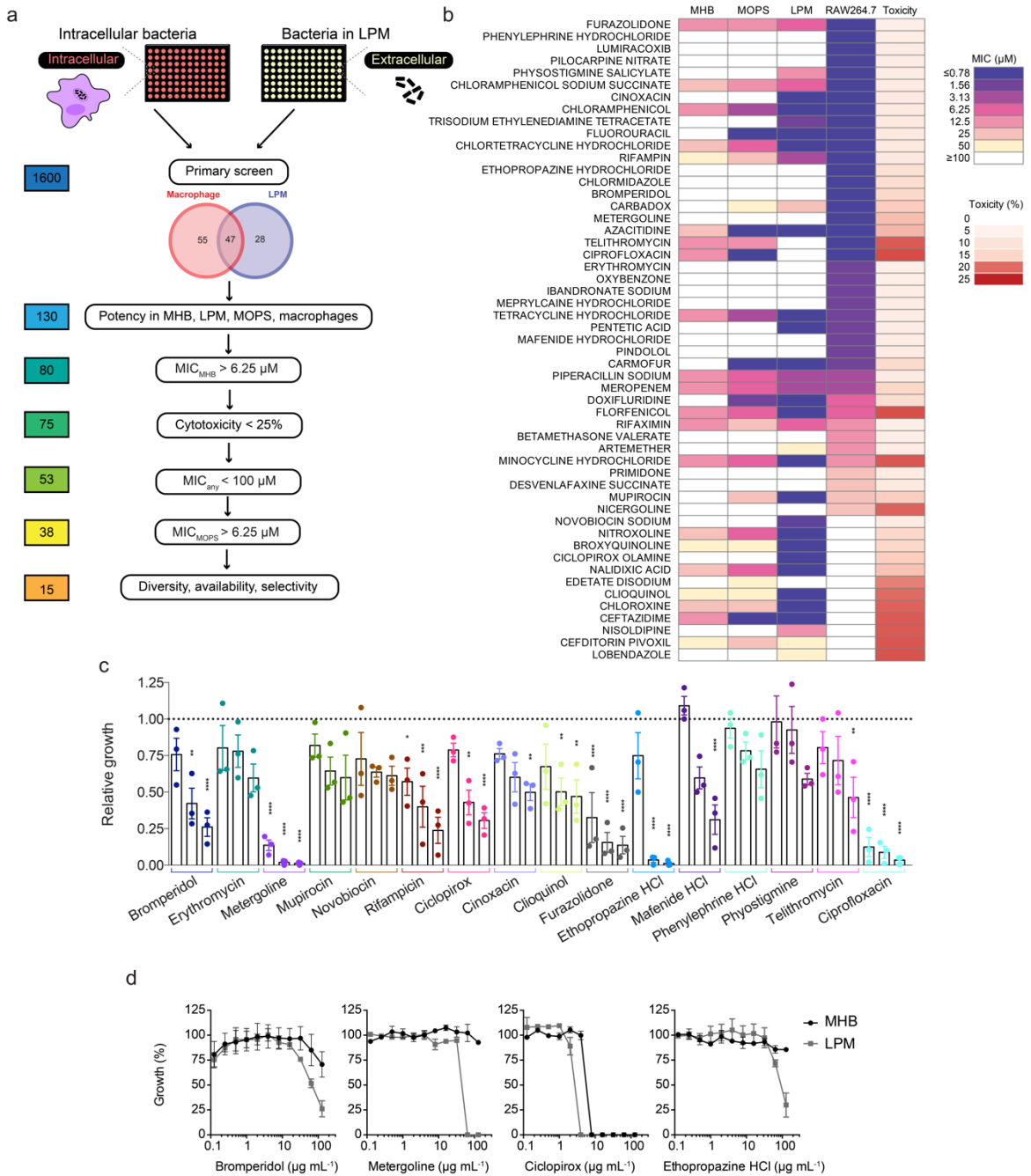


Figure 2.2. Chemical screen identifies novel compound activities against intracellular *S. Tm*.

a Screening workflow to identify compounds with intracellular antimicrobial activity against *S. Tm* grown in acidic LPM media and internalized in RAW264.7 macrophages. Secondary screening pipeline is shown below with the number of compounds remaining at each step to the left. **b** Potency and toxicity analysis of all primary screen actives represented as a heat map. Shown are the minimum inhibitory concentrations (MIC) for all compounds against *S. Tm* grown in MHB, LPM, MOPS (OD_{600}) and inside RAW264.7 macrophages (luminescence, RLU); the final column (Toxicity) reports lactate dehydrogenase release from RAW264.7 macrophages after 2 h of exposure to 50 μ M compound. All values shown reflect the mean of duplicate measurements. **c** Intracellular *S. Tm* replication measured in primary bone marrow-derived macrophages (BMMs) isolated from C57BL/6 mice. Relative growth reflects replication over 4 h, normalized to bacterial growth in BMMs treated with DMSO. Compounds were added at 8, 64, and 128 μ g mL⁻¹, as shown in increasing concentrations for each. Bar plots depict the mean of three independent biological replicates, error bars indicate s.e.m. Groups were compared via two-way ANOVA with Bonferroni correction for multiple testing. * $P < 0.05$, ** $P < 0.01$, *** $P < 0.001$, **** $P < 0.0001$. **d** Potency analysis of *S. Tm* growth inhibition for bromperidol, metergoline, ciclopirox, ethopropazine in MHB (black) and LPM (grey). Growth is normalized to a DMSO control (set to 100%), error bars indicate s.e.m. for two biological replicates.

Figure 2.3

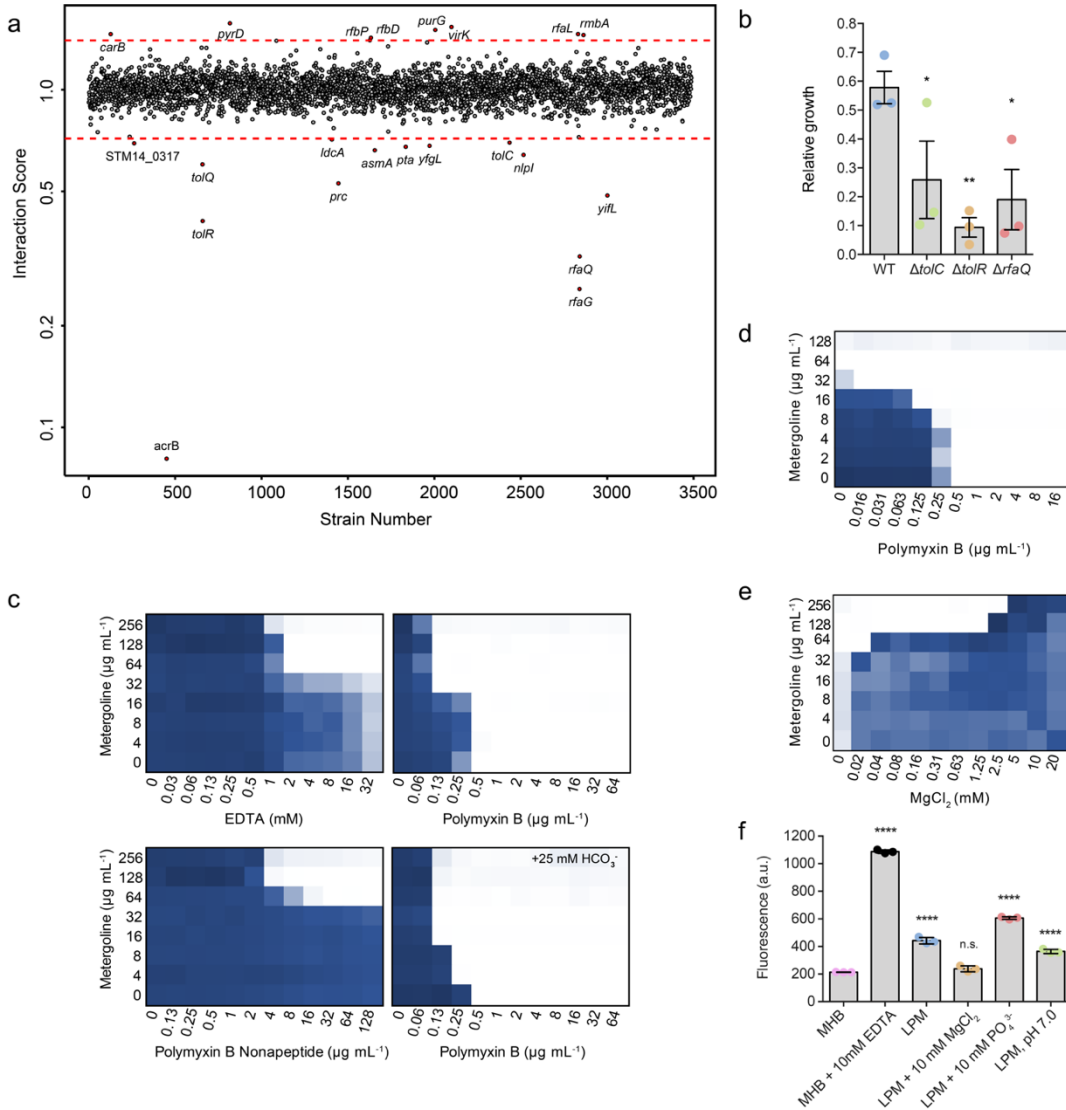


Figure 2.3. Impact of OM integrity and efflux on metergoline activity in MHB and LPM.

a Index plot showing sensitivity of SGD collection mutant strains grown in MHB with $100 \mu\text{g mL}^{-1}$ metergoline. Strains are sorted based on chromosomal position of the deleted gene. The chemical-genetic interaction score was calculated by dividing normalized growth of each mutant in the presence of metergoline divided by normalized growth in MHB. Red lines indicate 3 s.d. from the mean of the

dataset and values represent the mean of duplicate screens. The deleted genes within sensitive (below red) or resistant (above red) mutant strains are indicated. **b** Intracellular *S. Tm* (WT str. 14028S and indicated SGD mutants) replication measured in bone-marrow derived macrophages isolated from C57BL/6 mice, treated with 8 $\mu\text{g mL}^{-1}$ metergoline. Relative growth reflects replication over 4 h, normalized to bacterial growth in macrophages treated with DMSO. Bar plots depict the mean of three independent infections, error bars indicate s.e.m. SGD mutant groups were compared to WT *S. Tm* with a Kruskal-Wallis test with Dunn's multiple test correction. * $P < 0.05$, *** $P < 0.001$. **c** Chequerboard broth microdilution assay showing dose-dependent potentiation of metergoline by membrane-perturbing agents against *S. Tm* grown in MHB. Where indicated, sodium bicarbonate was added to media at a final concentration of 25 mM. **d** As in panel **c** but with a $\Delta\text{to}I\text{C}$ strain of *S. Tm*. **e** Chequerboard assay showing antagonism between Mg^{2+} and metergoline in LPM. In panels **c**, **d**, **e**, higher growth is indicated in dark blue and no detectable growth in white. Results are representative of at least two independent experiments. **f** NPN uptake assay for WT *S. Tm* grown in variants of LPM, MHB, or MHB with 10 mM EDTA. Values were normalized to account for background fluorescence prior to plotting. Bar plots depict the mean of triplicate experiments, error bars indicate s.d. All groups were compared to MHB via one-way ANOVA with Holm-Sidak's multiple test correction. **** $P < 0.0001$.

Figure 2.4

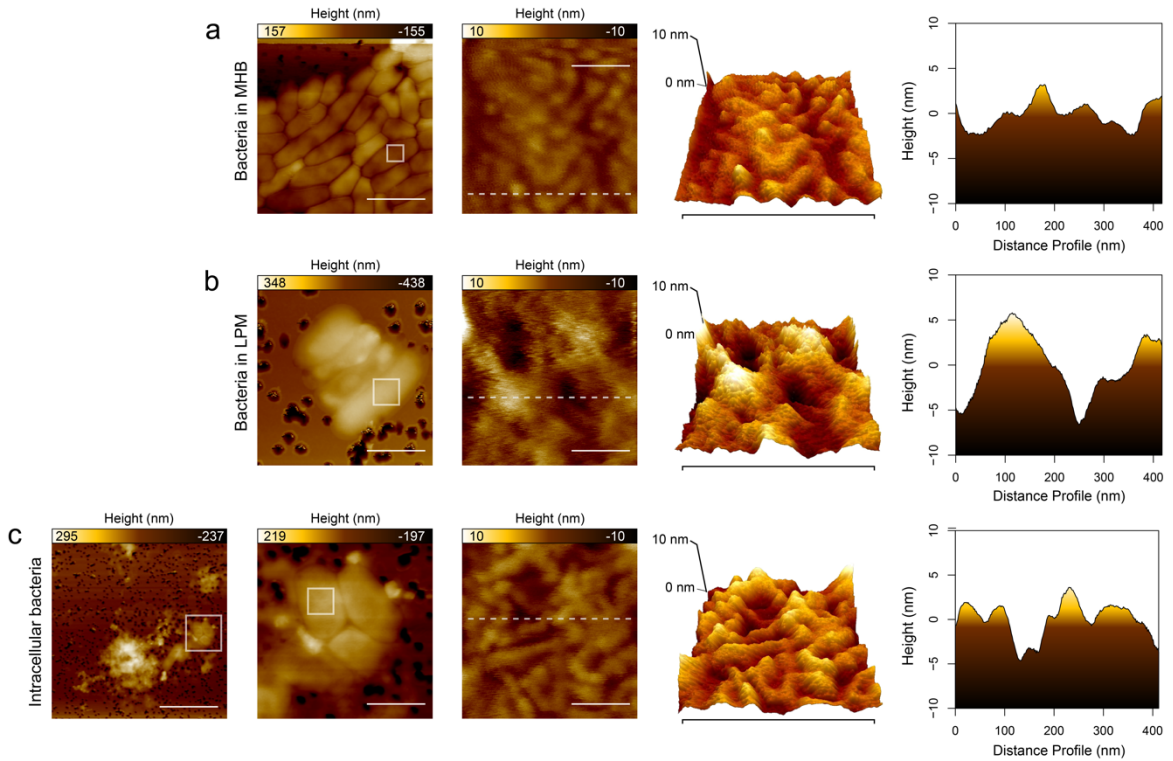


Figure 2.4. Atomic force microscopy (AFM) on *S. Tm* grown in MHB, LPM, or bone-marrow derived macrophages.

Images taken at increasing resolution as well as a 3D surface projection are shown for bacteria grown in **a** MHB, **b** LPM, or **c** immediately following lysis of infected macrophages (see Materials and Methods). Two-dimensional surface roughness projects (far right) show the surface topology of each sample. Scale bars from left to right show the following distance: **a** 2 μM , 0.1 μM , 0.4 μM ; **b** 1 μM , 0.1 μM , 0.4 μM ; **c** 4 μM , 1 μM , 0.1 μM , 0.4 μM

Figure 2.5

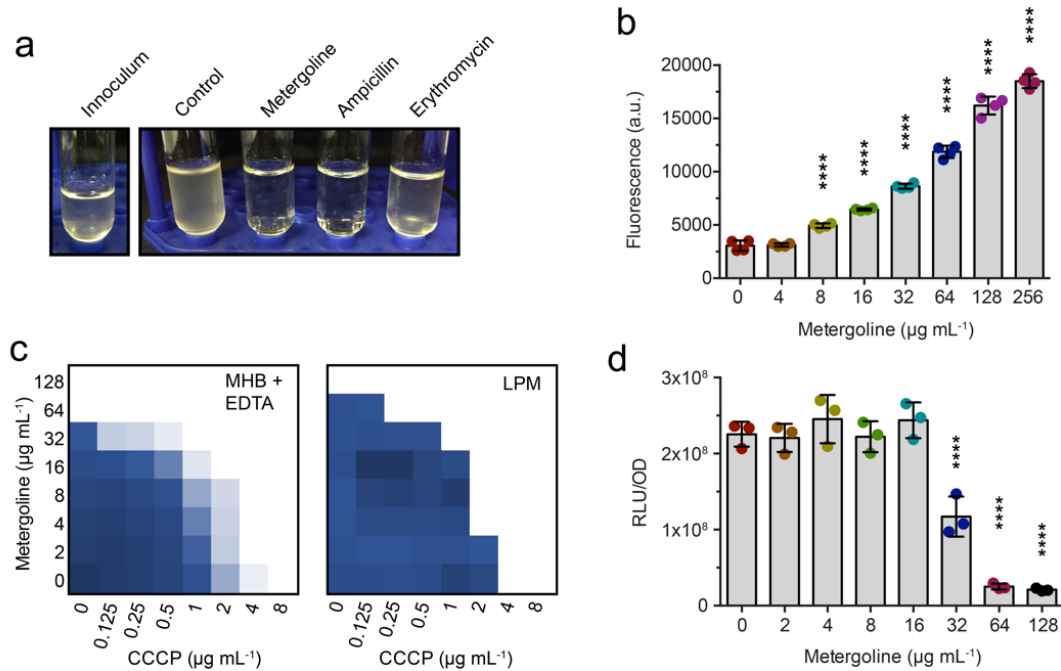


Figure 2.5. Metergoline is bacteriolytic and perturbs the *S. Tm* cytoplasmic membrane.

a Turbidity of cultures of *S. Tm* $\Delta\text{tol}/\text{C}$ in MHB after growth to mid-log phase (left, inoculum) then 2.5 h of growth at 37°C in the presence of metergoline ($200 \mu\text{g mL}^{-1}$), ampicillin ($16 \mu\text{g mL}^{-1}$), erythromycin ($16 \mu\text{g mL}^{-1}$), or a DMSO control. Note that erythromycin is bacteriostatic and culture turbidity did not change relative to the inoculum; ampicillin (bactericidal) and metergoline both cleared culture turbidity. **b** DiSC₃(5) assay on late-log phase *S. Tm* grown in MHB supplemented with 10 mM EDTA to enable DiSC₃(5) binding to the cytoplasmic membrane. Cells were loaded with DiSC₃(5) prior to a 1 min incubation with increasing concentrations of metergoline. Bar plots depict the mean of two biological replicates, error bars indicate s.d. All groups were compared against $0 \mu\text{g mL}^{-1}$ metergoline via one-way ANOVA with Holm-Sidak's multiple test correction. **** $P < 0.0001$. **c** Chequerboard broth microdilution assay showing synergy between metergoline and CCCP against *S. Tm* grown in MHB with 10

mM EDTA or LPM. **d** *S. Tm* grown in MHB with 1 mM EDTA to early-log phase, then exposed to metergoline for 30 min. Cellular ATP levels were estimated by luciferase activity (relative light units, RLU) normalized to optical density (OD₆₀₀). Bar plots depict the mean of two biological replicates, error bars indicate s.d. Groups were compared against 0 µg mL⁻¹ metergoline via one-way ANOVA with Holm-Sidak's multiple test correction. ****P<0.0001.

Figure 2.6

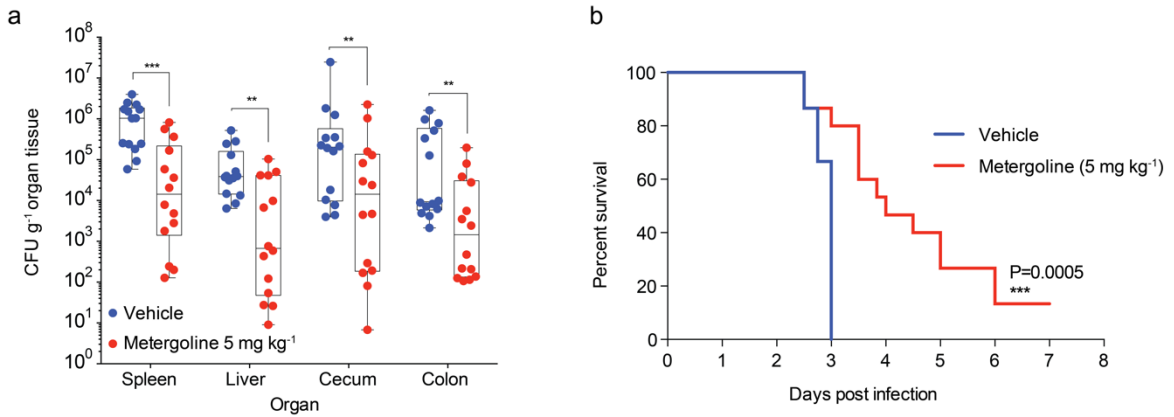


Figure 2.6. *In vivo* efficacy of metergoline in a murine model of systemic *S. Tm* infection.

C57BL/6 mice were infected intraperitoneally with $\sim 10^5$ CFU *S. Tm*. **a** Groups of mice were treated twice daily (every 12 h) with metergoline (5 mg kg^{-1} , red bars) or DMSO (5% in DMEM, blue bars) by i.p. injection. Treatments were administered beginning at the time of infection. Mice were euthanized at experimental endpoint (60 h post infection). Bacterial load in the spleen, liver, cecum, and colon was determined by selective plating on streptomycin. Data shown are the means of three separate experiments ($n=5$ per group). Box plot whiskers show the minimum to maximum values per group, lines in box plots show the median of each group. Groups were analyzed with a two-way ANOVA and corrected for multiple comparisons with a Holm-Sidak test. **b** For survival experiments, groups of mice were treated twice daily (every 12 h) beginning at the time of infection with metergoline (5 mg kg^{-1} , red) or DMSO (5% in DMEM, blue) by i.p. injection, and were euthanized at clinical endpoint. Survival curves shown are from three separate experiments ($n=5$ per group). Groups were analyzed with a Gehan-Breslow-Wilcoxon test for survival curve differences.

Tables

Table 2.1

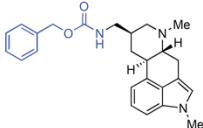
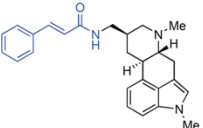
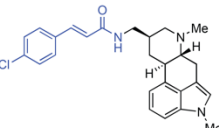
| Compound ^a | Minimum Inhibitory Concentration ($\mu\text{g mL}^{-1}$) | | | | | RAW264.7 | |
|--|--|-------------------------------|-----|-----------------------------------|-------------|---------------------|---------------------------|
| | MHB | S. Tm WT EDTA ^b | LPM | $\Delta\text{to}/\text{C}$ MHB | MRSA MHB | Growth ^c | Toxicity (%) ^d |
|  metergoline | >128 | 64 | 128 | 32 | 32 | 0.08 | 2.9 |
|  MLBC-01 | >128 | 32 | 128 | 8 | 16 | 0.07 | 18.07 |
|  MLBC-02 | >128 | 8 | 32 | 4 | 0.5 | 0.08 | 8.9 |

Table 2.1. Structure activity relationship analysis of metergoline and two synthetic analogues.

^aBlue highlights in chemical compounds depict structural differences between metergoline and MLBC-01 and MLBC-02

^bWT *S. Tm* was grown in MHB with 10 mM EDTA

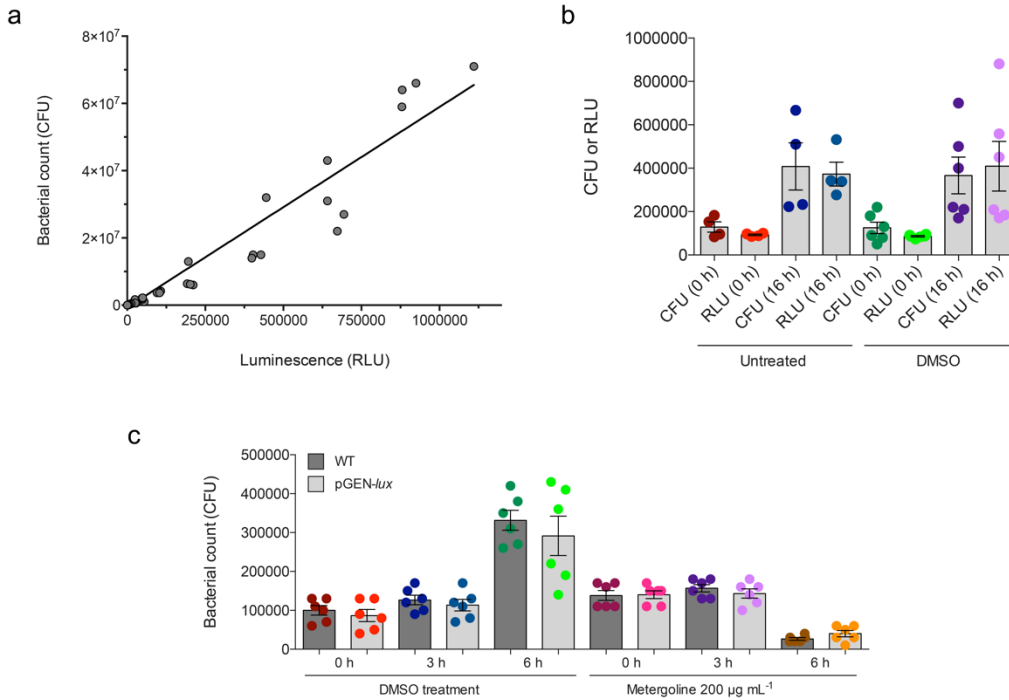
^cIntracellular activity was measured by addition of $8 \mu\text{g mL}^{-1}$ compound to RAW264.7 macrophages infected with WT *S. Tm* and is reported as fold-growth inhibition relative to a DMSO-treated control

^dToxicity was estimated by lactate dehydrogenase release from uninfected RAW264.7 cells

All numbers reflect the mean from two (MIC) or three (RAW264.7) experiments.

Supplementary Figures

Supplementary Figure 2.1

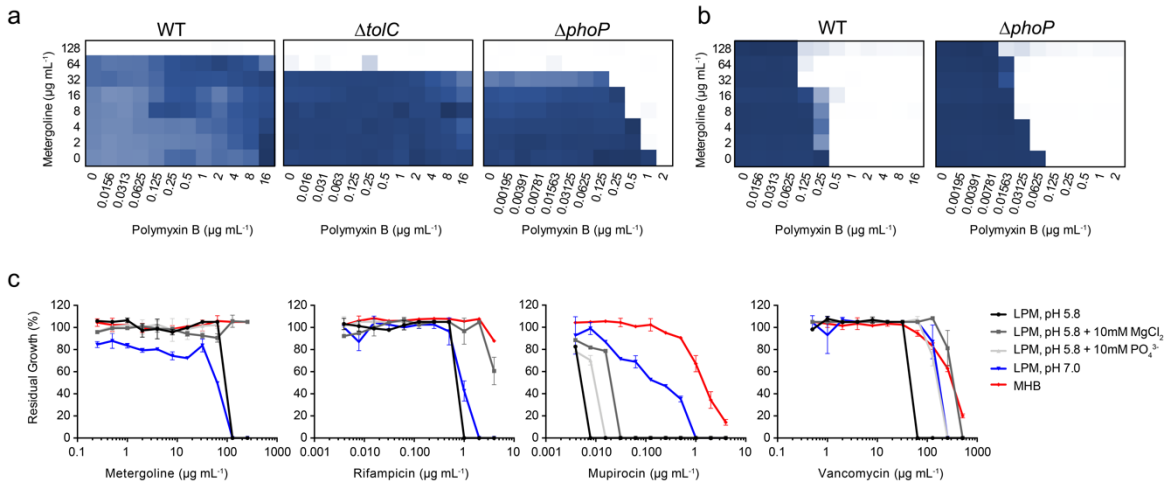


Supplementary Figure 2.1. Optimization of intracellular screening workflow.

a Colony forming unit (CFU) to luminescence correlation from *S. Tm* transformed with the pGEN plasmid expressing constitutive luciferase from the *em7* promoter (pGEN-*lux*). **b** Luminescence (relative light units, RLU) and CFU of *S. Tm* transformed with pGEN-*lux*, internalized in untreated (left) or DMSO-treated (right) RAW264.7 macrophages, measured directly after gentamicin treatment to kill extracellular bacteria (0 h) and 16 h later. Bar plots depict the mean of 4-6 biological replicates, error bars indicate s.e.m. **c** *S. Tm* (dark grey) and *S. Tm* transformed with pGEN-*lux* (light grey) were internalized into RAW264.7 macrophages and treated with DMSO (left) or 200 $\mu\text{g mL}^{-1}$ metergoline (right). Macrophages were lysed and CFU were enumerated immediately after

gentamicin treatment (0 h), at 3 h post-infection, and at 6 h post-infection. Bar plots depict the mean of 6 biological replicates, error bars indicate s.e.m.

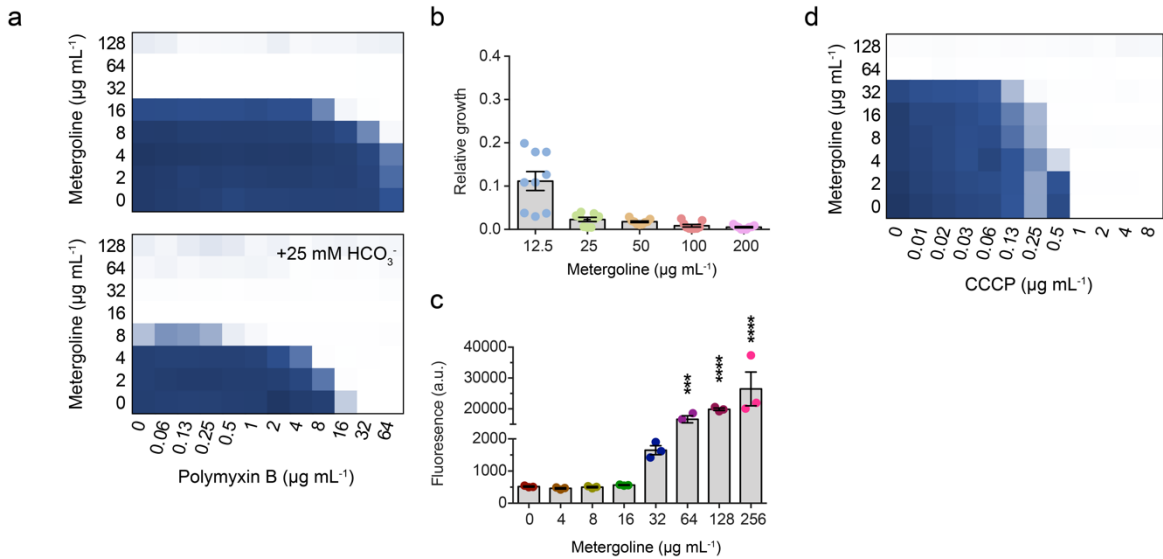
Supplementary Figure 2.2



Supplementary Figure 2.2. Impact of LPM or mutants on metergoline activity.

a Chequerboard broth microdilution assay measuring synergy between metergoline and polymyxin B in LPM. *S. Tm* WT, $\Delta tolC$, or $\Delta phoP$ were grown in LPM with the indicated concentrations of polymyxin B and metergoline. Darker colour indicates higher cell density. **b** Chequerboard broth microdilution assay measuring synergy between metergoline and polymyxin B in MHB. In **a** and **b**, data shown are representative of at least two experiments. **c** Potency analysis of metergoline, rifampicin, mupirocin, or vancomycin in MHB or variants of LPM. LPM was adjusted to pH 7.0 or supplemented with 10 mM MgCl_2 or 10 mM PO_4^{3-} as indicated. Residual growth was calculated as a percentage relative to an untreated control in each media. Points and error bars show the mean and s.e.m. from two biological replicates.

Supplementary Figure 2.3

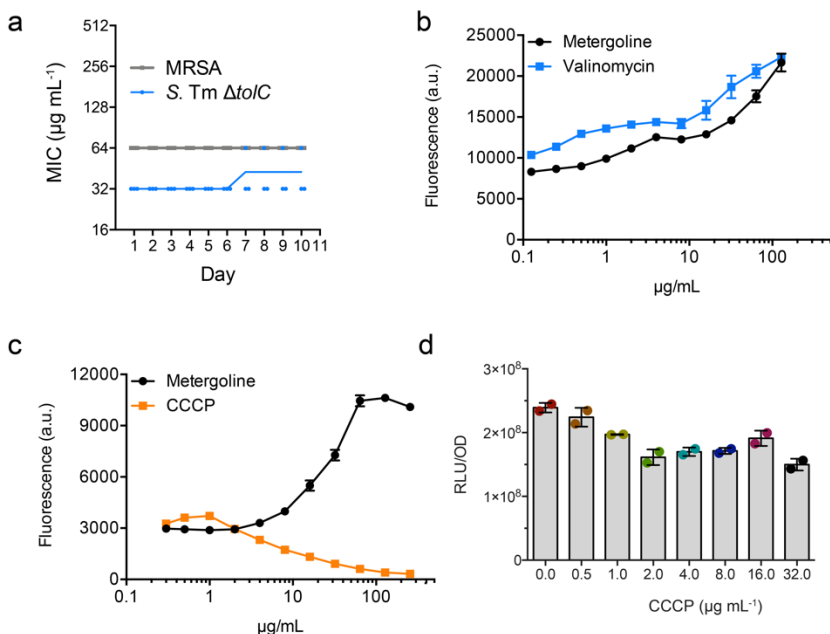


Supplementary Figure 2.3. Activity of metergoline against methicillin-resistant *Staphylococcus aureus* (MRSA).

a Chequerboard broth microdilution assay showing synergy between polymyxin B and metergoline against MRSA grown in MHB, or MHB supplemented with 25 mM bicarbonate (HCO_3^-). **b** Intracellular replication of MRSA measured in bone-marrow derived macrophages isolated from C57BL/6 mice. Relative growth reflects replication over 4 h, normalized to bacterial growth in macrophages treated with DMSO. Metergoline was added at the indicated concentrations. Bar plots depict the mean of 9 biological replicates, error bars indicate s.e.m. **c** The effect of metergoline on cytoplasmic membrane potential was measured by the DiSC₃(5) assay, following a 1 min exposure to the indicated concentrations of metergoline. Bar plots depict the mean fluorescence of three biological replicates, error bars indicate s.e.m. All groups were compared to 0 $\mu\text{g mL}^{-1}$ metergoline via one-way ANOVA with Holm-Sidak's multiple test correction. *** $P < 0.001$, **** $P < 0.0001$. **d** Chequerboard analysis showing synergy between metergoline

and CCCP against MRSA grown in MHB. In **a** and **b** darker colour indicates higher bacterial growth and data are representative of two experiments.

Supplementary Figure 2.4

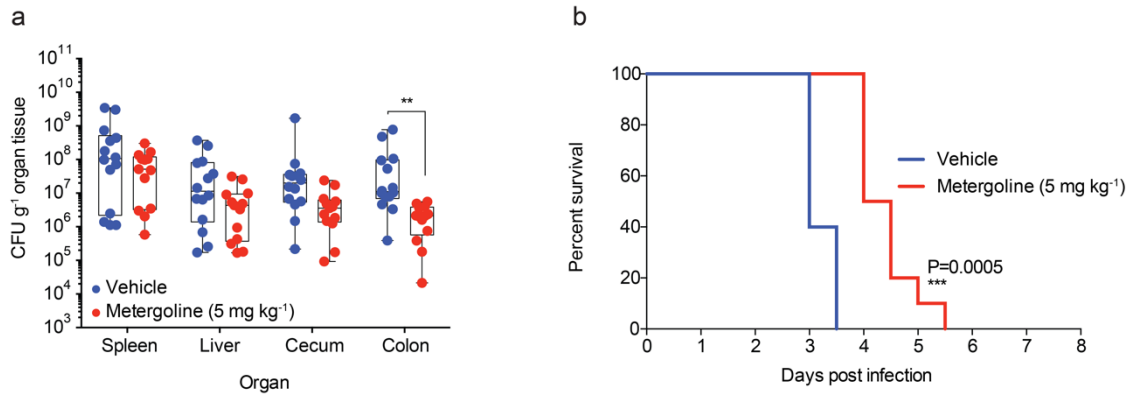


Supplementary Figure 2.4. Serial-passage experiment with metergoline and control experiments for DiSC₃(5) and ATP assays.

a The MIC of metergoline against three independent lineages of MRSA or ΔtolC *S. Tm* was measured daily for 10 d (see Methods). Cells from the highest concentration of metergoline with detectable growth were used each day to inoculate MIC plates. Points show the MIC for individual lineages and the connected line shows the mean MIC. **b-c** Effect of metergoline, valinomycin (**b**), and CCCP (**c**) on inner membrane potential was measured by the DiSC₃(5) assay. WT *S. Tm* was grown in MHB with 10 mM EDTA to an OD₆₀₀ ~ 1. Cells were loaded with DiSC₃(5) prior to 1 min incubation with compound. Note that 100 mM KCl was added to cells in **b** as valinomycin is K⁺-dependent. Error bars show s.e.m. for technical triplicates. **d** WT *S. Tm* was grown in MHB with 1 mM EDTA to OD₆₀₀ = 0.2 and then grown in the presence of CCCP for 30 min at 37°C. Cellular ATP levels were estimated by luciferase activity (relative light units,

RLU) normalized to optical density (OD_{600}). Bar plots depict the mean of two biological replicates, error bars indicate s.d.

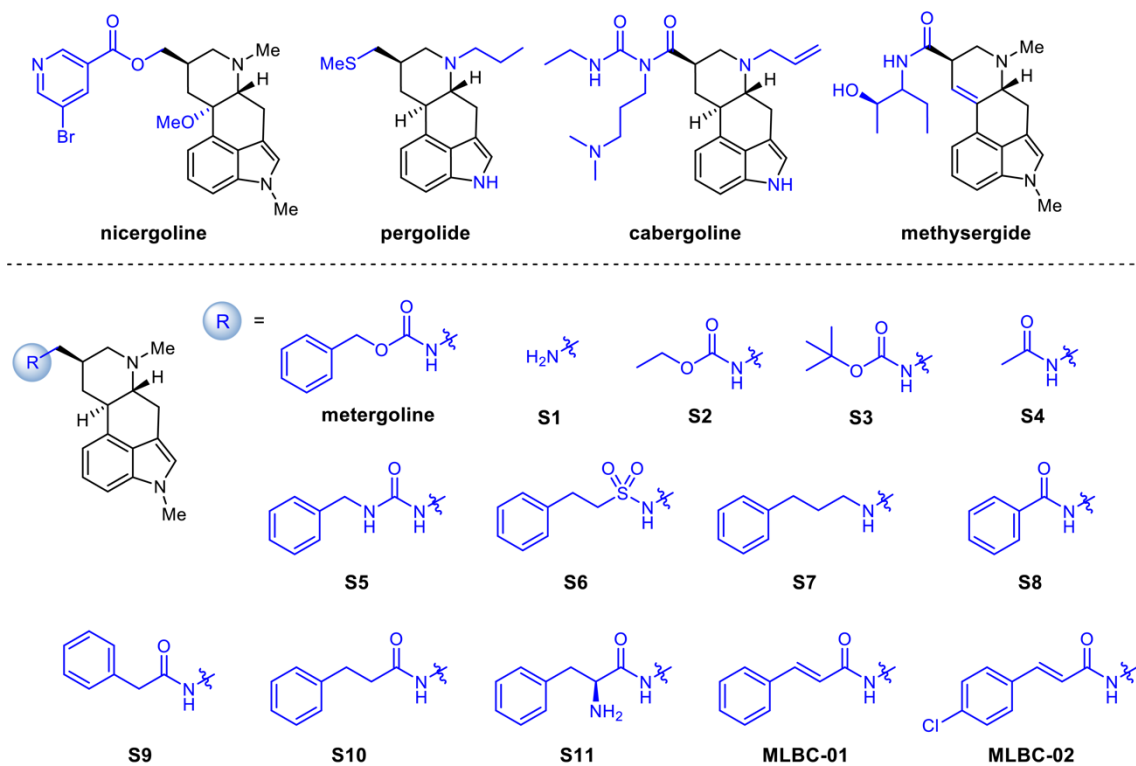
Supplementary Figure 2.5



Supplementary Figure 2.5. *In vivo* efficacy of metergoline following delayed treatment administration.

a Groups of mice were treated twice daily (every 12 h) with metergoline (5 mg kg⁻¹, red), or DMSO (5% in DMEM, blue) by i.p. injection. Treatments were administered beginning 12 h after initial infection. Mice were euthanized at experimental endpoint (60 h post-infection). Bacterial load in the spleen, liver, cecum, and colon was determined by selective plating in the presence of 150 µg mL⁻¹ streptomycin. Data shown are from three separate experiments (n=5 per group). Box plot whiskers show the minimum to maximum values per group, lines in box plots show the median of each group. Groups were analyzed with a two-way ANOVA and corrected for multiple comparisons with a Holm-Sidak test. **b** For survival experiments, groups of mice (n=10) were treated twice daily (every 12 h) with metergoline (5 mg kg⁻¹, red), or DMSO (5% in DMEM, blue) by i.p. injection, and were euthanized at clinical endpoint. Survival curves shown are from two independent experiments. Groups were analyzed with a Gehan-Breslow-Wilcoxon test for survival curve differences. *P<0.05, **P<0.01, ***P<0.001, ****P<0.0001.

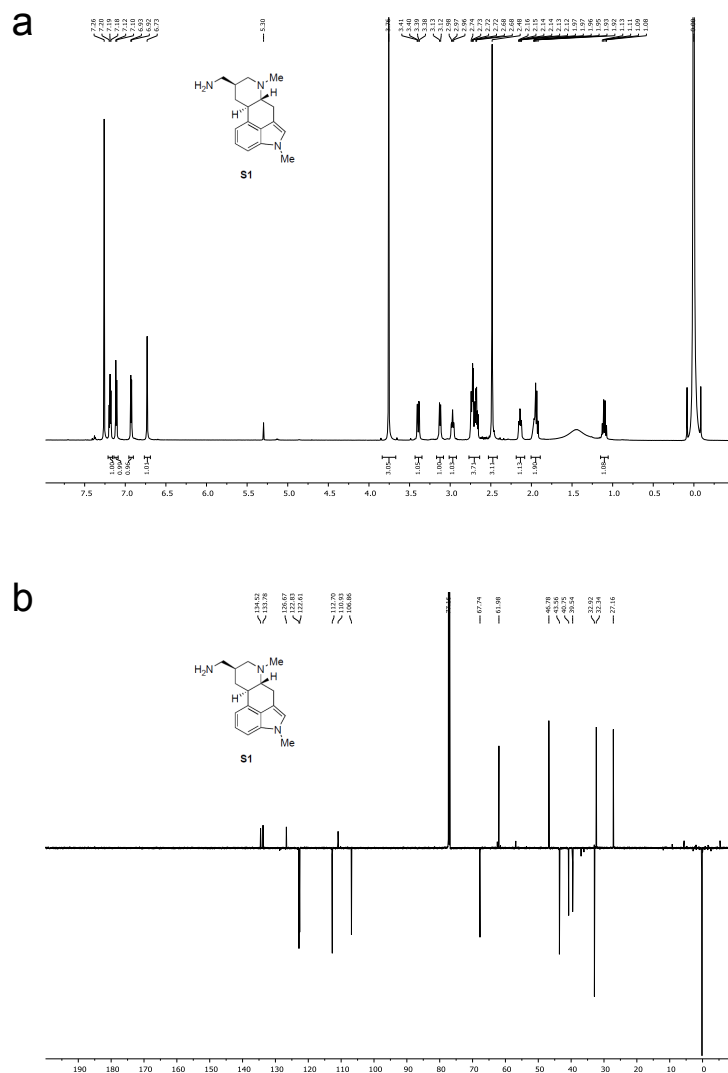
Supplementary Figure 2.6



Supplementary Figure 2.6. Structure of metergoline analogues.

Structural features differing from metergoline are indicated in blue.

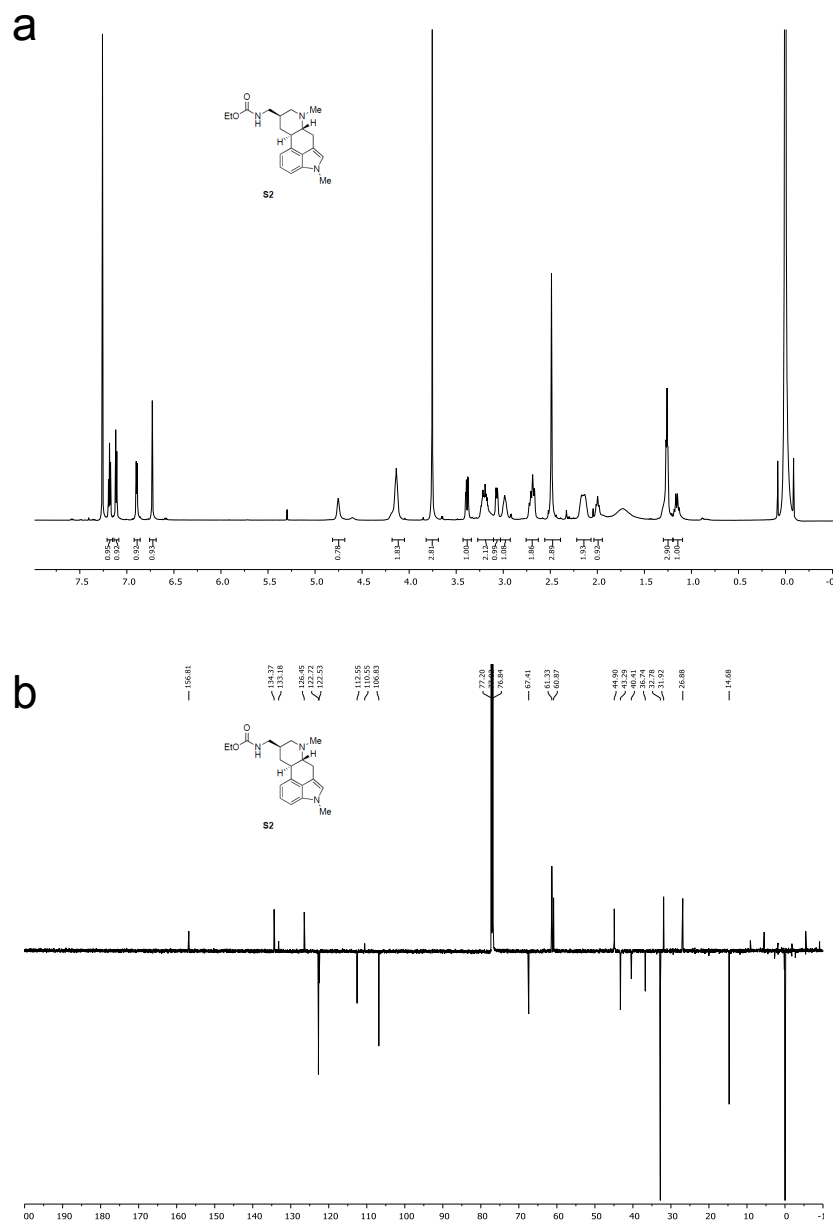
Supplementary Figure 2.7



Supplementary Figure 2.7. NMR spectra for aminomethyl ergoline (S1).

a ^1H NMR, 700 MHz, CDCl_3 . **b** ^{13}C NMR, 175 MHz, CDCl_3 . The structure of compound **S1** is shown.

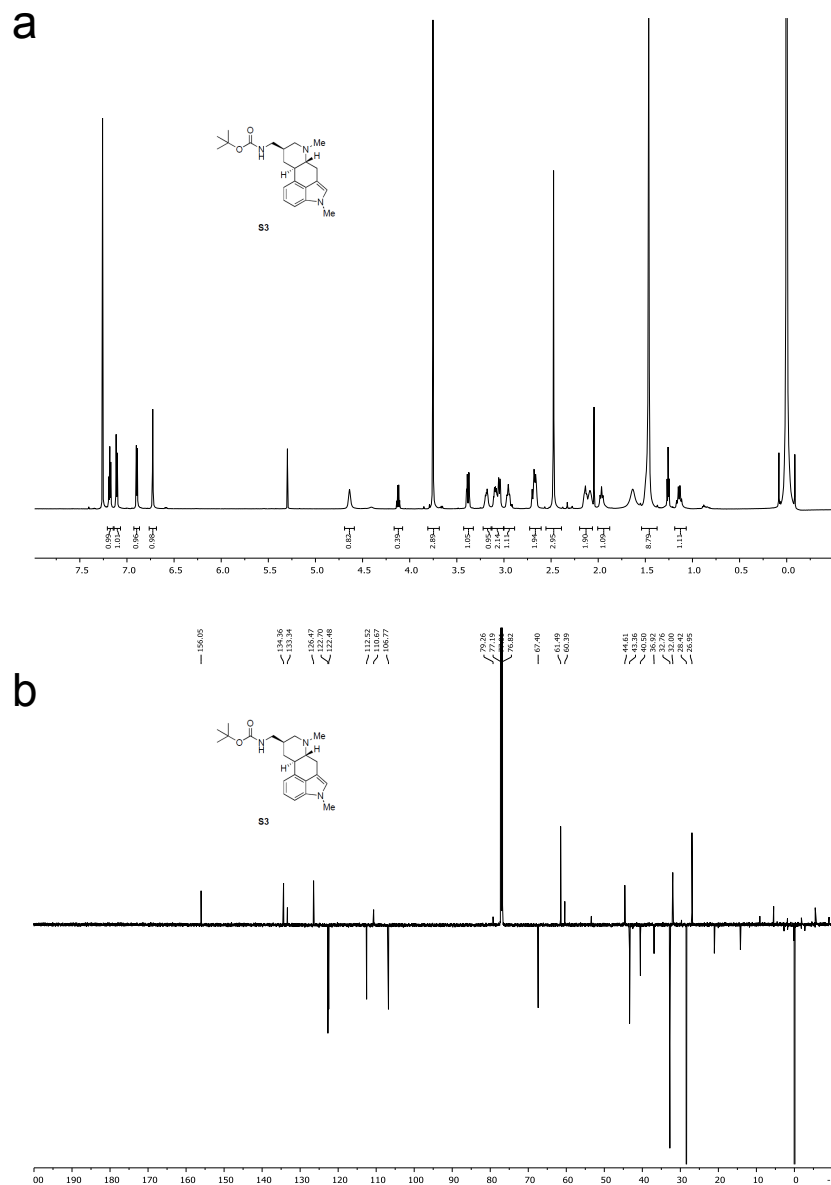
Supplementary Figure 2.8



Supplementary Figure 2.8. NMR spectra for ethyl carbamate derivative (**S2**).

a ^1H NMR, 700 MHz, CDCl_3 . **b** ^{13}C NMR, 175 MHz, CDCl_3 . The structure of compound **S2** is shown.

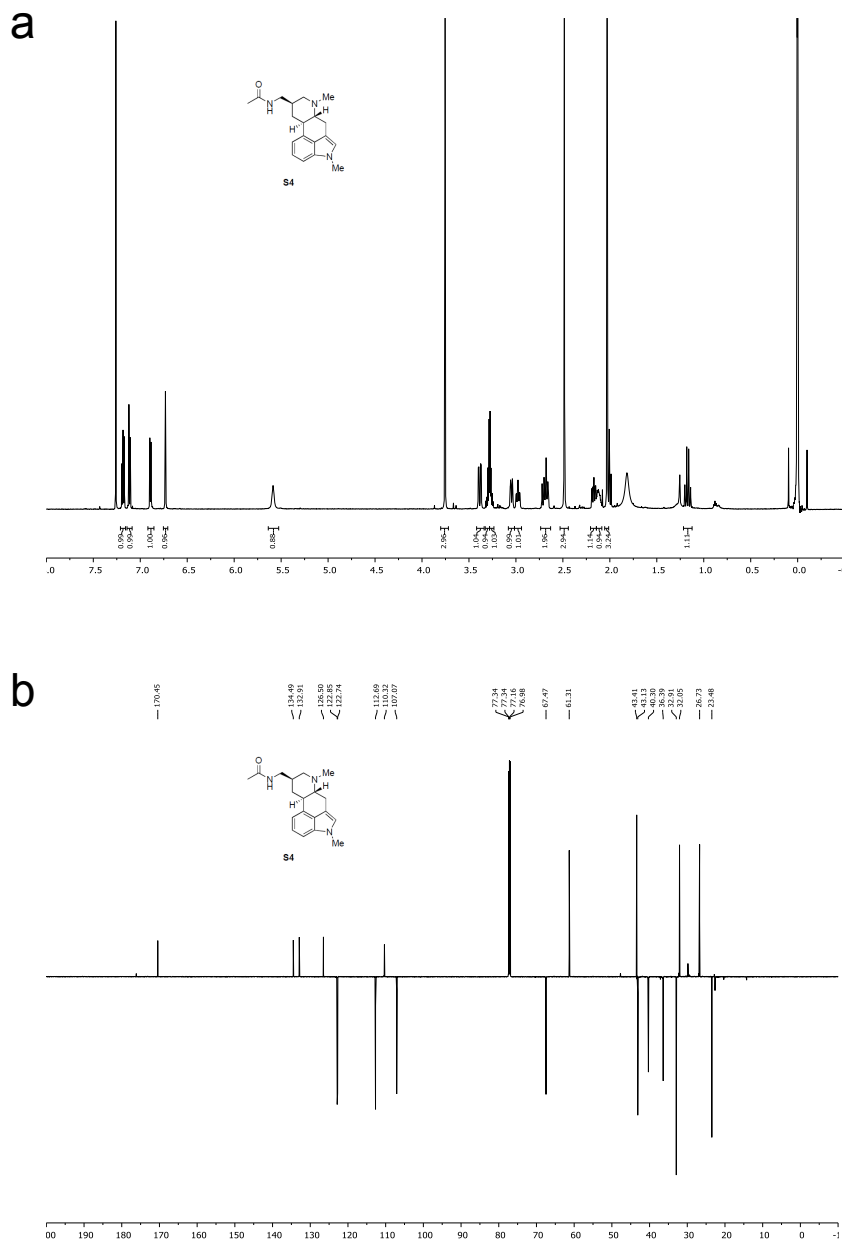
Supplementary Figure 2.9



Supplementary Figure 2.9. NMR spectra for N-Boc ergoline derivative (**S3**).

a ^1H NMR, 700 MHz, CDCl_3 . **b** ^{13}C NMR, 175 MHz, CDCl_3 . The structure of compound **S3** is shown.

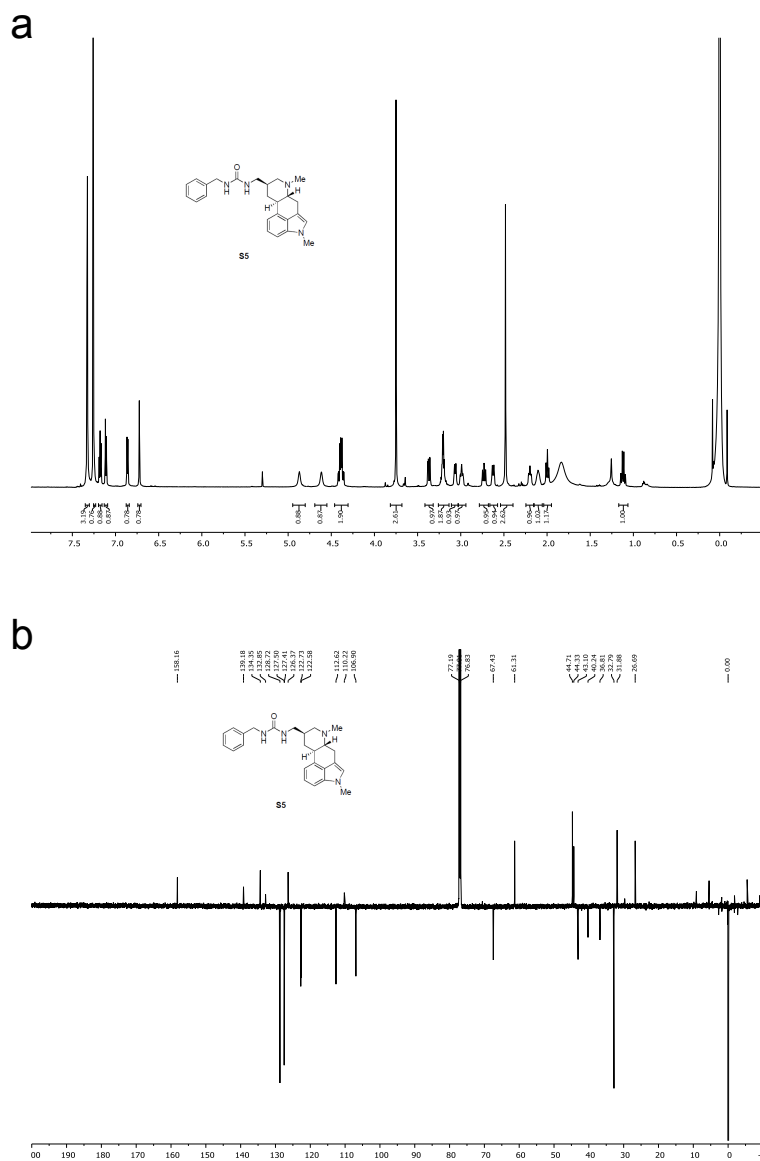
Supplementary Figure 2.10



Supplementary Figure 2.10. NMR spectra for N-Acetyl ergoline derivative (S4).

a ^1H NMR, 600 MHz, CDCl_3 . **b** ^{13}C NMR, 175 MHz, CDCl_3 . The structure of compound **S4** is shown.

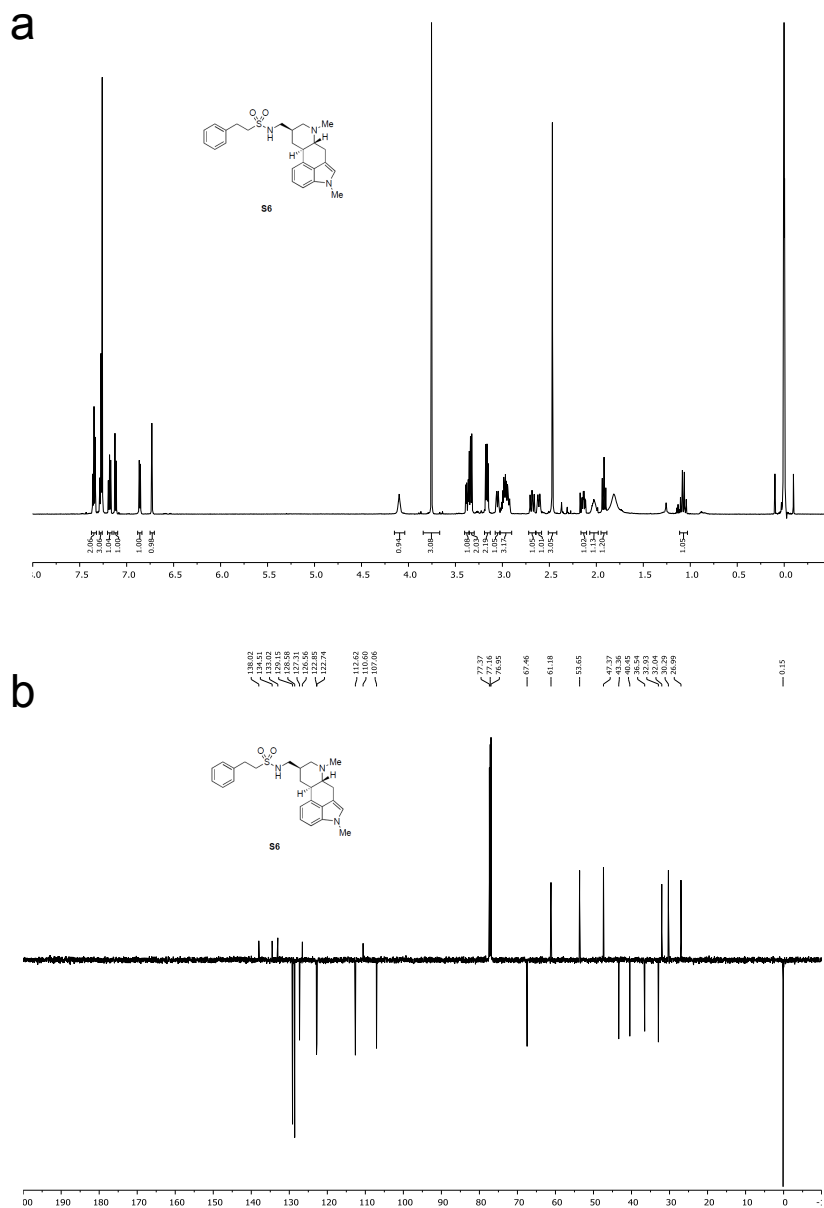
Supplementary Figure 2.11



Supplementary Figure 2.11. NMR spectra for N-(N'-Benzyl) urea derivative (**S5**).

a ¹H NMR, 700 MHz, CDCl₃. **b** ¹³C NMR, 175 MHz, CDCl₃. The structure of compound **S5** is shown.

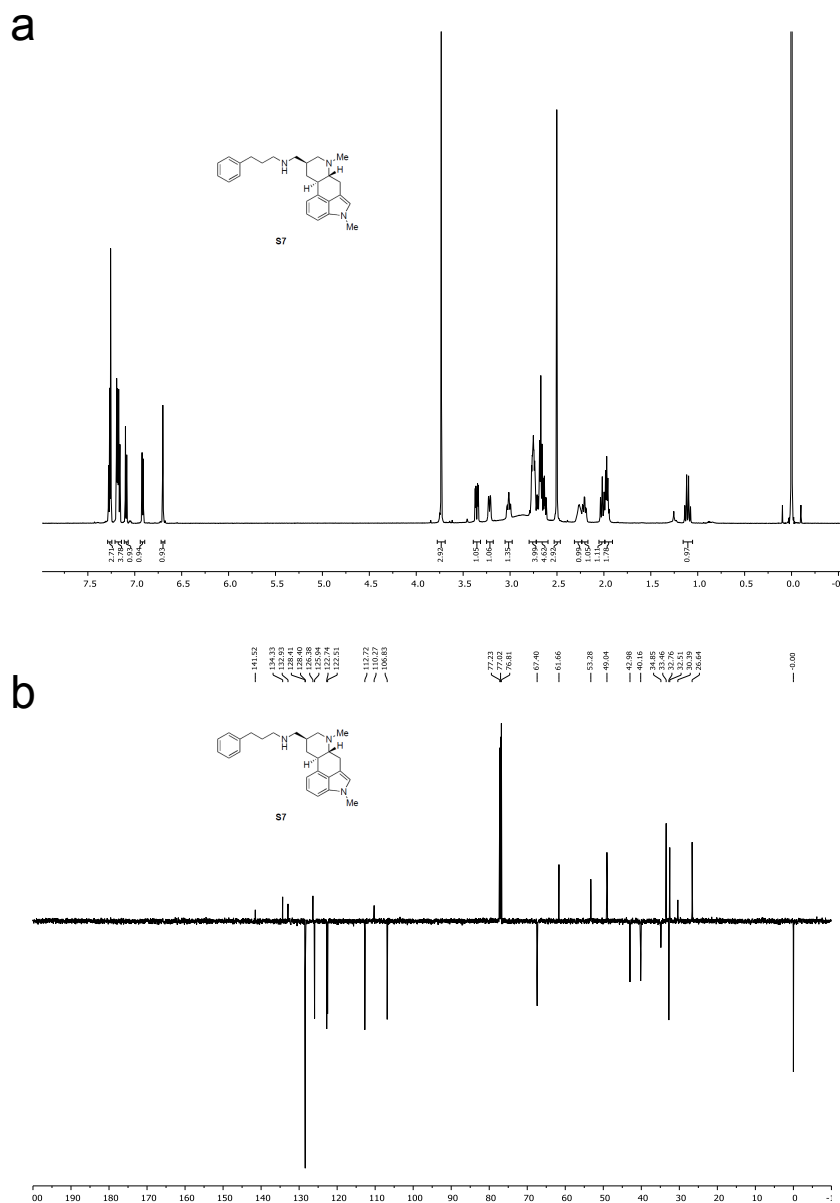
Supplementary Figure 2.12



Supplementary Figure 2.12. NMR spectra for N-(2-Phenylethylsulfonyl) ergoline derivative (**S6**).

a ^1H NMR, 600 MHz, CDCl_3 . **b** ^{13}C NMR, 150 MHz, CDCl_3 . The structure of compound **S6** is shown.

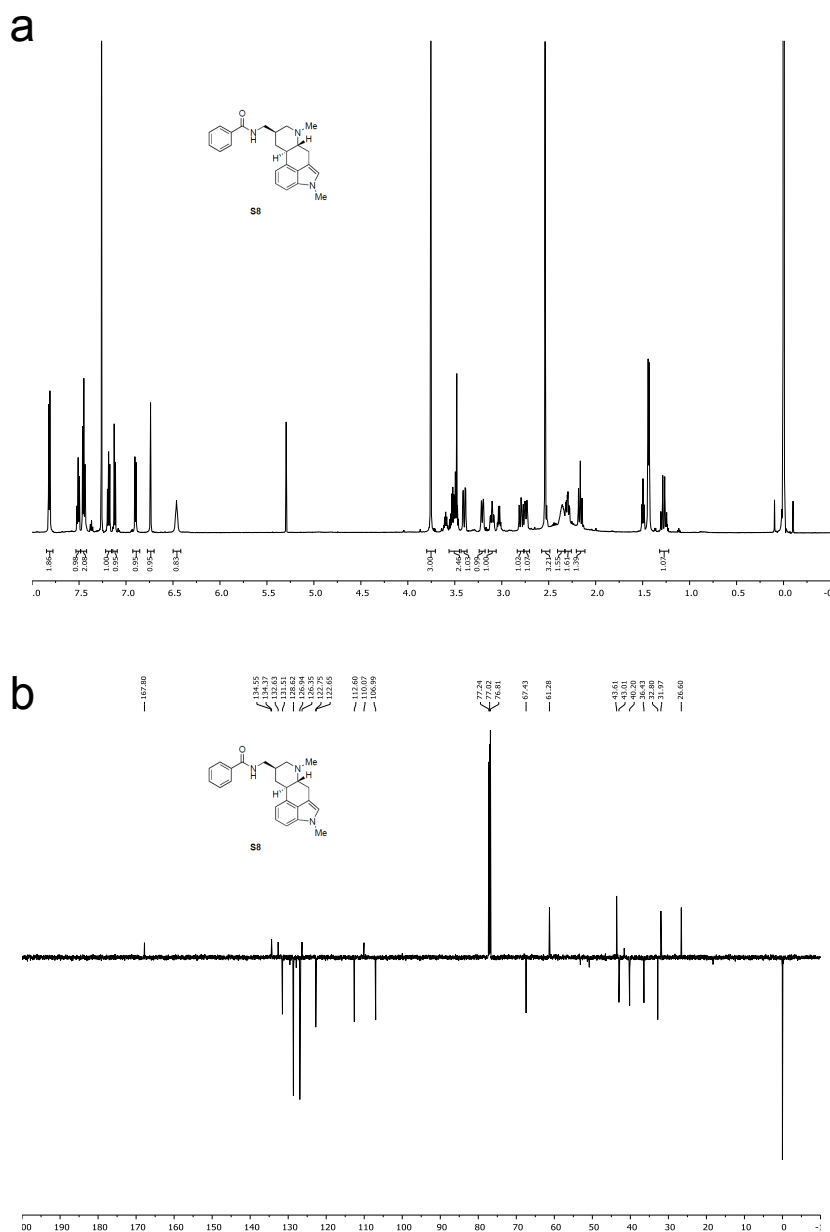
Supplementary Figure 2.13



Supplementary Figure 2.13. NMR spectra for N-(3-Phenylpropyl) ergoline derivative (**S7**).

a ^1H NMR, 600 MHz, CDCl_3 . **b** ^{13}C NMR, 150 MHz, CDCl_3 . The structure of compound **S7** is shown.

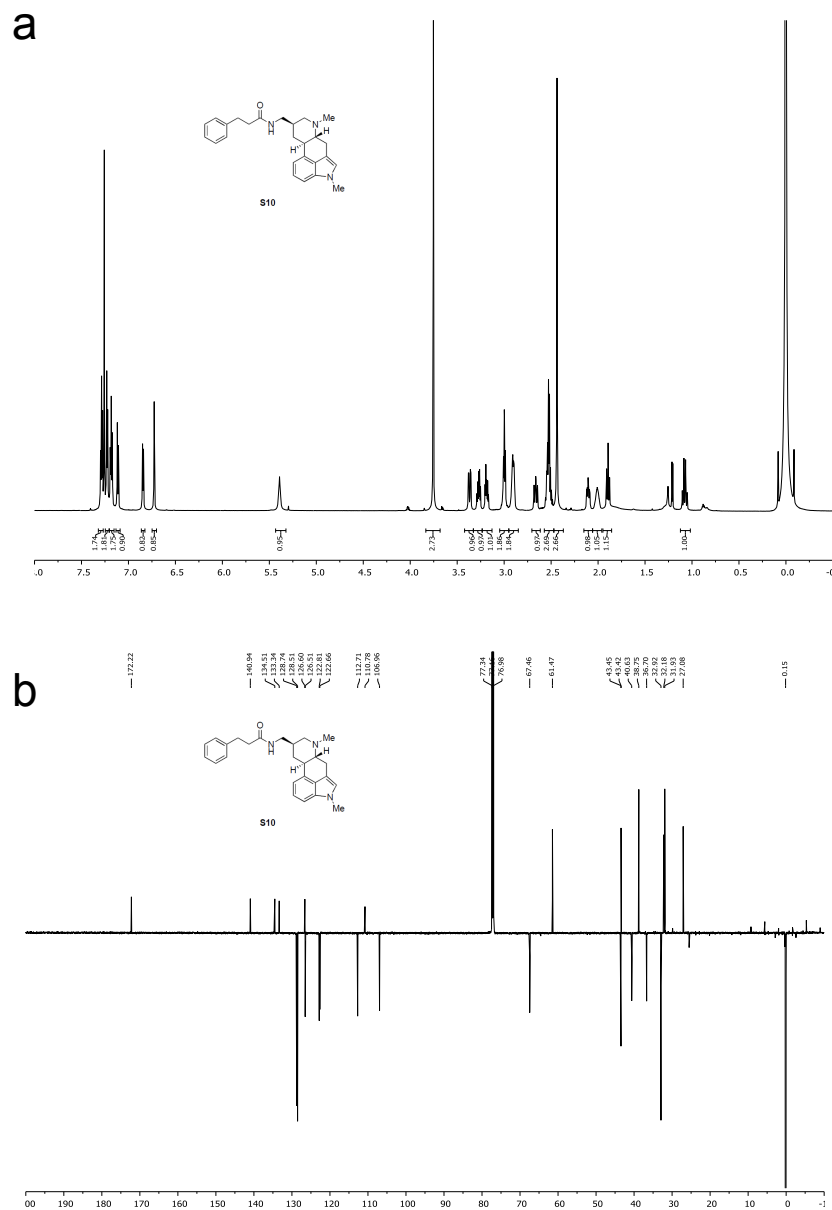
Supplementary Figure 2.14



Supplementary Figure 2.14. NMR spectra for N-Benzoyl ergoline derivative (**S8**).

a ^1H NMR, 600 MHz, CDCl_3 . **b** ^{13}C NMR, 150 MHz, CDCl_3 . The structure of compound **S8** is shown.

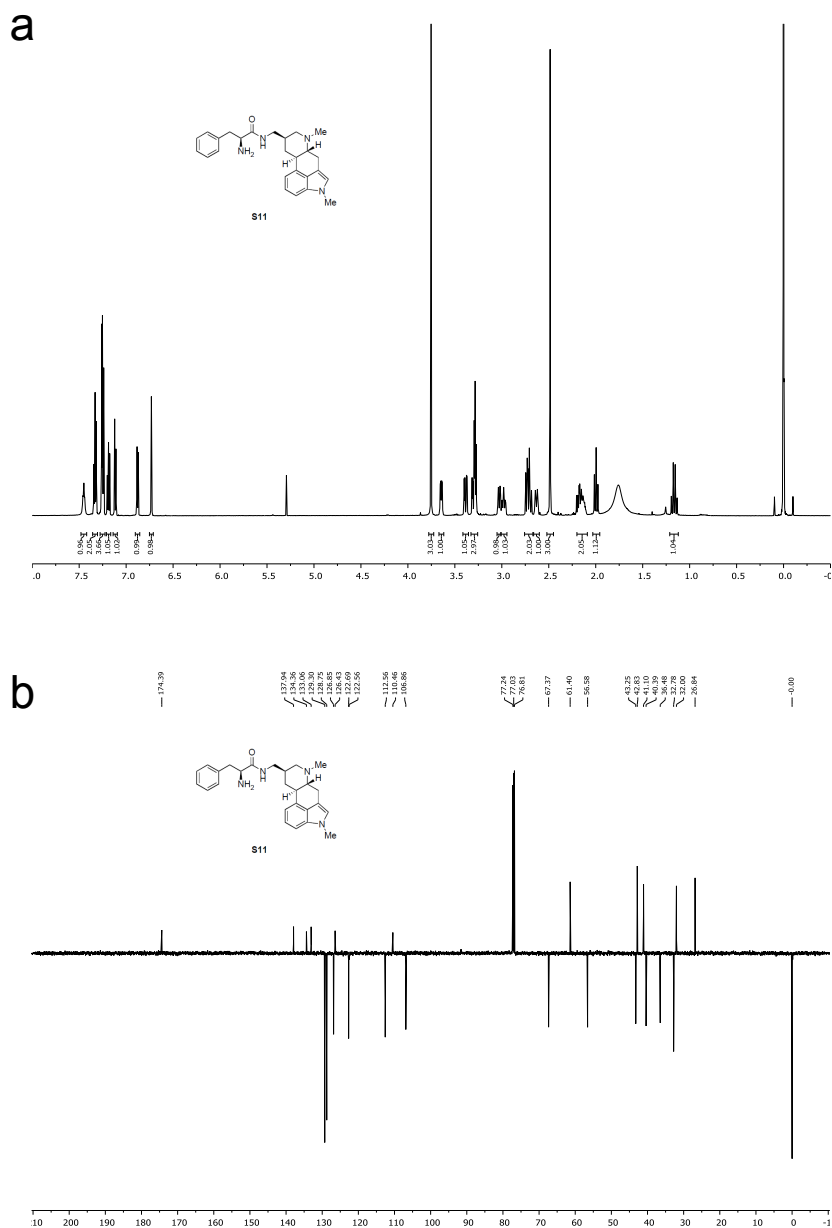
Supplementary Figure 2.16



Supplementary Figure 2.16. NMR spectra for N-(3-Phenylpropanoyl) ergoline derivative (**S10**).

a ^1H NMR, 700 MHz, CDCl_3 . **b** ^{13}C NMR, 175 MHz, CDCl_3 . The structure of compound **S10** is shown.

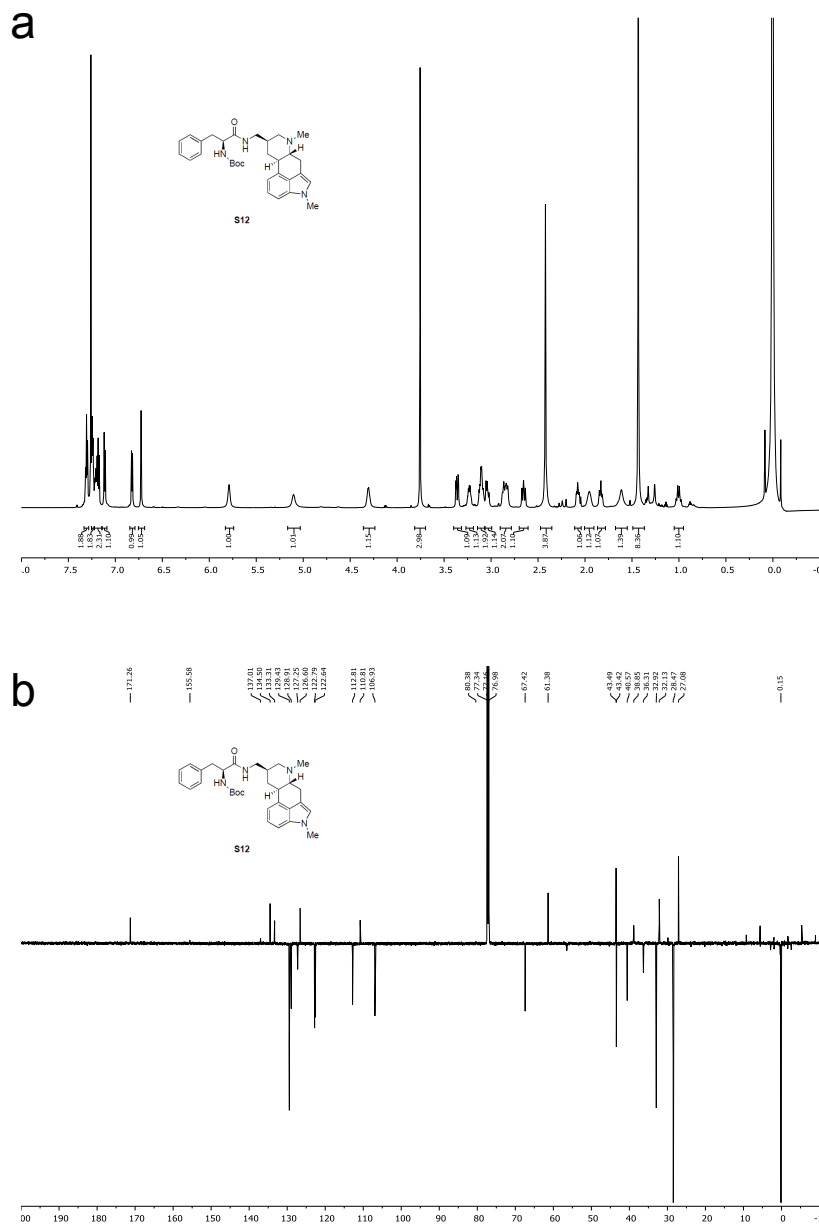
Supplementary Figure 2.17



Supplementary Figure 2.17. NMR spectra for N-L-Phenylalanyl ergoline derivative (**S11**).

a ^1H NMR, 600 MHz, CDCl_3 . **b** ^{13}C NMR, 150 MHz, CDCl_3 . The structure of compound **S11** is shown.

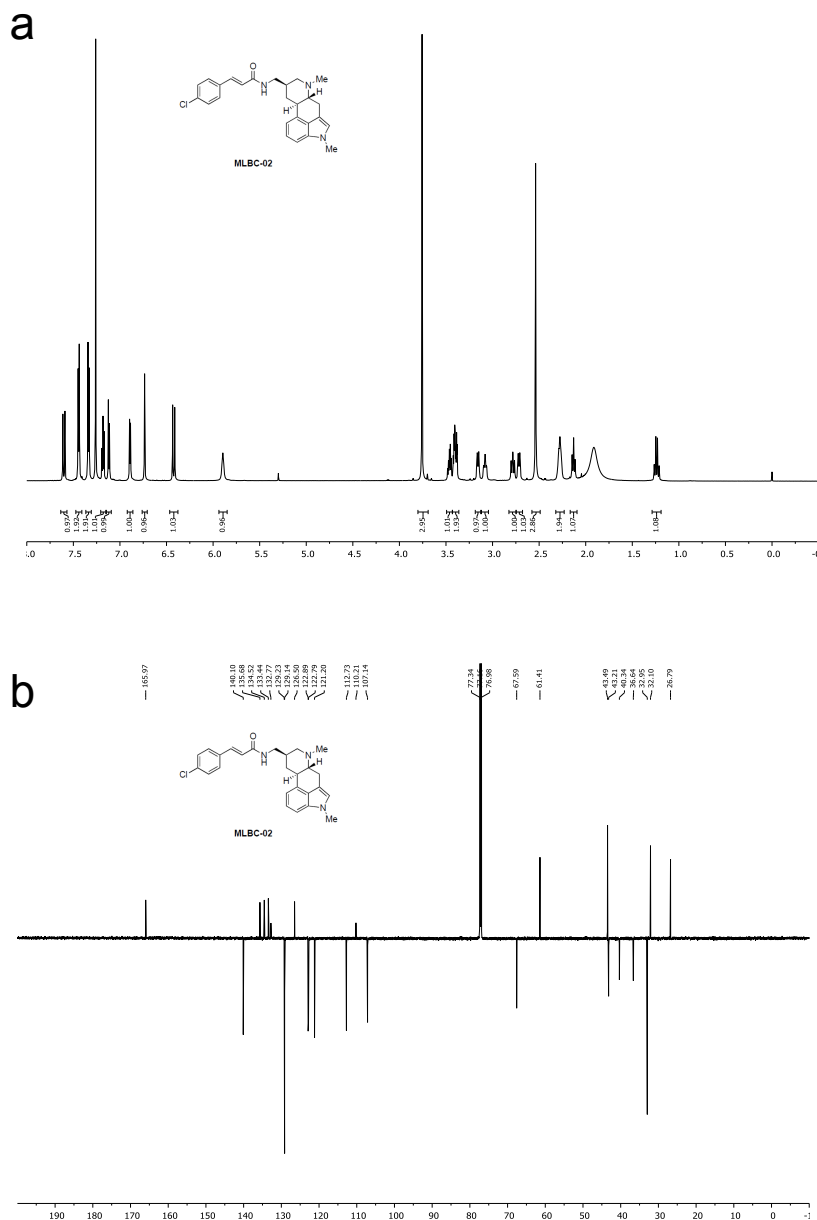
Supplementary Figure 2.18



Supplementary Figure 2.18. NMR spectra for N-(N-Boc-L-Phenylalanyl) ergoline derivative (**S12**).

a ^1H NMR, 700 MHz, CDCl_3 . **b** ^{13}C NMR, 175 MHz, CDCl_3 . The structure of compound **S12** is shown.

Supplementary Figure 2.20



Supplementary Figure 2.20. NMR spectra for N-trans-Cinnamoyl derivative (MLBC-02).

a ^1H NMR, 700 MHz, CDCl_3 . **b** ^{13}C NMR, 175 MHz, CDCl_3 . The structure of compound **MLBC-02** is shown.

Supplementary Tables

Supplementary Table 2.1

| Category | Parameter | Description |
|--------------------------|------------------------------------|---|
| Assay | Type of assay | Cell-based |
| | Target | Whole organism <i>Salmonella</i> Typhimurium SL1344 |
| | Primary measurement | Measurement of optical density at 600 nm, luminescence |
| | Assay protocol | Methods section 'High-throughput compound screening' |
| Library | Library size | 1600 |
| | Library composition | Synthetic small molecules, off-patent FDA approved molecules, known bioactives |
| Screen | Source | Microsource |
| | Format | 96-well plates (Corning), 3 replicates |
| | Concentration(s) tested | 10 uM, 0.2% DMSO |
| | Plate controls | High controls: 0.1% DMSO Low controls: 100 ug/mL rifampicin |
| | Reagent/compound dispensing system | Biomek FX liquid handler (Beckman Coulter Inc., Fullerton, CA) |
| | Detection instrument and software | Envision (Perkin Elmer, Waltham, MA) |
| | Assay validation/QC | For LPM screen: average (n=3) Z' score = 0.713, for RAW264.7 data see Figure S1 |
| | Correction factors | Optical density readings were background corrected; Luminescence values were normalized to T ₀ |
| | Normalization | Plate and well effects normalized with interquartile mean |
| Post-HTS analysis | Hit criteria | Compounds reducing normalized growth more than 3σ below the LPM, 4.68%; RAW264.7, 6.44% |
| | Hit rate | |
| | Additional assay(s) | Dose-response and MIC determination <i>in vitro</i> and in macrophages |

Supplementary Table 2.1. Small molecule screening data.

Supplementary Table 2.2

| Compound | Minimum Inhibitory Concentration ($\mu\text{g mL}^{-1}$) | | | | | RAW264.7 | |
|--------------|--|-------------------|------|---------------------|------|---------------------|---------------------------|
| | S. Tm WT | | | ΔtolC | MRSA | Growth ^b | Toxicity (%) ^c |
| | MHB | EDTA ^a | LPM | MHB | MHB | | |
| Metergoline | >128 | 64 | 128 | 32 | 32 | 0.08 | 2.9 |
| nicergoline | >128 | 64 | >128 | 128 | 128 | 0.59 | 7.37 |
| pergolide | >128 | >128 | >128 | >128 | >128 | 0.93 | 18.81 |
| cabergoline | >128 | >128 | >128 | >128 | >128 | 0.75 | 17.24 |
| methysergide | >128 | >128 | >128 | >128 | >128 | 1.01 | 15.57 |
| S1 | >128 | 16 | >128 | >128 | >128 | 0.39 | 6.01 |
| S2 | >128 | 128 | >128 | >128 | >128 | 0.85 | 6.94 |
| S3 | >128 | >128 | >128 | 128 | >128 | 0.23 | 14.02 |
| S4 | >128 | >128 | >128 | >128 | >128 | 0.84 | 16.54 |
| S5 | >128 | 128 | >128 | 64 | 128 | 0.49 | 14.95 |
| S6 | >128 | 64 | 128 | 64 | 64 | 0.08 | 19.86 |
| S7 | >128 | 32 | 64 | 64 | 16 | 0.58 | 17.78 |
| S8 | >128 | 128 | >128 | 128 | >128 | 0.65 | 17.60 |
| S9 | >128 | 128 | >128 | >128 | >128 | 0.86 | 19.18 |
| S10 | >128 | >128 | >128 | 128 | >128 | 0.87 | 20.78 |
| S11 | >128 | 32 | 64 | >128 | >128 | 0.56 | 12.64 |
| MLBC-01 | >128 | 32 | 128 | 8 | 16 | 0.07 | 18.07 |
| MLBC-02 | >128 | 8 | 32 | 4 | 0.5 | 0.08 | 8.9 |

Supplementary Table 2.2. Activity of metergoline and 17 structurally related compounds.

^aWT S. Tm was grown in MHB with 10 mM EDTA

^bIntracellular activity was measured by addition of 8 $\mu\text{g mL}^{-1}$ compound to RAW264.7 macrophages infected with WT S. Tm and is reported as old-growth inhibition relative to a DMSO-treated control

^cToxicity was estimated by lactate dehydrogenase release from uninfected RAW264.7 cells

All numbers reflect the mean from two (MIC) or three (RAW264.7) experiments.

Supplementary Table 2.3

| Position | δ C, mult | δ H, (mult, <i>J</i> in Hz, integration) | COSY | HMBC |
|----------|----------------------|---|---|-----------------------------|
| 1' | 32.9 CH ₃ | 3.76 (s, 3H) | | C2, C15 |
| 2 | 122.7 CH | 6.73 (s, 1H) | H4 _{eq} , H4 _{ax} | C1', C3, C15, C16 |
| 3 | 110.7 C | | | |
| 4 | 27.1 CH ₂ | 2.70 (dd, <i>J</i> = 14.7, 10.6 Hz, 1H, ax) | H2, H4 _{eq} , H5 | C2, C3, C5, C10 |
| | | 3.38 (dd, <i>J</i> = 14.6, 4.3 Hz, 1H, eq) | H2, H4 _{ax} , H5 | C2, C3, C5, C10, C16 |
| 5 | 67.5 CH | 2.16 (td, <i>J</i> = 10.6, 4.3 Hz, 1H) | H4 _{ax} , H4 _{eq} , H10 | C4, C6', C7, C9, C10 |
| 6' | 43.4 CH ₃ | 2.48 (s, 3H) | | C4, C5, C7, C8 |
| 7 | 61.6 CH ₂ | 1.99 (dd, <i>J</i> = 11.3, 11.1 Hz, 1H, ax) | H7 _{eq} , H8 | C5, C6', C9 |
| | | 3.05 (d, <i>J</i> = 11.1 Hz, 1H, eq) | H7 _{ax} , H8 | C5, C6', C8, C9 |
| 8 | 36.8 CH | 2.07–2.13 (m, 1H) | H8'A, H8'B, H7 _{ax} , H7 _{eq} , H9 _{ax} , H9 _{eq} | C7 |
| 8' | 43.5 CH ₂ | 3.27 (m, <i>J</i> = 13.5, 6.0 Hz, 1H, A) | H8, H8'B | C7, C8, C9, C18 |
| | | 3.29 (m, <i>J</i> = 13.5, 6.8 Hz, 1H, B) | | |
| 9 | 32.2 CH ₂ | 1.17 (q, <i>J</i> = 12.4 Hz, 1H, ax) | H8, H9 _{eq} , H10 | C5, C7, C8, C8', C10, C11 |
| | | 2.65 (m, 1H, eq) | H8, H9 _{ax} , H10 | C5, C7, C8, C10 |
| 10 | 40.4 CH | 2.97 (ddd, <i>J</i> = 12.4, 10.6, 3.4 Hz) | H5, H9 _{ax} , H9 _{ax} | C5, C9, C11 |
| 11 | 133.3 C | | | |
| 12 | 112.7 CH | 6.89 (d, <i>J</i> = 7.1 Hz, 1H) | H13 | C3, C10, C13, C14, C15, C16 |
| 13 | 122.8 CH | 7.18 (dd, <i>J</i> = 7.1, 8.1 Hz, 1H) | H12, H14 | C11, C12, C15, C16 |
| 14 | 107.0 CH | 7.11 (d, <i>J</i> = 8.1 Hz, 1H) | H13 | C11, C12, C16 |
| 15 | 134.5 C | | | |
| 16 | 126.6 C | | | |
| 17 | | 5.57 (brs, 1H) | H8'A, H8'B | C18 |
| 18 | 170.3 C | | | |
| 19 | 23.6 CH ₃ | 2.03 (s, 3H) | | C18 |

Supplementary Table 2.3. NMR data for N-acetyl ergoline derivative S4.

¹H NMR (700 MHz) and ¹³C NMR (175 MHz) experiments were recorded in CDCl₃ at 23 °C. Positional assignments are based on HSQC and HMBC correlation experiments. Stereochemical assignments were deduced from coupling constants.

Supplementary Methods

Synthetic Experimental Procedures: General

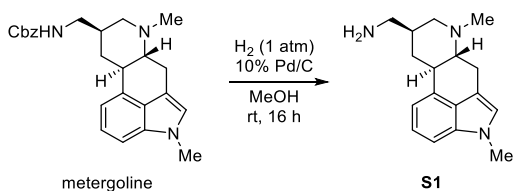
Chemical shifts in ^1H NMR and ^{13}C NMR spectra are reported in parts per million (ppm) relative to tetramethylsilane (TMS), with calibration of the residual solvent peaks according to values reported by Gottlieb et al. (chloroform: δ_{H} 7.26, δ_{C} 77.16; acetone: δ_{H} 2.05, δ_{C} 29.84, 206.26; methanol: δ_{H} 3.31, δ_{C} 49.00; DMSO: δ_{H} 2.50, δ_{C} 39.52; acetonitrile: δ_{H} 1.94, δ_{C} 1.32, 118.26) (Gottlieb et al., 1997). When peak multiplicities are given, the following abbreviations are used: s, singlet; d, doublet; t, triplet; q, quartet; sept., septet; dd, doublet of doublets; m, multiplet; br, broad; app., apparent; *gem*, geminal. ^1H NMR spectra were acquired at 600 or 700 MHz with a default digital resolution (Brüker parameter: FIDRES) of 0.18 and 0.15 Hz/point, respectively. Coupling constants reported herein therefore have uncertainties of ± 0.4 Hz and ± 0.30 Hz, respectively. All assignments of protons and carbons relied on data from 2-dimensional NMR experiments including COSY, HMQC, and HMBC. The ^{13}C NMR (DEPTq) spectra provided herein show CH and CH_3 carbon signals below the baseline and C and CH_2 carbons above the baseline. Melting points (mp) are uncorrected. Reactions were carried out at room temperature (rt) if temperature is not specified. An automated flash chromatography system (Teledyne CombiFlash Rf 200) was used for the purification of compounds on silica gel (either 40–60 μM or 20–40 μM particle size).

General Procedure A

To a solution of amine **S1** (1.0 equiv), EDC·HCl (1.2 equiv), HOBt (1.2 equiv), and a carboxylic acid (1.2 equiv) in CH_2Cl_2 (0.02 M) was added *i*-Pr₂NEt (3 equiv). The reaction mixture was stirred at rt for 3–16 h and the progress of the

reaction followed by thin-layer chromatography (TLC). Upon completion, the reaction mixture was diluted with CH_2Cl_2 , washed with saturated aqueous Na_2CO_3 , dried over Na_2SO_4 , and concentrated under reduced pressure. Products were purified by flash chromatography ($\text{MeOH}/\text{CH}_2\text{Cl}_2$) on silica gel.

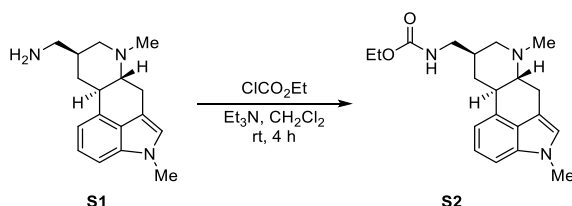
Aminomethyl ergoline (**S1**)



To a stirring solution of metergoline (1.00 g, 2.48 mmol) in MeOH (75 mL) was added 10% Pd/C (50 mg). The solution was degassed by stirring under vacuum for approximately 30–60 seconds, followed by back-filling with argon via balloon. After repeating the process 10 times, the flask was back-filled with H_2 gas from a balloon and the reaction stirred overnight at rt. After 14 h, the reaction vessel was purged of H_2 with argon and TLC analysis indicated the starting material was consumed. The reaction mixture was then filtered through a pad of Celite and the resulting yellow solution concentrated under reduced pressure to provide the primary amine as a viscous amber oil that was used in following reactions without further purification. The crude oil was diluted with CH_2Cl_2 , aliquotted into reaction vials, and concentrated under reduced pressure. A small amount of the crude amine **S1** solidified after concentrating from CH_2Cl_2 into an amorphous solid. Mp: 135–138 °C (lit. 151–153 °C) (Singh, 2014). $R_f = 0.03$ (10% MeOH/ CH_2Cl_2). ^1H NMR (700 MHz, CDCl_3): 7.19 (dd, $J = 7.1, 8.1$ Hz, 1H), 7.11 (d, $J = 8.1$ Hz, 1H), 6.93 (d, $J = 7.1$ Hz, 1H), 6.72 (s, 1H), 3.76 (s, 3H), 3.39 (dd, $J = 14.6, 4.2$ Hz, 1H), 3.12 (d, $J = 9.6$ Hz, 1H), 2.97 (m, 1H), 2.75–2.65 (m, 4H), 2.48 (s, 3H), 2.14 (td, $J = 10.6, 4.2$ Hz, 1H), 2.00–1.90 (m, 2H), 1.10 (q, $J = 12.1$ Hz, 1H). ^{13}C NMR (CDCl_3): 27.2, 32.3, 32.9, 39.5, 40.7, 43.6, 46.8, 62.0, 67.7, 106.9, 110.9, 112.7,

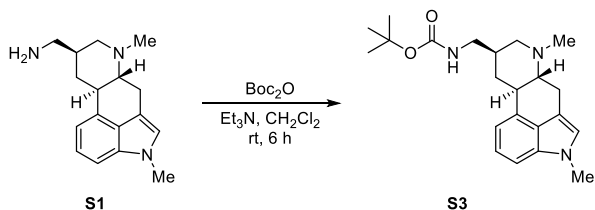
122.7, 122.6, 126.7, 133.8, 134.5. LCMS (ESI) m/z : 270.1965 calculated for $C_{17}H_{24}N_3^+$ ($[M + H]^+$); 270.1962 observed.

Ethyl carbamate ergoline derivative (S2)



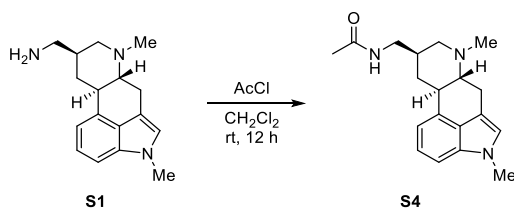
Et_3N (31 μ L, 0.22 mmol) was added to a solution of ethyl chloroformate (31 mg, 0.14 mmol) and amine **S1** (30 mg, 0.11 mmol) in CH_2Cl_2 (5 mL) and the reaction stirred for 6 h at rt. TLC analysis at 4 h indicated that the reaction was complete, and the solution was diluted with CH_2Cl_2 (25 mL), washed with saturated Na_2CO_3 (20 mL), dried over Na_2SO_4 , and concentrated under reduced pressure. Flash chromatography (0 \rightarrow 20% MeOH/ CH_2Cl_2) provided the ethyl carbamate **S2** as a yellow glassy solid (21 mg, 0.062 mmol, 56%). R_f = 0.28 (5% MeOH/ CH_2Cl_2). 1H NMR (700 MHz, $CDCl_3$): δ 7.18 (dd, J = 7.0, 8.1 Hz, 1H), 7.11 (d, J = 8.1 Hz, 1H), 6.90 (d, J = 7.0 Hz, 1H), 6.73 (s, 1H), 4.75 (brs, 1H), 4.17–4.10 (m, 2H), 3.75 (s, 3H), 3.38 (dd, J = 14.5, 4.2 Hz, 1H), 3.23–3.15 (m, 2H), 3.07 (d, J = 10.6 Hz, 1H), 3.00–2.95 (m, 1H), 2.75–2.65 (m, 2H), 2.49 (s, 3H), 2.20–2.10 (m, 2H), 2.00 (app t, J = 10.6 Hz, 1H), 1.26 (t, J = 6.8 Hz, 3H), 1.16 (app q, J = 12.2 Hz, 1H). ^{13}C NMR (125 MHz, $CDCl_3$): δ 156.8, 134.4, 133.2, 126.4, 122.7, 122.5, 112.6, 110.6, 106.8, 67.4, 61.3, 60.9, 44.9, 43.3, 40.4, 36.7, 32.8, 31.9, 26.9, 14.7. LCMS (ESI) m/z : 342.2176 calculated for $C_{20}H_{28}N_3O_2^+$ ($[M + H]^+$); 342.2203 observed.

N-Boc ergoline derivative (S3)



Et₃N (31 μ L, 0.22 mmol) was added to a solution of Boc₂O (31 mg, 0.14 mmol) and amine **S1** (30 mg, 0.11 mmol) in CH₂Cl₂ (5 mL) and the reaction stirred for 6 h at rt. TLC analysis at 6 h indicated that the reaction was complete, and the solution was diluted with CH₂Cl₂ (25 mL), washed with saturated Na₂CO₃ (20 mL), dried over Na₂SO₄, and concentrated under reduced pressure. Flash chromatography (0→20% MeOH/CH₂Cl₂) provided the *t*-butyl carbamate **S3** as a viscous oily solid (32 mg, 0.087 mmol, 86%). R_f = 0.26 (5% MeOH/CH₂Cl₂). ¹H NMR (700 MHz, CDCl₃): δ 7.18 (dd, J = 7.1, 8.1 Hz, 1H), 7.11 (d, J = 8.1 Hz, 1H), 6.90 (d, J = 7.1 Hz, 1H), 6.73 (s, 1H), 4.70–4.59 (brs, 1H), 3.75 (s, 3H), 3.38 (dd, J = 14.5, 4.2 Hz, 1H), 3.23–3.16 (m, 1H), 3.12–3.02 (m, 2H), 2.95 (m, 1H), 2.72–2.64 (m, 2H), 2.47 (s, 3H), 2.16–2.11 (m, 1H) 2.11–2.06 (m, 1H), 1.96 (app t, J = 10.9 Hz, 1H), 1.46 (s, 9H), 1.14 (app q, J = 12.2 Hz, 1H). ¹³C NMR (175 MHz, CDCl₃): δ 156.1, 134.4, 133.3, 126.5, 122.7, 122.5, 112.5, 110.7, 106.8, 79.3, 67.4, 61.5, 44.6, 43.4, 40.5, 36.9, 32.8, 32.0, 28.4 (3C), 27.0. LCMS (ESI) m/z : 370.2489 calculated for C₂₂H₃₂N₃O₂⁺ ([M + H]⁺); 370.2526 observed.

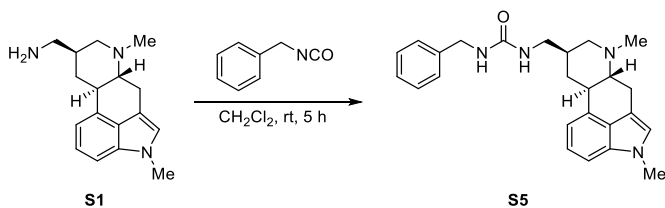
N-Acetyl ergoline derivative (**S4**)



In a modification of a known procedure (Singh, 2014), acetyl chloride (16 μ L, 0.22 mmol) was added to a solution of amine **S1** (30 mg, 0.11 mmol) in CH₂Cl₂ (5 mL) and stirred overnight at rt. After 12 h, the reaction mixture was diluted with CH₂Cl₂

(25 mL), washed with saturated Na_2CO_3 (20 mL), dried over Na_2SO_4 , and concentrated under reduced pressure to give a yellow oil that solidified under vacuum. Flash chromatography (0→20% MeOH/ CH_2Cl_2) provided acetamide **S4** (30 mg, 0.10 mmol, 88%) as an amorphous yellow solid. $R_f = 0.08$ (5% MeOH/ CH_2Cl_2). Mp: 191–194 °C (lit. 191–193 °C) (Singh, 2014). ^1H NMR (700 MHz, CDCl_3): 7.18 (dd, $J = 7.1, 8.2$ Hz, 1H), 7.11 (d, $J = 8.2$ Hz, 1H), 6.89 (d, $J = 7.1$ Hz, 1H), 6.73 (s, 1H), 5.59 (brs, 1H), 3.76 (s, 3H), 3.38 (dd, $J = 14.6, 4.3$ Hz, 1H), 3.29 (A of ABX, $J = 13.5, 6.8$ Hz, 1H), 3.27 (B of ABX, $J = 13.5, 6.0$ Hz, 1H), 3.05 (d, $J = 11.2$ Hz, 1H), 2.97 (ddd, $J = 12.3, 10.6, 3.4$ Hz, 1H), 2.65–2.72 (m, 2H), 2.48 (s, 3H), 2.16 (td, $J = 10.6$ Hz, $J = 4.3$ Hz, 1H), 2.07–2.15 (m, 1H), 2.03 (s, 3H), 1.99 (dd, $J = 11.3, 11.1$ Hz, 1H), 1.17 (q, $J = 12.3$ Hz, 1H). ^{13}C NMR (150 MHz, CDCl_3): 170.2, 134.4, 133.1, 126.4, 122.7, 122.6, 112.5, 110.5, 106.9, 67.4, 61.4, 43.4, 43.3, 40.5, 36.6, 32.8, 32.1, 26.9, 23.4. LCMS (ESI) m/z : 312.2070 calculated for $\text{C}_{19}\text{H}_{26}\text{N}_3\text{O}^+$ ($[\text{M} + \text{H}]^+$); 312.2076 observed.

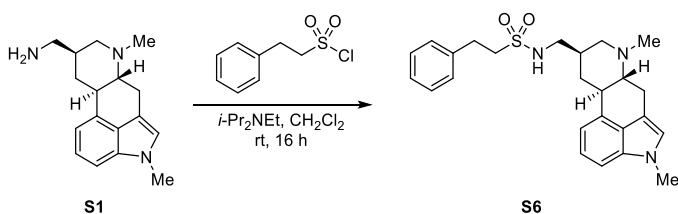
***N*-(*N'*-Benzyl) urea derivative (S5)**



Benzyl isocyanate (15 μL , 0.12 mmol) was added to a solution of amine **S1** (30 mg, 0.11 mmol) in CH_2Cl_2 (5 mL) and stirred at rt for 5 h. The reaction mixture was diluted with CH_2Cl_2 (25 mL), washed with saturated Na_2CO_3 (20 mL), dried over Na_2SO_4 , and concentrated under reduced pressure. Flash chromatography (0→10% MeOH/ CH_2Cl_2) provided the *N*-benzyl urea derivative **S5** as a beige solid (28 mg, 0.069 mmol, 63%). $R_f = 0.12$ (5% MeOH/ CH_2Cl_2). Mp: sintered at 200–205 °C; melted at 265–270 °C (dec). ^1H NMR (700 MHz, CDCl_3): δ 7.32–7.34 (t, 3H), 7.23–7.26 (m, 2H), 7.18 (dd, $J = 7.1, 8.1$ Hz, 2H), 7.11 (d, $J = 8.1$ Hz,

1H), 6.86 (d, $J = 7.1$ Hz, 1H), 6.72 (s, 1H), 4.87 (brs, 1H), 4.61 (brs, 1H), 4.41 (A or ABX, $J = 15.0, 5.9$ Hz, 1H), 4.37 (B or ABX, $J = 15.0, 5.8$ Hz, 1H), 3.75 (s, 3H), 3.37 (dd, $J = 14.5, 4.2$ Hz, 1H), 3.20 (m, 1H), 3.06 (brd, $J = 10.6$ Hz, 1H), 3.02–2.98 (m, 1H), 2.73 (app t, $J = 12.4$, Hz, 1H), 2.62 (d, $J = 12.0$ Hz, 1H), 2.48 (s, 3H), 2.20 (td, $J = 10.6$ Hz, $J = 4.0$ Hz, 1H), 2.15–2.05 (m, 1H), 2.00 (t, $J = 11.4$ Hz, 1H), 1.12 (q, $J = 12.3$ Hz, 1H). ^{13}C NMR (175 MHz, CDCl_3): δ 158.2, 139.2, 134.4, 132.9, 128.7 (2C), 127.5 (2C), 127.4, 126.4, 122.7, 122.6, 112.6, 110.2, 106.9, 67.4, 31.3, 44.7, 44.3, 43.1, 40.2, 36.8, 32.8, 31.9, 26.7. LCMS (ESI) m/z : 403.2492 calculated for $\text{C}_{25}\text{H}_{31}\text{N}_4\text{O}^+$ ($[\text{M} + \text{H}]^+$); 403.2565 observed.

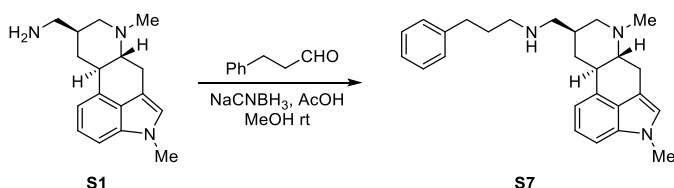
***N*-(2-Phenylethylsulfonyl) ergoline derivative (S6)**



To a solution of amine **S1** (30 mg, 0.11 mmol) and 2-phenylethanesulfonyl chloride (26 mg, 0.13 mmol) in CH_2Cl_2 (5 mL) was added *i*-Pr₂NEt (58 μL , 0.33 mmol). After stirring the reaction mixture at rt for 5 h, it was diluted with CH_2Cl_2 (25 mL), washed with saturated Na_2CO_3 (20 mL), dried over Na_2SO_4 , and concentrated under reduced pressure to give a yellow oily solid. Flash chromatography (0→10% MeOH/ CH_2Cl_2) provided sulfonamide **S6** as a pale yellow amorphous solid (27 mg, 0.062 mmol, 56%). $R_f = 0.24$ (5% MeOH/ CH_2Cl_2). ^1H NMR (600 MHz, CDCl_3): 7.35 (t, $J = 7.5$ Hz, 2H), 7.29–7.25 (m, 3H), 7.18 (dd, $J = 8.2, 7.1$ Hz, 1H), 7.12 (d, $J = 8.2$ Hz, 1H), 6.86 (d, $J = 7.1$ Hz, 1H), 6.73 (s, 1H), 4.10 (brs, 1H), 3.75 (s, 3H), 3.37 (dd, $J = 14.7, 4.4$ Hz, 1H), 3.35–3.31 (m, 2H), 3.18–3.14 (m, 1H), 3.05 (d, $J = 10.6$ Hz, 1H), 3.02–2.90 (m, 3H), 2.72–2.66 (m, 1H), 2.64–2.58 (m, 1H), 2.47 (s, 3H), 2.13 (td, $J = 10.8$ Hz, $J = 4.3$ Hz, 1H), 1.92 (t, $J = 11.3$ Hz, 1H), 1.08 (q, $J = 12.3$ Hz, 1H). ^{13}C NMR (150

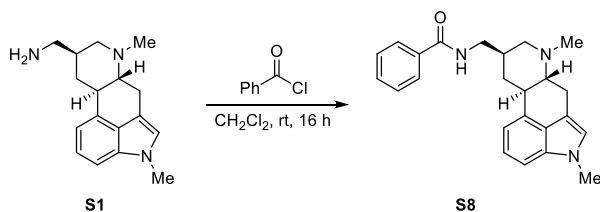
MHz, CDCl₃): 138.0, 134.5, 133.0, 129.2 (2C), 128.6 (2C), 127.3, 126.6, 122.9, 122.7, 112.6, 110.6, 107.0, 67.5, 61.2, 53.7, 47.4, 43.4, 40.5, 36.5, 32.9, 32.0, 30.3, 27.0. LCMS (ESI) *m/z*: 438.2210 calculated for C₂₅H₃₂N₃O₂S⁺ ([M + H]⁺); 438.2301 observed.

***N*-(3-Phenylpropyl) ergoline derivative (S7)**



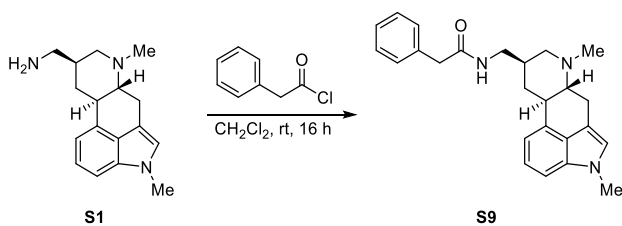
Amine **S1** (36 mg, 0.13 mmol) and 3-phenylpropanal (20 mg, 0.15 mmol) were combined and stirred with Na₂SO₄ (50 mg) in MeOH (5 mL) at rt. After stirring for 15 min, NaCNBH₃ (51 mg, 0.82 mmol) and AcOH (50 μL) were added and the solution stirred at rt for 2 h. The reaction mixture was diluted with CH₂Cl₂ (50 mL), washed with saturated Na₂CO₃ (30 mL), dried over Na₂SO₄, and concentrated under reduced pressure. Flash chromatography (0→20% MeCN/H₂O) provided amine **S7** as an off-white amorphous solid (32 mg, 0.083 mmol, 63%). *R*_f = 0.10 (10% MeOH/CH₂Cl₂). ¹H NMR (600 MHz, CDCl₃): 7.28–7.24 (m, 2H), 7.20–7.15 (m, 4H), 7.09 (d, *J* = 8.2 Hz, 1H), 6.92 (d, *J* = 7.1 Hz, 1H), 6.70 (s, 1H), 3.73 (s, 3H), 3.36 (dd, *J* = 14.6, 4.3 Hz, 1H), 3.22 (brd, *J* = 10.4 Hz, 1H), 3.01 (brt, *J* = 10.4, 3.5 Hz, 1H), 2.78–2.73 (m, 4H), 2.72–2.61 (m, 5H), 2.50 (s, 3H), 2.30–2.22 (m, 1H), 2.21 (td, *J* = 10.7, 4.2 Hz, 1H), 2.02 (t, *J* = 11.7 Hz, 1H), 1.99–1.97 (m, 2H), 1.11 (q, *J* = 12.3 Hz, 1H). ¹³C NMR (150 MHz, CDCl₃): 141.5, 134.3, 133.0, 128.4 (4C), 126.4, 125.9, 122.7, 122.5, 112.7, 110.3, 106.8, 67.4, 61.7, 53.3, 49.0, 43.0, 40.2, 34.9, 33.5, 32.8, 32.5, 30.4, 26.6. LCMS (ESI) *m/z*: 388.2747 calculated for C₂₄H₃₄N₃⁺ ([M + H]⁺); 388.2785 observed.

***N*-Benzoyl ergoline derivative (S8)**



Benzoyl chloride (20 mg, 0.15 mmol) was added to a solution of the amine **S1** (30 mg, 0.11 mmol) in CH_2Cl_2 (5 mL) and stirred overnight at rt. After 16 h, the reaction mixture was diluted with CH_2Cl_2 (25 mL), washed with saturated Na_2CO_3 (20 mL), dried over Na_2SO_4 , and concentrated under reduced pressure. Flash chromatography (0→20% MeOH/ CH_2Cl_2) provided amide **S8** as an amber oily solid (32 mg, 0.085 mmol, 77%). $R_f = 0.20$ (5% MeOH/ CH_2Cl_2). ^1H NMR (700 MHz, CDCl_3): 7.82 (d, $J = 7.3$ Hz, 2H), 7.51 (t, $J = 7.4$ Hz, 1H), 7.45 (dd, $J = 7.3, 7.4$ Hz, 2H), 7.19 (dd, $J = 7.1, 8.2$ Hz, 1H), 7.13 (d, $J = 8.2$ Hz, 1H), 6.90 (d, $J = 7.1$ Hz, 1H), 6.74 (s, 1H), 6.50–6.44 (brs, 1H), 3.75 (s, 3H), 3.55–3.45 (m, 2H), 3.40 (dd, $J = 14.6, 4.3$ Hz, 1H), 3.21 (d, $J = 12.4$ Hz, 1H), 3.14–3.07 (m, 1H), 2.85–2.75 (m, 1H), 2.74 (d, $J = 12.6$ Hz, 1H), 2.54 (s, 3H), 2.39–2.33 (m, 1H), 2.30 (td, $J = 4.4, 10.8$ Hz, 1H), 2.16 (t, $J = 11.4$ Hz, 1H), 1.31 (q, $J = 12.4$ Hz, 1H). ^{13}C NMR (150 MHz, CDCl_3): 167.8, 134.6, 134.4, 132.6, 131.5, 128.6 (2C), 126.9 (2C), 126.4, 122.8, 122.7, 112.6, 110.1, 107.0, 67.4, 61.3, 43.6, 43.0, 40.2, 36.4, 32.8, 32.0, 26.6. LCMS (ESI) m/z : 374.2227 calculated for $\text{C}_{24}\text{H}_{28}\text{N}_3\text{O}^+$ ($[\text{M} + \text{H}]^+$); 374.2296 observed.

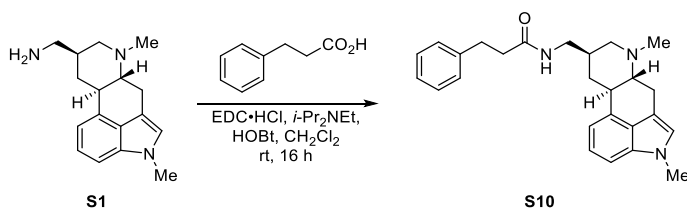
N-Phenylacetyl ergoline derivative (S9)



Phenylacetyl chloride (22 μL , 0.17 mmol) was added to a solution of the amine **S1** (30 mg, 0.11 mmol) in CH_2Cl_2 (5 mL) and stirred overnight at rt. After 16 h, the

reaction mixture was diluted with CH_2Cl_2 (25 mL), washed with saturated Na_2CO_3 (20 mL), dried over Na_2SO_4 , and concentrated under reduced pressure. Flash chromatography (0→20% $\text{MeOH}/\text{CH}_2\text{Cl}_2$) provided amide **S9** as an amorphous pale yellow solid (20 mg, 0.050 mmol, 45%). $R_f = 0.22$ (5% $\text{MeOH}/\text{CH}_2\text{Cl}_2$). ^1H NMR (700 MHz, CDCl_3): 7.38–7.36 (t, $J = 7.5$ Hz, 2H), 7.34–7.28 (m, 3H), 7.18 (dd, $J = 7.1, 8.2$ Hz, 1H), 7.12 (d, $J = 8.2$ Hz, 1H), 6.81 (d, $J = 7.1$ Hz, 1H), 6.73 (s, 1H), 5.75–5.68 (brs, 1H), 3.75 (s, 3H), 3.60 (s, 2H), 3.37 (dd, $J = 14.5, 4.3$ Hz, 1H), 3.31–3.26 (m, 1H), 3.22–3.17 (m, 1H), 3.14–3.04 (m, 2H), 2.86 (app t, $J = 12.7$ Hz, 1H), 2.57–2.53 (m, 1H), 2.55 (s, 3H), 2.38–2.33 (m, 1H), 2.24–2.16 (m, 1H), 2.09 (t, $J = 11.4$ Hz, 1H), 1.13 (q, $J = 12.4$ Hz, 1H). ^{13}C NMR (175 MHz, CDCl_3): 171.3, 135.0, 134.3, 132.0, 129.5 (2C), 129.1 (2C), 128.3, 127.4, 126.2, 122.8, 112.6, 109.5, 107.1, 67.3, 60.7, 43.9, 42.9, 42.5, 39.6, 35.7, 32.8, 31.5, 26.1. LCMS (ESI) m/z : 388.2383 calculated for $\text{C}_{25}\text{H}_{30}\text{N}_3\text{O}^+$ ($[\text{M} + \text{H}]^+$); 388.2448 observed.

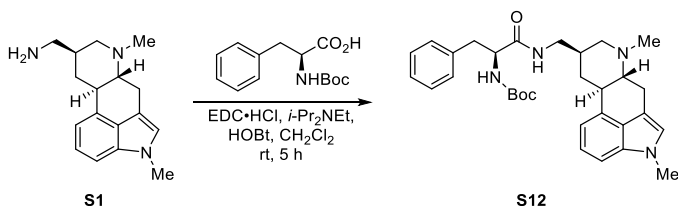
***N*-(3-Phenylpropanoyl) ergoline derivative (S10)**



According to General Procedure A, $i\text{-Pr}_2\text{NEt}$ (58 μL , 0.33 mmol) was added to a solution of amine **S1** (30 mg, 0.11 mmol), $\text{EDC}\cdot\text{HCl}$ (25 mg, 0.13 mmol), HOBT (18 mg, 0.13 mmol), and hydrocinnamic acid (20 mg, 0.13 mmol) in CH_2Cl_2 (5 mL). After stirring the reaction mixture overnight at rt for 16 h, it was diluted with CH_2Cl_2 (25 mL), washed with saturated Na_2CO_3 (20 mL), dried over Na_2SO_4 , and concentrated under reduced pressure to give a yellow solid. Flash chromatography (0→15% $\text{MeOH}/\text{CH}_2\text{Cl}_2$) provided amide **S10** as a pale yellow oil that later solidified (36 mg, 0.089 mmol, 81%). $R_f = 0.19$ (5% $\text{MeOH}/\text{CH}_2\text{Cl}_2$).

^1H NMR (700 MHz, CDCl_3): 7.29 (t, $J = 7.6$ Hz, 2H), 7.23 (d, $J = 7.1$ Hz, 2H), 7.20–7.16 (m, 2H), 7.12 (d, $J = 8.2$ Hz, 1H), 6.85 (d, $J = 7.0$ Hz, 1H), 6.73 (s, 1H), 5.41 (brs, 1H), 3.75 (s, 3H), 3.37 (dd, $J = 14.6, 4.3$ Hz, 1H), 3.27 (dt, $J = 13.7, 6.9$ Hz, 1H), 3.22–3.16 (m, 1H), 3.02–2.97 (m, 2H), 2.94–2.87 (m, 2H), 2.70–2.64 (m, 1H), 2.57–2.47 (m, 3H), 2.44 (s, 3H), 2.11 (td, $J = 10.8$ Hz, $J = 4.3$ Hz, 1H), 2.05–1.95 (m, 1H), 1.89 (t, $J = 11.3$ Hz, 1H), 1.08 (q, $J = 12.3$ Hz, 1H). ^{13}C NMR (175 MHz, CDCl_3): 172.2, 140.9, 134.5, 133.3, 128.7 (2C), 128.5 (2C), 126.6, 126.5, 122.8, 122.7, 112.7, 110.8, 107.0, 67.5, 61.5, 43.5, 43.4, 40.6, 38.7, 36.7, 32.9, 32.2, 31.9, 27.1. LCMS (ESI) m/z : 402.2540 calculated for $\text{C}_{26}\text{H}_{32}\text{N}_3\text{O}^+$ ($[\text{M} + \text{H}]^+$); 402.2536 observed.

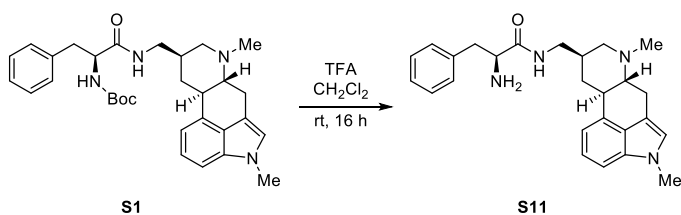
***N*-(*N*-Boc-*L*-Phenylalanyl) ergoline derivative (**S12**)**



According to General Procedure A, *i*-Pr₂NEt (117 μL , 0.67 mmol) was added to a solution of amine **S1** (60 mg, 0.22 mmol), EDC·HCl (51 mg, 0.27 mmol), HOBT (36 mg, 0.27 mmol), and *N*-Boc-*L*-phenylalanine (65 mg, 0.13 mmol) in CH_2Cl_2 (10 mL). After stirring the reaction mixture at rt for 3.5 h, it was diluted with CH_2Cl_2 (25 mL), washed with saturated Na_2CO_3 (20 mL), dried over Na_2SO_4 , and concentrated under reduced pressure to give a yellow oily solid. Flash chromatography (0→10% MeOH/ CH_2Cl_2) provided the *N*-Boc-Phe derivative **S12** as an off-white solid (69.3 mg, 0.13 mmol, 60%). $R_f = 0.19$ (5% MeOH/ CH_2Cl_2). Mp: 210–213 $^\circ\text{C}$. ^1H NMR (700 MHz, CDCl_3): δ 7.31 (t, $J = 7.5$ Hz, 2H), 7.24 (d, $J = 7.3$ Hz, 2H), 7.22–7.16 (m, 2H), 7.11 (d, $J = 8.1$ Hz, 1H), 6.82 (d, $J = 7.0$ Hz, 1H), 6.73 (s, 1H), 5.79 (brs, 1H), 5.10 (brs, 1H), 4.31 (brs, 1H), 3.76 (s, 3H), 3.36 (dd, $J = 14.6, 4.2$ Hz, 1H), 3.23 (dt, $J = 12.9, 6.2$ Hz, 1H), 3.15–3.08 (m, 2H),

3.08–3.00 (m, 1H), 2.89–2.80 (m, 2H), 2.65 (app t, $J = 12.4$, Hz, 1H), 2.42 (s, 3H), 2.08 (td, $J = 10.5$ Hz, $J = 4.0$ Hz, 1H), 2.00–1.91 (m, 1H), 1.83 (t, $J = 11.1$ Hz, 1H), 1.00 (q, $J = 12.2$ Hz, 1H). ^{13}C NMR (175 MHz, CDCl_3): δ 171.3, 155.6, 137.0, 134.5, 133.3, 129.4 (4C), 128.9, 127.3, 126.6, 122.8, 122.6, 112.8, 110.8, 106.9, 80.4, 67.4, 61.4, 43.5, 43.4, 40.6, 38.9, 36.3, 32.9, 32.1, 28.5 (3C), 27.1. LCMS (ESI) m/z : 517.3173 calculated for $\text{C}_{31}\text{H}_{41}\text{N}_4\text{O}_3^+$ ($[\text{M} + \text{H}]^+$); 517.3384 observed.

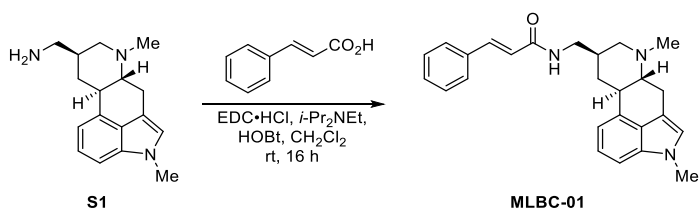
***N*-L-Phenylalanine ergoline derivative (S11)**



TFA (3 mL) was added to a stirring solution of the Boc-protected Phe derivative **S1** (49 mg, 0.12 mmol) in CH_2Cl_2 (10 mL) and the reaction mixture stirred at rt for 2.5 h. The reaction mixture was concentrated under reduced pressure, redissolved in CH_2Cl_2 (25 mL), and washed with saturated Na_2CO_3 (25 mL). The organic solution was dried over Na_2SO_4 , concentrated under reduced pressure, and flash chromatography (0→25% MeOH/ CH_2Cl_2) provided the free amine **S11** as a white amorphous solid (40 mg, 0.095 mmol, 80%). $R_f = 0.30$ (10% MeOH/ CH_2Cl_2). ^1H NMR (600 MHz, CDCl_3): 7.47–7.43 (m, 1H), 7.33 (t, $J = 7.6$ Hz, 2H), 7.27–7.24 (m, 3H), 7.19 (dd, $J = 7.1$, 8.2 Hz, 1H), 7.12 (d, $J = 8.2$ Hz, 1H), 6.85 (d, $J = 7.1$ Hz, 1H), 6.73 (s, 1H), 3.75 (s, 3H), 3.64 (dd, $J = 9.2$, 4.1 Hz, 1H), 3.38 (dd, $J = 14.6$, 4.3 Hz, 1H), 3.33–3.27 (m, 3H), 3.03 (brd, $J = 11.2$ Hz, 1H), 3.00–2.96 (m, 1H), 2.75–2.67 (m, 2H), 2.63 (brd, $J = 12.8$ Hz, 1H), 2.49 (s, 3H), 2.17 (td, $J = 10.7$ Hz, $J = 4.3$ Hz, 1H), 2.15–2.10 (m, 1H), 2.00 (t, $J = 11.4$ Hz, 1H), 1.08 (q, $J = 12.4$ Hz, 1H). ^{13}C NMR (150 MHz, CDCl_3): 174.4, 137.9, 134.4, 133.1, 129.3 (2C), 128.8 (2C), 126.9, 126.4, 122.7, 122.6, 112.6, 110.5,

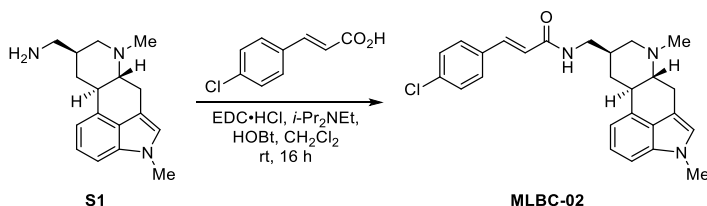
106.9, 67.4, 61.4, 56.6, 43.3, 42.8, 41.1, 40.4, 36.5, 32.8, 32.0, 26.8. LCMS (ESI) m/z : 417.2649 calculated for $C_{26}H_{33}N_4O^+$ ($[M + H]^+$); 417.2723 observed.

***N-trans*-Cinnamoyl ergoline derivative (MLBC-01)**



According to General Procedure A, $i-Pr_2NEt$ (58 μL , 0.33 mmol) was added to a solution of amine **S1** (30 mg, 0.11 mmol), $EDC \cdot HCl$ (25 mg, 0.13 mmol), $HOBT$ (18 mg, 0.13 mmol), and *trans*-cinnamic acid (20 mg, 0.14 mmol) in CH_2Cl_2 (5 mL). After stirring the reaction mixture at rt for 5 h, it was diluted with CH_2Cl_2 (25 mL), washed with saturated Na_2CO_3 (20 mL), dried over Na_2SO_4 , and concentrated under reduced pressure to give a yellow oily solid. Flash chromatography (0→15% $MeOH/CH_2Cl_2$) provided the *N*-cinnamoyl derivative **MLBC-01** as a pale yellow amorphous solid (31 mg, 0.078 mmol, 71%). $R_f = 0.24$ (5% $MeOH/CH_2Cl_2$). 1H NMR (700 MHz, $CDCl_3$): 7.66 (d, $J = 15.6$ Hz, 1H), 7.52 (d, $J = 6.7$ Hz, 1H), 7.40–7.34 (m, 3H), 7.18 (dd, $J = 7.1, 8.2$ Hz, 1H), 7.11 (d, $J = 8.2$ Hz, 1H), 6.91 (d, $J = 7.1$ Hz, 1H), 6.73 (s, 1H), 6.43 (d, $J = 15.6$ Hz, 1H), 5.73 (brs, 1H), 3.76 (s, 3H), 3.48–3.40 (m, 2H), 3.39 (dd, $J = 14.6, 4.3$ Hz, 1H), 3.10 (app d, $J = 11.1$ Hz, 1H), 3.02–1.98 (m, 1H), 2.75–2.67 (m, 2H), 2.49 (s, 3H), 2.23–2.19 (brs, 1H), 2.19 (td, $J = 10.6$ Hz, $J = 4.2$ Hz, 1H), 2.06 (app t, $J = 11.7$ Hz, 1H), 1.23 (q, $J = 12.4$ Hz, 1H). ^{13}C NMR (175 MHz, $CDCl_3$): 166.2, 141.4, 135.0, 134.5, 133.3, 129.8, 129.0 (2C), 128.0 (2C), 126.6, 122.9, 122.7, 120.7, 112.7, 10.8, 107.0, 67.5, 61.6, 43.6, 43.5, 40.7, 37.0, 32.9, 32.3, 27.1. LCMS (ESI) m/z : 400.2383 calculated for $C_{26}H_{32}N_3O^+$ ($[M + H]^+$); 400.2438 observed.

***N*-(4-Chloro-*trans*-cinnamoyl) ergoline derivative (MLBC-02)**



According to General Procedure A, *i*-Pr₂NEt (194 μ L, 1.11 mmol) was added to a solution of amine **S1** (100 mg, 0.37 mmol), EDC·HCl (85 mg, 0.44 mmol), HOBT (60 mg, 0.44 mmol), and 4-chlorocinnamic acid (81 mg, 0.44 mmol) in CH₂Cl₂ (10 mL). After stirring the reaction mixture overnight at rt for 16 h, it was diluted with CH₂Cl₂ (50 mL), washed with saturated Na₂CO₃ (2 \times 40 mL), dried over Na₂SO₄, and concentrated under reduced pressure to give an off-white solid. Flash chromatography (0 \rightarrow 15% MeOH/CH₂Cl₂) provided amide **MLBC-02** as a white solid (133 mg, 0.31 mmol, 83%). ¹H NMR (700 MHz, CDCl₃): 7.60 (d, *J* = 15.6 Hz, 1H, H₂₀), 7.44 (d, *J* = 8.1 Hz, 2H, H₂₂), 7.34 (d, *J* = 8.1 Hz, 2H, H₂₃), 7.18 (dd, *J* = 8.2, 7.1 Hz, 1H, H₁₃), 7.11 (d, *J* = 8.2 Hz, 1H, H₁₄), 6.89 (d, *J* = 7.1 Hz, 1H, H₁₂), 6.73 (s, 1H, H₂), 6.42 (d, *J* = 15.6 Hz, 1H, H₁₉), 5.94–5.87 (brs, 1H, NH), 3.76 (s, 3H, C₁'), 3.46 (dt, *J* = 14.1, 7.2 Hz, 1H, H₈'A), 3.43–3.36 (m, 2H, H₈'B + H₄eq), 3.16 (app d, *J* = 11.2, 1H, H₇eq), 3.08 (brt, *J* = 10.6, 3.1 Hz, 1H, H₁₀), 2.78 (app t, *J* = 12.8 Hz, 1H, H₄ax), 2.72 (brd, *J* = 10.6, 3.1 Hz, 1H, H₉eq), 2.54 (s, 3H), 2.32–2.23 (m, 2H, H₅ + H₈), 2.13 (app t, *J* = 11.2 Hz, 1H, H₇ax), 1.24 (app q, *J* = 12.4 Hz, 1H, H₉ax). ¹³C NMR (150 MHz, CDCl₃): 166.0, 140.1, 135.7, 134.5, 133.4, 132.8, 129.2 (2C), 129.1 (2C), 126.5, 122.9, 122.8, 121.2, 112.7, 110.2, 107.1, 67.6, 61.4, 43.5, 43.2, 40.3, 36.6, 33.0, 32.1, 26.8. LCMS (ESI) *m/z*: 434.1994 calculated for C₂₆H₂₉³⁵Cl N₃O⁺ ([M + H]⁺); 434.21842 observed.

CHAPTER 3 – Targeting two-component systems uncovers a small molecule inhibitor of *Salmonella* virulence

Preface

The work presented in this chapter was previously published in:

Tsai CN, MacNair CR, Cao MPT, Perry JN, Magolan J, Brown ED, Coombes BK. Targeting two-component systems uncovers a small molecule inhibitor of *Salmonella* virulence. *Cell Chemical Biology* (2020) 27, 793-805.

Permission has been granted by the publisher to reproduce the material herein.

I wrote the manuscript with input from Coombes BK. I performed all experiments, with the following exceptions: MacNair CR assisted with screening of the *Salmonella* deletion library (Figure 3.5), Cao MPT and Magolan J synthesized dephostatin (STAR Method, Synthesis of Dephostatin), Perry JN assisted with RT-qPCR experiments (Figure 3.2b).

*References within this and all other chapters have been compiled into one list at the end of the thesis, to avoid redundancy between sections.

Summary

Salmonella serovars are leading causes of gastrointestinal disease and have become increasingly resistant to fluoroquinolone and cephalosporin antibiotics. Overcoming this healthcare crisis requires new approaches in antibiotic discovery and the identification of unique bacterial targets. In this work, we describe a chemical-genomics approach to identify inhibitors of *Salmonella* virulence. From a cell-based, promoter reporter screen of ~50,000 small molecules, we identified dephostatin as a non-antibiotic compound that inhibits intracellular virulence factors and polymyxin resistance genes. Dephostatin disrupts signaling through both the SsrA-SsrB and PmrB-PmrA two-component regulatory systems and restores sensitivity to the last-resort antibiotic, colistin. Cell-based experiments and mouse models of infection demonstrate that dephostatin attenuates *Salmonella* virulence *in vitro* and *in vivo*, suggesting that perturbing regulatory networks is a promising strategy for the development of anti-infectives.

Keywords

Salmonella, SPI-2, antibiotic discovery, anti-virulence, chemical screening, colistin resistance

Introduction

Salmonella enterica serovar Typhimurium (*Salmonella*) is a major cause of gastrointestinal illness in healthy individuals and invasive non-typhoidal disease in immunocompromised adults and young children (Ao et al., 2015). In invasive infections, *Salmonella* infects and replicates within host cells to spread systemically, often requiring antibiotic therapy for resolution (Watson and Holden, 2010). Unfortunately, several first-line treatments for salmonellosis have been compromised by the recent emergence of fluoroquinolone and cephalosporin resistance (Ashton et al., 2017; Phoon et al., 2015; Stanaway et al., 2019), necessitating the discovery of new antibiotic targets to feed the development pipeline.

Traditional antibiotic discovery efforts have aimed to disrupt bacterial viability with bacteriostatic or bactericidal molecules (Lewis, 2013). A complementary strategy is to target bacterial virulence, where the goal of therapy is to attenuate pathogen fitness by disrupting virulence pathways without direct antimicrobial action (Rasko and Sperandio, 2010). Virulence factors and their associated regulatory control systems are often non-essential for bacterial survival and can be species-specific; therefore, anti-virulence agents may exert less selective pressure for resistance evolution and have minimal off-target effects on the host microbiota (Johnson and Abramovitch, 2017). Several previous studies have validated this approach (Amara et al., 2009; Anantharajah et al., 2016; Flores-Mireles et al., 2016; Lin et al., 2012; Oganessian et al., 2014; Sauter et al., 2008; Sully et al., 2014). However, there have been few attempts to identify *Salmonella*-specific anti-virulence agents (Curtis et al., 2014; Felise et al., 2008; Hudson et al., 2007; Negrea et al., 2007; Rooks et al., 2017; Zhang et al., 2018), warranting further research in this area.

In many *Salmonella* serovars, the horizontally acquired pathogenicity island, SPI-2, is essential for virulence (Ochman et al., 1996; Shea et al., 1996). This gene cluster encodes a type three secretion system (T3SS) that translocates over 30 unique protein effectors into host cells during infection (Figueira and Holden, 2012), which protect against the host immune response, modify the intracellular *Salmonella*-containing vacuole, and drive progression of systemic mammalian infection (Knuff and Finlay, 2017). SPI-2 gene expression is controlled by several two-component regulatory systems (TCSs), which have garnered recent attention as attractive targets for anti-virulence therapies due to their importance for gene regulation across bacterial taxa (Bem et al., 2014). Canonical TCSs consist of a histidine kinase that is auto-phosphorylated upon detection of an environmental stimulus, and a response regulator that becomes activated after phosphoryl group transfer (Jacob-Dubuisson et al., 2018).

Salmonella has over 20 TCSs, forming a complex network that regulates SPI-2 and other virulence genes (Ilyas et al., 2017). While the SsrA-SsrB and PhoQ-PhoP TCSs activate SPI-2 in a manner unique to *Salmonella* species (Navarre et al., 2005; Walther et al., 2007; Walther et al., 2011), PhoQ-PhoP and PmrB-PmrA control immune evasion and polymyxin resistance in several Enterobacteriaceae (Chen and Groisman, 2013; Gunn et al., 1998). SsrA-SsrB, PhoQ-PhoP, and PmrB-PmrA are activated in environments with acidic pH and low Mg^{2+} (Kato and Groisman, 2004; Kato et al., 2003; Mulder et al., 2015; Perez and Groisman, 2007), whereas PhoQ-PhoP and PmrB-PmrA individually sense antimicrobial peptides (Bijlsma and Groisman, 2005) and high Fe^{3+}/Al^{3+} (Wösten et al., 2000), respectively. Considering this overlap in signal detection, we aimed to identify chemical inhibitors of one or more of these three TCSs, predicting that disruption of any regulatory protein in these systems would perturb *Salmonella* virulence. Using a canonical SPI-2 promoter as a reporter for input from the SsrA-SsrB, PhoQ-PhoP, and PmrB-PmrA TCSs, we conducted a cell-based chemical

screen of ~50,000 small molecules. We identified the nitrosoaniline compound dephostatin, a *Streptomyces*-derived natural product previously characterized as a eukaryotic protein tyrosine phosphatase (PTP) inhibitor (Fujiwara et al., 1997; Masaya et al., 1993). Dephostatin inhibits both SPI-2 and polymyxin resistance genes, attenuates *Salmonella* virulence in macrophages, and potentiates colistin efficacy *in vitro* and in a murine model of systemic infection. This work suggests that inactivating regulatory signaling is a promising anti-virulence strategy to enhance the efficacy of existing antibiotics while also attenuating bacterial fitness during infection.

Results

Identifying chemical repressors of virulence gene transcription

The TCSs SsrA-SsrB, PhoQ-PhoP, and PmrB-PmrA are attractive anti-virulence targets in *Salmonella* due to their regulation of intracellular virulence (SPI-2) and polymyxin resistance genes. To quantify the fitness benefit conferred by each of these systems *in vivo*, we tested the fitness of single gene deletions in each sensor kinase (Δ ssrA, *phoQ*::Cm, Δ pmrB) and response regulator (Δ ssrB, *phoP*::Cm, Δ pmrA) individually and in competitive infections against a marked wild-type strain (*ushA*::Kn) (Coombes et al., 2005). All regulatory mutants, excluding Δ pmrB, were significantly attenuated in mono-infections of genetically susceptible mice (Figure 3.1a). Similarly, wild-type bacteria significantly out-competed each regulatory mutant in the spleen, and all but *phoQ*::Cm and Δ pmrA in the liver (Supplementary Figure 3.1a). These data are consistent with previous reports (Yoon et al., 2009), and also suggest a more moderate fitness defect of sensor kinase deletions relative to entire TCS mutants. Together, these results indicate that inhibiting TCS function is sufficient to attenuate virulence *in vivo*.

We next sought to establish an approach amenable to high-throughput screening to assess the activity of multiple TCSs with a single reporter. The SPI-2 T3SS is encoded across four operons with 6 distinct promoters (regulatory: *ssrA*, small apparatus: *ssaB*, effector: *sseA*, large apparatus: *ssaG*, *ssaM*, *ssaR*) (Tomljenovic-Berube et al., 2010). Activity of each of these promoters can be induced during growth in acidic media with low Mg^{2+} (LPM), as these environmental cues are sensed by the SsrA, PhoQ, and PmrB sensor kinases (Coombes et al., 2004). We selected *sseA* as a representative SPI-2 gene and monitored its promoter activity over 5 h of growth in LPM using a luciferase transcriptional reporter (*PsseA-lux*) (Figure 3.1b). Consistent with our previous reports (Osborne and Coombes, 2011), we observed that deletions of *ssrA*, *ssrB*, *phoQ*, or *phoP* significantly reduced *sseA* promoter activity relative to wild-type cells. We found that deletions of *pmrB* or *pmrA* also reduced luciferase expression from the *sseA* promoter, revealing a previously unknown regulatory connection. Together, these data validated the use of the *sseA* promoter as a reporter for signaling through multiple TCSs, which we considered the putative targets of our chemical screen.

We next screened 48,787 compounds comprised of diverse synthetic molecules, known bioactive compounds, and natural products, against wild-type *Salmonella* expressing *PsseA-lux*. Of these, 558 compounds inhibited the luminescence signal induced after 5 h of growth in LPM (Supplementary Figure 3.1b). In parallel, we monitored bacterial growth after ~20 h of incubation, leading us to exclude 94 compounds with negative effects on cell viability, which were not our interest (Supplementary Figure 3.1c). We then re-tested 192 of the remaining 464 compounds in dose-response assays and excluded 28 compounds that inhibited bacterial growth in LPM ($IC_{50} \leq 100 \mu M$), 16 compounds that failed to inhibit *PsseA-lux* activity ($\geq 50 \mu M$ required for 50% promoter inhibition), and 11 compounds that inhibited bacterial growth in LB ($IC_{50} \leq 100 \mu M$).

To further prioritize compounds with specificity for SPI-2 inhibition, we monitored the activity of the *hilA* promoter, as this gene is a transcriptional activator of SPI-1 and has not been reported to directly regulate SPI-2 genes (Pérez-Morales et al., 2017). We reasoned that non-specific repressors of bacterial transcription or bioluminescence production would inhibit *PhlA* and *PsseA* induction, and therefore sought to identify compounds with potent inhibitory activity against only *PsseA* (54 compounds). Based on their availability and diversity, 20 compounds were reordered for further experimental validation, of which we excluded 6 compounds with poor solubility, 5 minimally potent compounds against *PsseA-lux* (Supplementary Figure 3.1d), and 3 compounds that inhibited bacterial growth in LPM (Supplementary Figure 3.1e).

Owing to its potency and lack of growth-inhibitory activity, we selected methyl-3,4-dephostatin (hereafter dephostatin) for subsequent mechanistic investigation and examination of *in vivo* efficacy (Figure 3.1c). Dephostatin is a *Streptomyces*-derived molecule with previously characterized inhibitory activity against the eukaryotic PTPs CD45, PTP1B, and SHPTP-1 (Fujiwara et al., 1997; Masaya et al., 1993). Larger quantities of dephostatin were synthesized in-house (see STAR Methods) and confirmed to inhibit *PsseA-lux* with similar potency to commercial stocks.

Dephostatin represses intracellular virulence through SsrB

Our screen and counterselection workflow were designed to enrich for hits that inhibited one of the TCSs with transcriptional input into *sseA*, a proxy virulence gene in our system. To examine the broader activity of dephostatin, we tested the effect of dephostatin treatment on expression of all six promoters in SPI-2 (*ssrA*, *ssaB*, *sseA*, *ssaG*, *ssaM*, and *ssaR*). Dephostatin treatment significantly inhibited the activity of all six promoters, consistent with comprehensive inhibition across

the SPI-2 locus, whereas dephostatin had no effect on the transcriptional activity of an unrelated gene, *ompC*, that is unlinked from SPI-2 and receives transcriptional input from the EnvZ-OmpR TCS (Lee et al., 2000) (Figure 3.2a). In agreement with these data, *ssrA*, *ssaB*, *sseA*, *ssaG*, *ssaM*, and *ssaR* mRNA transcripts were reduced after growth of cells in the presence of dephostatin, whereas dephostatin had no effect on *ompC* transcript levels (Figure 3.2b). To establish a functional growth readout for dephostatin activity, we replaced the *sseA* gene with a chloramphenicol acetyltransferase gene (*cat*) on the chromosome such that chloramphenicol resistance was driven by the native *sseA* promoter (*P_{sseA}-Cm*). Under growth conditions known to activate SsrA-SsrB and SPI-2 gene expression (Coombes et al., 2004), this strain was resistant to chloramphenicol in the absence of dephostatin. However, increasing the concentration of dephostatin suppressed this resistance (Figure 3.2c). Taken together, these findings are consistent with dephostatin acting at or upstream of the SsrA-SsrB TCS to dismantle the signaling network controlling SPI-2 virulence gene expression.

Dephostatin is a low molecular weight, redox-active compound that possesses catechol and nitrosamine moieties (Figure 3.1c). Under acidic and oxidizing conditions, nitric oxide can undergo protonation to dinitrogen trioxide (N₂O₃) via a nitrite intermediate (NO₂⁻) (Herold and Röck, 2005), which has been shown to S-nitrosylate the redox-active thiol of Cys203 in SsrB (Husain et al., 2010). The labile nature of catechol and nitrosamine groups combined with the acidic conditions under which we observed repression of SPI-2 genes led us to speculate that a release of nitric oxide from dephostatin may be partially responsible for its mode of action. To test this, we quantified nitrite liberated from increasing concentrations of dephostatin under our experimental conditions and observed ~125 µM nitrite released after 2 h of incubation in LPM, which remained constant over 20 h (Figure 3.2d). Further, an SsrB_{C203S} variant, which cannot be

S-nitrosylated by reactive NO_2^- (Husain et al., 2010), was resistant to the inhibitory effect of dephostatin on SPI-2 gene expression (Figure 3.2e). Together, these data suggested that the inhibitory activity of dephostatin requires an interaction with SsrB at Cys203.

Since the activity of the SPI-2 T3SS is required for intracellular survival in macrophages (Jennings et al., 2017), we reasoned that any inhibitory effect of dephostatin on SsrA-SsrB signaling would compromise intracellular bacterial survival. In the presence of dephostatin, the number of intracellular *Salmonella* following infection of bone marrow-derived murine macrophages was significantly reduced (Figure 3.2f). Under these culture conditions, dephostatin caused negligible and non-significant host cell cytotoxicity (Figure 3.2g). Taken together, these data indicate that dephostatin inhibits the transcriptional activity of the SPI-2 T3SS, a key intracellular virulence factor in *Salmonella*, thereby compromising intracellular survival.

Dephostatin inhibits non-SPI-2 virulence genes

SsrB controls a large regulon of integrated virulence genes within and outside of SPI-2 (Desai et al., 2016; Ilyas et al., 2018; Tomljenovic-Berube et al., 2010). Since our data strongly suggested that the activity of dephostatin was integrated through SsrA-SsrB signaling, we hypothesized that dephostatin treatment might have a broader effect on the *Salmonella* transcriptome. To investigate this, we sequenced total RNA from *Salmonella* grown under conditions that activate SsrA-SsrB (LPM) and in LB as a control, in the presence or absence of dephostatin. We compared all transcript levels across these conditions, with a focus on a subset of 422 SsrB-regulated genes that we previously annotated as belonging to processes involved in outer membrane biogenesis and modification, transcription, translation, metabolism, motility, and virulence (SPI-1, SPI-2) (Ilyas et al., 2018)

(Figure 3.2). Among the 20% of genes from this annotated subset that were most significantly repressed by dephostatin, 24 genes were associated with SPI-2 and 15 genes were known regulatory targets of the PhoQ-PhoP and PmrB-PmrA TCSs (Chen and Groisman, 2013; Colgan et al., 2016) (Figure 3.3a, Supplementary Figure 3.2). Of note, this pattern of repression was specific to cells grown in LPM and not LB, suggesting an interaction between dephostatin and the TCS regulators required for environmental sensing of acidic pH and low Mg^{2+} .

To confirm these data, we monitored the activity of several PhoP- and PmrA-regulated promoters in dephostatin-treated *Salmonella* grown in LPM to activate sensing by the PhoQ and PmrB sensor kinases (Chen and Groisman, 2013; Coombes et al., 2004): *phoP*, *pagC*, *slyA*, and *pmrD* are all members of the PhoP regulon (Will et al., 2014), while *eptA* and *pbgP* are under the direct control of PmrA (Gunn et al., 1998). We found that dephostatin significantly repressed the promoter activity of the PmrA-regulated genes *eptA* and *pbgP* relative to DMSO-treated cells and had little influence on genes in the PhoP regulon (Figure 3.3b). In agreement with these data, *eptA* and *pbgP* mRNA transcripts were significantly reduced after growth of cells in the presence of dephostatin, whereas dephostatin marginally increased transcript levels of *pmrD*, which is under PmrA-mediated repression (Kato et al., 2003) (Figure 3.3c). Further experiments suggested that the effect of dephostatin on SsrA-SsrB was independent from its interaction with PmrA-regulated genes, because a Δ *ssrB* mutant was not attenuated for *PeptA* activity (Figure 3.3d) and dephostatin repressed the *eptA* and *pbgP* promoters even in a strain expressing SsrB_{C203S} (Figure 3.3e). Lastly, we found that the restoration of neutral pH or high Mg^{2+} levels abrogated *PsseA* (Figure 3.3f) and *PeptA* (Figure 3.3g) repression by dephostatin, indicating that this activity likely required the sensing of both environmental signals. Together, these results were consistent with dephostatin having a second mechanism of action targeting the

PmrB-PmrA regulon, independent of its interaction with SsrA-SsrB. However, we also note that this transcriptomic dataset revealed several significantly repressed genes that appear unrelated to either of these TCSs (Supplementary Figure 3.2), suggesting some off-target activity of dephostatin.

Dephostatin selectively potentiates polymyxin antibiotics against *Salmonella*

In several Enterobacteriaceae, the PmrB-PmrA TCS controls outer membrane modifications that are crucial for polymyxin resistance through chemical modifications to bacterial lipopolysaccharide (LPS) (Chen and Groisman, 2013). Specifically, the PmrA-regulated genes *eptA* (*pmrC*) and *pbgP* (*arnT/pmrK*) regulate the addition of phosphoethanolamine and 4-aminoarabinose to lipid A, altering the charge of the outer membrane to decrease electrostatic attraction to polymyxin antibiotics (Gunn et al., 1998). To examine the secondary activity of dephostatin against the PmrA regulon, we tested dephostatin in combination with colistin, polymyxin B (PMB), and cathelicidin-related antimicrobial peptide (CRAMP), which all induce cellular lysis after interacting with the Gram-negative outer membrane and can be resisted with PmrA-regulated LPS modifications. Interestingly, we observed synergy between dephostatin and all three chemical partners (Figure 3.4a), suggesting that repression of *eptA* and *pbgP* in this system enhances sensitivity to outer membrane perturbation.

We then sought to determine the directionality of potentiation between dephostatin and polymyxins. Specifically, we asked whether (i) dephostatin enhanced sensitivity of polymyxins by repressing PmrA gene targets, or (ii) polymyxins enhanced sensitivity to dephostatin by improving its ability to permeate the bacterial outer membrane. The latter would indicate cryptic antimicrobial activity of dephostatin, consistent with previous reports showing that

outer membrane permeabilization potentiates antibiotics with normally poor activity against Gram-negative bacteria (Brennan-Krohn et al., 2018; Ellis et al., 2019). To address this, we examined the interaction between EDTA or polymyxin B nonapeptide (PMBN) with dephostatin, as both EDTA and PMBN induce outer membrane permeabilization but are distinct from polymyxin antibiotics. EDTA is a non-specific metal chelator that induces outer membrane disruption and is not resisted by PmrA-regulated LPS modifications, while PMBN perturbs the outer membrane without inducing cell lysis and is non-antibacterial (Viljanen and Vaara, 1984). We observed no synergistic interaction between dephostatin in combination with either EDTA or PMBN (Figure 3.4b), validating dephostatin as a bona fide anti-virulence agent.

The ability of dephostatin to potentiate colistin was further confirmed in the invasive, multidrug-resistant ST313 sequence type of *Salmonella* (Figure 3.4c). The ST313 lineage is similar to the ST19 sequence type used in all of our experiments with respect to most SPI-2 and polymyxin resistance determinants, but also shows evidence of genome degradation, harbors several antibiotic resistance genes, and is associated with invasive non-typhoidal infections with very high case fatality rates (Kingsley et al., 2009). Interestingly, we also found that dephostatin-colistin synergy was generally unique to *Salmonella* species. Whereas we observed only modest synergy between dephostatin-colistin against *Yersinia enterocolitica* and *Klebsiella pneumoniae*, we found no synergy between the other Gram-negative bacterial species *Escherichia coli*, *Citrobacter rodentium*, *Pseudomonas aeruginosa* and *Acinetobacter baumannii* (Supplementary Figure 3.3a).

We next screened ~20 additional antibiotics covering several major drug classes for changes in their minimal inhibitory concentration (MIC) in the presence of dephostatin. We observed no potentiation of DNA-damaging molecules,

macrolides, translation inhibitors, beta-lactams, or transcriptional inhibitors (Supplementary Figure 3.3). We note that dephostatin did not synergize with any antibiotics typically restricted to Gram-positive bacteria, supporting our premise that dephostatin exhibits selectivity towards polymyxin antibiotic potentiation due to its inhibitory effect on the PmrA regulon. We also found that this activity was abolished in media with neutral pH or high Mg^{2+} levels (Figure 3.4d), consistent with our expression data (Figure 3.3f, Figure 3.3g), and further suggestive of a specific interaction between dephostatin and the TCSs required to sense these environmental signals.

Chemicals that target the bacterial inner membrane are known to synergize with polymyxin antibiotics (Farha et al., 2013), as well as with other inner membrane disruptors (Sekyere and Amoako, 2017). To exclude disruption of the proton motive force as a potential mechanism of action, we examined the impact of dephostatin on the inner membrane. We determined that dephostatin did not significantly alter fluorescence produced by 3,3'-dipropylthiadicarbo-cyanine iodide (DiSC₃(5)) (Figure 3.4e), a probe that accumulates in the inner membrane in a manner dependent on the proton motive force (Bakker and Mangerich, 1981; Mitchell, 2011). Moreover, dephostatin did not exhibit antibacterial synergy with CCCP, an ionophore that dissipates the proton gradient across the inner membrane (Figure 3.4f). Taken together, these data suggest that dephostatin does not target the bacterial inner membrane, consistent with a selective effect of this compound on TCS inhibition.

Synergy between dephostatin and colistin requires PmrA-regulated genes

Given the therapeutic potential of dephostatin-colistin synergy, we sought to further interrogate the mechanism underlying this combination. For this, we implemented a chemical-genomics approach, predicting that mutants with a

deletion of the gene encoding the secondary target of dephostatin would be sensitized to colistin, and would exhibit no further increase in colistin sensitivity in the presence of dephostatin (El-Halfawy et al., 2019). To test these hypotheses, we screened 3,549 non-essential gene deletion mutants of *Salmonella* (Santiviago et al., 2009), at a subinhibitory concentration of colistin in the presence and absence of dephostatin. We performed these screens in LPM, a minimal media that induces gene expression conferring colistin resistance. In all downstream analyses, we excluded any strain that had fitness defects when grown in LPM, as we have previously reported that this media limits the growth of strains lacking non-essential nutrient biosynthesis, metabolism, and cell envelope homeostasis genes (Ellis et al., 2019) (Supplementary Figure 3.4a).

As an initial data filter, we looked for any mutant that had increased sensitivity to dephostatin alone; however, we observed no significant growth defects for any mutants in the presence of dephostatin relative to no-compound controls (Supplementary Figure 3.4b). We then examined the mutants with increased sensitivity to colistin alone, revealing several mutants in genes regulated by PmrA (*pmrD*, *arnT*, *arnF*, *arnD*, *udg*, *arnA*, *pmrA*), as well as genes involved in motility (*motA*, *fliN*, *flgJ*, *flgE*) and outer membrane integrity (*tolQ*, *bamB*, *pgm*) (Figure 3.5a). Among the mutants with increased sensitivity to colistin, *arnDFT*, *pmrAF*, *phoQ*, *flgE*, *udg*, and *safC* were not further potentiated for colistin sensitivity in the presence of dephostatin (Figure 3.5b). We confirmed the resistance of these mutants to dephostatin-colistin synergy with checkerboard assays (Supplementary Figure 3.4c) and observed the most pronounced loss of potentiation for *arnT*, *phoQ*, *udg*, *arnD*, *pmrA*, *pgm*, and *pmrF* mutants (Figure 3.5c). Excluding *phoQ* and *pgm*, these genes are all regulated by PmrA, supporting our hypothesis that dephostatin disrupts signaling through the PmrB-PmrA TCS to enhance the antibacterial activity of colistin.

We next sought to isolate mutants resistant to the combination of dephostatin and colistin to elucidate the mechanism of action underlying this potentiation. We were unable to produce resistant mutants when plating on solid media containing dephostatin and colistin (~4x MIC), nor after ~30 serial passages (see STAR Methods) (Supplementary Figure 3.5a). However, continued passaging in liquid culture eventually yielded two strains resistant to dephostatin-colistin synergism. Whole genome sequencing revealed that both strains had acquired a single point mutation (L85R) in PmrB (*pmrB*_{L85R}). Of note, a similar mutation in *pmrB* was previously isolated from clinical isolates of colistin-resistant *Klebsiella pneumoniae*, although the mechanism underlying this is currently unknown (Cannatelli et al., 2014).

We transferred *pmrB*_{L85R} into a wild-type *Salmonella* background by allelic replacement and examined the susceptibility of this strain to dephostatin-colistin synergy. Although the PmrB_{L85R}-expressing strain was resistant to colistin-dephostatin synergism, this strain was also inherently more resistant to colistin alone relative to wild-type *Salmonella* (Supplementary Figure 3.5b). These results likely indicated that *pmrB*_{L85R} bypasses the effect of dephostatin to confer high-level colistin resistance through a separate mode of action. In line with this, we determined that the *pmrB*_{L85R} mutant was as susceptible as wild-type *Salmonella* to dephostatin-mediated repression of PmrA-regulated genes (Supplementary Figure 3.5c). To conclude from these findings, we found no evidence for a resistance pathway specific to dephostatin-colistin synergy.

***In vivo* efficacy of dephostatin and colistin in a murine infection model**

Finally, to begin proof of concept studies with dephostatin, we evaluated the efficacy of dephostatin against a systemic *Salmonella* infection as both a monotherapy and in combination with colistin. In these experiments, we

administered dephostatin at the highest concentration possible (5 mg/kg) given water solubility constraints, but selected a colistin concentration equivalent to approximately one quarter of the human equivalent dose (Nation and Li, 2009). Treatment with dephostatin or colistin independently led to $\sim 0.5\text{-log}_{10}$ and $\sim 3.2\text{-log}_{10}$ reductions in bacterial burdens, respectively, relative to vehicle-treated controls (Figure 3.6a). Dephostatin in combination with colistin resulted in a $\sim 4.3\text{-log}_{10}$ decrease in *Salmonella* burden when compared to the vehicle-treated group, and a further, significant $\sim 1.1\text{-log}_{10}$ reduction when compared to the colistin-treated group. Together, these results indicate that dephostatin has the potential for significant dose-sparing of toxic antibiotic partners, like colistin. Indeed, the concentrations of dephostatin and colistin used in our experiments were well-tolerated with no adverse effects on uninfected mice. Importantly, we cannot exclude the possibility of an additional interaction between dephostatin and the host phosphoproteome during these infections, given the previously characterized inhibitory activity of this compound against eukaryotic PTPs (Fujiwara et al., 1997).

We also tested the potential for dephostatin and colistin to prolong survival of *Salmonella*-infected animals. When administered as a monotherapy, dephostatin did not significantly extend animal survival beyond that of the vehicle-treated group. Treatment with colistin extended survival of 87.5% of mice to ~ 5 days post infection and 25% of mice survived to the end of the experiment (Figure 3.6b). However, 62.5% of mice treated with both dephostatin and colistin survived the infection indicating a significant improvement over monotherapy. Of note, in these experiments, treatments were administered beginning at the time of infection; we speculate that improvements in the pharmacokinetic properties of dephostatin would be required if the time before treatment was increased. Together, these results support dephostatin as an anti-virulence agent with the ability to potentiate antibiotic efficacy *in vivo*.

Discussion

The emergence of multidrug-resistant *Salmonella* strains requires the development of new anti-infectives with unique mechanisms of action. In this work, we developed a screen designed to enrich for anti-virulence compounds targeting *Salmonella* signaling pathways required for intracellular survival, and uncovered the nitrosoaniline natural product, dephostatin. Although more work is needed to fully characterize the mode of action of dephostatin, we predict an interaction with SsrB and PmrA to disrupt signaling through both regulons. However, we cannot rule out additional transcriptional inhibitory effects for dephostatin. While a strain expressing SsrB_{C203S} is insensitive to the SPI-2 inhibitory action of dephostatin, it is currently unclear whether this is entirely distinct from the impact of dephostatin on the PmrA regulon. Further, our chemical genomics data suggest that several PmrA-regulated genes are required for dephostatin-colistin synergism, indicating that dephostatin likely influences a master regulatory process upstream of these gene products. Probing the mechanism underlying the broad transcriptional inhibition elicited by dephostatin will require extensive future work, as our results indicate possible multimodal activity.

The previously characterized inhibitory activity of dephostatin against eukaryotic PTPs (Fujiwara et al., 1997; Masaya et al., 1993) suggests that administering this compound to infected macrophages and mice may have impacted host physiology in a bacterial-independent manner. Indeed, recent reports have demonstrated that PTP activity is required for LPS tolerance via TLR4 signaling, and that chemical inhibitors of PTPs, such as dephostatin, restore endotoxin sensitivity (Suzuki et al., 2001). It is possible that this additional mode of action may have contributed to our infection outcomes, as the inhibition of LPS

tolerance in infected macrophages or mice may lead to a hyperinflammatory response following challenge with *Salmonella*, potentially restricting bacterial growth. Further experiments using TLR4-deficient cell lines or animals will aid in determining if signaling through this immunological axis is important for dephostatin activity.

We encountered difficulty in isolating mutants resistant to dephostatin-colistin synergism. The single suppressor mutation we isolated (*pmrB*_{L85R}) was specific to colistin resistance and therefore indirectly bypassed dephostatin activity. While these results complicate our characterization of a potential mode of action, they also provide intriguing evidence to consider anti-virulence agents as ‘resistance-proof’ treatments for infection (Allen et al., 2014). Because dephostatin does not influence bacterial viability and likely has multiple molecular targets, it is possible that selective pressure for resistance evolution is diminished. Indeed, this is consistent with previous literature suggesting that ideal antibiotic agents may circumvent resistance evolution by targeting multiple processes (Silver, 2007; Tyers and Wright, 2019). Further experimental work is required to approximate the strength of selection in this and other combination treatment schemes, but we consider this evidence encouraging to support the development of anti-virulence agents in combination with existing antibiotics.

Colistin is considered an antibiotic of last resort for multidrug-resistant Enterobacteriaceae that fail to respond to conventional treatments (Brennan-Krohn et al., 2018). Concerningly, the therapeutic use of this potent antimicrobial has been increasing, leading to increased levels of colistin resistance. Our work suggests that compounds like dephostatin have the potential to overcome intrinsic polymyxin resistance, and therefore may aid in maintaining the clinical efficacy of this important antimicrobial class. To this end, we present evidence that *in vitro*, the combination of dephostatin with colistin considerably delays the

time required to obtain elevated colistin resistance. We also find that dephostatin is able to potentiate colistin activity even against a multidrug-resistant, ST313 sequence type strain of invasive *Salmonella*. Strains within this lineage are the leading cause of severe bloodstream infections in sub-Saharan Africa (Canals et al., 2019b; Van Puyvelde et al., 2019) and have acquired resistance to multiple first-line antibiotic treatments. Continued research to identify therapeutic options for this global health threat is essential.

Although dephostatin displayed efficacy *in vivo* only in combination with colistin, there is a growing body of work supporting the potential of anti-virulence molecules as antibiotic adjuvants (El-Halfawy et al., 2019; Harris et al., 2014; Kirienko et al., 2019). This approach is particularly suited to last-resort antibiotics that have problematic safety profiles as monotherapies; for example, co-administering dephostatin with colistin allowed for a favorable outcome during murine salmonellosis despite colistin dose sparing to one quarter the human-equivalent dose. The therapeutic potential of dosing regimens that reduce the frequency or concentration of colistin required for infection treatment cannot be overstated. Our findings complement a number of recently reported colistin adjuvants that disarm intrinsic or acquired resistance, or are independently antibacterial (Barker et al., 2017; Harris et al., 2014; MacNair et al., 2018; MacNair et al., 2020; Stokes et al., 2017; Zimmerman et al., 2020). Combinations of this nature are a particularly promising therapeutic strategy in the antibiotic resistance era, and further studies will be required to determine the clinical significance of dephostatin-colistin synergism.

Our approach validates the utility of a high-throughput, reporter-based assay to identify small molecules that suppress multiple virulence factors. While it is difficult to completely abolish *Salmonella* virulence with the repression of any single gene, targeting top-level TCS regulators provides an opportunity to

simultaneously inhibit several virulence determinants within the same regulatory network. For this reason, dephostatin is uniquely positioned amongst anti-virulence agents, with an ability to suppress SPI-2 genes but also potentiate polymyxin antibiotics. Chemical compounds with similar activity profiles may be particularly useful to treat systemic infections with heterogeneous virulence gene expression, in which bacterial sub-populations in different host sites may require different virulence processes for survival (Tsai and Coombes, 2019). To this end, leveraging our existing knowledge of the regulatory networks required for bacterial virulence across cellular compartments and tissues will aid in the development of effective anti-virulence therapies. Indeed, several recent studies have laid the foundation for future discovery in this chemical space, identifying a number of chemical compounds that inhibit master regulators of virulence (Carabajal et al., 2020; El-Halfawy et al., 2019; Gao et al., 2018; Rasko et al., 2008; Starkey et al., 2014; Zheng et al., 2016). Continued research in this area is essential to continue yielding new anti-infectives that broadly inhibit bacterial virulence.

Significance

There is an urgent need to discover and develop new anti-infective agents. The shortage of antibiotics under development is an acute problem for the Gram-negative pathogen *Salmonella* Typhimurium, which now has high-priority status for new drug development. Here, we describe a chemical-genomics approach to identify inhibitors of key virulence pathways in *Salmonella*. We uncover the nitrosoaniline natural product dephostatin, which we show to suppress intracellular virulence in *Salmonella* through perturbation of the two-component system, SsrA-SsrB. Further, we show that dephostatin also disrupts the activity of the PmrB-PmrA two-component system that controls outer membrane modifications required for polymyxin resistance. Accordingly, we discover that

dephostatin sensitizes *Salmonella* to the last-resort antibiotics colistin and polymyxin B and find that co-administration of dephostatin and colistin in a mouse model of lethal *Salmonella* infection significantly prolongs animal survival while considerably dose-sparing colistin. This work exemplifies the therapeutic potential of disrupting regulatory signaling to attenuate bacterial virulence, thereby enabling new drug combinations to emerge.

Acknowledgements

We are grateful to W. Elhenawy, D. Little, and R. Gordzevich for helpful discussions of this work. We thank the McMaster Genome Facility for performing RNA and genome sequencing, the McMaster Centre for Microbial Chemical Biology for assistance with high-throughput screening, and J. Hinton for providing the D23580 *Salmonella* strain. C.N.T. and C.R.M. were supported by Frederick Banting and Charles Best Canada Graduate Scholarships. Chemical synthesis was supported by McMaster's Faculty of Health Sciences and a generous endowed gift from the Boris Family. This work was supported by grants to B.K.C. from the Canadian Institutes of Health Research (FRN-156361) and from the Boris Family Fund for Health Research Excellence.

Author Contributions

Conceptualization, C.N.T. and B.K.C.; Methodology, C.N.T. and B.K.C.; Investigation, C.N.T., C.R.M., M.P.T.C., J.N.P.; Resources, J.M., E.D.B., B.K.C.; Writing – Original Draft, C.N.T. and B.K.C.; Writing – Review & Editing, C.N.T., C.R.M. and B.K.C.; Supervision, B.K.C.; Funding Acquisition, B.K.C.

Declaration of Interests

The authors declare no competing interests.

STAR Methods

RESOURCE AVAILABILITY

Lead Contact

Further information and requests for resources and reagents should be directed to and will be fulfilled by the Lead Contact, Brian Coombes (coombes@mcmaster.ca).

Materials Availability

All unique/stable reagents generated in this study are available from the Lead Contact without restriction.

Data and Code Availability

The accession number for the RNA-sequencing dataset reported in this paper is GEO: GSE147414. The accession number for the whole-genome sequencing dataset reported in this paper is SRA: PRJNA613819.

EXPERIMENTAL MODEL AND SUBJECT DETAILS

Bacterial Strains and Culture Conditions

All experiments with *Salmonella* were performed with strain SL1344 or derivatives unless otherwise noted. Routine propagation of bacteria was in LB media (10 g/L NaCl, 10 g/L Tryptone, 5 g/L yeast extract) supplemented with appropriate antibiotics (streptomycin, 100 µg/ml; chloramphenicol, 34 µg/ml; gentamicin, 15 µg/ml; kanamycin, 50 µg/ml; ampicillin, 100 µg/ml). Where indicated, bacteria were sub-cultured 1:50 and grown in LPM (referred to as acidic pH low Mg²⁺ media) (5 mM KCl, 7.5 mM (NH₄)₂SO₄, 0.5 mM K₂SO₄, 80

mM MES pH 5.8, 0.1% casamino acids, 0.3% (v/v) glycerol, 24 μM MgCl_2 , 337 μM PO_4^{3-}) or LPM pH 7.4 (referred to as neutral pH low Mg^{2+} media) (5 mM KCl, 7.5 mM $(\text{NH}_4)_2\text{SO}_4$, 0.5 mM K_2SO_4 , 100 mM Tris pH 7.4, 0.1% casamino acids, 0.3% (v/v) glycerol, 24 μM MgCl_2 , 337 μM PO_4^{3-}). Where indicated, 10 mM MgCl_2 was added to LPM (referred to as acidic pH high Mg^{2+} media). Bacteria were grown at 37°C.

Mice

All animal experiments were performed according to the Canadian Council on Animal Care guidelines using protocols approved by the Animal Review Ethics Board at McMaster University under Animal Use Protocol #17-03-10. Six- to ten-week-old female C57BL/6 mice were purchased from Charles River Laboratories and were used for all murine infections or for isolation of murine bone marrow-derived macrophages. Mice were stored in a Biosafety Level 2 SPF barrier facility at the McMaster Central Animal Facility. Mice were fed a regular chow diet *ad libitum*. Before all infections and treatments, mice were relocated at random from a housing cage to treatment or control cages.

Cell Culture

Cells were maintained in a humidified incubator at 37°C with 5% CO_2 . RAW264.7 macrophages were grown in DMEM containing 10% FBS (Gibco) and seeded in tissue culture-treated 96-well plates (Corning) 20 h prior to infection. Bone marrow-derived macrophages were collected from the femur and tibia of mice and maintained in RPMI containing 10% FBS (Gibco), 10% L929 fibroblast conditioned media, and 100 U penicillin-streptomycin. Cells were differentiated for 7 days in 150 mm Petri dishes, then lifted with ice-cold PBS for seeding in tissue culture-treated 96-well plates (Corning) 20 h prior to infection. L929 fibroblast conditioned media was collected from the supernatants of L929 fibroblasts grown in DMEM with 10% FBS for ten days.

METHOD DETAILS

Cloning and Mutant Generation

Primers for cloning and mutant generation are listed in Table 3.1. All DNA manipulation procedures followed standard molecular biology protocols. Primers were synthesized by Sigma-Aldrich. PCRs were performed with Phusion, Phire II, or Taq DNA polymerases (ThermoFisher). All deletions were confirmed by PCR and verified by DNA sequencing performed by Genewiz Incorporated. Unmarked, in-frame gene deletions were generated via homologous recombination from a suicide plasmid as described previously (Coombes et al., 2007). Briefly, ~500 bp upstream and downstream of each target gene were PCR-amplified and spliced together by overlap-extension PCR. The resulting deletion allele was cloned into the KpnI/SacI digested suicide plasmid pRE112 (Edwards et al., 1998), then transformed into SM10 λ *pir* to create a donor strain for conjugation. Deletion constructs were introduced into wild-type *Salmonella* via conjugal transfer and merodiploids were first selected on chloramphenicol, followed by selection for mutants using SacB-based counterselection on 5% (w/v) sucrose. For generation of P*sseA*-Cm, ~500 bp upstream of *sseA*, a promoterless chloramphenicol resistance cassette, and ~500 bp downstream of *sseA* were PCR-amplified and spliced together by overlap-extension PCR. This allele was subsequently used for allelic exchange. Similar methods were used for the generation of the *ssrB*_{C203S} and *pmrB*_{L85R} strains, in which the indicated point mutations were introduced by overlap-extension PCR and chromosomally replaced by allelic exchange. Transcriptional reporters were generated by cloning ~500-800 bp regulatory regions upstream of query genes from SL1344 into the BamHI/SnaBI-digested pGEN-*luxCDABE* plasmid (Lane et al., 2007). Sequence-verified plasmids were transformed into wild-type SL1344.

Survival and Competitive Indices of Mutants

Mice were infected intraperitoneally (i.p.) with $\sim 10^5$ CFU *Salmonella* in 0.1 M Hepes (pH 8.0) with 0.9% NaCl. For survival experiments, mice were euthanized at clinical endpoint, determined using body condition scoring analyzing weight loss, reduced motility, and hunched posture. For competitive infections, the inoculum was comprised of a 1:1 ratio of a marked wild-type strain resistant to kanamycin (*ushA::Kn*) (Coombes et al., 2005) and a second competing mutant strain. At ~ 60 -70 h after infection, mice were euthanized and the spleen and liver were homogenized in cold PBS, serially diluted, and plated on LB medium containing streptomycin for determination of total CFU. Colonies were replica-plated under kanamycin selection for enumeration of SL1344 *ushA::Kn*. The

competitive index was calculated using the formula:
$$\frac{\left[\frac{\text{mutant}}{\text{wt}}\right]_{\text{output}}}{\left[\frac{\text{mutant}}{\text{wt}}\right]_{\text{input}}}$$

Transcriptional Reporter Assays

Wild-type or mutant *Salmonella* was transformed with the pGEN-*luxCDABE* plasmid (Lane et al., 2007) containing various promoters. Cells were grown in LB until mid-log phase, then sub-cultured 1:50 into LPM, following which luminescence and OD₆₀₀ were read every hour for 5 h. Luminescence (RLU) was normalized to OD₆₀₀. When individual time points are not shown, normalized RLU reflects luminescence/OD₆₀₀ values at 0 h subtracted from those at 5 h. For all assays, DMSO and dephostatin concentrations were 0.25% and 32 $\mu\text{g/ml}$, respectively.

Chemical Screening

All high-throughput compound screening was performed at the Centre for Microbial Chemical Biology (McMaster University). The chemical library screened contained 48,787 diverse small molecules assorted from Sigma-Aldrich, MicroSource, and Enamine. An overnight culture of *Salmonella* *PsseA-lux* was sub-cultured $\sim 1:50$ in LB with 100 $\mu\text{g/ml}$ ampicillin and grown for 2-2.5 h. This

culture was diluted ~1:100 into LPM and dispensed into 384-well black, clear flat-bottom (Corning) plates to a final volume of 30 μ L per well. 60 nL of each compound (5 mM stocks) was added (Echo 550 Liquid Handler) for a final concentration of 10 μ M compound per well. OD₆₀₀ and luminescence were read immediately after compound addition, after 5-6 h, and again after 18-22 h. Plate and well effects were normalized by interquartile-mean based methods (Mangat et al., 2014) and compounds reducing growth more than 2.25 s.d. below the mean were considered actives. Screening was performed in duplicate.

RNA Isolation and RT-qPCR

Wild-type *Salmonella* was grown in LB until mid-log phase, then sub-cultured 1:100 into LPM and grown in the presence of DMSO (0.25%) or dephostatin (32 μ g/ml) for 5-6 h. 5 ml of each strain was pelleted by centrifugation and resuspended in 1 ml Trizol (Invitrogen) for cell lysis. RNA was extracted by chloroform (BioShop) separation following the manufacturer's protocol, precipitated with 100% isopropanol (BioShop) and washed with 75% ethanol (Sigma) before treatment with Dnase I (Turbo DNA-free kit). DNase I was inactivated with 2.5 mM EDTA and RNA was resuspended in DEPC water. For RT-qPCR experiments, cDNA was synthesized from purified RNA using qScript cDNA Supermix (Quantabio) and diluted 1:10 before use. The housekeeping gene *16S* was used for normalization, RT-qPCR was performed in a LightCycler 480 (Roche) with PerfeCTa SYBR Green Supermix (Quantabio). For all experiments, normalized ratios (dephostatin/DMSO) were calculated relative to *16S* transcript levels.

Growth Curves

Strains were grown until mid-log phase in LB, then diluted 1:100 into LPM. OD₆₀₀ was measured at 15 min intervals for ~24 h using a Tecan Sunrise. For

experiments with PsseA-Cm, media was supplemented with 10 µg/ml chloramphenicol and dephostatin at the indicated concentrations.

Measurement of Nitric Oxide

Two-fold serial dilutions of dephostatin (beginning at 64 µg/ml) and sodium nitrite (beginning at 250 µM) were made in LPM and mixed with equal volumes of 1x Griess reagent (Sigma) for a final volume of 100 µL/well in black 96-well clear flat bottom plates (Corning). Plates were incubated in the dark at room temperature for 10 min, then absorbance was read at 540 nm (Biotek Neo). Readings were taken continuously every 10 min for 3 h, then again after incubation overnight (~20 h). Absorbance values for sodium nitrite were used to generate a standard curve and approximate nitrite levels in wells containing dephostatin.

Intracellular Replication Assays

Differentiated bone marrow-derived macrophages were seeded 20 h prior to infection at $\sim 10^5$ cells per well in RPMI containing 10% FBS (Gibco) with 100 ng/ml LPS from *Salmonella enterica* serovar Minnesota R595 (Millipore). Overnight cultures of wild-type SL1344 were diluted to obtain a multiplicity of infection of $\sim 50:1$ and added to each well. Plates were spun down at 500 x g for 2 min, then incubated for 30 min at 37°C with 5% CO₂. Media was aspirated and replaced with fresh RPMI with 10% FBS and 100 µg/ml gentamicin to kill extracellular bacteria for 30 min at 37°C with 5% CO₂. Again, media was aspirated, wells were washed 3 times with PBS, and 200 µL fresh RPMI with 10% FBS containing DMSO or dephostatin at 16, 32, 64, or 128 µg/ml was added to each well. At this time or 6 h later, media was aspirated, wells were washed once in PBS, then adhered macrophages were lysed in sterile water. Bacterial colony-forming units (CFUs) from each lysed well were enumerated by serially diluting in PBS and plating on LB plates. Fold change in CFU (CFU at 6 h divided by at 0 h) was calculated to represent replication over the course of the experiment.

Cytotoxicity Assays

RAW264.7 macrophages were left to adhere for 20 h at $\sim 10^5$ cells per well in DMEM containing 10% FBS (Gibco). Dephostatin was premixed into DMEM then added to wells. After 4 h of treatment, the culture supernatant was collected for analysis of lactate dehydrogenase release. Cytotoxicity was quantified colorimetrically (Pierce LDH cytotoxicity kit) wherein LDH activity is measured by subtracting A_{490} from A_{680} . Lysis control wells were treated with 10X lysis buffer for 1 hour. Percent cytotoxicity was calculated with the formula:

$$\frac{LDH_{Compound\ Treated} - LDH_{Spontaneous}}{LDH_{Maximum} - LDH_{Spontaneous}} \times 100\%$$

where $LDH_{Spontaneous}$ is the amount of LDH activity in the supernatant of untreated cells and $LDH_{Maximum}$ is the amount of LDH activity in the supernatant of lysis control wells. The LDH activity in cell-free culture medium was subtracted from each value prior to normalization.

RNA-sequencing

Purified RNA was analyzed with a BioAnalyzer chip and treated with RiboZero for rRNA depletion, cDNA was barcoded for each sample. cDNA was sequenced on an Illumina HiSeq 2000 platform with single-end reads. Raw reads were processed with FastQC and trimmed with Cutadapt (Martin, 2011) to remove Truseq adapter sequences. Sequencing data was aligned against the reference genome for *Salmonella* (NC_016810) using BWA (mem algorithm) (Koehors et al., 2017) and analyzed using featureCounts (Liao et al., 2014) and the R package DESeq2 (Love et al., 2014).

Chequerboard Broth Microdilution Assays

8x8 matrices of compound were created in 96-well plates with two-fold serial dilutions of each compound at 8 concentrations. After overnight growth in LB, bacteria were diluted 1:5000 into LPM and added to each well of the 8x8 matrix.

After addition of bacteria, plates were incubated at 37°C for ~18-22 h, before and after which the OD₆₀₀ was measured. At least two biological replicates were performed for each assay.

DiSC₃(5) Assay

Cells were grown to late-log phase (OD₆₀₀ ~ 1) in MHB supplemented with 5 mM EDTA, as outer membrane disruption is required for the highly lipophilic 3'3'-dipropylthiadicarbocyanine iodide (DiSC₃(5)) to access the cytoplasmic membrane. Cells were harvested by centrifugation, washed twice in buffer (5 mM HEPES pH 7.0, 20 mM glucose), and resuspended in buffer to a final OD₆₀₀ of 0.085 with 1 µM DiSC₃(5) before incubation for 30 min at 37°C. 75 µL of DiSC₃(5)-loaded cells was then added to two-fold dilutions of dephostatin or colistin in 96-well black clear-bottom plates (Corning) and fluorescence (excitation = 620 nm, emission = 685 nm) was read immediately after using a Tecan M1000 Infinite Pro plate reader. The fluorescence intensity was stable for at least 15 min when the plate was shielded from light.

Genetic Screening

The *Salmonella* single-gene deletion (SGD) library was pinned from frozen DMSO stocks at 384-colony density onto LB agar medium containing 50 µg/ml kanamycin using a Singer RoToR HDA (Singer Instruments) and grown for 20 h at 37°C. The SGD was then grown overnight in 384-well clear flat-bottom plates (Corning) in LB supplemented with 50 µg/ml kanamycin (30 µL/well). The Singer RoToR HDA was used to inoculate assay plates containing 30 µL/well LPM alone or supplemented with dephostatin (64 µg/ml), colistin (8 µg/ml), or dephostatin and colistin (64 and 8 µg/ml, respectively). Optical density at 600 nm (OD₆₀₀) was measured with a Tecan M1000 Infinite Pro plate reader at the time of inoculation (T₀) and after ~20 h (T₂₀) of incubation at 37°C. Growth was calculated by

subtracting reads at T_0 from those at T_{20} . Experiments were performed in duplicate.

Suppressor Isolation and Variant Analysis

Spontaneous resistant mutants were selected for by serial passage in liquid culture. A single colony of wild-type SL1344 was grown overnight in LPM at 37°C. The susceptibility of this strain to colistin was repeatedly tested by diluting bacteria 1:2000 into 200 µL LPM per well of 96-well microtiter plates, containing two-fold serial dilutions of colistin, beginning at 256 µg/ml. Every other day, the highest well with observable growth was sub-cultured and grown overnight in LPM containing 8 µg/ml dephostatin and the corresponding colistin concentration at which growth was observed. Serial passaging was done in duplicate. When strains displayed resistance to >256 µg/ml colistin, genomic DNA was extracted using the QIAamp DNA mini kit (Qiagen). Samples were sequenced on a MiSeq 2x250 platform with paired-end reads. Raw reads were processed with FastQC and trimmed with Cutadapt (Martin, 2011) to remove Nextera transposase sequences. Sequencing data was aligned against the reference genome for *Salmonella* (NC_016810) and analyzed using breseq (Barrick et al., 2014) in polymorphism mode with default settings.

Treatment of Infected Animals

Mice were infected intraperitoneally (i.p.) with $\sim 10^5$ CFU *Salmonella* (SL1344) in 0.1 M HEPES (pH 8.0) with 0.9% NaCl. Groups of mice were administered treatments every 24 h by i.p. injection beginning at the time of infection. 5% DMSO in water was given to vehicle control groups of mice, dephostatin solubilized in 5% DMSO in water was administered at 2.5 or 5 mg/kg, and colistin solubilized in water was administered at 5 or 10 mg/kg. Experimental endpoint was defined as 60 h post-infection for CFU determination, at which *Salmonella*-infected mice exhibited ~ 10 -12% weight loss and displayed signs of clinical

illness. For these experiments, mice were euthanized, and the spleen and liver were homogenized in cold PBS, serially diluted, and plated on LB medium containing streptomycin for determination of total CFU. Clinical endpoint in survival experiments was determined using body condition scoring analyzing weight loss, reduced motility, and hunched posture.

Synthesis of Dephostatin

Dephostatin (compound 5, 3,4-Dihydroxy-*N*-methyl-*N*-nitrosoaniline) was synthesized from 4-nitrocatechol (compound 1) via the intermediate compounds 2 (3,4-Bis[(*tert*-butyldimethylsilyl)oxy]nitrobenzene), 3 (3,4-Bis[(*tert*-butyldimethylsilyl)oxy]-*N*-methylaniline), and 4 (3,4-Bis[(*tert*-butyldimethylsilyl)oxy]-*N*-methyl-*N*-nitrosoaniline), using the route shown in Supplementary Figure 3.6. For the following description of synthesis procedures, all chemical shifts in ^1H NMR and ^{13}C NMR spectra are reported in parts per million (ppm) relative to tetramethylsilane (TMS), with calibration of the residual solvent peaks according to values previously reported (Gottlieb et al., 1997) (chloroform: δ_{H} 7.26, δ_{C} 77.16; acetone: δ_{H} 2.05, δ_{C} 29.84, 206.26). When peak multiplicities are given, the following abbreviations are used: s, singlet; d, doublet; t, triplet; q, quartet; sept., septet; dd, doublet of doublets; m, multiplet; br, broad; app., apparent; *gem*, geminal. ^1H NMR and ^{13}C spectra were recorded at 700 MHz and 175 MHz, respectively, with a digital resolution (Brüker parameter: FIDRES) of 0.15 Hz/point and coupling constants reported herein therefore have uncertainties of ± 0.3 Hz. Reactions were carried out at room temperature (rt) if temperature is not specified. Unless otherwise noted, an automated flash chromatography system (Teledyne CombiFlash Rf 200) was used for the purification of compounds on silica gel (either 40–60 μM or 20–40 μM particle size). Low Resolution Mass Spectrometry (LRMS) measurements were recorded on an Advion Expression CMS Compact Mass Spectrometer. Compound 2: A solution of 4-nitrocatechol (compound 1) (0.994 g, 6.407 mmol), *tert*-

butylchlorodimethylsilane (TBS-Cl, 2.414 g, 16.02 mmol), imidazole (1.090 g, 16.02 mmol) and dimethylaminopyridine (DMAP, 0.020 g, 0.164 mmol) in DMF (12.5 ml) was stirred at rt for 16 h. The reaction was poured into water (70 ml) and extracted with EtOAc (3 × 50 ml). The organic layers were combined and washed with water (3 × 50 ml), dried over Na₂SO₄, and concentrated *in vacuo* to an orange oil. Flash chromatography (0:100→10:90 EtOAc/Hex) provided the TBS-protected catechol compound 2 as a pale yellow solid (2.34 g, 6.09 mmol, 95%). *R_f* = 0.69 (EtOAc/Hex 10:90). ¹H NMR (700 MHz, CDCl₃): δ 0.25 (s, 6H, one of Si(CH₃)₂), 0.26 (s, 6H, one of Si(CH₃)₂), 0.99 (s, 9H, one of SiC(CH₃)₃), 1.00 (s, 9H, one of SiC(CH₃)₃), 6.87 (d, *J* = 8.9 Hz, 1H, ArH), 7.71 (d, *J* = 2.8 Hz, 1H, ArH), 7.77 (dd, *J* = 8.9 Hz, *J* = 2.8 Hz, 1H, ArH). ¹³C NMR (175 MHz, CDCl₃): δ -3.9 (2C), -4.0 (2C), 18.6, 18.7, 25.9 (3C), 26.0 (3C), 116.4, 117.9, 120.1, 141.8, 147.2, 153.8. LRMS (APCI) *m/z*: 384.2 calcd for C₁₈H₃₄NO₄Si₂ (M + H); 384.3 obsd. All data were in accordance with the literature (Li et al., 2012).

Compound 3: 2-Propanol (14 ml) was added to a two-neck flask containing 10% Pd/C (0.307 g, 2.89 mmol). A solution of ammonium formate (0.994 g, 15.8 mmol) in water (1.39 ml) was transferred to the same flask. The reaction mixture was stirred for 2 mins to activate Pd/C. Next, the nitroarene compound 2 (0.403 g, 1.050 mmol) and HCHO (37% solution in water, 0.83 ml, 10.0 mmol) were added. The reaction mixture was degassed to remove oxygen, and stirred under nitrogen flow overnight at rt. The Pd/C catalyst was then removed by filtration through Celite and the filtrate concentrated by rotary evaporation. The resulting mixture was diluted with CH₂Cl₂ (20 ml), washed with brine (20 ml), dried over Na₂SO₄, and concentrated *in vacuo* to a dark brown oil. Flash chromatography (0:100→10:90 EtOAc/Hex) provided the *N*-methylaniline derivative 3 as a brown oil (67 mg, 0.26 mmol, 26%). *R_f* = 0.25 (EtOAc/Hex 10:90). ¹H NMR (700 MHz, CDCl₃): δ 0.15 (s, 6H, one of Si(CH₃)₂), 0.19 (s, 6H, one of Si(CH₃)₂), 0.97 (s, 9H, one of SiC(CH₃)₃), 0.98 (s, 9H, one of SiC(CH₃)₃), 2.76 (s, 3H, NHCH₃), 6.12 (dd, *J* = 8.6 Hz, *J* = 2.8 Hz, 1H, ArH), 6.17 (d, *J* = 2.8 Hz, 1H, ArH), 6.67 (d, *J* = 8.6

Hz, 1H, ArH). LRMS (APCI) m/z : 368.2 calcd for $C_{19}H_{38}NO_2Si_2$ (M + H); 368.5 obsd. All spectral data were in accordance with the literature (Byun et al., 2007).

Compound 4: To a solution of aniline (compound 3) (0.401 g, 1.091 mmol) in THF (42 ml) were added 1 M HCl (10.1 ml) and $NaNO_2$ (90.3 mg, 1.309 mmol) successively at 0 °C. The solution was stirred at 0 °C for 3.5 h before the organic solvent was removed by rotary evaporation. The aqueous mixture was extracted with CH_2Cl_2 (2 × 40 ml) and the combined organic extracts were dried over Na_2SO_4 and concentrated *in vacuo* to a dark-brown oil. Flash chromatography (0:100→5:95 EtOAc/Hex) provided the *N*-nitroso compound 4 as a brown powder (365 mg, 0.921 mmol, 84%). R_f = 0.58 (EtOAc/Hex 10:90). 1H NMR (700 MHz, $CDCl_3$): δ 0.22 (s, 12H, 2 × $Si(CH_3)_2$), 0.99 (s, 9H, one of $Si(CH_3)_3$), 1.00 (s, 9H, one of $Si(CH_3)_3$), 3.41 (s, 3H, $NHCH_3$), 6.89–6.92 (m, 2H, ArH), 7.08 (d, J = 1.9 Hz, 1H, ArH). ^{13}C NMR (175 MHz, $CDCl_3$): δ –3.95 (2C), –3.96 (2C), 18.6 (br, 2C), 26.0 (br, 6C), 32.1, 112.5, 113.1, 121.3, 136.3, 146.8, 147.7. MS (APCI) m/z : 396.2 calcd for $C_{19}H_{37}N_2O_3Si_2$ (M + H); 397.6 obsd. The data were in accordance with the literature (Tanaka and Umezawa, 1995). Compound 5: The synthesis of dephostatin (compound 5) was carried out following the route previously reported (Tanaka and Umezawa, 1995; Watanabe et al., 1994), except that TBAF was used instead of NaF-HF for the TBS removal. To a solution of compound 4 (96.1 mg, 0.242 mmol) in THF (5.3 ml) were added TBAF (1 M in THF, 0.28 ml, 0.28 mmol) successively at 0 °C. The solution was stirred at 0 °C for 1 h, then stirred at rt for another 3 h. The solvent was removed by rotary evaporation, and the resulting crude was poured into a solution of satd NH_4Cl and extracted with EtOAc (5 × 10 ml). The combined organic layers were combined, dried over Na_2SO_4 , and concentrated *in vacuo* to a brown oil. Due to the tendency of dephostatin to oxidize, flash chromatography (5:95→10:90 MeOH/ $CHCl_3$) was carried out with a glass column *under nitrogen flow*. Dephostatin (compound 5) was isolated as an orange powder (23.9 mg, 0.142 mmol, 58%). R_f = 0.26 (MeOH/ $CHCl_3$ 10:90). 1H NMR (700 MHz, acetone- d_6): δ

3.38 (s, 3H, NCH_3), 6.89–6.95 (m, 2H, ArH), 7.13 (d, $J = 2.2$ Hz, 2H, ArH), 8.29 (br, 2H, OH). ^{13}C NMR (175 MHz, acetone- d_6): δ 32.3, 108.8, 112.4, 116.4, 136.5, 145.7, 146.7. LRMS (APCI) m/z : 169.1 calcd for $\text{C}_7\text{H}_9\text{N}_2\text{O}_3$ (M + H); 169.3 obsd. Characterization data were in accordance with the literature (Tanaka and Umezawa, 1995; Watanabe et al., 1994).

QUANTIFICATION AND STATISTICAL ANALYSIS

Data were analyzed using RStudio version 1.0.143 with R version 3.2.2, and GraphPad Prism 8.0 software (GraphPad Inc., San Diego, CA). Unless otherwise noted, groups were compared via two-way analysis of variance (ANOVA). Each figure legend contains information on the type of multiple comparison test used as well as mean and dispersion measures. P values of <0.05 were considered significant. An explanation of the software used for RNA-sequencing and variant analysis can be found in each experimental method description.

Figures

Figure 3.1

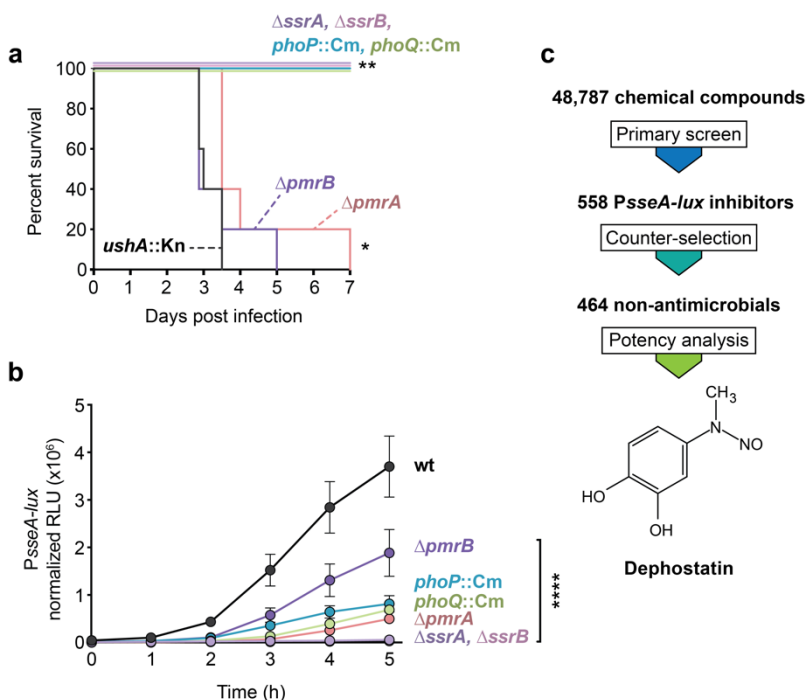


Figure 3.1. Identifying chemical repressors of virulence gene transcription.

(a) Survival plot of mice (n=5 per group). Groups were analyzed with a Gehan-Breslow-Wilcoxon test for survival curve differences. *P<0.05, **P<0.01. (b) Transcriptional reporter assay. Data are the means with standard error from three independent experiments. Significance is shown for values compared at time = 5 h. ****P<0.0001 (Bonferroni's multiple comparisons test). (c) Workflow of screen prioritization methods and chemical structure of Dephostatin. See also Supplementary Figure 3.1.

Figure 3.2

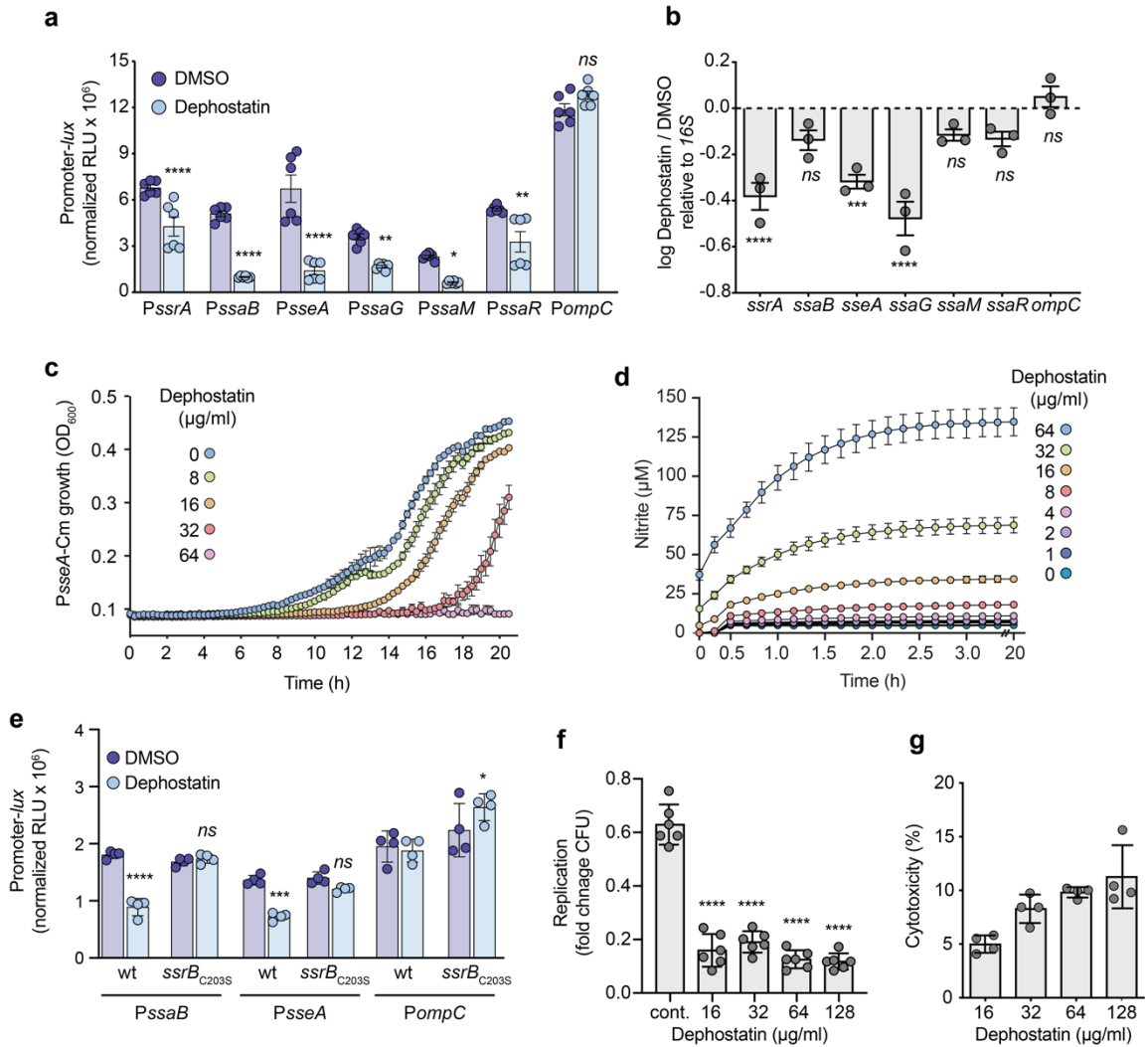


Figure 3.2. Dephostatin represses intracellular virulence through SsrB.

(a) Transcriptional reporter assay. Data are the means with standard error. Values for dephostatin were compared against those for DMSO. *P<0.05, **P<0.01, ****P<0.0001 (Bonferroni's multiple comparisons test). (b) Gene expression measured by RT-qPCR. Data are the means with standard error. Groups were compared against a value of 0 using one-way ANOVA ***P<0.001, ****P<0.0001 (Dunnett's multiple comparisons test). (c) Growth of PsseA-Cm.

Data are the means with standard error from two independent experiments. (d) Nitric oxide release from dephostatin, dots and error indicate mean and s.d. from three independent experiments. (e) As in (a). (f) Infection of bone marrow-derived macrophages. Data are the means with standard error. Groups were compared against DMSO-treated macrophages (cont.) via one-way ANOVA. **** $P < 0.0001$ (Dunnett's multiple comparisons test). (g) Percentage cytotoxicity after exposure to dephostatin. Data are the means with standard error.

Figure 3.3

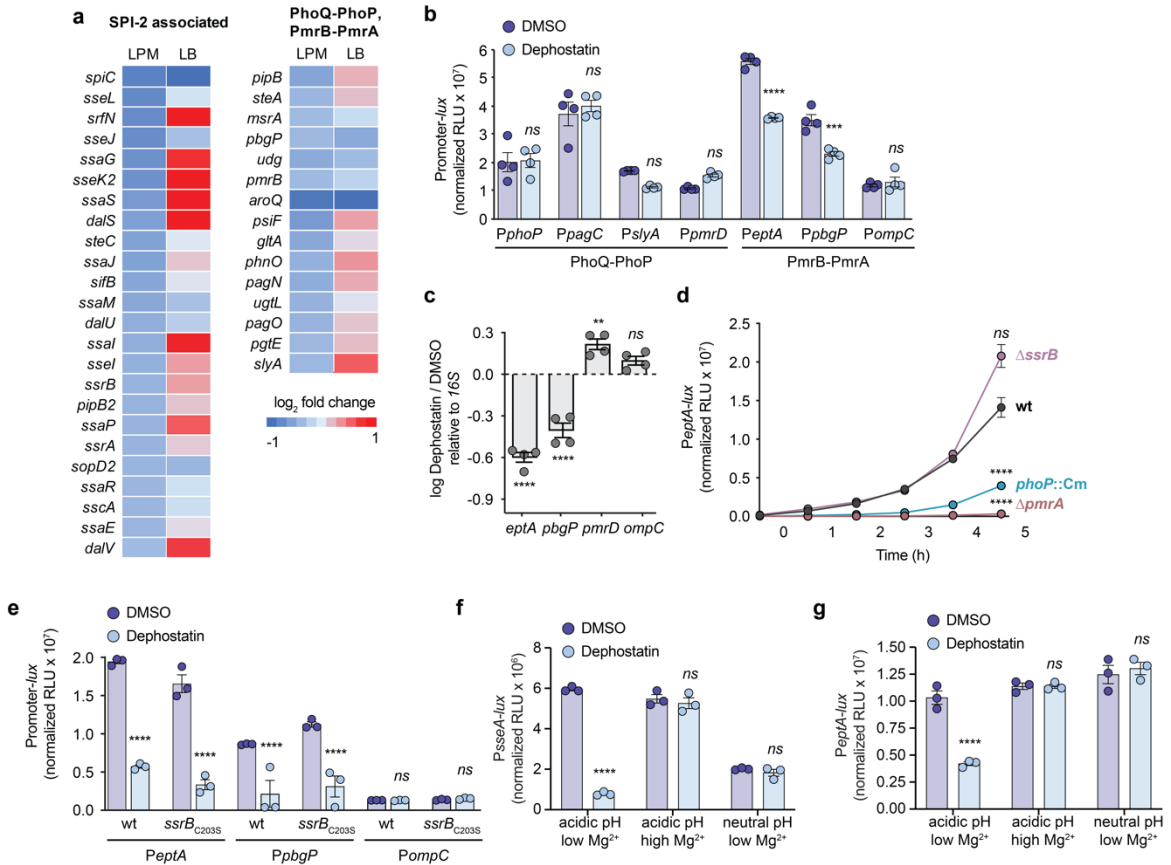


Figure 3.3. Dephostatins inhibit non-SPI-2 virulence genes.

(a) log₂ fold change in gene expression following RNA-sequencing of dephostatins-treated cells relative to DMSO-treated. Blue, downregulated; red, upregulated. (b) Transcriptional reporter assay. Data are the means with standard error. Values for dephostatins were compared against those for DMSO. ***P<0.001, ****P<0.0001 (Bonferroni's multiple comparisons test). (c) Gene expression measured by RT-qPCR. Data are the means with standard error. Groups were compared against a value of 0 (i.e. no change in expression) via one-way ANOVA. **P<0.01, ****P<0.0001 (Bonferroni's multiple comparisons test). (d) Transcriptional reporter assay. Data are the means with standard error from three independent experiments. Significance is shown for values compared

at time = 5 h. ****P<0.0001 (Bonferroni's multiple comparisons test). (e-g) As in (b). In (f) and (g), growth media types are indicated.

See also Supplementary Figure 3.2.

Figure 3.4

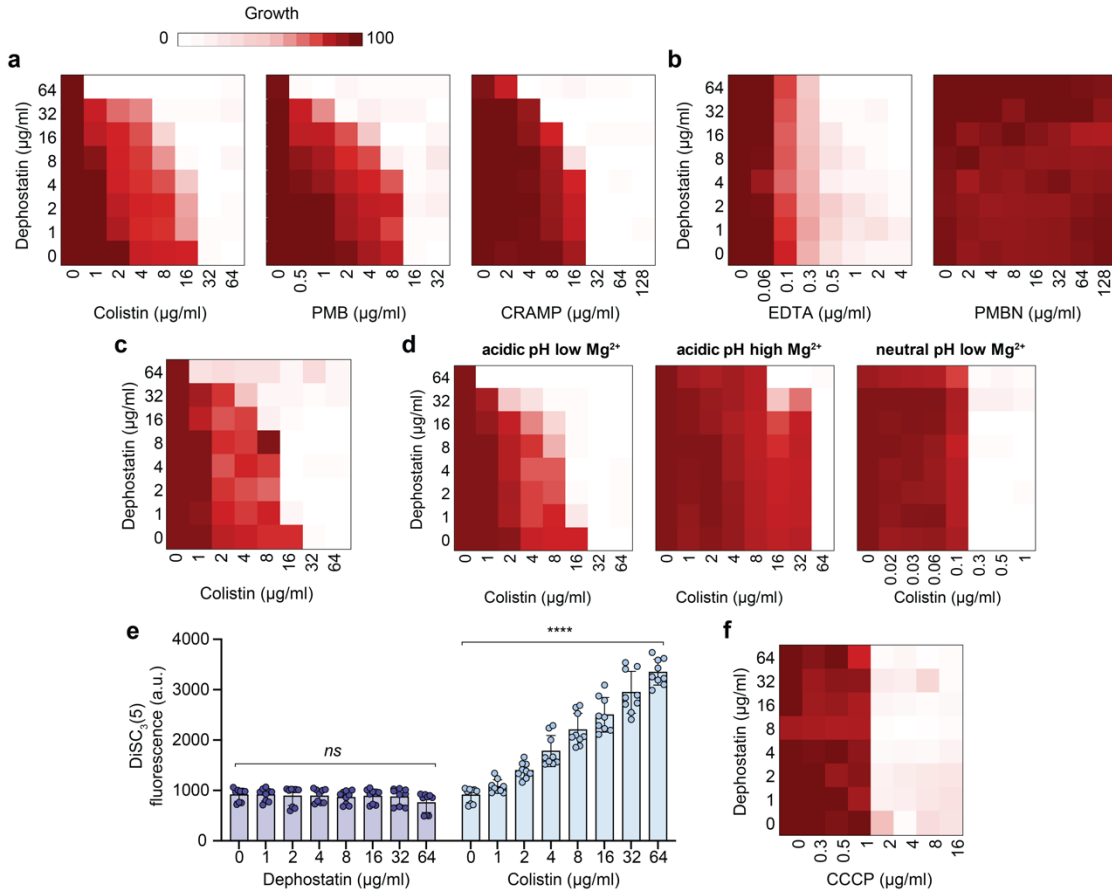


Figure 3.4. Dephostatin selectively potentiates polymyxin antibiotics against *Salmonella*.

(a) Chequerboard broth microdilution assays between dephostatin and colistin, polymyxin B (PMB), or cathelin-related antimicrobial peptide (CRAMP). (b) As in (a), for dephostatin and EDTA or polymyxin B nonapeptide (PMBN). (c) As in (a), for dephostatin and colistin against the ST313 sequence type (str. D23580) of *Salmonella*. (d) As in (a), for dephostatin and colistin in the indicated media types. (e) DiSC₃(5) assay, bar plots depict the mean of three biological replicates, error bars indicate standard error. Concentrations of each compound were compared against 0 µg/ml. ****P<0.0001 (Dunnett's multiple comparisons test). (f) As in (a), for dephostatin and carbonyl cyanide m-chlorophenyl hydrazone

(CCCP). In (a-d) and (f), higher growth is indicated in dark red, no detectable growth is indicated in white, and results are representative of at least two independent experiments.

See also Supplementary Figure 3.3.

Figure 3.5

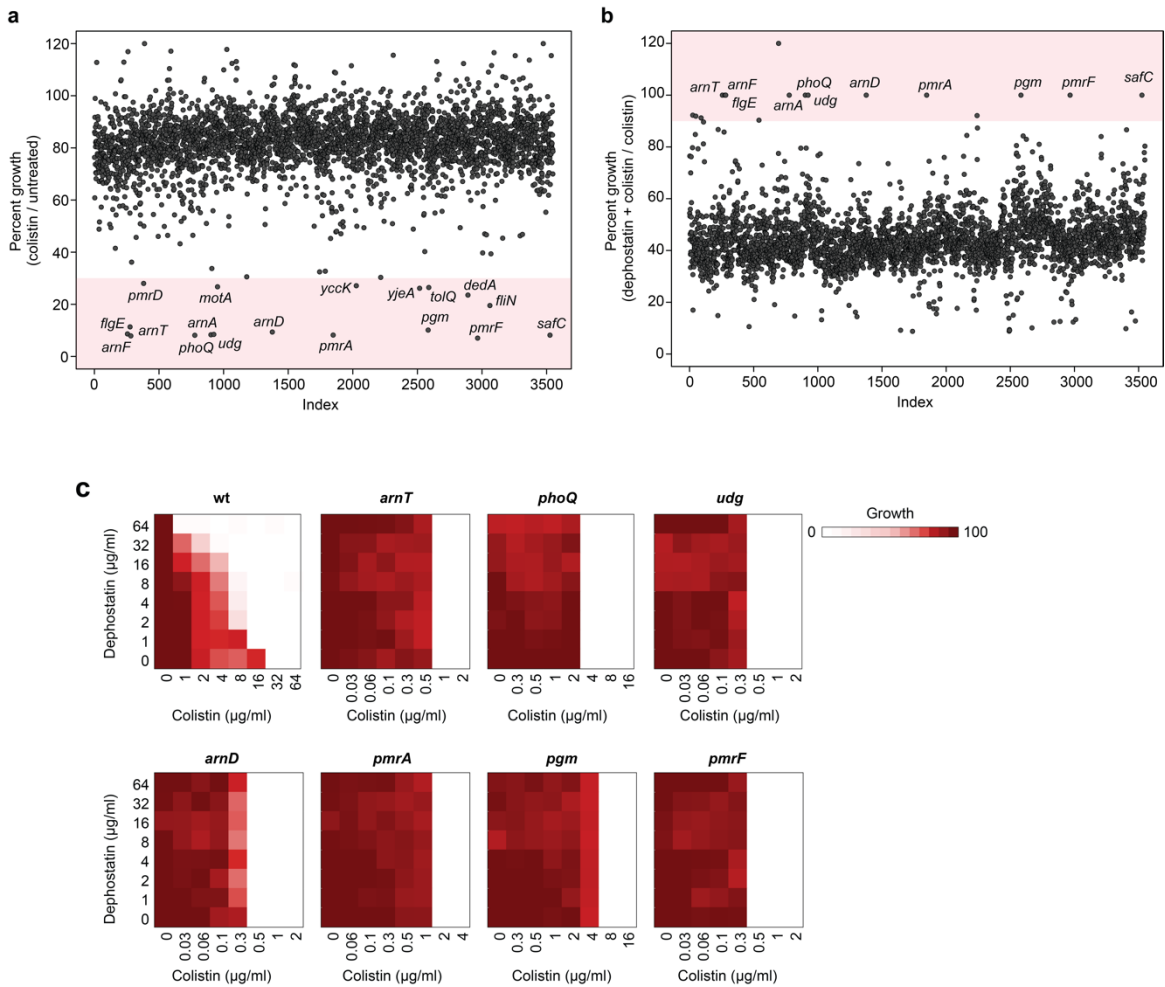


Figure 3.5. Synergy between dephostatin and colistin requires PmrA-regulated genes.

(a) Screening of SGD strains. Percent growth was calculated based on growth in the presence of colistin relative to its respective control (untreated strain) growing in LPM. Each dot is the mean of two technical replicates. (b) As in (a). Percent growth was calculated based on growth in the presence of colistin and dephostatin relative to its respective control (colistin-treated strain) growing in LPM. (c) Chequerboard assays of dephostatin and colistin against resistant deletion mutants. Higher growth is indicated in dark red, no detectable growth is

indicated in white, and results are representative of at least two independent experiments.

See also Supplementary Figure 3.4 and Supplementary Figure 3.5.

Figure 3.6

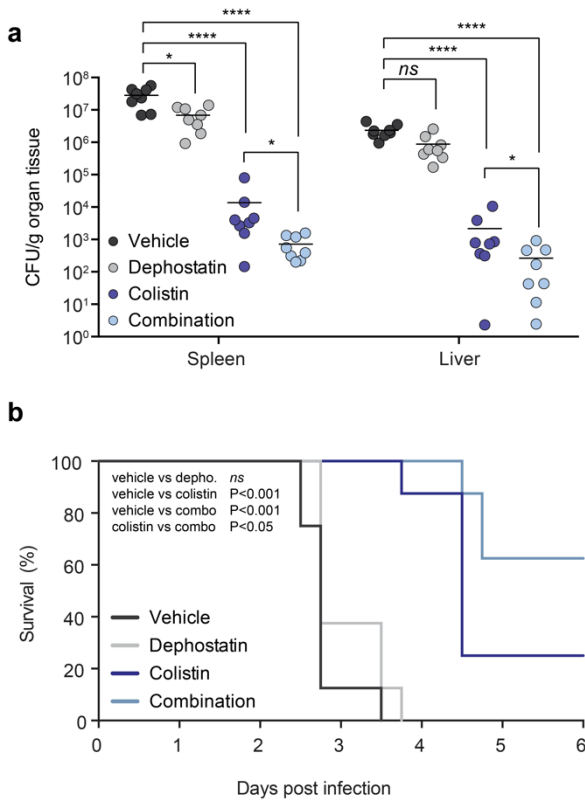
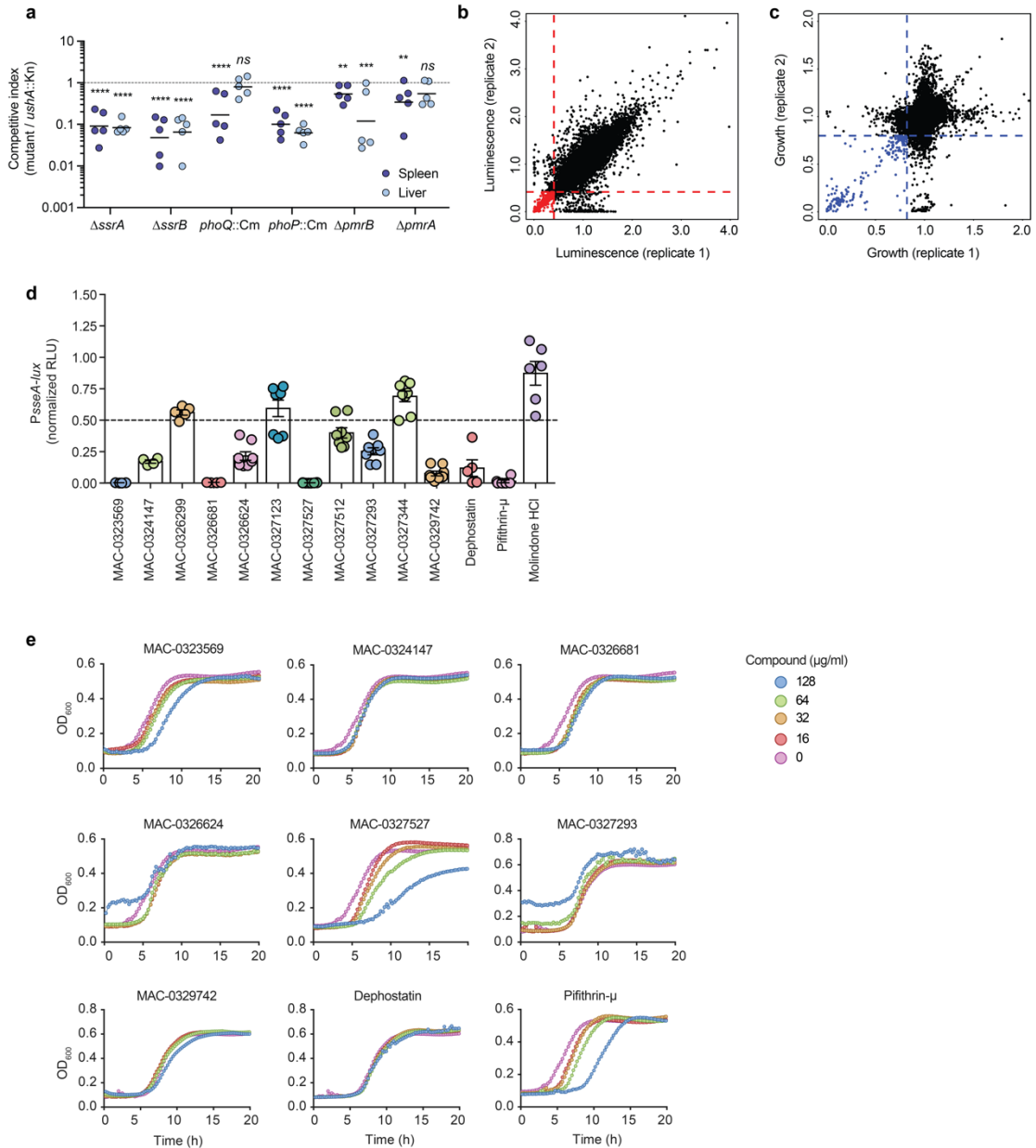


Figure 3.6. *In vivo* efficacy of dephostatin and colistin in a murine infection model.

(a) Mice were treated with vehicle (5% DMSO v/v in water, black), dephostatin (2.5 mg/kg, grey), colistin (10 mg/kg, dark blue), or dephostatin and colistin (2.5 and 10 mg/kg respectively, light blue) and euthanized at experimental endpoint (60 h post infection). Each point is representative of an individual animal, lines indicate arithmetic means of each group. * $P < 0.05$, **** $P < 0.0001$ (Holm-Sidak's multiple comparisons test). (b) Mice were treated with vehicle (5% DMSO v/v in water, black), dephostatin (5 mg/kg, grey), colistin (5 mg/kg, dark blue), or dephostatin and colistin (5 and 5 mg/kg respectively, light blue) and euthanized at clinical endpoint. Survival curves shown are from two separate experiments ($n = 4$ per group) and groups were analyzed with a Gehan-Breslow-Wilcoxon test. * $P < 0.05$, *** $P < 0.001$.

Supplementary Figures

Supplementary Figure 3.1

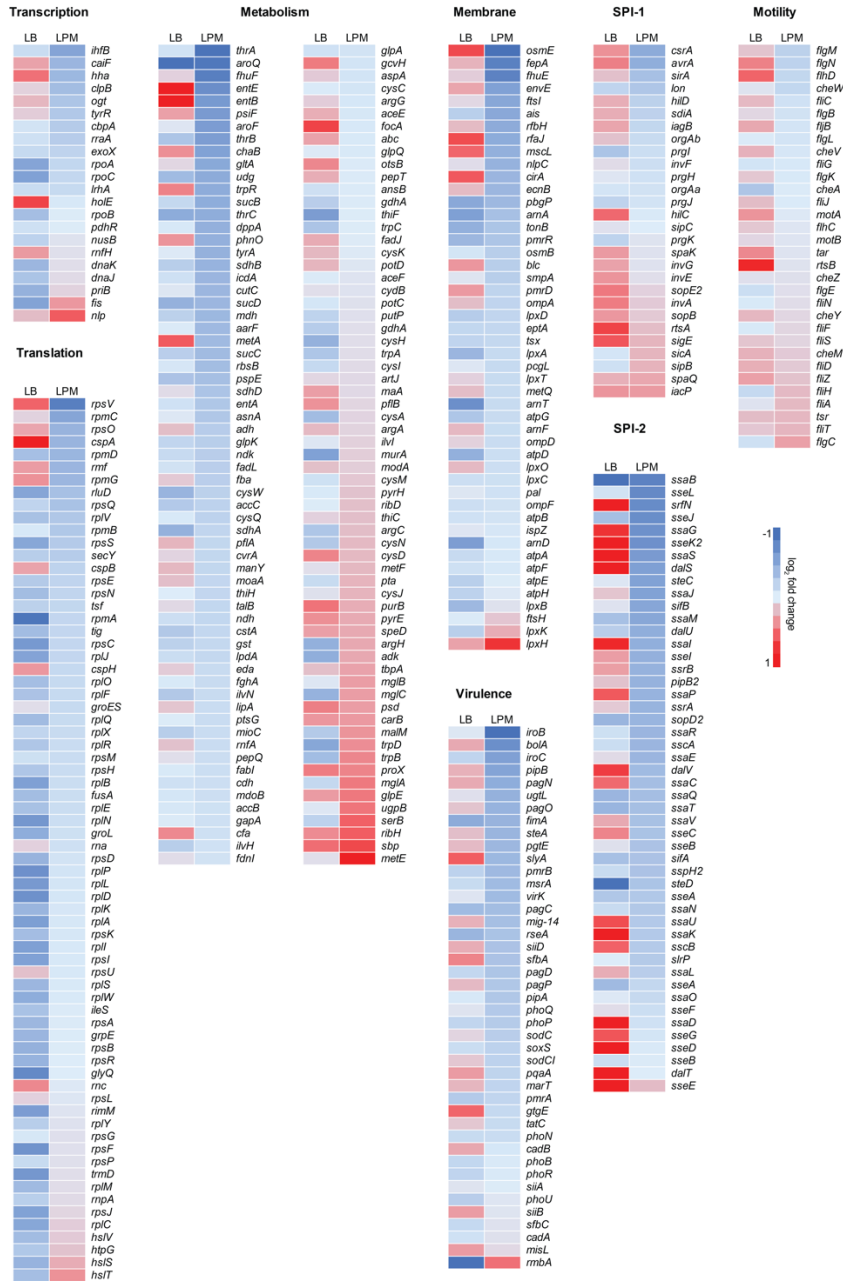


Supplementary Figure 3.1. Screening workflow to identify chemical repressors of virulence gene transcription, related to Figure 3.1.

(a) Each data point represents 1 animal, horizontal lines indicate geometric means. The broken line indicates a competitive index of 1, representing equal

fitness. Groups were compared to a value of 1 (equal fitness) ** $P < 0.01$, *** $P < 0.001$, **** $P < 0.0001$ (Holm-Sidak's multiple comparisons test). (b) Bioluminescence production from *PsseA-lux* was monitored over 5 h, values on graph represent interquartile mean-normalized, background subtracted RLU per well. Red lines indicate 2.25 s.d. from the mean of dataset. (c) As in (b) showing normalized interquartile mean-normalized, background subtracted OD_{600} monitored over ~20 h of incubation. Blue lines indicate 2.25 s.d. from the mean of the dataset. (d) Transcriptional reporter assay of *PsseA-lux* in *Salmonella* grown with 128 $\mu\text{g}/\text{mL}$ dephostatin. Normalized luminescence was calculated by subtracting luminescence at 0 h from 5 h, then dividing by corresponding values for cells treated with DMSO (vehicle control). The dotted line indicates 50% inhibition of luminescence. (e) OD_{600} monitored every 15 min for 20 h of growth of wild-type *Salmonella* in the presence of the indicated compounds.

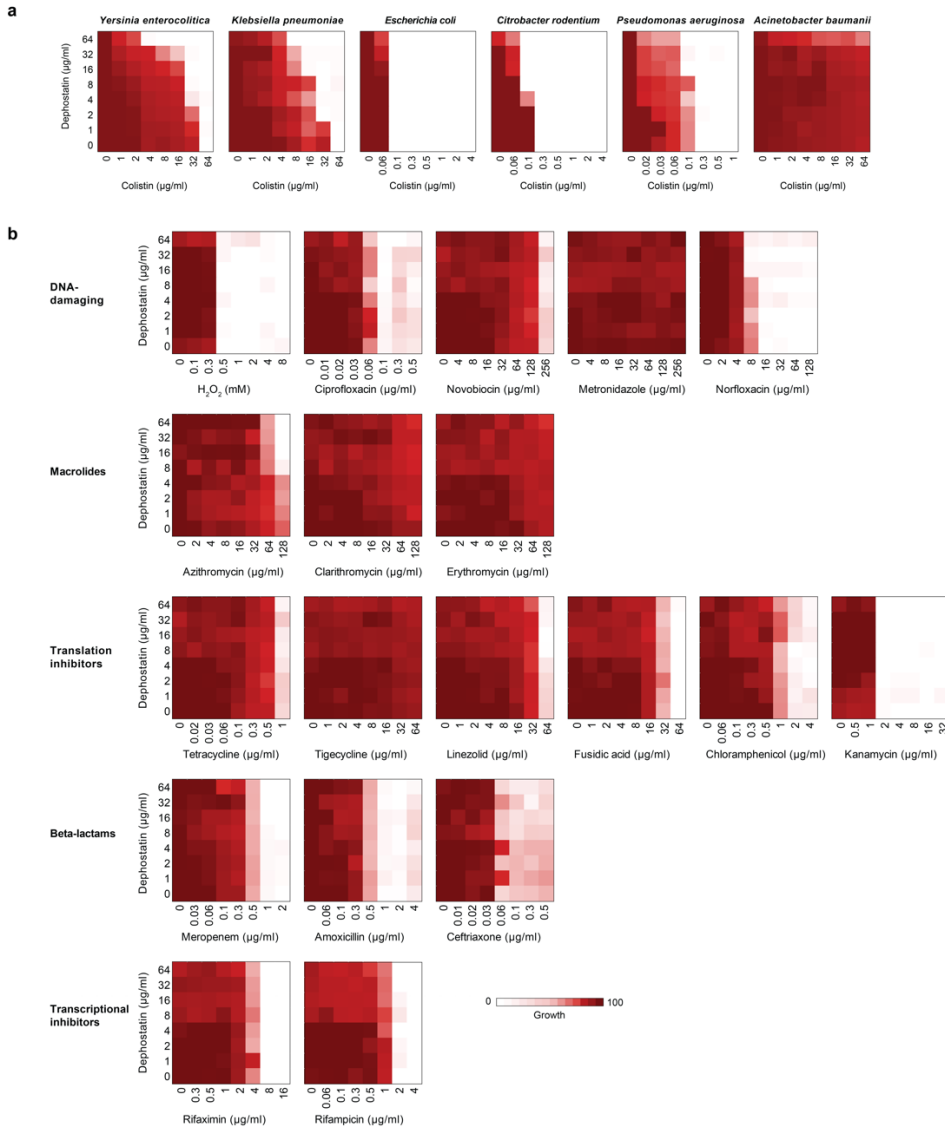
Supplementary Figure 3.2



Supplementary Figure 3.2. Dephostatin represses transcription of SPI-2 and other virulence genes, related to Figure 3.3.

Heat maps depict the \log_2 fold change in gene expression for cells grown with dephostatin compared to DMSO. Genes are grouped by functional category. Blue, downregulated; red, upregulated.

Supplementary Figure 3.3

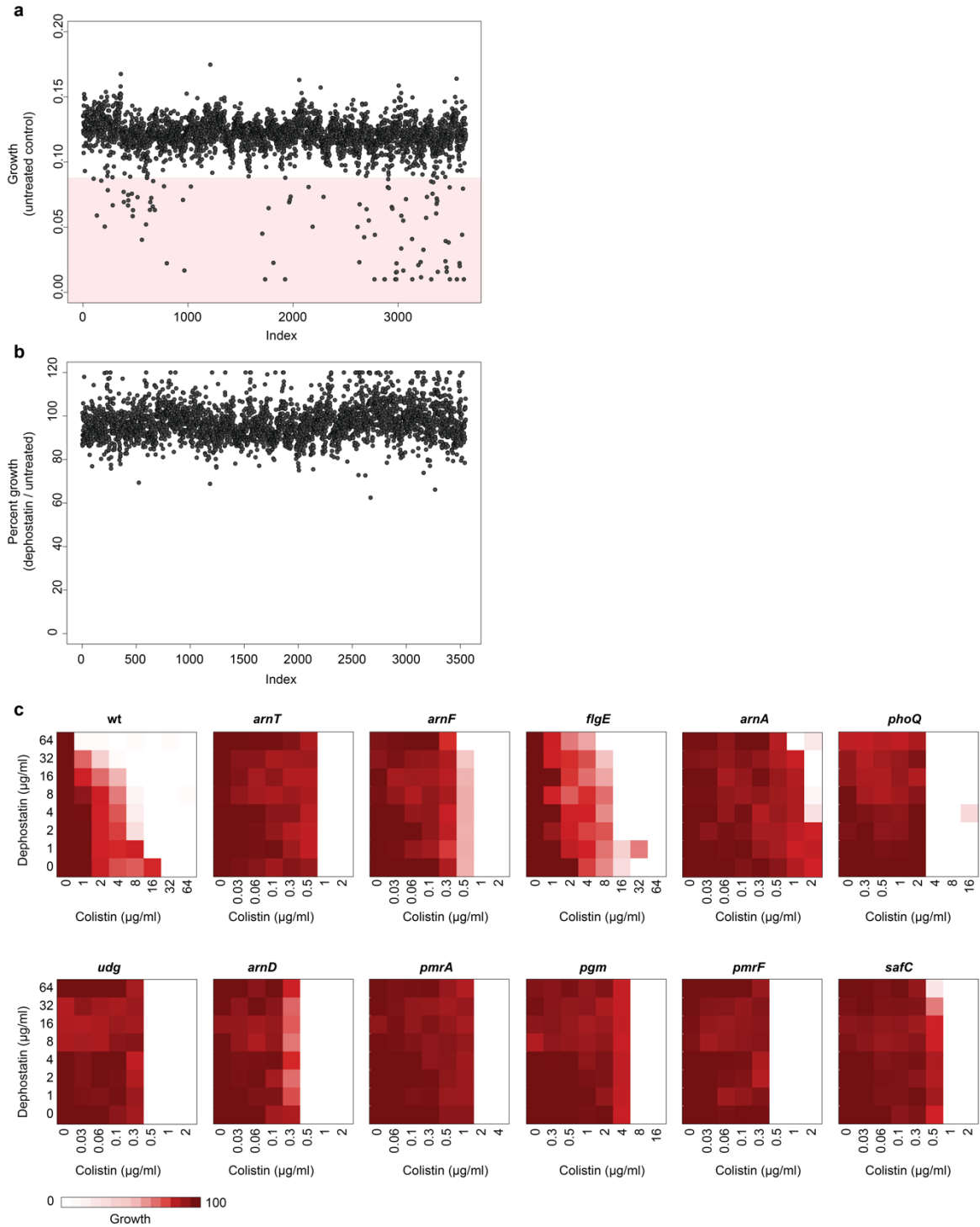


Supplementary Figure 3.3. Selectivity of dephostatin-polymyxin synergy, related to Figure 3.4.

Chequerboard broth microdilution assays showing the presence or absence of dose-dependent potentiation between dephostatin and the antibiotics indicated above. (a) Bacterial species are indicative above each chequerboard, for dephostatin in combination with colistin. (b) Antibiotics are grouped by functional class or target (left labels). In (a) and (b), higher growth is indicated in dark red,

no detectable growth is indicated in white, and results are representative of at least two independent experiments.

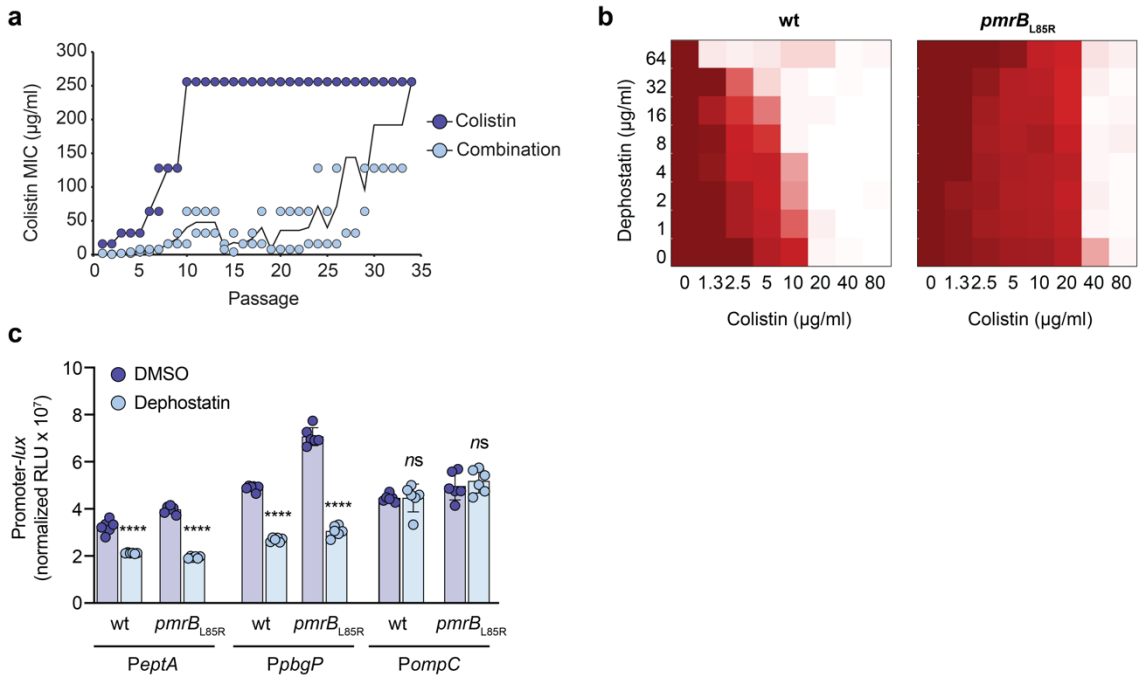
Supplementary Figure 3.4



Supplementary Figure 3.4. Screening of the *Salmonella* single-gene deletion (SGD) collection, related to Figure 3.5.

(a) Screening of SGD strains in LPM (untreated control). Growth was calculated by subtracting the pre-reads (0 h) from reads after ~20 h of incubation. Each dot is the mean of two technical replicates. The red rectangle indicates 2 s.d. from the mean of the dataset, indicating a cutoff for strains attenuated for growth. (b) Screening of SGD strains in LPM with 64 $\mu\text{g/ml}$ dephostatin. Growth was calculated by subtracting the pre-reads (0 h) from reads after ~20 h of incubation, percent growth was calculated based on growth in the presence of dephostatin relative to its respective control (untreated strain) growing in LPM. Each dot is the mean of two technical replicates. (c) Chequerboard broth microdilution assays showing the presence or absence of dose-dependent potentiation between dephostatin and colistin, for the genetic mutants as indicated. Higher growth is indicated in dark red, no detectable growth is indicated in white, and results are representative of at least two independent experiments.

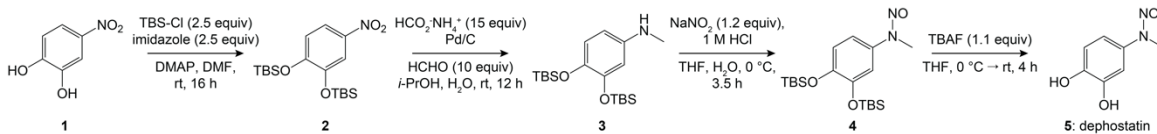
Supplementary Figure 3.5



Supplementary Figure 3.5. Analysis of genetic suppressors to dephostatin-colistin synergy, related to Figure 3.5.

(a) Serial passage experiment with colistin alone or in the presence of 8 µg/ml dephostatin. Cells from the highest concentration of colistin with detectable growth were used every other day to re-inoculate MIC plates. Points show the MIC for individual lineages and the connected line shows the mean MIC. (b) Checkerboard assays of dephostatin and colistin in combination against the indicated suppressor mutant (*pmrB_{L85R}*). Higher growth is indicated in dark red, no detectable growth is indicated in white, and results are representative of at least two independent experiments. (c) Transcriptional reporter assay of the indicated promoters. Bars and error indicate mean and s.e.m. For each promoter, values for dephostatin were compared against those for DMSO. ****P<0.0001 (Holm-Sidak's multiple comparisons test).

Supplementary Figure 3.6



Supplementary Figure 3.6. Dephostatin synthesis route, related to STAR Method: Synthesis of Dephostatin.

Dephostatin (compound **5**, 3,4-Dihydroxy-*N*-methyl-*N*-nitrosoaniline) was synthesized from 4-nitrocatechol (compound **1**) via the intermediate compounds **2** (3,4-Bis[(*tert*-butyldimethylsilyl)oxy]nitrobenzene), **3** (3,4-Bis[(*tert*-butyldimethylsilyl)oxy]-*N*-methylaniline), and **4** (3,4-Bis[(*tert*-butyldimethylsilyl)oxy]-*N*-methyl-*N*-nitrosoaniline).

Supplementary Tables

Supplementary Table 3.1

| Primer (forward) | Primer (reverse) | Sequence (forward) | Sequence (reverse) | Description |
|------------------|------------------|---|--|--|
| CT9-9 | CT9-10 | ggggagctctctgtattgattgccggtctgacgc | actgaggaagctaacaggcgttta | <i>ΔpmrB</i> (flanking region 1) |
| CT9-11 | CT9-12 | acgcctgttagctttcctcagtgcc | gggggtaccaggatggcctgcatttctgacgcg | <i>ΔpmrB</i> (flanking region 2) |
| CT9-3 | CT9-4 | ggggagctcccacagcggcgtgcgtagctcatg | tgaggagactaagcagtgagcct | <i>ΔpmrA</i> (flanking region 1) |
| CT9-5 | CT9-6 | atcaggctcactcgttagtctcct | gggggtaccggcagccacggccaacctattaca | <i>ΔpmrA</i> (flanking region 2) |
| CT8-18 | CT8-19 | gggggatccagaagaaacgggtaagt | gggtacgtaattgattaaacctctgtt | pGEN- <i>PompC-luxCDABE</i> |
| CT5-19 | CT5-20 | aggccttcgggtgtaaaagt | gactcaagcctgccagtttc | 16S RT-qPCR |
| CT5-5 | CT5-6 | aaatccgggctaaggtgagt | taaactccttctcggcctcct | <i>ssrA</i> RT-qPCR |
| CT5-13 | CT5-14 | gtctgaggagggattcatgc | tgctgaagcagtagtgca | <i>ssaB</i> RT-qPCR |
| CT5-17 | CT5-18 | aaatccgggctaaggtgagt | taaactccttctcggcctcct | <i>sseA</i> RT-qPCR |
| CT5-3 | CT5-4 | agtgatagtctcaccaca | gcgcttaatacatcgattctg | <i>ssaG</i> RT-qPCR |
| CT9-71 | CT9-72 | acggccttagcaaccaata | ttgaggaataacctggaacg | <i>ssaM</i> RT-qPCR |
| CT5-11 | CT5-12 | gattgcctttgcaactgat | tcggcccataatgaataag | <i>ssaR</i> RT-qPCR |
| CT7-9 | CT7-10 | gcagcgcagatttctcagac | cgtaaccgttgctgatgcc | <i>ompC</i> RT-qPCR |
| CT6-2 | CT6-3 | gggggagctcacttgaccgggtagaagat | tatatccagtgtttttctccattcccctccatatacacgata | <i>PsseA-Cm</i> (upstream of <i>sseA</i>) |
| CT6-4 | CT6-5 | ttatctatcgtgtataggggggaaatggagaaaaaatcactggata | tcctgaagacattatgctttacctttt | <i>PsseA-Cm</i> (<i>Cm</i> cassette) |
| CT6-6 | CT6-7 | cgatgagtggcagggaggagcgtaaaaggtaaagcataatgtcttca | acgctcctccctgcc | <i>PsseA-Cm</i> (downstream of <i>sseA</i>) |
| CT10-36 | CT10-42 | ggggagctctcaattcgcctctgtggaatggtt | gggggtaccgaattgttatctgccctgac | <i>ssrB_{C203S}</i> (region 1) |
| CT10-43 | CT10-39 | ttctcgggcagagtaagtaactc | gggggtaccattttaaaattgtagagcatgta | <i>ssrB_{C203S}</i> (region 2) |
| CT7-69 | CT7-70 | gggggatcctctgcacctcgtgggca | gggtacgtacatctcttccctgtgt | pGEN- <i>PphoP-luxCDABE</i> |
| CT7-71 | CT7-72 | gggggatcccacctcgttatataa | gggtacgtacaactcctaataactactt | pGEN- <i>PpagC-luxCDABE</i> |
| CT7-63 | CT7-64 | gggggatccgatctcagcagagatgta | gggtacgtattcatctcctataatt | pGEN- <i>PslxA-luxCDABE</i> |
| CT7-65 | CT7-66 | gggggatcccgctggcgcgacgcagct | gggtacgtagcggcccgttcacgctg | pGEN- <i>PpmrD-luxCDABE</i> |
| CT8-44 | CT8-45 | gggggatccagtgctgggtgc | gggtacgtagtgtgatgctccat | pGEN- <i>PeptA-luxCDABE</i> |
| CT8-50 | CT8-51 | gggggatccgatcgcaccgctcg | gggtacgtacattttccttcag | pGEN- <i>PpbpP-luxCDABE</i> |
| CT8-56 | CT8-57 | cctaccgtaaaactcgtgc | gagcgatcgatgatgacc | <i>eptA</i> RT-qPCR |
| CT8-62 | CT8-63 | gataacaaccggcccgaaaa | gcgccgagtaaacgatcat | <i>pbpP</i> RT-qPCR |
| CT7-1 | CT7-2 | atgttctgtgctgtgcgatag | tcaaccgctgccattcgt | <i>pmrD</i> RT-qPCR |
| CT10-8 | CT10-11 | ggggagctccgcagtaacgtcgcataccgcgca | gggggtacctataggccgcatcaggcatggagg | <i>pmrB_{L5R}</i> |

Supplementary Table 3.1. Primers used in this study, related to STAR Method: Cloning and mutant generation.

CHAPTER 4 – Host-directed small molecules sensitize multidrug resistant *Salmonella* to macrophage immunity

Preface

As of May 2021, the work presented in this chapter is in preparation for submission:

Tsai CN, MacNair CR, Perry JN, Brown ED, Coombes BK. Host-directed small molecules sensitize multidrug resistant *Salmonella* to macrophage immunity. *In preparation.*

I wrote the manuscript with input from Coombes BK. I performed all experiments, with the following exceptions: MacNair CR and Perry JN assisted with the LPM chemical screen (Figure 4.1c).

*References within this and all other chapters have been compiled into one list at the end of the thesis, to avoid redundancy between sections.

Abstract

Bloodstream infections caused by non-typhoidal strains of *Salmonella enterica* are a major global health concern. These infections are especially problematic in sub-Saharan Africa, resulting in almost 50,000 deaths each year. Interestingly, the majority of bloodstream infections in this region are caused by a single sequence type (ST) 313 of *S. enterica*, which has acquired resistance to several first-line antibiotics. To combat this rising health threat, it is imperative that we explore new therapeutic strategies that sidestep conventional mechanisms of antibiotic resistance, such as host-directed therapy (HDT). Here, we identify several HDT compounds that modulate macrophage immunity to restrict ST313 replication. By performing two parallel chemical screens in cultured macrophages and nutrient-limited growth media, we enrich for small molecules that restrict intracellular ST313 replication without directly targeting bacterial viability. We identify and characterize the immunomodulatory activity of four such compounds (berbamine, cantharidin, indatraline, patulin), which significantly attenuate ST313 infection.

Introduction

Salmonella enterica is an important global pathogen that causes disease in a wide range of animal hosts. Pathogenic lifestyles within this species exist along a spectrum, from non-typhoidal serovars that occupy a broad host range and cause uncomplicated gastroenteritis, to typhoidal serovars that are comparatively more restricted and linked to bloodstream infection (Langridge et al., 2015). In previous years, our lab and others have primarily focused on non-typhoidal, non-invasive serovars, using the ST19 sequence type of *Salmonella enterica* serovar Typhimurium (hereinafter *Salmonella*). However, new clades of non-typhoidal, highly invasive *Salmonella* strains are emerging, which appear to more closely resemble typhoidal serovars during human infection (Wheeler et al., 2018). These variants have been shown to cause lethal septicaemia – clinically termed invasive non-typhoidal *Salmonella* (iNTS) disease – with HIV-positive, malaria-infected, or malnourished individuals at particular risk (Gordon et al., 2008).

iNTS is of particular concern in sub-Saharan Africa, where a single sequence type of *Salmonella* (ST313) is dominant (Feasey et al., 2012). Concerningly, ST313 isolates tend to be multidrug resistant to chloramphenicol, ampicillin, kanamycin, streptomycin, sulfonamides, and trimethoprim, rendering many first-line treatment options ineffective (Su et al., 2004). Some lineages within this sequence type have also been identified to express extended-spectrum beta-lactamases that decrease ceftriaxone sensitivity (a commonly prescribed antibiotic for complicated iNTS infections) (Feasey et al., 2014); further, an emerging extensively drug resistant lineage in the Democratic Republic of the Congo is concurrently azithromycin-resistant (Van Puyvelde et al., 2019).

The dissemination of iNTS antibiotic resistance is adding urgency to an already serious threat, as any further restriction in treatment options has the potential to

greatly increase global morbidity and mortality. To address this crisis, we must consider alternative therapeutic strategies that are impervious to existing resistance mechanisms, such as host-directed therapy (HDT) (Hancock et al., 2012). By chemically modulating the activity of the host immune system, HDT may perturb host cell pathways that pathogens exploit for virulence, enhance antimicrobial activity initiated by the immune system, or blunt excessive instances of inflammation (Kaufmann et al., 2018). Such an approach may be particularly useful for recalcitrant intracellular pathogens such as *Salmonella*, which naturally subvert immune-based killing by manipulating host cell signaling. However, HDT has been relatively underexplored in the context of bacterial infection, despite achieving great success in other therapeutic areas through suppression or stimulation of autoimmune and inflammatory responses (Ulevitch, 2004). The most significant progress in this area has been made in investigating HDT as a treatment option for tuberculosis, wherein modulators of cytokine and antimicrobial peptide production, autophagy, and phagosomal maturation have been shown to restrict intramacrophage replication of *Mycobacterium tuberculosis* (Kaufmann et al., 2018).

Here, we investigated HDT as an anti-infective strategy against multidrug resistant ST313 *Salmonella*. We hypothesized that small molecules with immunomodulatory activity may ablate the natural ability for intracellular *Salmonella* to exploit host signaling pathways for virulence gene expression and immune evasion, and therefore focused on macrophage immunity as these cells comprise a major axis of the innate immune response to *Salmonella* infection. Adapting our previously published intramacrophage screening platform (Ellis et al., 2019), we screened 3840 chemical compounds for immunomodulatory activity against RAW264.7 macrophages, to identify those that altered intracellular ST313 *Salmonella* replication. By counter-selecting against any small molecules that were antimicrobial in physiologically relevant growth conditions

(acidic, nutrient-limited media), we enriched for those with putative host-targeting activity. Follow-up studies revealed 4 compounds (berbamine, cantharidin, indatraline, patulin) to be potent inhibitors of intracellular *Salmonella* replication that also modulate macrophage immunity.

Results

Screening for immunomodulatory compounds against ST313

To identify HDT compounds active against ST313 *Salmonella*, we chose to screen an annotated chemical library of 3840 small molecules, comprised of previously approved drugs, natural products, and other compounds with known biological activity. In our first chemical screen, each compound was added to a well of RAW264.7 macrophages that had been pre-treated with lipopolysaccharide (LPS) for ~20 h; cells were then incubated with compound for a further 4 h to provide time for intracellular accumulation or drug activity. The compound-containing media was then removed from macrophages, and cells were infected with opsonized ST313 *Salmonella* expressing pGEN-*lux*-Gm (Lane et al., 2007). With slight modifications to our previously reported high-throughput infection method (Ellis et al., 2019), macrophages were treated with fosfomycin to prevent extracellular bacterial replication, and intramacrophage bacterial viability was monitored by reading luminescence immediately after fosfomycin treatment and 6 h later (Figure 4.1a).

Considering our goal of identifying compounds with host-specific activity, we next screened the same annotated library for antimicrobial activity against ST313 *Salmonella* grown in acidic, nutrient-limited media (LPM). As our previous work indicated an overlap in chemical sensitivity for *Salmonella* grown in LPM and in macrophages (Ellis et al., 2019), we reasoned that LPM-active antimicrobials

may also possess bacterial-targeting activity against *Salmonella* grown in macrophages (provided that they were able to accumulate within these cells in our screening approach). In this secondary screen, compounds were added to ST313 *Salmonella* and growth was monitored for 20 h (Figure 4.1b).

After normalizing each screening dataset independently (Mangat et al., 2014), we directly compared bacterial luciferase production over 6 h of intramacrophage replication (Figure 4.1a) to bacterial OD₆₀₀ after 20 h of growth in LPM (Figure 4.1b), for ST313 *Salmonella* exposed to each compound (Figure 4.1c). Using a standard deviation cutoff to identify hit significance, we found that 92 compounds restricted ST313 growth in LPM, while 30 compounds restricted ST313 luminescence in macrophages (28 of which did not impact bacterial viability in LPM). These 28 presumed HDT compounds were then re-screened for potency; we found that 8 compounds within this set, when tested at 100 µM, resulted in a net, dose-dependent reduction in fold-change (over 6 h of replication) in intramacrophage ST313 luminescence (Figure 4.1d).

Analyzing specificity, toxicity, and potency of putative HDT compounds

Based on chemical diversity and commercial availability, we prioritized 6 of the 8 remaining compounds to be re-ordered and further characterized (amodiaquine, berbamine, cantharidin, cetrimonium bromide, indatraline, patulin). We then determined the minimum inhibitory concentration (MIC) of each compound against ST313 grown in extracellular media conditions (LB, LPM, DMEM), to identify those with antimicrobial activity at concentrations not detected by our initial LPM screen (Figure 4.2a). Opting to exclude any compounds with an MIC < 16 µg/mL in any media type, we were left with 4 compounds (amodiaquine, berbamine, cantharidin and indatraline) that had either no MIC or an MIC > 16 µg/mL in LB, LPM, and DMEM.

We next sought to determine the toxicity of each compound towards macrophages, reasoning that ST313 luminescence may have decreased for certain compounds due to their induction of macrophage lysis in the earlier stages of our screening protocol. As a proxy for cytotoxicity, we monitored lactate dehydrogenase (LDH) release from uninfected macrophages treated with the 4 remaining compounds (Figure 4.2b). With these data, we were able to select the maximum, non-toxic concentration of each compound to be used for our follow-up assays (32 µg/mL for amodiaquine and berbamine, 64 µg/mL for cantharidin, and 8 µg/mL for indatraline).

Finally, we validated the ability for each compound to attenuate ST313 replication by enumerating bacterial CFU rather than monitoring luminescence production. Following a similar infection protocol as was used in our initial macrophage screen, we pre-treated macrophages with amodiaquine, berbamine, cantharidin, and indatraline at the maximum concentrations previously determined to not induce cytotoxicity, then removed each compound and infected macrophages with ST313 to enumerate CFU at 0, 6, and 20 h post-infection. These data aligned with our previous results, as treatment with each compound significantly reduced ST313 replication at both 6 (Figure 4.2c) and 20 h (Figure 4.2d) post-infection, relative to control-treated macrophages.

Characterization of immunomodulatory activity

Given the compound library we chose for screening, all 4 putative HDT compounds are drugs with previously annotated biological activity (Figure 4.3a). Briefly, amodiaquine is an aminoquinoline derivative with known anti-malarial and anti-inflammatory properties (Olliaro et al., 1996); berbamine is an anti-cancer drug with inhibitory activity towards bcr/abl fusion gene and NF-κB (Liang et al.,

2009; Xu et al., 2006); cantharidin is a beetle-secreted terpenoid used as a blistering agent (Moed et al., 2001); indatraline is a non-selective monoamine transporter that blocks dopamine, norepinephrine, and serotonin reuptake (Cho et al., 2016). To begin investigating the possible impact of each compound on macrophage immunity, we monitored the transcription of several key inflammatory-associated genes in RAW264.7 macrophages: *IL-1 β* , *TNF- α* , the NF- κ B target gene *NFKBIA*, inducible nitric oxide synthase (*NOS2*), *COX-2*, and NADPH oxidase (*NOX2*). We noted several distinct patterns of gene expression: amodiaquine significantly decreased *NFKBIA* expression and significantly increased *NOS2* expression (Figure 4.3b); berbamine significantly decreased *IL-1 β* , *TNF- α* , and *NOX2* expression (Figure 4.3c); cantharidin significantly increased *IL-1 β* , *NOS2*, and *COX-2* expression (Figure 4.3d); and indatraline significantly decreased *IL-1 β* , *TNF- α* , and *COX-2* expression (Figure 4.3e). These data indicated that amodiaquine and cantharidin exerted primarily pro-inflammatory effects, while berbamine and indatraline were primarily anti-inflammatory. Experiments are currently ongoing to continue elucidating the mechanism of action and potential *in vivo* efficacy of these immunomodulatory compounds.

Discussion

It has become increasingly important to identify non-traditional therapeutics for multidrug resistant pathogens. In this work, we sought to identify HDT compounds that attenuate ST313 viability in macrophages, as these cells represent one of the most important niches colonized by *Salmonella* during infection. Using a parallel chemical screening approach, we identified four compounds (amodiaquine, berbamine, cantharidin, and indatraline) to all significantly restrict *Salmonella* replication in macrophages while simultaneously modulating inflammatory host gene expression.

This work is still in progress, and several important experiments remain to continue understanding how and why these four compounds restrict intracellular *Salmonella* replication. Importantly, while our chemical screen was designed to enrich for compounds with host-specific immunomodulatory activity, it remains possible that one or more of our compounds is also directly antimicrobial against intracellular *Salmonella*. Indeed, this would be consistent with our previous reports of elevated chemical sensitivity for bacteria in intracellular environments (Ellis et al., 2019). To begin separating the possible host/bacterial-targeting mechanisms of actions for each compound, I intend to test for possible antimicrobial activity against efflux-deficient or outer membrane-impaired *Salmonella*. If these compounds were inactive against even these highly susceptible variants, a promising route of investigation may be to examine their activity in macrophages deficient for certain immune pathways or cytokines. If the compound-mediated inhibition of *Salmonella* replication no longer occurred in macrophages lacking a specific component of innate immunity, it would suggest a host-specific mechanism for the compound in question. Based on our preliminary RT-qPCR results, bone marrow-derived macrophages from mice lacking *IL-1 β* , *TNF- α* , or *NOS2* may be particularly useful to examine; similarly, chemical inhibitors of macrophage immune processes may be used.

It will also be important to understand the full extent of transcriptomic change elicited by compound treatment. To this end, it may be worthwhile to extract and sequence total RNA from macrophages treated with these four compounds, both after compound treatment but before bacterial infection, and after bacterial infection. Such an experiment could reveal broader patterns in gene expression induced by these compounds, across multiple groups of pro- and anti-inflammatory genes. There is evidence that some of these hit compounds may have specific transcriptional effects on phagocytic cells – berbamine was

previously shown to reduce IL-1 cytokine production (Seow et al., 1992); cantharidin has been characterized as an inducer of apoptosis (Maroufi et al., 2012) and an inhibitor of protein phosphatase activity (Honkanen, 1993); indatraline was previously identified (but not further characterized) as a hit within another intramacrophage *Salmonella* screen (Nagy et al., 2020) and is also known to induce autophagy (Li et al., 2016). All four compounds should also be examined for their possible inhibitory activity against *Salmonella in vivo*, using our established model of systemic salmonellosis in genetically susceptible mice. Serum levels of cytokines and signaling molecules in these animals could also be monitored, to better understand the impact of each compound on the host immune system during infection.

It is also interesting to consider the effects of immunomodulation on intracellular *Salmonella* virulence gene expression. A hallmark of *Salmonella* pathogenesis is its ability to sense and respond to changing environmental cues encountered during infection, including instances of inflammation that may have been modulated by our compounds of interest. For example, nitric oxide generated by the *NOS2*-encoded inducible nitric oxide synthase is known to posttranslationally modify the master regulator SsrB in *Salmonella*, contributing positively to fitness during infection (Husain et al., 2010). It is possible that the chemical inhibition of this and other inflammatory signals would have simultaneously blunted virulence gene expression in *Salmonella*, amplifying its intracellular attenuation. Continuing to investigate this possibility would perhaps require testing of deletion mutants in *Salmonella* that lack important virulence gene regulators, to test for a loss of compound-mediated inhibition. Bacterial gene expression during infection could also be monitored, using either promoter-reporter constructs or RNA extraction and RT-qPCR, although these experiments would have to also account for an expected reduction in bacterial viability.

Methods

Bacterial strains and culture conditions

Salmonella experiments were performed with strain D23580 (ST313). For compound screening and secondary assays, this strain was transformed with pGEN-*lux*-Gm (Lane et al., 2007). Routine propagation of bacteria was in LB media (10 g/L NaCl, 10 g/L Tryptone, 5 g/L yeast extract) supplemented with appropriate antibiotics (streptomycin, 100 µg/ml; gentamicin, 15 µg/ml). Where indicated, bacteria were grown in LPM (acidic pH low Mg²⁺ media) (5 mM KCl, 7.5 mM (NH₄)₂SO₄, 0.5 mM K₂SO₄, 80 mM MES pH 5.8, 0.1% casamino acids, 0.3% (v/v) glycerol, 24 µM MgCl₂, 337 µM PO₄³⁻). Bacteria were grown at 37°C.

Cell culture maintenance

Cells were maintained in a humidified incubator at 37°C with 5% CO₂. RAW264.7 macrophages were grown in DMEM containing 10% FBS (Gibco) and seeded in tissue culture-treated 96-well (100 µL/well, 10⁵ cells/well) or 384-well (50 µL/well, 5 x 10⁴ cells/well) plates (Corning) ~20-24 h prior to use, with 100 ng/mL LPS from *Salmonella enterica* serovar Minnesota R595 (Millipore).

Reagents

All high-throughput compound screening was performed at the Centre for Microbial Chemical Biology (McMaster University). The chemical library screened contained 3840 diverse small molecules assorted from Sigma-Aldrich and MicroSource; screening stocks (5 mM) were stored at -20°C in DMSO. Hit compounds that were re-ordered included: amodiaquine (Sigma-Aldrich), berbamine (Cedarlane), cantharidin (Sigma-Aldrich), cetrimonium bromide

(Cedarlane), indatraline (Sigma-Aldrich), patulin (Cedarlane). Compounds were routinely dissolved in DMSO at a concentration of 10 mg/mL and stored at -20°C .

Macrophage chemical screening

100 nL of each compound (5 mM stocks) was added (Echo 550 Liquid Handler) directly to 384-well black, clear flat-bottom plates (Corning) containing LPS-pretreated RAW264.7 macrophages in 50 μL DMEM + 10% FBS, for a final concentration of 10 μM compound per well. Macrophages were incubated with compounds for 4 h at 37°C with 5% CO_2 . A culture of ST313 expressing pGEN-*lux*-Gm was grown overnight in LB with 15 $\mu\text{g}/\text{mL}$ gentamicin. 30 min prior to infection (~ 3.5 h after compound addition), bacteria were opsonized for 30 min in 20% human serum (Innovative Research) in PBS at 37°C . Compound-containing media was then removed from macrophages, and replaced with 50 $\mu\text{L}/\text{well}$ of opsonized bacteria (diluted in DMEM + 10% FBS to achieve a multiplicity of infection (MOI) of 50:1). Plates were centrifuged at $200 \times g$ for 3 min, then incubated for 30 min at 37°C with 5% CO_2 . Bacteria-containing media was then removed from macrophages and replaced with 50 $\mu\text{L}/\text{well}$ of DMEM + 10% FBS + 100 $\mu\text{g}/\text{mL}$ fosfomycin to eliminate extracellular bacteria. Plates were incubated again for 30 min at 37°C with 5% CO_2 . Fosfomycin-containing media was then removed from macrophages and replaced with 50 $\mu\text{L}/\text{well}$ of DMEM + 10% FBS + 10 $\mu\text{g}/\text{mL}$ fosfomycin. Luminescence was read immediately after this media replacement step ($\text{Lux}_{0\text{ h}}$, Figure 1a), plates were incubated for 6 h at 37°C with 5% CO_2 , then luminescence was measured a second time ($\text{Lux}_{6\text{ h}}$, Figure 1a). Δ luminescence was calculated by dividing $\text{Lux}_{6\text{ h}}$ by $\text{Lux}_{0\text{ h}}$ to represent fold change replication over the course of the experiment.

LPM chemical screening

A culture of ST313 was grown overnight in LB, then subcultured ~1:50 in LB and grown for 2.5 h. This culture was then diluted ~1:350 into LPM and dispensed into 384-well clear flat-bottom plates (Corning) to a final volume of 30 μ L per well. 60 nL of each compound (5 mM stocks) was added (Echo 550 Liquid Handler) directly to bacteria-containing media, for a final concentration of 10 μ M compound per well. OD_{600} was read immediately after compound addition ($OD_{0\text{ h}}$, Figure 1b) and again after 20 h of incubation at 37°C ($OD_{20\text{ h}}$, Figure 1b). Δ growth was calculated by subtracting $OD_{0\text{ h}}$ from $OD_{20\text{ h}}$.

Data analysis and secondary screening of chemicals

Both the macrophage and LPM screens were performed in technical duplicate. Plate and well effects were normalized by interquartile-mean based methods (Mangat et al., 2014), and compounds reducing growth more than 2.65 s.d. below the mean of each dataset were considered 'hits'. For secondary screening of hit compounds, a similar protocol to the initial macrophage screen was followed, with the exception that compounds were serially diluted two-fold starting at 100 μ M to a final concentration of 0.78 μ M in DMEM + 10% FBS, prior to the 4 h incubation period with macrophages.

MIC determination for hit compounds

A culture of ST313 was grown overnight in LB, then diluted ~1:10000 into LB, LPM, or DMEM + 10% FBS. Compounds were serially diluted two-fold starting at 64 μ g/mL to a final concentration of < 0.1 μ g/mL, then added to bacteria-containing media. OD_{600} was read immediately after compound addition then again after ~20 h of incubation at 37°C.

Cytotoxicity assays

RAW264.7 macrophages were seeded into 96-well plates in DMEM + 10% FBS + 100 ng/mL LPS as described above. Compounds were serially diluted two-fold starting at 64 µg/mL to a final concentration of 0.5 µg/mL, then added directly to macrophages. After 4 h of incubation with compounds at 37°C with 5% CO₂, plates were centrifuged at 500 x g for 2 min and culture supernatant was collected for quantification of lactate dehydrogenase (LDH) release. Cytotoxicity was quantified colorimetrically (G-biosciences Cytoscan™-LDH Cytotoxicity Assay) wherein LDH activity is measured by recording A₄₉₀ after 20 min incubation with substrate mix at 37°C. Lysis control wells were treated with 10X lysis buffer for 45 min prior to supernatant collection. Percent cytotoxicity was calculated with the formula: $\frac{LDH_{Compound\ Treated} - LDH_{Spontaneous}}{LDH_{Maximum} - LDH_{Spontaneous}} \times 100\%$ where LDH_{Spontaneous} is the amount of LDH activity in the supernatant of untreated cells and LDH_{Maximum} is the amount of LDH activity in the supernatant of lysis control wells. The LDH activity in cell-free culture medium was subtracted from each value prior to normalization to account for serum.

Intramacrophage CFU enumeration

RAW264.7 macrophages were seeded into 96-well plates in DMEM + 10% FBS + 100 ng/mL LPS as described above. A single concentration of each compound (determined based on cytotoxicity testing) was added directly to wells with 6 technical replicates, with an equivalent volume of DMSO added to control wells. Macrophages were incubated with compounds for 4 h at 37°C with 5% CO₂.

A culture of ST313 was grown overnight in LB, then 30 min prior to infection (~3.5 h after compound addition), bacteria were opsonized for 30 min in 20% human serum (Innovative Research) in PBS at 37°C. Compound-containing media was

then removed from macrophages, and replaced with 100 μ L/well of opsonized bacteria (diluted in DMEM + 10% FBS to achieve a multiplicity of infection (MOI) of 50:1). Plates were centrifuged at 200 x g for 3 min, then incubated for 30 min at 37°C with 5% CO₂. Bacteria-containing media was then removed from macrophages and replaced with 100 μ L/well of DMEM + 10% FBS + 100 μ g/mL fosfomycin to eliminate extracellular bacteria. Plates were incubated again for 30 min at 37°C with 5% CO₂. Fosfomycin-containing media was then removed from macrophages and replaced with 100 μ L/well of DMEM + 10% FBS + 10 μ g/mL fosfomycin. Immediately after this media replacement step, adhered macrophages from half of the wells (triplicate) were lysed in sterile water. Bacterial colony-forming units (CFUs) from each lysed well were enumerated by serially diluting in PBS and plating on LB plates. After 6 h of incubation at 37°C with 5% CO₂, adhered macrophages from the other other half of the wells were lysed in sterile water for plating and CFU enumeration. Fold change in CFU/mL was calculated (CFU at 6 h divided by at 0 h) to represent replication over the course of the experiment. For experiments with 20 h of incubation, an identical protocol was followed, with the exception of a modified MOI of 20:1 to prevent excessive macrophage lysis overnight.

RNA isolation and RT-qPCR

RAW264.7 macrophages were seeded into 96-well plates in DMEM + 10% FBS + 100 ng/mL LPS as described above. A single concentration of each compound (determined based on cytotoxicity testing) was added directly to wells with 3 technical replicates, with an equivalent volume of DMSO added to control wells. Macrophages were incubated with compounds for 4 h at 37°C with 5% CO₂.

Compound-containing media was removed, then adhered macrophages were scraped and resuspended in 100 μ L Trizol (Invitrogen) for cell lysis. RNA was

extracted by chloroform (BioShop) separation following the manufacturer's protocol, precipitated with 100% isopropanol (BioShop) and washed with 75% ethanol (Sigma) before treatment with Dnase I (Turbo DNA-free kit). DNase I was inactivated with 2.5 mM EDTA and RNA was resuspended in DEPC water. For RT-qPCR experiments, cDNA was synthesized from purified RNA using qScript cDNA Supermix (Quantabio) and diluted 1:10 before use. *GAPDH* was used for normalization, RT-qPCR was performed in a LightCycler 480 (Roche) with PerfeCTa SYBR Green Supermix (Quantabio). For all experiments, normalized ratios (compound/DMSO) were calculated relative to *GAPDH* transcript levels.

Quantification and statistical analysis

Data were analyzed using RStudio version 1.0.143 with R version 3.2.2, and GraphPad Prism 8.0 software (GraphPad Inc., San Diego, CA). Each figure legend contains information on the type of statistical test used as well as mean and dispersion measures. P values of < 0.05 were considered significant.

Figures

Figure 4.1

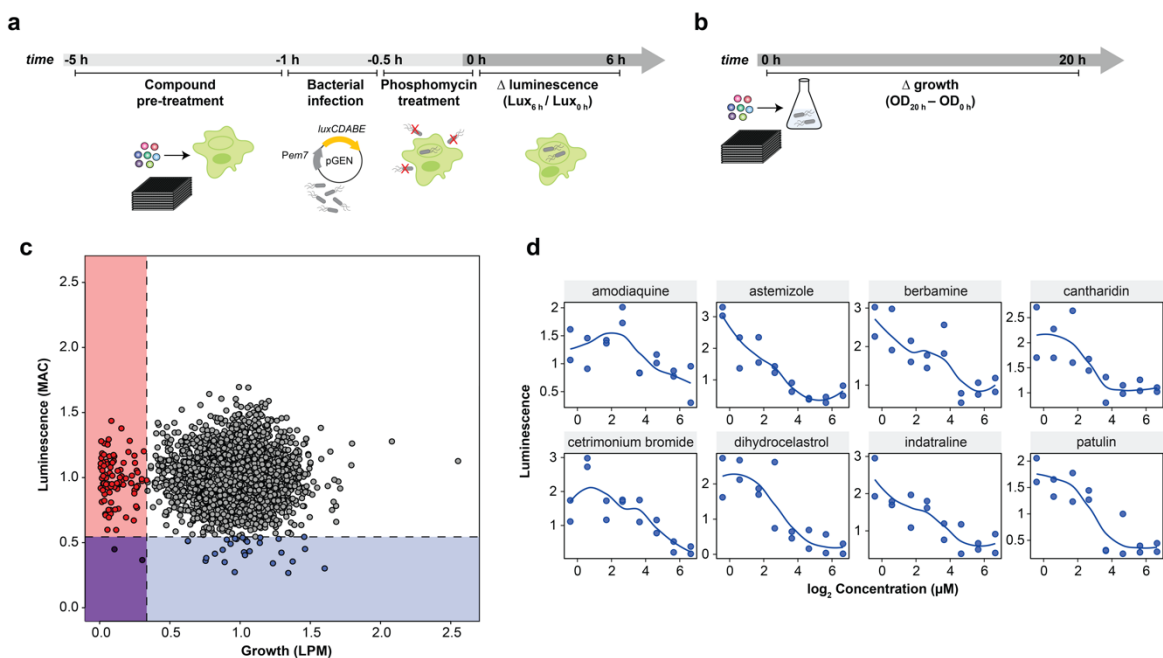


Figure 4.1. Immunomodulatory compounds restrict *Salmonella* replication in macrophages.

(a) Workflow of screening methods for small molecule screen in macrophages. RAW264.7 macrophages in 384-well plates were pre-treated with compounds for 4 h, infected with ST313 expressing the luminescent pGEN-*luxCDABE* plasmid for 30 min, then treated with fosfomycin to kill extracellular bacteria for 30 min. Luminescence was read at 0 and 6 h to approximate bacterial viability. (b) Workflow of screening methods for small molecule screen in LPM. OD_{600} was read at 0 and 20 h after compound addition. (c) Plot of screening data from macrophage and LPM chemical screens. Along y axis, luminescence production from pGEN-*luxCDABE* was monitored over 6 h, values on graph represent interquartile mean-normalized RLU per well, at 6 h divided by 0 h. Along x axis, bacterial growth was monitored, values on graph represent interquartile mean-

normalized, background subtracted OD₆₀₀ over 20 h of incubation. Red dots, blue dots, and purple dots indicate compounds that significantly reduced growth, luminescence, and both, respectively, 2.65 s.d. from the mean of the dataset (indicated by dotted lines). (d) Re-screening of hit compounds against *Salmonella* in macrophages. Dots indicate data (luminescence produced from pGEN-*luxCDABE*) from two technical replicates.

Figure 4.2

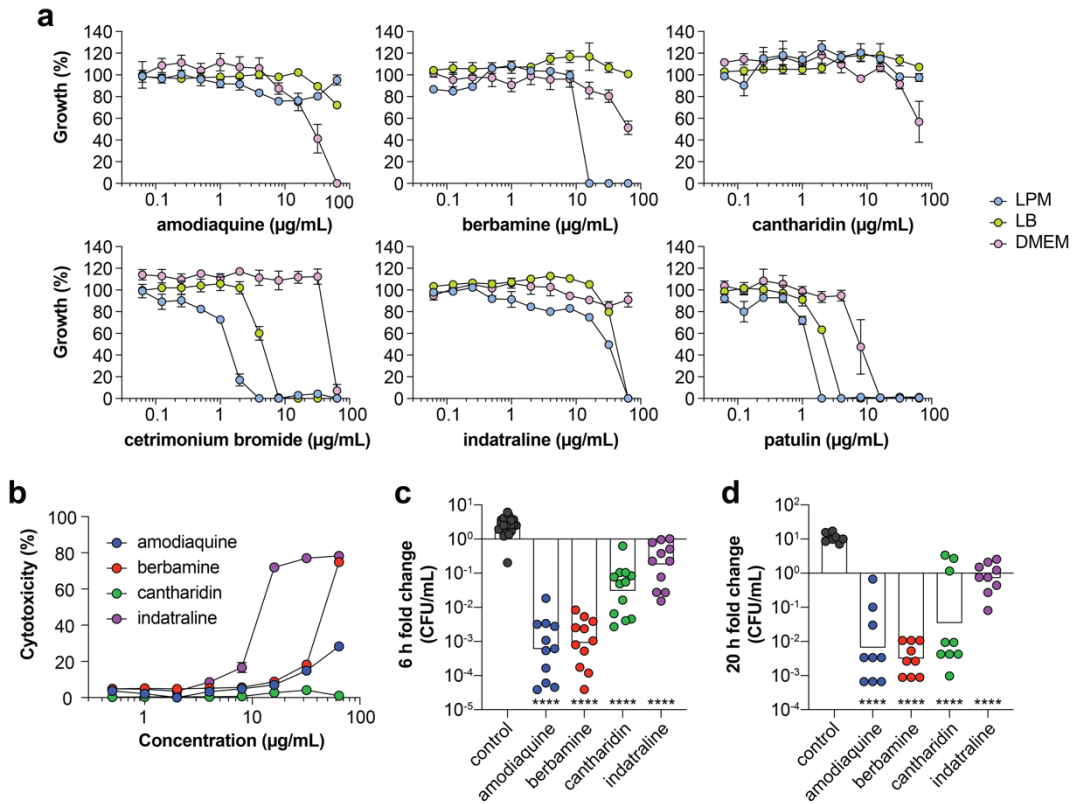


Figure 4.2. Potency analysis of putative HDT compounds.

(a) Growth normalized to a DMSO control (set to 100%) of ST313 in the presence of hit compounds. Data is from two-four biological replicates, dots and error indicate mean and s.e.m. (b) Percentage cytotoxicity after exposure to indicated compounds. Dots indicate mean and s.e.m. from three independent experiments. (c) Compound treatment and bacterial infection of RAW264.7 macrophages for 6 h. Bars indicate mean CFU/mL. Groups were compared against control-treated macrophages (equivalent concentration of DMSO) via one-way ANOVA and corrected for multiple comparisons with Bonferroni's test. ****p < 0.0001. (d) As in (c), for 20 h of bacterial infection.

Figure 4.3

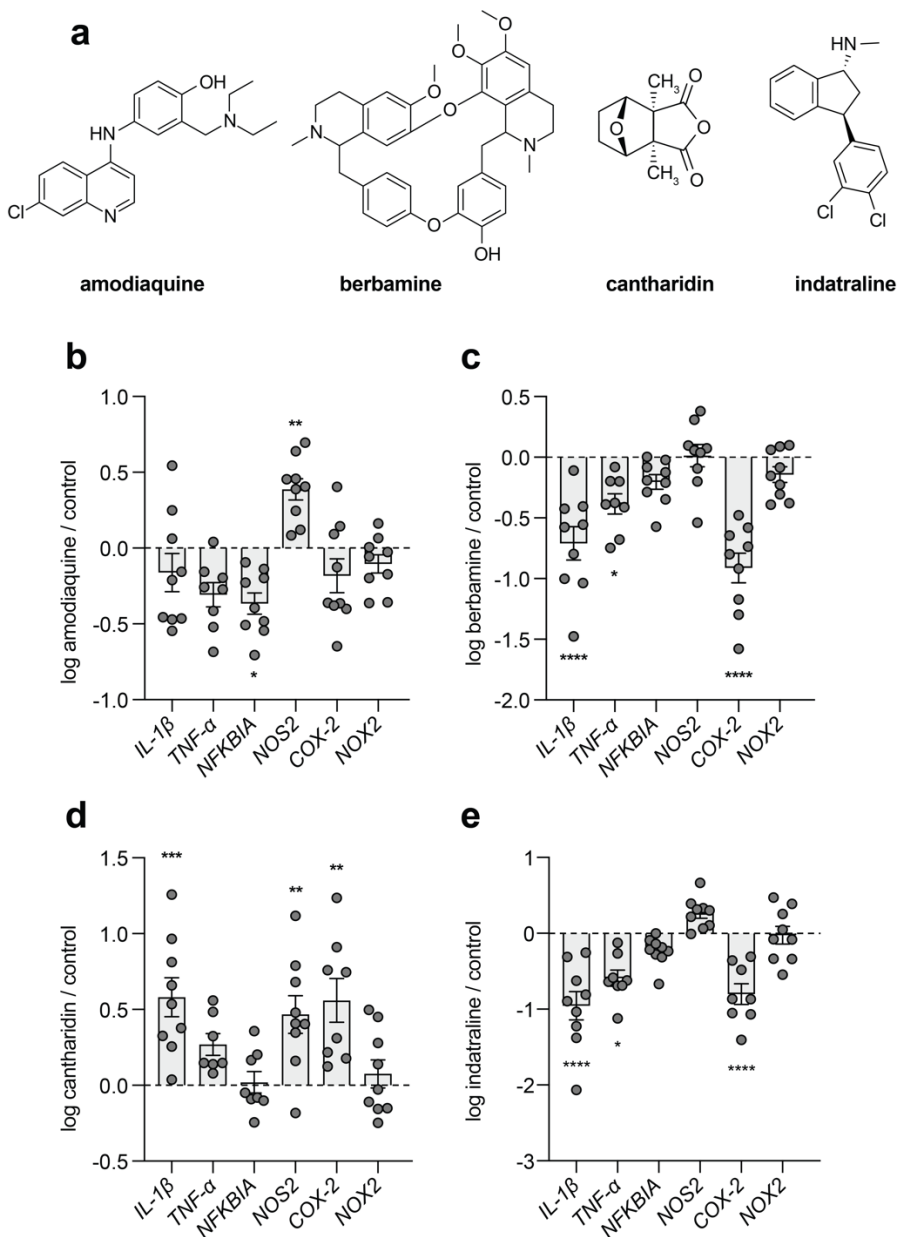


Figure 4.3. Immunomodulatory activity of hit compounds.

(a) Chemical structures of hit compounds. (b-e) Gene expression measured by RT-qPCR. Bars indicate mean and s.e.m. Groups were compared against a

value of 0 via one-way ANOVA and corrected for multiple comparisons with Dunnett's test. * $p < 0.05$, ** $p < 0.01$, *** $p < 0.001$, **** $p < 0.0001$.

CHAPTER 5 – Conclusions

Summary

The work presented in this thesis describes three non-traditional discovery approaches that leverage the setting of infection and the activity of the host immune system to identify conditionally active anti-infective compounds. Chapter 2 describes the discovery of an intracellular-specific antimicrobial, metergoline, which inhibits intramacrophage *Salmonella* replication and extends animal survival in a murine model of systemic salmonellosis. Chapter 3 presents a promoter reporter-based screen to identify the anti-virulence compound, dephostatin, which antagonizes SsrA/B and PmrB/A TCS signaling and enhances sensitivity to colistin *in vitro* and *in vivo*. Chapter 4 investigates the potential for immunomodulatory compounds to restrict *Salmonella* replication in macrophages with host-targeting activity, leading to the identification of four small molecules that attenuate infections caused by a multidrug resistant strain of *Salmonella*. This final chapter considers these new anti-infectives within the landscape of modern drug discovery and proposes some future avenues of investigation within this research area.

Conditional antimicrobial activity and outer membrane disruption

In chapter 2, we performed a chemical screen to enrich for antimicrobial compounds that are selectively active against intramacrophage *Salmonella*. The premise of this work was founded in previously published studies (Ersoy et al., 2017; Farha et al., 2017) that suggested antibiotic sensitivity may differ between traditional *in vitro* growth conditions and others that more closely resembled the setting of infection. Historically, this idea emerged from the notable antibiotic prontosil, which was inactive *in vitro* yet efficacious *in vivo* due to a requirement for host-mediated metabolic conversion (Bentley, 2009). Analogously, we observed that metergoline was active only in Mg²⁺-deplete environments, as its

entry required *in cellulo* permeabilization of the outer membrane (OM) of *Salmonella*.

In the years since this work was published, similar findings derived from screening in infection-relevant conditions have been reported many times. This list is far from comprehensive, but some notable examples include: the hyperactivity of rifabutin against *Acinetobacter baumannii* in only nutrient-limited media (Luna et al., 2020); the selective activity of ruthenium red and several other chemical compounds against *Klebsiella pneumoniae* grown in human blood serum (Weber et al., 2020); the intramacrophage-specific antimicrobial activity of clofazimine (Nagy et al., 2020) and an inner membrane perturbant (Dombach et al., 2020) against *Salmonella*; the enhanced activity of avibactam against multidrug resistant *K. pneumoniae* in the presence of the human cathelicidin antimicrobial peptide LL-37 (Ulloa et al., 2019); the *in vitro* and *in vivo* activity of a biotin biosynthesis inhibitor only in conditions mimicking biotin levels in human environments (Carfrae et al., 2020); the restoration of azithromycin activity against macrolide-resistant bacteria in the presence of physiological bicarbonate concentrations (Farha et al., 2020); and the sensitization of Gram-negative bacteria to antibiotics with conventionally Gram-positive-specific activity in human blood serum (Heesterbeek et al., 2019). It is clear that the use of these host-mimicking growth conditions has the potential to consistently unmask otherwise inactive antimicrobials, and therefore could add to our existing antibiotic arsenal in a meaningful way.

It is worth noting that a majority of these recently identified compounds were conditionally active due to some form of immune-mediated Gram-negative OM permeabilization (i.e. nutritional immunity strategies to deplete ions essential for membrane integrity, antimicrobial peptides that induce membrane perturbation, complement proteins that create OM pores, amongst other factors). Indeed,

compounds that require OM perturbation for their activity are likely the low-hanging fruit of host-mimicking drug screens, given the formidable nature of the OM as a barrier to drug entry (Brown et al., 2014). For those interested in continuing to uncover *in vivo* actives that require membrane permeabilization, these technically challenging screens (for example, the maintenance of cultured macrophages or other immune cell lines is more difficult and prone to error than the use of standard growth media) may be replaced by screening in the presence of an OM perturbant. Indeed, there is precedent indicating that OM perturbants paired with otherwise inactive compounds have significant clinical potential as combinatorial anti-infective therapies (MacNair and Brown, 2020; MacNair et al., 2018; Stokes et al., 2017). Conversely, enriching for conditionally active anti-infectives that do not require membrane permeabilization – a more elusive class of compounds, in my opinion – may require an additional layer of screening to triage hit compounds, such as counter-selecting against chemicals that synergize with conventional OM perturbants like colistin.

Chemicals identified from infection-mimicking screens can also serve as biological probes of conditional gene essentiality in pathogens. Many questions remain in the study of *Salmonella*-host cell interactions *in vivo*; unfortunately, those that are most pressing are difficult to interrogate under conventional laboratory growth conditions. Screening annotated chemical collections gives researchers access to hit compounds with often well-characterized primary targets, providing chemical probes that can be exploited for mechanistic studies. Moving forward with these types of screens for *Salmonella* may allow researchers to explore which bacterial factors are required for survival under the many unique host microenvironments it encounters, and how these differ in timing and expression throughout the heterogeneous landscape of infection.

Advantages and disadvantages of inhibiting bacterial virulence

In chapter 3, we looked to anti-virulence inhibitors as an alternative anti-infective strategy. In this study, we selected TCSs as virulence targets given their demonstrated importance during pathogenesis and the implicit possibility for us to abolish multiple axes of *Salmonella* virulence with the inhibition of a single top-level regulator. Although the exact mechanism of action of dephostatin remains unknown, its relatively non-specific activity may have been advantageous – its inhibition of multiple TCSs (at least two, to our knowledge) attenuated *Salmonella* virulence within more than one important pathway, facilitating the synergistic interaction between dephostatin and colistin. Indeed, this and other recently published studies validate regulatory systems as targets for anti-virulence therapies (Carabajal et al., 2020; El-Halfawy et al., 2019; Gao et al., 2018; Maura et al., 2017), but it remains to be seen whether this approach will be translated into clinical practice.

An important aspect of this study was the possibility to explore the proposed evolutionary benefit of anti-virulence therapies. Many have claimed that virulence inhibitors are likely to exert weaker selection for bacterial resistance evolution, compared to conventional antibiotics. While the latter target bacterial survival itself and produce strong selective pressure for resistance, the former would ideally have no influence on bacterial growth *in vitro* and would not exert the fitness cost normally associated with antimicrobial exposure. To this end, our attempts to isolate suppressors resistant to dephostatin and colistin produced only a single mutation associated with colistin resistance alone, suggesting that dephostatin may indeed exert less selective pressure than a conventional antimicrobial. However, further experimentation is required to examine the ‘resistance-proof’ potential of anti-virulence agents, such as serial passaging experiments in settings that more closely resemble the setting of infection.

Although our and others' (Gerdt and Blackwell, 2014; Mellbye and Schuster, 2011; Rezzoagli et al., 2018; Ross-Gillespie et al., 2014) *in vitro* studies supporting a resistance-proof claim are compelling, the ablation of virulence gene expression during infection is almost certain to confer a fitness disadvantage to an invading pathogen. Ultimately, it may be more important to ask whether there is an advantage for anti-virulence compounds to impose niche-specific selective pressure on bacteria (i.e. only in the setting of infection), compared to conventional antibiotics that are more likely to select for bacterial resistance irrespective of environment.

There are several limitations of anti-virulence therapies that must also be evaluated in future studies. One perspective that emerges from this work is the narrow-spectrum activity of dephostatin, similar to that of other anti-virulence agents that have been identified – indeed, most virulence factors are species or even strain-specific (Dickey et al., 2017). Unfortunately, the prohibitively slow nature of current diagnostic methods has favoured broad-spectrum therapies, which enable treatment before a definitive diagnosis can be reached. In these cases, anti-virulence agents would likely need to be administered in combination with existing antibiotics to achieve appropriate levels of bacterial coverage. Further, clinical advancement of these alternative treatments would require an improved understanding of the heterogeneity of virulence for individual pathogens. Immune responses to infection are often heterogeneous and are met with similarly variable responses in bacterial virulence, suggesting that the administration of anti-virulence therapies would need to be timed appropriately. It is also likely that these treatments will be sensitive to the immune status of the infected individual, as robust immune system activity would ultimately be required to clear even an attenuated infection. Finally, the non-essentiality of virulence factors *in vitro* precludes traditional susceptibility testing for minimum inhibitory

concentration (MIC) and breakpoint determination, complicating the nature of pre-clinical and susceptibility studies.

Taken together, these disadvantages have and will continue to complicate anti-virulence drug development – already, several candidates have failed to progress through clinical trials (Theuretzbacher and Piddock, 2019). However, I remain optimistic that these antibiotic alternatives may one day be useful in clinical practice, if only in combination with other anti-infective treatments. Improvements in diagnostic testing to accurately identify pathogens and perhaps even test for virulence factor expression will be paramount to this future goal. Moreover, future research must focus on characterizing the interactions between putative anti-virulence drugs and existing antibiotic treatment options, as data on these combinations will be required to prove superiority to standard-of-care monotherapies. We can hope to identify new anti-virulence agents that synergize with existing antibiotics, allowing for dose-sparing and enhanced efficacy against even drug-resistant pathogens.

Direct targeting of the host immune system during infection

In chapter 4, we investigated host-directed therapy (HDT) as a third approach to mitigate *Salmonella* infection. For this work, we were specifically interested in finding HDT compounds that would target the ST313 sequence type of *Salmonella*, as strains within this lineage are capable of causing more serious illness during human infections and are also antibiotic resistant. We reasoned that the distinct immunomodulatory activity of HDT compounds could sensitize ST313 to host immune processes and attenuate infection.

A proposed benefit of HDT is its potential to circumvent traditional selective pressure for resistance evolution, by targeting only the host immune system.

Such compounds are also likely to exert broad-spectrum activity – given the conservation of immune responses against multiple bacterial species – which is advantageous for standard-of-care empiric therapies. However, very few HDTs have advanced through clinical trials as stand-alone anti-infectives, and in practice would likely need to be administered in combination with antibiotics or other therapeutics. Future work in this research area should be directed to identifying HDT compounds that stimulate and repress the immune system during *Salmonella* infection, as controlling excessive instances of inflammation is as important as amplification when necessary. It will be especially important to ensure that such compounds do not induce overstimulation of the immune system, as a disruption of this delicate balance may lead to excessive host tissue damage. In practice, the administration of HDT compounds (similar to the other unconventional anti-infectives discussed herein) is likely to require a paradigm shift into personalized medicine, where treatments are tailored to both appropriately diagnosed infections and patients.

Similar to our work in chapter 2, a potentially interesting route of investigation into anti-*Salmonella* HDTs is their use as probes for the molecular mechanisms of host-pathogen interactions. Relative to the ST19 sequence type of *Salmonella*, several questions remain regarding the differential adaptation of ST313 to infective environments within human hosts. To this end, using HDT screens to interrogate ST313 susceptibility to different forms of macrophage immunomodulation holds great promise. Elucidating the mechanism of action of putative HDT compounds may reveal previously unknown aspects of the intracellular lifestyle of ST313, such as its interactions with immune pathways that trigger cytokine production, autophagy, phagosomal maturation, and inflammasome activation. This would complement the recent literature describing the differences between ST313 and ST19, in which ST313 is described as having undergone specific genome degradation consistent with adaptation to human

colonization (Kingsley et al., 2009). As has been shown in other enteric pathogens adapting to a more invasive, extraintestinal lifestyle, several genes required for growth in the inflamed gut have been lost, inactivated or are down-regulated in ST313 (Canals et al., 2019a; Canals et al., 2019b). The phenotypes associated with these adaptations include decreases in the ability to ferment melibiose (Yang et al., 2015), metabolize L-tartaric acid and dihydroxyacetone as alternative carbon sources, and utilize purine and pyrimidine nucleotides as sources of phosphorus (Okoro et al., 2015). It is currently unknown if the loss of these metabolic processes has impacted the intracellular lifestyle of ST313, but I would consider it to be highly probable – depending on macrophage polarization status, *Salmonella* has access to divergent nutrient profiles that may require metabolic adaptation.

Final remarks

Antibiotic resistance has reached critical levels and is threatening the very foundation of modern medicine. It is now crucial that we explore non-traditional approaches in drug discovery to uncover new therapeutic options for infection. Strategies such as antibiotic potentiation, the use of infection-relevant screening conditions, virulence inhibition, and host-directed immunomodulation are all promising, but remain in their infancy. These unconventional approaches have and will continue to face significant challenges, and their future clinical development will require a modified outlook on narrow-spectrum activity, drastic improvements in diagnostics, alterations in pre-clinical assays for compound activity, and rigorous species-specific investigation into the heterogeneous landscape of infection. It will only be with persistent academic investment into these research areas that the austere threat of a post-antibiotic age may be avoided.

REFERENCES

- Allen, R.C., Papat, R., Diggle, S.P., and Brown, S.P. (2014). Targeting virulence: can we make evolution-proof drugs? *Nature Reviews Microbiology* 12, 300-308.
- Amara, N., Mashiach, R., Amar, D., Krief, P., Spieser, S.A.H., Bottomley, M.J., Aharoni, A., and Meijler, M.M. (2009). Covalent inhibition of bacterial quorum sensing. *Journal of the American Chemical Society* 131, 10610-10619.
- Amro, N.A., Kotra, L.P., Wadu-Mesthrige, K., Bulychev, A., Mobashery, S., and Liu, G.-y. (2000). High-resolution atomic force microscopy studies of the *Escherichia coli* outer membrane: structural basis for permeability. *Langmuir* 16, 2789-2796.
- Anantharajah, A., Faure, E., Buyck, J.M., Sundin, C., Lindmark, T., Meccas, J., Yahr, T.L., Tulkens, P.M., Mingeot-Leclercq, M.P., Guery, B., *et al.* (2016). Inhibition of the injectisome and flagellar type III secretion systems by INP1855 impairs *Pseudomonas aeruginosa* pathogenicity and inflammasome activation. *Journal of Infectious Diseases* 214, 1105-1116.
- Ao, T.T., Feasey, N.A., Gordon, M.A., Keddy, K.H., Angulo, F.J., and Crump, J.A. (2015). Global burden of invasive nontyphoidal *Salmonella* disease, 2010. *Emerging Infectious Diseases* 21, 941-949.
- Årdal, C., Lacotte, Y., and Ploy, M.-C. (2020). Financing pull mechanisms for antibiotic-related innovation: opportunities for Europe. *Clinical Infectious Diseases* 71, 1994-1999.
- Arpaia, N., Godec, J., Lau, L., Sivick, K.E., McLaughlin, L.M., Jones, M.B., Dracheva, T., Peterson, S.N., Monack, D.M., and Barton, G.M. (2011). TLR signaling is required for *Salmonella* Typhimurium virulence. *Cell* 144, 675-688.
- Ashton, P.M., Owen, S.V., Kaindama, L., Rowe, W.P.M.M., Lane, C.R., Larkin, L., Nair, S., Jenkins, C., de Pinna, E.M., Feasey, N.A., *et al.* (2017). Public health surveillance in the UK revolutionises our understanding of the invasive *Salmonella* Typhimurium epidemic in Africa. *Genome Medicine* 9, 92-92.
- Aussel, L., Zhao, W., Hébrard, M., Guilhon, A.-a., Viala, J.P.M., Henri, S., Chasson, L., Gorvel, J.-p., Barras, F., and Méresse, S. (2011). *Salmonella* detoxifying enzymes are sufficient to cope with the host oxidative burst. *Molecular Microbiology* 80, 628-640.

Bader, M.W.M.W., Sanowar, S., Daley, M.E.M.E., Schneider, A.R.A.R., Cho, U., Xu, W., Klevit, R.E., Moual, H.L., and Miller, S.I. (2005). Recognition of antimicrobial peptides by a bacterial sensor kinase. *Cell* 122, 461-472.

Bakker, E.P., and Mangerich, W.E. (1981). Interconversion of components of the bacterial proton motive force by electrogenic potassium transport. *Journal of Bacteriology* 147, 820-826.

Bang, I.S., Audia, J.P., Park, Y.K., and Foster, J.W. (2002). Autoinduction of the *ompR* response regulator by acid shock and control of the *Salmonella enterica* acid tolerance response. *Molecular Microbiology* 44, 1235-1250.

Barker, W.T., Martin, S.E., Chandler, C.E., Nguyen, T.V., Harris, T.L., Goodell, C., Melander, R.J., Doi, Y., Ernst, R.K., and Melander, C. (2017). Small molecule adjuvants that suppress both chromosomal and *mcr-1* encoded colistin-resistance and amplify colistin efficacy in polymyxin-susceptible bacteria. *Bioorganic & Medicinal Chemistry* 25, 5749-5753.

Barrick, J.E., Colburn, G., Deatherage, D.E., Traverse, C.C., Strand, M.D., Borges, J.J., Knoester, D.B., Reba, A., and Meyer, A.G. (2014). Identifying structural variation in haploid microbial genomes from short-read resequencing data using breseq. *BMC Genomics* 15, 1039-1039.

Bartek, I.L., Reichlen, M.J., Honaker, R.W., Leistikow, R.L., Clambey, E.T., Scobey, M.S., Hinds, A.B., Born, S.E., Covey, C.R., Schurr, M.J., *et al.* (2016). Antibiotic bactericidal activity is countered by maintaining pH homeostasis in *Mycobacterium smegmatis*. *mSphere* 1, e00176-00116-00118.

Barthel, M., Hapfelmeier, S., Quintanilla-Martínez, L., Kremer, M., Rohde, M., Hogardt, M., Pfeffer, K., Rüssmann, H., and Hardt, W.-D. (2003). Pretreatment of mice with streptomycin provides a *Salmonella enterica* serovar Typhimurium colitis model that allows analysis of both pathogen and host. *Infection and Immunity* 71, 2839-2858.

Bäumler, A.J.A.J., Tsolis, R.M.R.M., Ficht, T.A.T.A., and Adams, L.G. (1998). Evolution of host adaptation in *Salmonella enterica*. *Infection and Immunity* 66, 4579-4587.

Bearson, B.L., Wilson, L., and Foster, J.W. (1998). A low pH-inducible, PhoPQ-dependent acid tolerance response protects *Salmonella* Typhimurium against inorganic acid stress. *Journal of Bacteriology* 180, 2409-2417.

Behnsen, J., Perez-Lopez, A., Nuccio, S.-P.S.P.S.-P., and Raffatellu, M. (2015). Exploiting host immunity: the *Salmonella* paradigm. *Trends in Immunology* 36, 112-120.

Bem, A.E., Velikova, N., Pellicer, M.T., Baarlen, P.v., Marina, A., Wells, J.M., Van Baarlen, P., Marina, A., and Wells, J.M. (2014). Bacterial histidine kinases as novel antibacterial drug targets. *ACS Chemical Biology* 10, 213-224.

Bentley, R. (2009). Different roads to discovery; Prontosil (hence sulfa drugs) and penicillin (hence β -lactams). *Journal of Industrial Microbiology and Biotechnology* 36, 775-786.

Bevins, C.L., and Salzman, N.H. (2011). Paneth cells, antimicrobial peptides and maintenance of intestinal homeostasis. *Nature Reviews Microbiology* 9, 356-368.

Bhan, M., Bahl, R., and Bhatnagar, S. (2005). Typhoid and paratyphoid fever. *The Lancet* 366, 749-762.

Bijlsma, J.J.E., and Groisman, E.A. (2005). The PhoP/PhoQ system controls the intramacrophage type three secretion system of *Salmonella enterica*. *Molecular Microbiology* 57, 85-96.

Birmingham, C.L., Smith, A.C., Bakowski, M.A., Yoshimori, T., and Brumell, J.H. (2006). Autophagy controls *Salmonella* infection in response to damage to the *Salmonella*-containing vacuole. *Journal of Biological Chemistry* 281, 11374-11383.

Bowdish, D.M.E., and Davidson, D.J. (2005). A re-evaluation of the role of host defence peptides in mammalian immunity. *Current Protein and Peptide Science* 6, 35-51.

Branchu, P., Bawn, M., and Kingsley, R.A. (2018). Genome variation and molecular epidemiology of *Salmonella enterica* serovar Typhimurium pathovariants. *Infection and Immunity* 86, e00079-00018.

Bravo, D., Silva, C., Carter, J.A., Hoare, A., Alvarez, S.A., Blondel, C.J., Zaldívar, M., Valvano, M.A., and Contreras, I. (2008). Growth-phase regulation of lipopolysaccharide O-antigen chain length influences serum resistance in serovars of *Salmonella*. *Journal of Medical Microbiology* 57, 938-946.

Brennan-Krohn, T., Pironti, A., and Kirby, J.E. (2018). Synergistic activity of colistin-containing combinations against colistin-resistant Enterobacteriaceae. *Antimicrobial Agents and Chemotherapy* 62, 801-801.

Brown, D.G., May-Dracka, T.L., Gagnon, M.M., and Tommasi, R. (2014). Trends and exceptions of physical properties on antibacterial activity for Gram-positive and Gram-negative pathogens. *Journal of Medicinal Chemistry* 57, 10144-10161.

Brown, E.D., and Wright, G.D. (2016). Antibacterial drug discovery in the resistance era. *Nature* 529, 336-343.

Brown, K.L.K.L., and Hancock, R.E.W.R.E.W. (2006). Cationic host defense (antimicrobial) peptides. *Current Opinion in Immunology* 18, 24-30.

Broz, P., Ruby, T., Belhocine, K., Bouley, D.M., Kayagaki, N., Dixit, V.M., and Monack, D.M. (2012). Caspase-11 increases susceptibility to *Salmonella* infection in the absence of caspase-1. *Nature* 490, 288-291.

Bumann, D., and Cunrath, O. (2017). Heterogeneity of *Salmonella*-host interactions in infected host tissues. *Current Opinion in Microbiology* 39, 57-63.

Bumann, D., and Schothorst, J. (2017). Intracellular *Salmonella* metabolism. *Cellular Microbiology* 19, e12766-e12766.

Byun, E., Hong, B., De Castro, K.A., Lim, M., and Rhee, H. (2007). One-pot reductive mono-N-alkylation of aniline and nitroarene derivatives using aldehydes. *Journal of Organic Chemistry* 72, 9815-9817.

Calva, E., and Oropeza, R. (2006). Two-component signal transduction systems, environmental signals, and virulence. *Microbial Ecology* 51, 166-176.

Campoy, S., Jara, M., and Busquets, N. (2002). Role of the high-affinity zinc uptake znuABC system in *Salmonella enterica* serovar Typhimurium virulence. *Infection and Immunity* 70, 4721-4725.

Canals, R., Chaudhuri, R.R., Steiner, R.E., Owen, S.V., Quinones-Olvera, N., Gordon, M.A., Baym, M., Ibba, M., and Hinton, J.C.D. (2019a). The fitness landscape of the African *Salmonella* Typhimurium ST313 strain D23580 reveals unique properties of the pBT1 plasmid. *PLoS Pathogens* 15.

Canals, R., Hammarlöf, D.L., Kröger, C., Owen, S.V., Fong, W.Y., Lacharme-Lora, L., Zhu, X., Wenner, N., Carden, S.E., Honeycutt, J., *et al.* (2019b). Adding function to the genome of African *Salmonella* Typhimurium ST313 strain D23580. *PLoS Biology* 17, e3000059.

Cannatelli, A., Di Pilato, V., Giani, T., Arena, F., Ambretti, S., Gaibani, P., D'Andrea, M.M., and Rossolinia, G.M. (2014). *In vivo* evolution to colistin resistance by PmrB sensor kinase mutation in KPC-producing *Klebsiella*

pneumoniae is associated with low-dosage colistin treatment. *Antimicrobial Agents and Chemotherapy* 58, 4399-4403.

Capra, E.J., and Laub, M.T. (2012). Evolution of two-component signal transduction systems. *Annual Review of Microbiology* 66, 325-347.

Carabajal, M.A., Asquith, C.R.M., Laitinen, T., Tizzard, G.J., Yim, L., Rial, A., Chabalgoity, J.A., Zuercher, W.J., and Vescovi, E.G. (2020). Quinazoline-based antivirulence compounds selectively target *Salmonella* PhoP/PhoQ signal transduction system. *Antimicrobial Agents and Chemotherapy* 64, e01744-01719.

Carfrae, L.A., MacNair, C.R., Brown, C.M., Tsai, C.N., Weber, B.S., Zlitni, S., Rao, V.N., Chun, J., Junop, M.S., and Coombes, B.K. (2020). Mimicking the human environment in mice reveals that inhibiting biotin biosynthesis is effective against antibiotic-resistant pathogens. *Nature Microbiology* 5, 93-101.

Casino, P., Rubio, V., and Marina, A. (2009). Structural insight into partner specificity and phosphoryl transfer in two-component signal transduction. *Cell* 139, 325-336.

Castanheira, S., and García-Del Portillo, F. (2017). *Salmonella* populations inside host cells. *Frontiers in Cellular and Infection Microbiology* 7, 432-432.

CDC (2019). Antibiotic resistance threats in the United States, 2019 (Atlanta, GA: U.S. Department of Health and Human Services).

Chau, N.E., Pérez-Morales, D., Elhenawy, W., Bustamante, V.H., Zhang, Y.E., and Coombes, B.K. (2021). (p)ppGpp-dependent regulation of the nucleotide hydrolase PpnN confers complement resistance in *Salmonella enterica* serovar Typhimurium. *Infection and Immunity* 89.

Chen, H.D., and Groisman, E.A. (2013). The biology of the PmrA/PmrB two-component system: the major regulator of lipopolysaccharide modifications. *Annual Review of Microbiology* 67, 83-112.

Cheung, J., and Hendrickson, W.A. (2010). Sensor domains of two-component regulatory systems. *Current Opinion in Microbiology* 13, 116-123.

Chiu, H.C., Kulp, S.K., Soni, S., Wang, D., Gunn, J.S., Schlesinger, L.S., and Chen, C.S. (2009). Eradication of intracellular *Salmonella enterica* serovar typhimurium with a small-molecule, host cell-directed agent. *Antimicrobial Agents and Chemotherapy* 53, 5236-5244.

Cho, Y.S., Yen, C.-n., Shim, J.S., Kang, D.H., Kang, S.W., Liu, J.O., and Kwon, H.J. (2016). Antidepressant indatraline induces autophagy and inhibits restenosis via suppression of mTOR/S6 kinase signaling pathway. *Scientific Reports* 6, 1-9.

Choi, J., and Groisman, E.A. (2013). The lipopolysaccharide modification regulator PmrA limits *Salmonella* virulence by repressing the type three-secretion system Spi/Ssa. *Proceedings of the National Academy of Sciences* 110, 9499-9504.

Christianson, S., Golding, G.R., Campbell, J., Program, C.N.I.S., and Mulvey, M.R. (2007). Comparative genomics of Canadian epidemic lineages of methicillin-resistant *Staphylococcus aureus*. *Journal of Clinical Microbiology* 45, 1904-1911.

Colgan, A.M., Kröger, C., Diard, M., Hardt, W.-D., Puente, J.L., Sivasankaran, S.K., Hokamp, K., and Hinton, J.C.D. (2016). The impact of 18 ancestral and horizontally-acquired regulatory proteins upon the transcriptome and sRNA landscape of *Salmonella enterica* serovar Typhimurium. *PLoS Genetics* 12, e1006258.

Colquhoun, J.M., Wozniak, R.A., and Dunman, P.M. (2015). Clinically relevant growth conditions alter *Acinetobacter baumannii* antibiotic susceptibility and promote identification of novel antibacterial agents. *PLoS ONE* 10, e0143033.

Commissaris, R.L., and Rech, R.H. (1982). Interactions of metergoline with diazepam, quipazine, and hallucinogenic drugs on a conflict behavior in the rat. *Psychopharmacology* 76, 282-285.

Coombes, B.K., Brown, N.F., Valdez, Y., Brumell, J.H., and Finlay, B.B. (2004). Expression and secretion of *Salmonella* pathogenicity island-2 virulence genes in response to acidification exhibit differential requirements of a functional type III secretion apparatus and SsaL. *Journal of Biological Chemistry* 279, 49804-49815.

Coombes, B.K., Lowden, M.J., Bishop, J.L., Wickham, M.E., Brown, N.F., Duong, N., Osborne, S., Gal-mor, O., and Finlay, B.B. (2007). SseL is a *Salmonella*-specific translocated effector integrated into the SsrB-controlled *Salmonella* pathogenicity island 2 type III secretion system. *Infection and Immunity* 75, 574-580.

Coombes, B.K., Wickham, M.E., Lowden, M.J., Brown, N.F., and Finlay, B.B. (2005). Negative regulation of *Salmonella* pathogenicity island 2 is required for contextual control of virulence during typhoid. *Proceedings of the National Academy of Sciences* 102, 17460-17465.

Côté, J.-P., French, S., Gehrke, S.S., Macnair, C.R., Mangat, C.S., Bharat, A., and Brown, E.D. (2016). The genome-wide interaction network of nutrient stress genes in *Escherichia coli*. *mBio* 7, 1-12.

Curtis, M.M., Russell, R., Moreira, C.G., Adebesein, A.M., Wang, C., Williams, N.S., Taussig, R., Stewart, D., Zimmern, P., Lu, B., *et al.* (2014). QseC inhibitors as an antivirulence approach for Gram-negative pathogens. *mBio* 5, e02165-02114.

Cuypers, W.L., Jacobs, J., Wong, V., Klemm, E.J., Deborggraeve, S., and Van Puyvelde, S. (2018). Fluoroquinolone resistance in *Salmonella*: insights by whole-genome sequencing. *Microbial Genomics* 82, 346-349.

Czyz, D.M., Potluri, L.-P.P., Jain-Gupta, N., Riley, S.P., Martinez, J.J., Steck, T.L., Crosson, S., Shuman, H.A., Gabay, J.E., Czyż, D.M., *et al.* (2014). Host-directed antimicrobial drugs with broad-spectrum efficacy against intracellular bacterial pathogens. *mBio* 5, e01534.

D'Elia, M.A., Pereira, M.P., Brown, E.D., D'Elia, M.A., Pereira, M.P., and Brown, E.D. (2009). Are essential genes really essential? *Trends in Microbiology* 17, 433-438.

Datsenko, K.A., and Wanner, B.L. (2000). One-step inactivation of chromosomal genes in *Escherichia coli* K-12 using PCR products. *Proceedings of the National Academy of Sciences* 97, 6640-6645.

Datta, S., Costantino, N., and Court, D.L. (2006). A set of recombineering plasmids for Gram-negative bacteria. *Gene* 379, 109-115.

Davies, J., and Davies, D. (2010). Origins and evolution of antibiotic resistance. *Microbiology and Molecular Biology Reviews* 74, 417-433.

Delcour, A.H. (2009). Outer membrane permeability and antibiotic resistance. *Biochimica et Biophysica Acta* 1794, 808-816.

Deng, W., Marshall, N.C., Rowland, J.L., McCoy, J.M., Worrall, L.J., Santos, A.S., Strynadka, N.C.J., and Finlay, B.B. (2017). Assembly, structure, function and regulation of type III secretion systems. *Nature Reviews Microbiology* 15, 323-337.

Desai, S.K., Winardhi, R.S., Periasamy, S., Dykas, M.M., Jie, Y., and Kenney, L.J. (2016). The horizontally-acquired response regulator SsrB drives a *Salmonella* lifestyle switch by relieving biofilm silencing. *eLife* 5, e10747.

Dickey, S.W., Cheung, G.Y.C., and Otto, M. (2017). Different drugs for bad bugs: antivirulence strategies in the age of antibiotic resistance. *Nature Reviews Drug Discovery* 16, 457-471.

Dombach, J.L., Quintana, J.L., Nagy, T.A., Wan, C., Crooks, A.L., Yu, H., Su, C.-C., Yu, E.W., Shen, J., and Detweiler, C.S. (2020). A small molecule that mitigates bacterial infection disrupts Gram-negative cell membranes and is inhibited by cholesterol and neutral lipids. *PLoS Pathogens* 16, e1009119.

Edwards, R.A., Keller, L.H., and Schifferli, D.M. (1998). Improved allelic exchange vectors and their use to analyze 987P fimbria gene expression. *Gene* 207, 149-157.

El-Halfawy, O.M., Czarny, T.L., Flannagan, R.S., Day, J., Bozelli, J.C., Kuiack, R.C., Salim, A., Eckert, P., Epand, R.M., McGavin, M.J., *et al.* (2019). Discovery of an antivirulence compound that reverses β -lactam resistance in MRSA. *Nature Chemical Biology* 16, 143-149.

Ellermeier, J.R., and Slauch, J.M. (2007). Adaptation to the host environment: regulation of the SPI1 type III secretion system in *Salmonella enterica* serovar Typhimurium. *Current Opinion in Microbiology* 10, 24-29.

Ellis, M.J., Tsai, C.N., Johnson, J.W., French, S., Elhenawy, W., Porwollik, S., Andrews-Polymenis, H., McClelland, M., Magolan, J., Coombes, B.K., *et al.* (2019). A macrophage-based screen identifies antibacterial compounds selective for intracellular *Salmonella* Typhimurium. *Nature Communications* 10, 197.

Eng, S.-K., Pusparajah, P., Ab Mutalib, N.-S., Ser, H.-L., Chan, K.-G., and Lee, L.-H. (2015). *Salmonella*: a review on pathogenesis, epidemiology and antibiotic resistance. *Frontiers in Life Science* 8, 284-293.

Ercoli, G., Fernandes, V.E., Chung, W.Y., Wanford, J.J., Thomson, S., Bayliss, C.D., Straatman, K., Crocker, P.R., Dennison, A., Martinez-Pomares, L., *et al.* (2018). Intracellular replication of *Streptococcus pneumoniae* inside splenic macrophages serves as a reservoir for septicaemia. *Nature Microbiology* 3, 600-610.

Ernst, R.K., Guina, T., and Miller, S.I. (2001). *Salmonella* Typhimurium outer membrane remodeling: role in resistance to host innate immunity. *Microbes and Infection* 3, 1327-1334.

Ersoy, S.C., Heithoff, D.M., Barnes, L., Tripp, G.K., House, J.K., Marth, J.D., Smith, J.W., and Mahan, M.J. (2017). Correcting a fundamental flaw in the paradigm for antimicrobial susceptibility testing. *EBioMedicine* 20, 173-181.

Fahnoe, K.C., Flanagan, M.E., Gibson, G., Shanmugasundaram, V., Che, Y., and Tomaras, A.P. (2012). Non-traditional antibacterial screening approaches for the identification of novel inhibitors of the glyoxylate shunt in Gram-negative pathogens. *PLoS ONE* 7, e51732.

Fang, F.C., DeGroot, M.A., Foster, J.W., Bäuml, A.J., Ochsner, U., Testerman, T., Bearson, S., Giárd, J.C., Xu, Y., Campbell, G., *et al.* (1999). Virulent *Salmonella* Typhimurium has two periplasmic Cu, Zn-superoxide dismutases. *Proceedings of the National Academy of Sciences* 96, 7502-7507.

Fang, F.C.F.C.F.C. (2004). Antimicrobial reactive oxygen and nitrogen species: Concepts and controversies. *Nature Reviews Microbiology* 2, 820-832.

Farha, M.A., and Brown, E.D. (2015). Unconventional screening approaches for antibiotic discovery. *Annals of the New York Academy of Sciences* 1354, 54-66.

Farha, M.A., French, S., Stokes, J.M., and Brown, E.D. (2017). Bicarbonate alters bacterial susceptibility to antibiotics by targeting the proton motive force. *ACS Infectious Diseases* 4, 382-390.

Farha, M.A., MacNair, C.R., Carfrae, L.A., El Zahed, S.S., Ellis, M.J., Tran, H.-K.R., McArthur, A.G., and Brown, E.D. (2020). Overcoming acquired and native macrolide resistance with bicarbonate. *ACS Infectious Diseases* 6, 2709-2718.

Farha, M.A., Verschoor, C.P., Bowdish, D., and Brown, E.D. (2013). Collapsing the proton motive force to identify synergistic combinations against *Staphylococcus aureus*. *Chemistry & Biology* 20, 1168-1178.

Fass, E., and Groisman, E.A. (2009). Control of *Salmonella* pathogenicity island-2 gene expression. *Current Opinion in Microbiology* 2, 199-204.

Feasey, N.A., Cain, A.K., Msefula, C.L., Pickard, D., Alaerts, M., Aslett, M., Everett, D.B., Allain, T.J., Dougan, G., and Gordon, M.A. (2014). Drug resistance in *Salmonella enterica* ser. Typhimurium bloodstream infection, Malawi. *Emerging Infectious Diseases* 20, 1957.

Feasey, N.A., Dougan, G., Kingsley, R.A., Heyderman, R.S., and Gordon, M.A. (2012). Invasive non-typhoidal *Salmonella* disease: an emerging and neglected tropical disease in Africa. *The Lancet* 379, 2489-2499.

Felise, H.B., Nguyen, H.V., Pfuetzner, R.A., Barry, K.C., Jackson, S.R., Blanc, M.-P., Bronstein, P.A., Kline, T., and Miller, S.I. (2008). An inhibitor of Gram-negative bacterial virulence protein secretion. *Cell Host & Microbe* 4, 325-336.

Feng, X., Zhu, W., Schurig-Briccio, L.A., Lindert, S., Shoen, C., Hitchings, R., Li, J., Wang, Y., Baig, N., Zhou, T., *et al.* (2015). Antiinfectives targeting enzymes and the proton motive force. *Proceedings of the National Academy of Sciences*, 201521910-201521988.

Figueira, R., and Holden, D.W. (2012). Functions of the *Salmonella* pathogenicity island 2 (SPI-2) type III secretion system effectors. *Microbiology* 158, 1147-1161.

Fischbach, M.A. (2011). Combination therapies for combating antimicrobial resistance. *Current Opinion in Microbiology* 14, 519-523.

Fleming, A. (1929). On the antibacterial action of cultures of a penicillium, with special reference to their use in the isolation of *B. influenzae*. *British Journal of Experimental Pathology* 10, 226.

Flores-Mireles, A.L., Walker, J.N., Potretzke, A., Schreiber, H.L., Pinkner, J.S., Bauman, T.M., Park, A.M., Desai, A., Hultgren, S.J., and Caparon, M.G. (2016). Antibody-based therapy for enterococcal catheter-associated urinary tract infections. *mBio* 7, e01653-01616.

Fowler, C.C., and Galán, J.E. (2018). Decoding a *Salmonella* Typhi regulatory network that controls typhoid toxin expression within human cells. *Cell Host & Microbe* 23, 65-76.e66.

Franchi, L. (2006). Cytosolic flagellin requires Ipaf for activation of caspase-1 and interleukin 1 β in *Salmonella*-infected macrophages *Nature Immunology*.

Fujiwara, S., Watanabe, T., Nagatsu, T., Gohda, J., Imoto, M., and Umezawa, K. (1997). Enhancement or induction of neurite formation by a protein tyrosine phosphatase inhibitor, 3,4-dephostatin, in growth factor-treated PC12h cells. *Biochemical and Biophysical Research Communications* 238, 213-217.

Galán, J.E. (1996). Molecular genetic bases of *Salmonella* entry into host cells. *Molecular Microbiology* 20, 263-271.

Gao, P., Ho, P.L., Yan, B., Sze, K.H., Davies, J., and Kao, R.Y.T. (2018). Suppression of *Staphylococcus aureus* virulence by a small-molecule compound. *Proceedings of the National Academy of Sciences* 409, 201720520-201720520.

Geddes, K., Cruz, F., Heffron, F., Iii, F.C., Heffron, F., Cruz, F., and Heffron, F. (2007). Analysis of cells targeted by *Salmonella* type III secretion *in vivo*. *PLoS Pathogens* 3, e196-e196.

Gerdt, J.P., and Blackwell, H.E. (2014). Competition studies confirm two major barriers that can preclude the spread of resistance to quorum-sensing inhibitors in bacteria. *ACS Chemical Biology* 9, 2291-2299.

Gordon, M.A., Graham, S.M., Walsh, A.L., Wilson, L., Phiri, A., Molyneux, E., Zijlstra, E.E., Heyderman, R.S., Hart, C.A., and Molyneux, M.E. (2008). Epidemics of invasive *Salmonella enterica* serovar enteritidis and *S. enterica* serovar Typhimurium infection associated with multidrug resistance among adults and children in Malawi. *Clinical Infectious Diseases* 46, 963-969.

Gottlieb, H.E., Kotlyar, V., and Nudelman, A. (1997). NMR chemical shifts of common laboratory solvents as trace impurities. *Journal of Organic Chemistry* 62, 7512-7515.

Groisman, E.A., and Parra-Lopez, C. (1992). Resistance to host antimicrobial peptides is necessary for *Salmonella* virulence. *Proceedings of the National Academy of Sciences* 89, 11939-11943.

Gunn, J.S. (2001). Mechanisms of bacterial resistance and response to bile. *Microbes and infection* 2, 1-7.

Gunn, J.S., Lim, K.B., Krueger, J., Kim, K., Guo, L., Hackett, M., and Miller, S.I. (1998). PmrA-PmrB-regulated genes necessary for 4-aminoarabinose lipid A modification and polymyxin resistance. *Molecular Microbiology* 27, 1171-1182.

Hancock, R.E.W., and Sahl, H.G. (2006). Antimicrobial and host-defense peptides as new anti-infective therapeutic strategies. *Nature Biotechnology* 24, 1551-1557.

Hancock, R.E.W.R.E.W., Nijnik, A., and Philpott, D.J.D.J.D.J.D.J. (2012). Modulating immunity as a therapy for bacterial infections. *Nature Reviews Microbiology* 10, 243-254.

Hand, W.L., King-Thompson, N.L., and Steinberg, T.H. (1983). Interactions of antibiotics and phagocytes. *Journal of Antimicrobial Chemotherapy* 12, 1-11.

Haraga, A., Ohlson, M.B., and Miller, S.I. (2008). Salmonellae interplay with host cells. *Nature Reviews Microbiology* 6, 53-66.

Harris, T.L., Worthington, R.J., Hittle, L.E., Zurawski, D.V., Ernst, R.K., and Melander, C. (2014). Small molecule downregulation of PmrAB reverses lipid A modification and breaks colistin resistance. *ACS Chemical Biology* 9, 122-127.

Heesterbeek, D.A., Bardoel, B.W., Parsons, E.S., Bennett, I., Ruyken, M., Doorduyn, D.J., Gorham Jr, R.D., Berends, E.T., Pyne, A.L., and Hoogenboom, B.W. (2019). Bacterial killing by complement requires membrane attack complex formation via surface-bound C5 convertases. *The EMBO journal* 38, e99852.

Helaine, S., Cheverton, A.M., Watson, K.G., Faure, L.M., Matthews, S.A., and Holden, D.W. (2014). Internalization of *Salmonella* by macrophages induces formation of nonreplicating persisters. *Science* 343, 204-208.

Helander, I.M., and Sandholm, T.M. (2000). Fluorometric assessment of Gram-negative bacterial permeabilization. *Journal of Applied Microbiology* 88, 213-219.

Herold, S., and Röck, G. (2005). Mechanistic studies of S-nitrosothiol formation by NO[•]/O₂ and by NO[•]/methemoglobin. *Archives of Biochemistry and Biophysics* 436, 386-396.

Honkanen, R.E. (1993). Cantharidin, another natural toxin that inhibits the activity of serine/threonine protein phosphatases types 1 and 2A. *FEBS Letters* 330, 283-286.

Hood, M.I., and Skaar, E.P. (2012). Nutritional immunity: transition metals at the pathogen–host interface. *Nature Reviews Microbiology* 10, 525-537.

Hooker, J.M., Kim, S.W., Reibel, A.T., Alexoff, D., Xu, Y., and Shea, C. (2010). Evaluation of [¹¹C]metergoline as a PET radiotracer for 5HTR in nonhuman primates. *Bioorganic & Medicinal Chemistry* 18, 7739-7745.

Hudson, D.L., Layton, A.N., Field, T.R., Bowen, A.J., Wolf-Watz, H., Elofsson, M., Stevens, M.P., and Galyov, E.E. (2007). Inhibition of type III secretion in *Salmonella enterica* serovar Typhimurium by small-molecule inhibitors. *Antimicrobial Agents and Chemotherapy* 51, 2631-2635.

Husain, M., Jones-Carson, J., Song, M., McCollister, B.D., Bourret, T.J., and Vázquez-Torres, A. (2010). Redox sensor SsrB Cys 203 enhances *Salmonella* fitness against nitric oxide generated in the host immune response to oral infection. *Proceedings of the National Academy of Sciences* 107, 14396-14401.

Hutchings, M.I., Truman, A.W., and Wilkinson, B. (2019). Antibiotics: past, present and future. *Current Opinion in Microbiology* 51, 72-80.

Ibberson, C.B., Stacy, A., Fleming, D., Dees, J.L., Rumbaugh, K., Gilmore, M.S., and Whiteley, M. (2017). Co-infecting microorganisms dramatically alter pathogen gene essentiality during polymicrobial infection. *Nature Microbiology* 2, 17079-17079.

Ilyas, B., Mulder, D.T., Little, D.J., Elhenawy, W., Banda, M.M., Pérez-Morales, D., Tsai, C.N., Chau, N.Y.E.E., Bustamante, V.H., and Coombes, B.K. (2018). Regulatory evolution drives evasion of host inflammasomes by *Salmonella* Typhimurium. *Cell Reports* 25, 825-832.

Ilyas, B., Tsai, C.N., Coombes, B.K., and Coombes, B.K. (2017). Evolution of *Salmonella*-host cell interactions through a dynamic bacterial genome. *Frontiers in Cellular and Infection Microbiology* 7, doi: 10.3389/fcimb.2017.00428.

Jacob-Dubuisson, F., Mechaly, A., Betton, J.-M., and Antoine, R. (2018). Structural insights into the signalling mechanisms of two-component systems. *Nature Reviews Microbiology* 16, 585–593.

Jennings, E., Thurston, T.L.M., and Holden, D.W. (2017). *Salmonella* SPI-2 type III secretion system effectors: molecular mechanisms and physiological consequences. *Cell Host & Microbe* 22, 217-231.

Johnson, B.K., and Abramovitch, R.B. (2017). Small molecules that sabotage bacterial virulence. *Trends in Pharmacological Sciences* 38, 339-362.

Jorgensen, I., Zhang, Y., Krantz, B.A., and Miao, E.A. (2016). Pyroptosis triggers pore-induced intracellular traps (PITs) that capture bacteria and lead to their clearance by efferocytosis. *The Journal of Experimental Medicine* 213, jem.20151613-20152128.

Kang, K., Wong, K.-S., Fong, W.-P., and Tsang, P.W.-K. (2011). Metergoline-induced cell death in *Candida krusei*. *Fungal Biology* 115, 302-309.

Kariuki, S., Revathi, G., Kariuki, N., Kiiru, J., Mwituria, J., Muyodi, J., Githinji, J.W., Kagendo, D., Munyalo, A., and Hart, C.A. (2006). Invasive multidrug-resistant non-typhoidal *Salmonella* infections in Africa: zoonotic or anthroponotic transmission? *Journal of Medical Microbiology* 55, 585-591.

Karlinsey, J.E., Stepien, T.A., Mayho, M., Singletary, L.A., Bingham-Ramos, L.K., Brehm, M.A., Greiner, D.L., Shultz, L.D., Gallagher, L.A., and Bawn, M. (2019). Genome-wide analysis of *Salmonella enterica* serovar Typhi in humanized mice reveals key virulence features. *Cell Host & Microbe* 26, 426-434. e426.

Kato, A., and Groisman, E.A. (2004). Connecting two-component regulatory systems by a protein that protects a response regulator from dephosphorylation by its cognate sensor. *Genes & Development* *18*, 2302-2313.

Kato, A., Latifi, T., and Groisman, E.A. (2003). Closing the loop: the PmrA/PmrB two-component system negatively controls expression of its posttranscriptional activator PmrD. *Proceedings of the National Academy of Sciences* *100*, 4706-4711.

Kaufmann, S.H., Dorhoi, A., Hotchkiss, R.S., and Bartenschlager, R. (2018). Host-directed therapies for bacterial and viral infections. *Nature Reviews Drug Discovery* *17*, 35.

Khatiwara, A., Jiang, T., Sung, S.-S., Dawoud, T., Kim, J.N., Bhattacharya, D., Kim, H.-B., Ricke, S.C., and Kwon, Y.M. (2012). Genome scanning for conditionally essential genes in *Salmonella enterica* serotype Typhimurium. *Applied and Environmental Microbiology* *78*, 3098-3107.

Kingsley, R.A., Msefula, C.L., Thomson, N.R., Kariuki, S., Holt, K.E., Gordon, M.A., Harris, D., Clarke, L., Whitehead, S., Sangal, V., *et al.* (2009). Epidemic multiple drug resistant *Salmonella* Typhimurium causing invasive disease in sub-Saharan Africa have a distinct genotype. *Genome Research* *19*, 2279-2287.

Kirienko, N.V., Vasil, M.L., Otto, M., Franco, O.L., Fleitas Martínez, O., Cardoso, M.H., and Ribeiro, S.M. (2019). Recent advances in anti-virulence therapeutic strategies with a focus on dismantling bacterial membrane microdomains, toxin neutralization, quorum-sensing interference and biofilm inhibition. *Frontiers in Cellular and Infection Microbiology* *1*, 74-74.

Klemm, E.J., Shakoor, S., Page, A.J., Qamar, F.N., Judge, K., Saeed, D.K., Wong, V.K., Dallman, T.J., Nair, S., Baker, S., *et al.* (2018). Emergence of an extensively drug-resistant *Salmonella enterica* serovar Typhi clone harboring a promiscuous plasmid encoding resistance to fluoroquinolones and third-generation cephalosporins. *mBio* *9*, e00105-00118-00110.

Knuff, K., and Finlay, B.B. (2017). What the SIF is happening - the role of intracellular *Salmonella*-induced filaments. *Frontiers in Cellular and Infection Microbiology* *7*, e335.

Koehors, J.J., Dam, J.C.J.v., Saccenti, E., Santos, V.A.P.M.d., Suarez-Diez, M., and Schaap, P.J. (2017). Fast and accurate long-read alignment with Burrows-Wheeler transform. *Oxford* *34*, 1401-1403.

Krishnamoorthy, G., Leus, I.V., Weeks, J.W., Wolloscheck, D., Rybenkov, V.V., and Zgurskaya, H.I. (2017). Synergy between active efflux and outer membrane diffusion defines rules of antibiotic permeation into Gram-negative bacteria. *mBio* 8, e01172-01117.

Kröger, C., Colgan, A., Srikumar, S., Händler, K., Sivasankaran, S.K., Hammarlöf, D.L., Canals, R., Grissom, J.E., Conway, T., Hokamp, K., *et al.* (2013). An infection-relevant transcriptomic compendium for *Salmonella enterica* serovar Typhimurium. *Cell Host & Microbe* 14, 683-695.

Lambris, J.D., Ricklin, D., and Geisbrecht, B.V. (2008). Complement evasion by human pathogens. *Nature Reviews Microbiology* 6, 132-142.

Lane, M.C.C., Alteri, C.J., Smith, S.N., and Mobley, H.L.T. (2007). Expression of flagella is coincident with uropathogenic *Escherichia coli* ascension to the upper urinary tract. *Proceedings of the National Academy of Sciences* 104, 16669-16674.

Langridge, G.C., Fookes, M., Connor, T.R., Feltwell, T., Feasey, N., Parsons, B.N., Seth-Smith, H.M.B., Barquist, L., Stedman, A., Humphrey, T., *et al.* (2015). Patterns of genome evolution that have accompanied host adaptation in *Salmonella*. *Proceedings of the National Academy of Sciences* 112, 863-868.

Latz, E., Xiao, T.S., and Stutz, A. (2013). Activation and regulation of the inflammasomes. *Nature Reviews Immunology* 13, 397-411.

Lawley, T.D., Chan, K., Thompson, L.J., Kim, C.C., Govoni, G.R., and Monack, D.M. (2006). Genome-wide screen for *Salmonella* genes required for long-term systemic infection of the mouse. *PLoS Pathogens* 2, e11-e11.

Lee, A.K., Detweiler, C.S., and Falkow, S. (2000). OmpR regulates the two-component system SsrA-SsrB in *Salmonella* pathogenicity island 2. *Journal of Bacteriology* 182, 771-781.

Leekha, S., Terrell, C.L., and Edson, R.S. (2011). General principles of antimicrobial therapy. Paper presented at: Mayo Clinic Proceedings (Elsevier).

Lehar, S.M., Pillow, T., Xu, M., Staben, L., Kajihara, K.K., Vandlen, R., DePalatis, L., Raab, H., Hazenbos, W.L., Hiroshi Morisaki, J., *et al.* (2015). Novel antibody-antibiotic conjugate eliminates intracellular *S. aureus*. *Nature* 527, 323-328.

Lewis, K. (2013). Platforms for antibiotic discovery. *Nature Reviews Drug Discovery* 12, 371-387.

Li, M., Shandilya, S.M.D., Carpenter, M.A., Rathore, A., Brown, W.L., Perkins, A.L., Harki, D.A., Solberg, J., Hook, D.J., Pandey, K.K., *et al.* (2012). First-in-class small molecule inhibitors of the single-strand DNA cytosine deaminase APOBEC3G. *ACS Chemical Biology* 7, 506-517.

Li, Y., McGreal, S., Zhao, J., Huang, R., Zhou, Y., Zhong, H., Xia, M., and Ding, W.-X. (2016). A cell-based quantitative high-throughput image screening identified novel autophagy modulators. *Pharmacological Research* 110, 35-49.

Liang, Y., Xu, R.-z., Zhang, L., and Zhao, X.-y. (2009). Berbamine, a novel nuclear factor κ B inhibitor, inhibits growth and induces apoptosis in human myeloma cells. *Acta Pharmacologica Sinica* 30, 1659-1665.

Liao, Y., Smyth, G.K., and Shi, W. (2014). featureCounts: an efficient general purpose program for assigning sequence reads to genomic features. *Bioinformatics* 30, 923-930.

Lin, L., Tan, B., Pantapalangkoor, P., Ho, T., Baquir, B., Tomaras, A., Montgomery, J.I., Reilly, U., Barbacci, E.G., Hujer, K., *et al.* (2012). Inhibition of LpxC protects mice from resistant *Acinetobacter baumannii* by modulating inflammation and enhancing phagocytosis. *mBio* 3, e00312-00312.

Liss, V., Swart, A.L., Kehl, A., Hermanns, N., Zhang, Y., Chikkaballi, D., Böhles, N., Deiwick, J., and Hensel, M. (2017). *Salmonella enterica* remodels the host cell endosomal system for efficient intravacuolar nutrition. *Cell Host & Microbe* 21, 390-402.

Lo, J.-H., Kulp, S.K., Chen, C.-S., and Chiu, H.-C. (2014). Sensitization of intracellular *Salmonella enterica* serovar Typhimurium to aminoglycosides *in vitro* and *in vivo* by a host-targeted antimicrobial agent. *Antimicrobial Agents and Chemotherapy* 58, 7375-7382.

Lobritz, M.A., Belenky, P., Porter, C.B.M., Gutierrez, A., Yang, J.H., Schwarz, E.G., Dwyer, D.J., Khalil, A.S., and Collins, J.J. (2015). Antibiotic efficacy is linked to bacterial cellular respiration. *Proceedings of the National Academy of Sciences* 112, 8173-8180.

Love, M.I., Huber, W., and Anders, S. (2014). Moderated estimation of fold change and dispersion for RNA-seq data with DESeq2. *Genome Biology* 15, 550-550.

Lukacs, G.L., Rotstein, O.D., and Grinstein, S. (1991). Determinants of the phagosomal pH in macrophages. *Journal of Biological Chemistry* 266, 24540-24548.

Luna, B., Trebosc, V., Lee, B., Bakowski, M., Ulhaq, A., Yan, J., Lu, P., Cheng, J., Nielsen, T., and Lim, J. (2020). A nutrient-limited screen unmasks rifabutin hyperactivity for extensively drug-resistant *Acinetobacter baumannii*. *Nature Microbiology* 5, 1134-1143.

MacNair, C.R., and Brown, E.D. (2020). Outer membrane disruption overcomes intrinsic, acquired, and spontaneous antibiotic resistance. *mBio* 11.

MacNair, C.R., Stokes, J.M., Carfrae, L.A., Fiebig-Comyn, A.A., Coombes, B.K., Mulvey, M.R., and Brown, E.D. (2018). Overcoming *mcr-1* mediated colistin resistance with colistin in combination with other antibiotics. *Nature Communications* 9, 458-458.

MacNair, C.R., Tsai, C.N., and Brown, E.D. (2020). Creative targeting of the Gram-negative outer membrane in antibiotic discovery. *Annals of the New York Academy of Sciences* 1459, 69-85.

Majowicz, S.E., Musto, J., Scallan, E., Angulo, F.J., Kirk, M., O'Brien, S.J., Jones, T.F., Fazil, A., and Hoekstra, R.M. (2010). The global burden of nontyphoidal *Salmonella* gastroenteritis. *Clinical Infectious Diseases* 50, 882-889.

Man, S.M., and Kanneganti, T.-D. (2015). Regulation of inflammasome activation. *Immunological Reviews* 265, 6-21.

Mangat, C.S., Bharat, A., Gehrke, S.S., and Brown, E.D. (2014). Rank ordering plate data facilitates data visualization and normalization in high-throughput screening. *Journal of Biomolecular Screening* 19, 1314-1320.

Maroufi, Y., Ghaffarifar, F., Dalimi, A.-A., Sharifi, Z., and Hassan, Z. (2012). Cantharidin-induced apoptosis in *Leishmania major* promastigotes and macrophages infected by *Leishmania major* amastigotes *in vitro*. *Journal of Mazandaran University of Medical Sciences* 22, 32-40.

Martin, M. (2011). Cutadapt removes adapter sequences from high-throughput sequencing reads. *EMBnetjournal* 17, doi: 10.14806/ej.14817.14801.14200.

Masaya, I., Hildeaki, K., Tsutomu, S., Cfflgusa, H., Masa, H., Tomio, T., and Kazuo, U. (1993). Dephostatin, a novel protein tyrosine phosphatase inhibitor produced by *Streptomyces*. *The Journal of Antibiotics* 46, 1342-1346.

Mascher, T., Helmann, J.D., and Udden, G. (2006). Stimulus perception in bacterial signal-transducing histidine kinases. *Microbiology and Molecular Biology Reviews* 70, 910-938.

Mastroeni, P., and Grant, A. (2017). Dynamics of spread of *Salmonella enterica* in the systemic compartment. *Microbes and Infection*, 1-9.

Mastroeni, P., Grant, A., Restif, O., and Maskell, D. (2009). A dynamic view of the spread and intracellular distribution of *Salmonella enterica*. *Nature Reviews Microbiology* 7, 73-80.

Maura, D., Drees, S.L., Bandyopadhyaya, A., Kitao, T., Negri, M., Starkey, M., Lesic, B., Milot, S., Déziel, E., and Zahler, R. (2017). Polypharmacology approaches against the *Pseudomonas aeruginosa* MvfR regulon and their application in blocking virulence and antibiotic tolerance. *ACS Chemical Biology* 12, 1435-1443.

McCarthy, A.J., Stabler, R.A., and Taylor, P.W. (2018). Genome-wide identification by transposon insertion sequencing of *Escherichia coli* K1 genes essential for in vitro growth, gastrointestinal colonizing capacity, and survival in serum. *Journal of Bacteriology* 200.

Mellbye, B., and Schuster, M. (2011). The sociomicrobiology of antivirulence drug resistance: a proof of concept. *mBio* 2, e00131-00111.

Miao, E.A., Alpuche-Aranda, C.M., Dors, M., Clark, A.E., Bader, M.W., Miller, S.I., and Aderem, A. (2006). Cytoplasmic flagellin activates caspase-1 and secretion of interleukin 1 β via Ipaf. *Nature Immunology* 7, 569-575.

Miao, E.A., Mao, D.P., Yudkovsky, N., Bonneau, R., Lorang, C.G., Warren, S.E., Leaf, I.A., and Aderem, A. (2010). Innate immune detection of the type III secretion apparatus through the NLRC4 inflammasome. *Proceedings of the National Academy of Sciences* 107, 3076-3080.

Mitchell, G., and Isberg, R.R. (2017). Innate immunity to intracellular pathogens: balancing microbial elimination and inflammation. *Cell Host & Microbe* 22, 166-175.

Mitchell, P. (2011). Chemiosmotic coupling in oxidative and photosynthetic phosphorylation. *Biochimica et Biophysica Acta* 41, 445-502.

Moed, L., Shwayder, T.A., and Chang, M.W. (2001). Cantharidin revisited: a blistering defense of an ancient medicine. *Archives of Dermatology* 137, 1357-1360.

Monack, D.M., Bouley, D.M., and Falkow, S. (2004a). *Salmonella* Typhimurium persists within macrophages in the mesenteric lymph nodes of chronically

infected *Nramp1*^{+/+} mice and can be reactivated by IFN γ neutralization. *The Journal of Experimental Medicine* 199, 231-241.

Monack, D.M., Mueller, A., and Falkow, S. (2004b). Persistent bacterial infections: the interface of the pathogen and the host immune system. *Nature Reviews Microbiology* 2, 747-765.

Mulder, D.T., McPhee, J.B., Reid-Yu, S.A., Stogios, P.J., Savchenko, A., and Coombes, B.K. (2015). Multiple histidines in the periplasmic domain of the *Salmonella enterica* sensor kinase SsrA enhance signaling in response to extracellular acidification. *Molecular Microbiology* 95, 678-691.

Müller, A.A., Dolowschiak, T., Sellin, M.E., Felmy, B., Verbree, C., Gadiant, S., Westermann, A.J., Vogel, J., LeibundGut-Landmann, S., and Hardt, W.-D. (2016). An NK cell perforin response elicited via IL-18 controls mucosal inflammation kinetics during *Salmonella* gut infection. *PLoS pathogens* 12, e1005723-e1005723.

Nagy, T.A., Crooks, A.L., Quintana, J.L., and Detweiler, C.S. (2020). Clofazimine reduces the survival of *Salmonella enterica* in macrophages and mice. *ACS Infectious Diseases* 6, 1238-1249.

Nair, S., Ashton, P., Doumith, M., Connell, S., Painset, A., Mwaigwisya, S., Langridge, G., de Pinna, E., Godbole, G., and Day, M. (2016). WGS for surveillance of antimicrobial resistance: a pilot study to detect the prevalence and mechanism of resistance to azithromycin in a UK population of non-typhoidal *Salmonella*. *Journal of Antimicrobial Chemotherapy* 71, 3400-3408.

Nation, R.L., and Li, J. (2009). Colistin in the 21st century. *Current Opinion in Infectious Diseases* 22, 535-543.

Navarre, W.W., Halsey, T.A., Walthers, D., Frye, J., McClelland, M., Potter, J.L., Kenney, L.J., Gunn, J.S., Fang, F.C., and Libby, S.J. (2005). Co-regulation of *Salmonella enterica* genes required for virulence and resistance to antimicrobial peptides by SlyA and PhoP/PhoQ. *Molecular Microbiology* 56, 492-508.

Needham, B.D., and Trent, M.S. (2013). Fortifying the barrier: the impact of lipid A remodelling on bacterial pathogenesis. *Nature Reviews Microbiology* 11, 467-481.

Negrea, A., Bjur, E., Ygberg, S.E., Elofsson, M., Wolf-Watz, H., and Rhen, M. (2007). Salicylidene acylhydrazides that affect type III protein secretion in *Salmonella enterica* serovar Typhimurium. *Antimicrobial Agents and Chemotherapy* 51, 2867-2876.

Nichols, R.J., Sen, S., Choo, Y.J., Beltrao, P., Zietek, M., Chaba, R., Lee, S., Kazmierczak, K.M., Lee, K.J., Wong, A., *et al.* (2011). Phenotypic landscape of a bacterial cell. *Cell* 144, 143-156.

Nikaido, H. (2003). Molecular basis of bacterial outer membrane permeability revisited. *Microbiology and Molecular Biology Reviews* 67, 593-656.

Ochman, H., Lawrence, J.G., and Groisman, E.A. (2000). Lateral gene transfer and the nature of bacterial innovation. *Nature*.

Ochman, H., Soncini, F.C., Solomon, F., and Groisman, E.A. (1996). Identification of a pathogenicity island required for *Salmonella* survival in host cells. *Proceedings of the National Academy of Sciences* 93, 7800-7804.

Oganesyan, V., Peng, L., Damschroder, M.M., Cheng, L., Sadowska, A., Tkaczyk, C., Sellman, B.R., Wu, H., and Dall'Acqua, W.F. (2014). Mechanisms of neutralization of a human anti- α -toxin antibody. *Journal of Biological Chemistry* 289, 29874-29880.

Oh, Y.J., Plochberger, B., Rechberger, M., and Hinterdorfer, P. (2017). Characterizing the effect of polymyxin B antibiotics to lipopolysaccharide on *Escherichia coli* surface using atomic force microscopy. *Journal of Molecular Recognition* 30, e2605-e2605.

Okoro, C.K., Barquist, L., Connor, T.R., Harris, S.R., Clare, S., Stevens, M.P., Arends, M.J., Hale, C., Kane, L., and Pickard, D.J. (2015). Signatures of adaptation in human invasive *Salmonella* Typhimurium ST313 populations from sub-Saharan Africa. *PLoS Neglected Tropical Diseases* 9, e0003611.

Olliaro, P., Nevill, C., LeBras, J., Ringwald, P., Mussano, P., Garner, P., and Brasseur, P. (1996). Systematic review of amodiaquine treatment in uncomplicated malaria. *The Lancet* 348, 1196-1201.

Osborne, S.E., and Coombes, B.K. (2011). Transcriptional priming of *Salmonella* pathogenicity island-2 precedes cellular invasion. *PLoS ONE* 6, e21648-e21648.

Perez, J.C., and Groisman, E.A. (2007). Acid pH activation of the PmrA/PmrB two-component regulatory system of *Salmonella enterica*. *Molecular Microbiology* 63, 283-293.

Pérez-Morales, D., Banda, M.M., Chau, N.Y.E., Salgado, H., Martínez-Flores, I., Ibarra, J.A., Ilyas, B., Coombes, B.K., and Bustamante, V.H. (2017). The

transcriptional regulator SsrB is involved in a molecular switch controlling virulence lifestyles of *Salmonella*. PLoS Pathogens 13, e1006497.

Peschel, A. (2017). How do bacteria resist human antimicrobial peptides? Trends in microbiology 10, 1-8.

Phoon, Y.W., Chan, Y.Y., and Koh, T.H. (2015). Isolation of multidrug-resistant *Salmonella* in Singapore. Singapore Medical Journal 56, e142-e144.

Porwollik, S., Santiviago, C.A., Cheng, P., Long, F., Desai, P., Fredlund, J., Srikumar, S., Silva, C.A., Chu, W., Chen, X., *et al.* (2014). Defined single-gene and multi-gene deletion mutant collections in *Salmonella enterica* sv. Typhimurium. PLoS ONE 9, e99820-e99820.

Prouty, A.M., Brodsky, I.E., Falkow, S., Gunn, J.S., and Gunn, C.J.S. (2004). Bile-salt-mediated induction of antimicrobial and bile resistance in *Salmonella* Typhimurium. Microbiology 150, 775-783.

Rasko, D.A., Moreira, C.G., De, R.L., Reading, N.C., Ritchie, J.M., Waldor, M.K., Williams, N., Taussig, R., Wei, S., Roth, M., *et al.* (2008). Targeting QseC signaling and virulence for antibiotic development. Science 321, 1078-1080.

Rasko, D.A., and Sperandio, V. (2010). Anti-virulence strategies to combat bacteria-mediated disease. Nature Reviews Drug Discovery 9, 117-128.

Reens, A.L., Crooks, A.L., Su, C.-C., Nagy, T.A., Reens, D.L., Podoll, J.D., Edwards, M.E., Yu, E.W., and Detweiler, C.S. (2018). A cell-based infection assay identifies efflux pump modulators that reduce bacterial intracellular load. PLoS Pathogens 14, e1007115-e1007115.

Rezzoagli, C., Wilson, D., Weigert, M., Wyder, S., and Kümmerli, R. (2018). Probing the evolutionary robustness of two repurposed drugs targeting iron uptake in *Pseudomonas aeruginosa*. Evolution, Medicine, and Public Health 2018, 246-259.

Ricklin, D., Hajishengallis, G., Yang, K., and Lambris, J.D. (2010). Complement: a key system for immune surveillance and homeostasis. Nature Immunology 11, 785-797.

Rooks, M.G., Veiga, P., Reeves, A.Z., Lavoie, S., Yasuda, K., Asano, Y., Yoshihara, K., Michaud, M., Wardwell-Scott, L., Gallini, C.A., *et al.* (2017). QseC inhibition as an antivirulence approach for colitis-associated bacteria. Proceedings of the National Academy of Sciences 114, 142-147.

Ross-Gillespie, A., Weigert, M., Brown, S.P., and Kümmerli, R. (2014). Gallium-mediated siderophore quenching as an evolutionarily robust antibacterial treatment. *Evolution, Medicine, and Public Health* 1, 18-29.

Rycroft, J.A., Gollan, B., Grabe, G.J., Hall, A., Cheverton, A.M., Larrouy-Maumus, G., Hare, S.A., and Helaine, S. (2018). Activity of acetyltransferase toxins involved in *Salmonella* persister formation during macrophage infection. *Nature Communications* 9, 1993-1993.

Sabbagh, S.C., Lepage, C., McClelland, M., and Daigle, F. (2012). Selection of *Salmonella enterica* serovar Typhi genes involved during interaction with human macrophages by screening of a transposon mutant library. *PLoS ONE* 7, e36643-e36643.

Santiviago, C.A., Reynolds, M.M., Porwollik, S., Choi, S.-H., Long, F., Andrews-Polymenis, H.L., and McClelland, M. (2009). Analysis of pools of targeted *Salmonella* deletion mutants identifies novel genes affecting fitness during competitive infection in mice. *PLoS Pathogens* 5, e1000477-e1000477.

Sastry, B.S.R., and Phillis, J.W. (1977). Metergoline as a selective 5-hydroxytryptamine antagonist in the cerebral cortex. *Canadian Journal of Physiology and Pharmacology* 55, 130-133.

Sauter, K.A.D., Melton-Celsa, A.R., Larkin, K., Troxell, M.L., O'Brien, A.D., and Magun, B.E. (2008). Mouse model of hemolytic-uremic syndrome caused by endotoxin-free Shiga toxin 2 (Stx2) and protection from lethal outcome by anti-Stx2 antibody. *Infection and Immunity* 76, 4469-4478.

Sekyere, J.O., and Amoako, D.G. (2017). Carbonyl cyanide m-chlorophenylhydrazine (CCCP) reverses resistance to colistin, but not to carbapenems and tigecycline in multidrug-resistant Enterobacteriaceae. *Frontiers in Microbiology* 8, 228-228.

Seow, W., Ferrante, A., Summors, A., and Thong, Y. (1992). Comparative effects of tetrandrine and berbamine on production of the inflammatory cytokines interleukin-1 and tumor necrosis factor. *Life Sciences* 50, PL53-PL58.

Shea, J.E., Hensel, M., and Gleeson, C. (1996). Identification of a virulence locus encoding a second type III secretion system in *Salmonella* Typhimurium. *Proceedings of the National Academy of Sciences* 93, 2593–2597.

Shi, Y., Cromie, M.J., Hsu, F.-f.F., Turk, J., and Groisman, E.A. (2004). PhoP-regulated *Salmonella* resistance to the antimicrobial peptides magainin 2 and polymyxin B. *Molecular Microbiology* 53, 229-241.

Silver, L.L. (2007). Multi-targeting by monotherapeutic antibacterials. *Nature Reviews Drug Discovery* 6, 41-55.

Singh, K.K., Gurminder; Mjambili, Faith; Smith, Peter J.; Chibale, Kelly (2014). Synthesis of metergoline analogues and their evaluation as antiplasmodial agents. *MedChemComm* 5, 165.

Slauch, J.M. (2011). How does the oxidative burst of macrophages kill bacteria? Still an open question. *Molecular Microbiology* 80, 580-583.

Sorbara, M.T., and Pamer, E.G. (2018). Interbacterial mechanisms of colonization resistance and the strategies pathogens use to overcome them. *Mucosal Immunology* 9, 1-1.

Srikumar, S., Kröger, C., Hébrard, M., Colgan, A., Owen, S.V., Sivasankaran, S.K., Cameron, A.D.S., Hokamp, K., and Hinton, J.C.D. (2015). RNA-seq brings new insights to the intra-macrophage transcriptome of *Salmonella* Typhimurium. *PLoS Pathogens* 11, 1-26.

Stanaway, J.D., Parisi, A., Sarkar, K., Blacker, B.F., Reiner, R.C., Hay, S.I., Nixon, M.R., Dolecek, C., James, S.L., Mokdad, A.H., *et al.* (2019). The global burden of non-typhoidal *Salmonella* invasive disease: a systematic analysis for the Global Burden of Disease Study 2017. *The Lancet Infectious Diseases* 19, 1312-1314.

Stanley, S.A., Barczak, A.K., Silvis, M.R., Luo, S.S., Sogi, K., Vokes, M., Bray, M.A., Carpenter, A.E., Moore, C.B., Siddiqi, N., *et al.* (2014). Identification of host-targeted small molecules that restrict intracellular *Mycobacterium tuberculosis* growth. *PLoS Pathogens* 10.

Starkey, M., Lepine, F., Maura, D., Bandyopadhyaya, A., Lesic, B., He, J., Kitao, T., Righi, V., Milot, S., Tzika, A., *et al.* (2014). Identification of anti-virulence compounds that disrupt quorum-sensing regulated acute and persistent pathogenicity. *PLoS Pathogens* 10, e1004321-e1004321.

Steeb, B., Claudi, B., Burton, N.A., Tienz, P., Schmidt, A., Farhan, H., Mazé, A., and Bumann, D. (2013). Parallel exploitation of diverse host nutrients enhances *Salmonella* virulence. *PLoS Pathogens* 9, e1003301-e1003301.

Stokes, J.M., MacNair, C.R., Ilyas, B., French, S., Côté, J.-P.P., Bouwman, C., Farha, M.A., Sieron, A.O., Whitfield, C., Coombes, B.K., *et al.* (2017). Pentamidine sensitizes Gram-negative pathogens to antibiotics and overcomes acquired colistin resistance. *Nature Microbiology* 2, 17028-17028.

Su, L.-H., Chiu, C.-H., Chu, C., and Ou, J.T. (2004). Antimicrobial resistance in nontyphoid *Salmonella* serotypes: a global challenge. *Clinical Infectious Diseases* 39, 546-551.

Sully, E.K., Malachowa, N., Elmore, B.O., Alexander, S.M., Femling, J.K., Gray, B.M., DeLeo, F.R., Otto, M., Cheung, A.L., Edwards, B.S., *et al.* (2014). Selective chemical inhibition of agr quorum sensing in *Staphylococcus aureus* promotes host defense with minimal impact on resistance. *PLoS Pathogens* 10, e1004174-e1004174.

Suzuki, T., Hiroki, A., Watanabe, T., Yamashita, T., Takei, I., and Umezawa, K. (2001). Potentiation of insulin-related signal transduction by a novel protein-tyrosine phosphatase inhibitor, Et-3,4-dephostatin, on cultured 3T3-L1 adipocytes. *Journal of Biological Chemistry* 276, 27511-27518.

Tanaka, S.I., and Umezawa, K. (1995). Synthesis and protein tyrosine phosphatase inhibitory activity of dephostatin analogs. *The Journal of Antibiotics* 48, 1460-1466.

Theuretzbacher, U., Bush, K., Harbarth, S., Paul, M., Rex, J.H., Tacconelli, E., and Thwaites, G.E. (2020). Critical analysis of antibacterial agents in clinical development. *Nature Reviews Microbiology* 18, 286-298.

Theuretzbacher, U., and Piddock, L.J.V. (2019). Non-traditional antibacterial therapeutic options and challenges. *Cell Host & Microbe* 26, 61-72.

Tomljenovic-Berube, A.M., Mulder, D.T., Whiteside, M.D., Brinkman, F.S.L., and Coombes, B.K. (2010). Identification of the regulatory logic controlling *Salmonella* pathoadaptation by the SsrA-SsrB two-component system. *PLoS Genetics* 6, e1000875-e1000875.

Tommasi, R., Brown, D.G., Walkup, G.K., Manchester, J.I., and Miller, A.A. (2015). ESKAPEing the labyrinth of antibacterial discovery. *Nature Reviews Drug Discovery* 14, 529-542.

Tsai, C.N., and Coombes, B.K. (2019). The role of the host in driving phenotypic heterogeneity in *Salmonella*. *Trends in Microbiology* 27, 508-523.

Tuinema, B.R., Reid-Yu, S.A., and Coombes, B.K. (2014). *Salmonella* evades D-amino acid oxidase to promote infection in neutrophils. *mBio* 5, 1-9.

Turner, K.H., Wessel, A.K., Palmer, G.C., Murray, J.L., and Whiteley, M. (2015). Essential genome of *Pseudomonas aeruginosa* in cystic fibrosis sputum. *Proceedings of the National Academy of Sciences* 112, 4110-4115.

Tyers, M., and Wright, G.D. (2019). Drug combinations: a strategy to extend the life of antibiotics in the 21st century. *Nature Reviews Microbiology* 17, 141-155.

Ulevitch, R.J. (2004). Therapeutics targeting the innate immune system. *Nature Reviews Immunology* 4, 512-520.

Ulloa, E.R., Dillon, N., Tsunemoto, H., Pogliano, J., Sakoulas, G., and Nizet, V. (2019). Avibactam sensitizes carbapenem-resistant NDM-1-producing *Klebsiella pneumoniae* to innate immune clearance. *Journal of Infectious Diseases* 220, 484-493.

Van Puyvelde, S., Pickard, D., Vandelannoote, K., Heinz, E., Barbé, B., de Block, T., Clare, S., Coomber, E.L., Harcourt, K., Sridhar, S., *et al.* (2019). An African *Salmonella* Typhimurium ST313 sublineage with extensive drug-resistance and signatures of host adaptation. *Nature Communications* 10, doi: 10.1038/s41467-41019-11844-z.

Vazquez-Torres, A., Xu, Y., and Jones-Carson, J. (2000). *Salmonella* pathogenicity island 2-dependent evasion of the phagocyte NADPH oxidase. *Science* 287, 1655-1658.

Velkinburgh, J.C.V., and Gunn, J.S. (1999). PhoP-PhoQ-Regulated Loci are required for enhanced bile resistance in *Salmonella* spp. *Infection and Immunity* 67, 1614-1622.

Viljanen, P., and Vaara, M. (1984). Susceptibility of gram-negative bacteria to polymyxin B nonapeptide. *Antimicrobial Agents and Chemotherapy* 25, 701-705.

Walthers, D., Carroll, R.K., Navarre, W.W., Libby, S.J., Fang, F.C., and Kenney, L.J. (2007). The response regulator SsrB activates expression of diverse *Salmonella* pathogenicity island 2 promoters and counters silencing by the nucleoid-associated protein H-NS. *Molecular Microbiology* 65, 477-493.

Walthers, D., Li, Y., Liu, Y., Anand, G., Yan, J., and Kenney, L.J. (2011). *Salmonella enterica* response regulator SsrB relieves H-NS silencing by displacing H-NS bound in polymerization mode and directly activates transcription. *Journal of Biological Chemistry* 286, 1895-1902.

Watanabe, T., Takeuchi, T., Otsuka, M., and Umezawa, K. (1994). Total synthesis of dephostatin, a novel protein tyrosine phosphatase inhibitor. *Journal of Chemical Society, Chemical Communications* 4, 437-438.

Watson, K.G., and Holden, D.W. (2010). Dynamics of growth and dissemination of *Salmonella in vivo*. *Cellular Microbiology* 12, 1389-1397.

Webber, M.A., Bailey, A.M., Blair, J.M.A., Morgan, E., Stevens, M.P., Hinton, J.C.D., Ivens, A., Wain, J., and Piddock, L.J.V. (2009). The global consequence of disruption of the AcrAB-TolC efflux pump in *Salmonella enterica* includes reduced expression of SPI-1 and other attributes required to infect the host. *Journal of Bacteriology* 191, 4276-4285.

Weber, B.S., De Jong, A.M., Guo, A.B., Dharavath, S., French, S., Fiebig-Comyn, A.A., Coombes, B.K., Magolan, J., and Brown, E.D. (2020). Genetic and chemical screening in human blood serum reveals unique antibacterial targets and compounds against *Klebsiella pneumoniae*. *Cell Reports* 32, 107927.

Wheeler, N.E., Gardner, P.P., and Barquist, L. (2018). Machine learning identifies signatures of host adaptation in the bacterial pathogen *Salmonella enterica*. *PLoS Genetics* 14, e1007333.

Will, W.R., Bale, D.H., Reid, P.J., Libby, S.J., and Fang, F.C. (2014). Evolutionary expansion of a regulatory network by counter-silencing. *Nature Communications* 5, 5270-5270.

Winterbourn, C.C., and Kettle, A.J. (2013). Redox reactions and microbial killing in the neutrophil phagosome. *Antioxidants & Redox signaling* 18, 642-660.

Wong, C.E., Sad, S., and Coombes, B.K. (2009). *Salmonella enterica* serovar Typhimurium exploits Toll-like receptor signaling during the host-pathogen interaction. *Infection and Immunity* 77, 4750-4760.

Wösten, M.M.S.M., Kox, L.F.F., Chamnongpol, S., Soncini, F.C., and Groisman, E.A. (2000). A signal transduction system that responds to extracellular iron. *Cell* 103, 113-125.

Wrande, M., Andrews-Polymenis, H., Twedt, D.J., Steele-Mortimer, O., Porwollik, S., McClelland, M., and Knodler, L.A. (2016). Genetic determinants of *Salmonella enterica* serovar Typhimurium proliferation in the cytosol of epithelial cells. *Infection and Immunity* 84, 3517-3526.

Wright, G.D. (2016). Antibiotic adjuvants: rescuing antibiotics from resistance. *Trends in Microbiology* xx, 1-10.

Wu, M., Maier, E., Benz, R., and Hancock, R.E.W. (1999). Mechanism of interaction of different classes of cationic antimicrobial peptides with planar bilayers and with the cytoplasmic membrane of *Escherichia coli*. *Biochemistry* 38, 7235-7242.

Xu, H.R., and Hsu, H.S. (1992). Dissemination and proliferation of *Salmonella* Typhimurium in genetically resistant and susceptible mice. *Journal of Medical Microbiology* 36, 377-381.

Xu, R., Dong, Q., Yu, Y., Zhao, X., Gan, X., Wu, D., Lu, Q., Xu, X., and Yu, X.-F. (2006). Berbamine: a novel inhibitor of bcr/abl fusion gene with potent anti-leukemia activity. *Leukemia Research* 30, 17-23.

Yang, J., Barrila, J., Roland, K.L., Kilbourne, J., Ott, C.M., Forsyth, R.J., and Nickerson, C.A. (2015). Characterization of the invasive, multidrug resistant non-typhoidal *Salmonella* strain D23580 in a murine model of infection. *PLoS Neglected Tropical Diseases* 9, e0003839-e0003839.

Yoon, H., McDermott, J.E., Porwollik, S., McClelland, M., and Heffron, F. (2009). Coordinated regulation of virulence during systemic infection of *Salmonella enterica* serovar Typhimurium. *PLoS Pathogens* 5, e1000306-e1000306.

Zhang, L., Dhillon, P., Yan, H., Farmer, S., and Hancock, R.E. (2000). Interactions of bacterial cationic peptide antibiotics with outer and cytoplasmic membranes of *Pseudomonas aeruginosa*. *Antimicrobial Agents and Chemotherapy* 44, 3317-3321.

Zhang, Y., Liu, Y., Wang, T., Deng, X., and Chu, X. (2018). Natural compound sanguinarine chloride targets the type III secretion system of *Salmonella enterica* serovar Typhimurium. *Biochemistry and Biophysics Reports* 14, 149-154.

Zheng, H., Colvin, C.J., Johnson, B.K., Kirchhoff, P., Wilson, M., Jorgensen-Muga, K., Larsen, S., and Abramovitch, R. (2016). Inhibitors of *Mycobacterium tuberculosis* DosRST signaling and persistence. *Nature Chemical Biology* 13, 218-225.

Zimmerman, S.M., Lafontaine, A.-A.J., Herrera, C.M., McLean, A.B., and Trent, M.S. (2020). A whole cell screen identifies small bioactives that synergize with polymyxin and exhibit antimicrobial activities against multidrug-resistant bacteria. *Antimicrobial Agents and Chemotherapy* 64, e01677-01619.

Zlitni, S., Ferruccio, L.F., and Brown, E.D. (2013). Metabolic suppression identifies new antibacterial inhibitors under nutrient limitation. *Nature Chemical Biology* 9, 796-804.

Zumla, A., Rao, M., Wallis, R.S., Kaufmann, S.H.E., Rustomjee, R., Mwaba, P., Vilaplana, C., Yeboah-Manu, D., Chakaya, J., Ippolito, G., *et al.* (2016). Host-directed therapies for infectious diseases: current status, recent progress, and future prospects. *The Lancet Infectious Diseases* 16, e47-e63.